SELECTED TOPICS FROM THE THEORY OF ELECTRON-ATOM AND ATOM-ATOM COLLISIONS

A THESIS

Presented to

The Faculty of the Division of Graduate Studies and Research

by

Walter Fredrick Morrison, Jr.

In Partial Fulfillment

of the Requirements for the Degree

Doctor of Philosophy

in the School of Physics

Georgia Institute of Technology

March, 1978

SELECTED TOPICS FROM THE THEORY

OF ELECTRON-ATOM AND ATOM-ATOM COLLISIONS

Approved:

Martin R. Flannery, Chairman

Ian R. Gatland

Earl W. McDaniel

Date approved by Chairman 8/23/77

ACKNOWLEDGMENTS

The author of a thesis is never solely responsible for his work, but must credit those who have guided, supported, and encouraged him. He is limited by space, however, and cannot acknowledge all the professors, friends, and fellow students to whom he owes thanks. He must therefore limit his written acknowledgments to those few to whom he is most indebted and trust that the others are aware of his gratitude.

I would first like to thank my advisor, Dr. M. R. Flannery, for his patient guidance and help. At those frequent moments when I was bewildered or confused, he forced me to puzzle things out for myself and benefit by my experience.

For their support, encouragement, and friendship I wish to thank Dr. and Mrs. E. W. McDaniel. One is rarely fortunate enough to find a professor with such a deep personal concern for his students.

I wish to thank my family for their unwaivering support and for the knowledge that I may always turn to them for help and advice.

Finally, I wish to thank my wife, Julia. It is her love, sacrifice and understanding that have enabled me to complete this thesis.

TABLE OF CONTENTS

TABLE OF CONTENTS (Continued)

LIST OF TABLES

LIST OF ILLUSTRATIONS

LIST OF ILLUSTRATIONS (Continued)

SUMMARY

The quantal phase shifts for H^+ - (He, Ne, Ar, Kr), K^+ - (He, Ne), and Li^+ - He systems have been calculated using interaction potentials obtained from the literature. The phase shifts were calculated over the range $k = 10^{-2}$ a.u. - 20 a.u. where k is the relative ion - atom momentum. The phase shifts were obtained by numerically integrating the radial equation, using a Numerov integrator, and matching the numerical and asymptotic solutions at large r.

The quantal elastic, diffusion, and viscosity cross sections were determined for the ion-rare gas systems mentioned above over the stated range of relative momenta by means of standard phase shift sums over angular momentum. For low relative momenta, as few as 30 phase shifts were necessary for covergence of the sum, while at the highest relative momenta as many as 200 phase shifts were required.

The classical diffusion and viscosity cross sections for the ion-rare gas systems previously mentioned and for the K^+ - Ar, Li^+ - (Ne, Ar), and Na^+ (He, Ne, Ar) systems were calculated over the stated range of relative momenta. At low relative momenta, the classical cross sections serve only as a "mean" about which the quantal cross sections oscillate, but the agreement between the classical and quantal values improves with increasing relative momenta until they eventually become indistinguishable.

Collision integrals and zero field reduced mobilities were calculated for each ion-rare gas system and compared to experimental

values as a test of the interaction potentials used in the calculation. Quantal values were obtained at various temperatures between 1 and 1000°K. The low energy quantal effects observed in the cross sections survived the averaging procedure of the collision integral only in the case of the very light ion systems, (H^+ - (He, Ne, Ar, Kr)), and then only at low temperatures. For the other ion-rare gas systems considered, classical and quantal calculations of the mobility differed by less than 1% over the entire temperature range.

The Vainshtein, Presnyakov and Sobel'man approximation was shown to be applicable to the excitation of metastable helium by electron impact. The expressions for the singlet-singlet and triplet-triplet excitation cross sections taking into account the exchange of incident and atomic electrons were derived.

The Born and the Vainshtein, Presnyakov and Sobel'man approximations were applied to the $2^{1,3}P$, $3^{1,3}S$, $3^{1,3}P$,$3^{1,3}D$ and $4^{1,3}P$ excitations arising from e^- - He ($2^{1,3}S$) collisions. Total excitation cross sections were calculated for the above transitions for electron impact energy up to 500 eV. Contrary to expectation, excitation to the $3^{1,3}D$ and $3^{1,3}S$ states dominate the $3^{1,3}P$ and $4^{1,3}P$ excitations except at incident energies above 100 eV.

The use of the so-called Massey-Mohr approximation in the theory of atomic collisions is discussed. It is pointed out that this approximation has a much more general application than envisioned by its creators.

PART I

Theoretical Calculation of the Mobility of Ions in Rare Gases

CHAPTER I

THEORETICAL INTRODUCTION

Definitions

Consider a localized trace amount of ions in an otherwise uniform gas of neutral atoms of an unlike element. The diffusion of the ions in the gas is described by Fick's law, which relates the ion flux density $\vec{J}$ to the negative of the gradient of the ionic number density through a constant of proportionality known as the binary diffusion coefficient, D_{12}. If a weak electric field is applied to the gas, the ions will drift through the gas with an average velocity proportional to the electric field strength. This constant of proportionality is known as the zero field mobility, K, and is related to the binary diffusion coefficient through the Einstein relation,

$$K = \frac{eD_{12}}{kT} \tag{I-1}$$

where e is the ionic charge, k is Boltzmann's constant, and T is the temperature of the neutral gas. The binary diffusion coefficient depends on the detailed ion-neutral interaction in a very complex manner through the collision integrals[2],

$$\Omega^{(\ell,s)}(T) = \frac{1}{2(kT)^{s+2}} \sqrt{\frac{kT}{2\pi\mu}} \int_0^\infty E^{s+1} e^{-E/kT} Q^{\ell}(E)\, dE \tag{I-2}$$

where μ and E are the reduced mass and relative energy of ion-neutral system, and the $Q^{\ell}(E)$ are the classical, semi-classical, or quantal transport cross sections as a function of E. Defining N_1 and N_2 as the ion and neutral gas number densities, the binary diffusion coefficient is given by

$$D_{12} = \frac{3kT\ (1 + \varepsilon_o)}{16\mu(N_1+N_2)\ \Omega^{(1,1)}(T)} \qquad \text{(I-3)}$$

where ε_o is a small correction factor[3] depending on higher order collision integrals, $\Omega^{(\ell,s)}(T)$. In general we consider only a trace amount of ions, such that $N_1 << N_2$, and choosing N_2 to be the standard number density, $N = 2.687 \times 10^{19}\ cm^{-3}$, we may define the zero field reduced mobility,

$$K_o(T) = \frac{3e\ \ (1+\varepsilon_o)}{16\mu N\ \Omega^{(1,1)}(T)} \qquad \text{(I-4)}.$$

Reduced Collision Integrals

In calculating the zero field reduced mobility, it becomes convenient to deal with dimensionless variables and reduced collision cross sections and integrals. Following the discussion of Hirschfelder, Curtiss, and Bird[2], we may write a general spherically symmetric interaction in the form,

$$V(r) = \varepsilon f(r/\sigma).$$

For potentials of the general form used to describe ion-neutral interactions,

$$V(r) = \frac{M\varepsilon}{N-M}\left[\left(\frac{\sigma}{r}\right)^N - \frac{N}{M}\left(\frac{\sigma}{r}\right)^M\right] \qquad \text{(I-5-a)},$$

or

$$V(r) = \frac{JM(1+\gamma)\ \varepsilon}{JN(1-\gamma)+2NM\gamma-JM(1+\gamma)}\left[\left(\frac{\sigma}{r}\right)^N - \frac{N}{J}\left(\frac{2\gamma}{1+\gamma}\right)\left(\frac{\sigma}{r}\right)^J - \frac{N}{M}\left(\frac{1-\gamma}{1+\gamma}\right)\left(\frac{\sigma}{r}\right)^M\right] \qquad \text{(I-5-b)},$$

ε and σ are the well depth and position of the potential minimum respectively, while for ion-neutral potentials of the form,

$$V(r) = \frac{M\varepsilon}{N-M}\left(\frac{N}{M}\right)\left(\frac{N}{N-M}\right)\left[\left(\frac{\alpha}{r}\right)^N - \left(\frac{\alpha}{r}\right)^M\right] \qquad \text{(I-5-c)}$$

ε is still the well depth, but σ now represents the radial position at which the interaction is equal to zero, and the position of the potential minimum is given by

$$r_{min} = \left(\frac{N}{M}\right)\left(\frac{1}{N-M}\right)\sigma \qquad \text{(I-5-d)}.$$

Another choice of ε and σ might be simply the units of energy and length used in defining the interaction.

Once ε and σ are determined, we may define reduced variables of the form,

$$E^* = E/\varepsilon \qquad \text{(I-6-a)}$$

$$V^* = V/\varepsilon \qquad \text{(I-6-b)}$$

$$T^* = kT/\varepsilon \qquad \text{(I-6-c)}$$

$$r^* = r/\sigma \qquad \text{(I-6-d)},$$

etc. For a rigid sphere of radius σ, the classical transport cross sections are given by[2],

$$Q^{(\ell)}_{\text{rigid sphere}} = \left[1 - \frac{1}{2}\left(\frac{1+(-1)^{\ell}}{1+\ell}\right)\right]\pi\,\sigma^2 \qquad \text{(I-7-a)}$$

and the corresponding collision integrals by,

$$\Omega^{(\ell,s)}_{\text{rigid sphere}} = \sqrt{\frac{kT}{2\pi\mu}}\;\frac{(s+1)!}{2}\;Q^{(\ell)}_{\text{rigid sphere}} \qquad \text{(I-7-b)}.$$

Using equations (7) we can define reduced transport cross sections and collision integrals,

$$Q^{(\ell)*}(E^*) = \frac{Q^{(\ell)}(E)}{Q^{(\ell)}_{\text{rigid sphere}}} \qquad \text{(I-8-a)}$$

$$\Omega^{(\ell,s)*}(T) = \frac{\Omega^{(\ell,s)}(T)}{\Omega^{(\ell,s)}_{\text{rigid sphere}}} \qquad \text{(I-8-b)},$$

and in the case of the diffusion cross section, $\ell = s = 1$, we obtain

$$\Omega^{(1,1)*}(T^*) = \frac{1}{\pi\sigma^2}\sqrt{\frac{2\pi\mu}{kT}}\;\Omega^{(1,1)}(T) \qquad \text{(I-8-c)}.$$

Using (I-8-c) we may now write the zero field reduced mobility, equation (4), in terms of the reduced collision integral:

$$K_o(T) = \frac{3e\sqrt{\frac{2\pi}{\mu kT}}\,(1+\varepsilon_o)}{16\pi\sigma^2 N\,\Omega^{(1,1)^*}(T^*)} \qquad \text{(I-9)}.$$

Development of the Scattering Cross Section

The theory of scattering is well developed and has been presented by a large number of authors[2,4-7], therefore only a few relevant results will be reproduced here.

Classical

The classical theory of scattering is based on well defined trajectories for the interacting particles. In the center of mass coordinate system (see Figure 1), we may define a quantity

$$b = \frac{\ell}{\sqrt{2\mu E}} \qquad \text{(I-10)}$$

known as the impact parameter, where ℓ is the angular momentum of the ficticious particle of mass μ about the center of mass. Straightforward analysis[2] leads us to the angle of deflection in the center of mass system

$$\Theta\,(b,E) = \pi - 2b \int_{r_m}^{\infty} \frac{dr}{r^2} \left[1 - \frac{V(r)}{E} - \frac{b^2}{r^2}\right]^{-\frac{1}{2}} \qquad \text{(I-11)}$$

as depicted in Figure 1, and where r_m, the distance of closest approach, is the outer most root of the denominator of the integral in

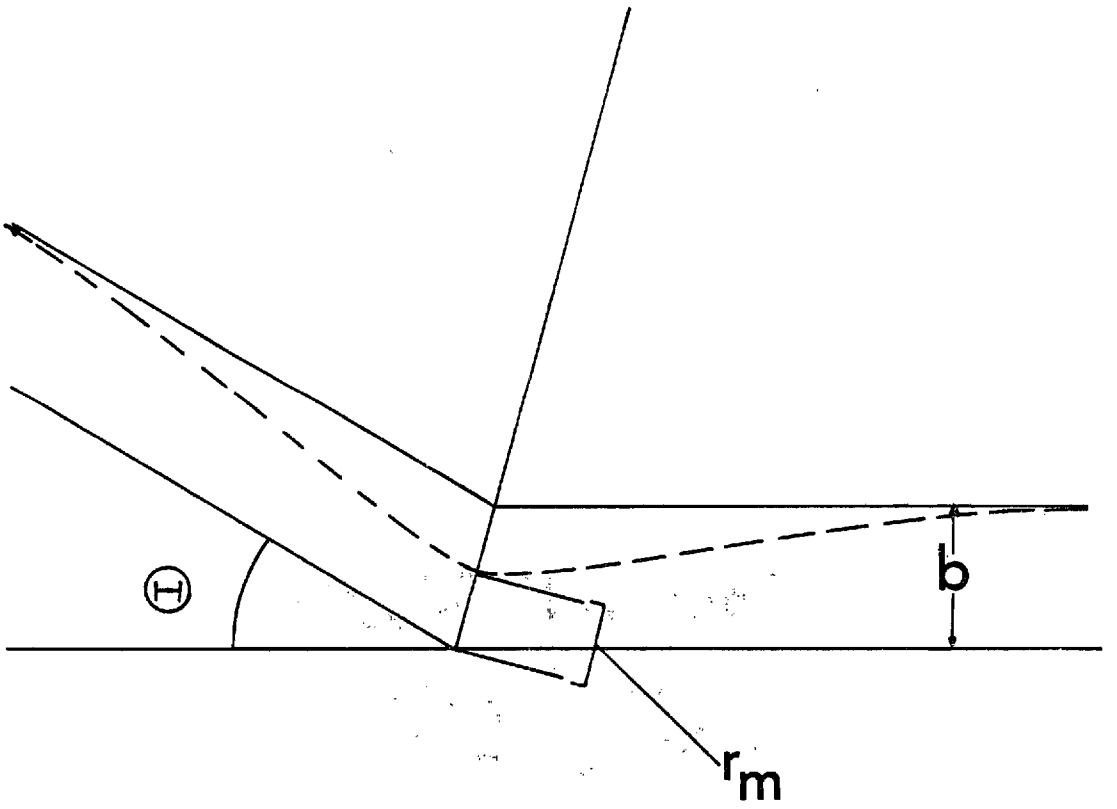

Figure 1. A Classical Scattering Trajectory.

equation (I-11). For a spherically symmetric interaction, the transport cross sections are given by,

$$Q^{\ell}(E) = 2\pi \int_0^{\infty} \left[1 - \cos^{\ell}\left(\Theta(b,E)\right)\right] b\,db \qquad \text{(I-12)},$$

where the infinite impact parameter corresponds to an angle of deflection of 0 and the zero impact parameter to an angle of deflection of π. Re-writing equations (I-11) and (I-12) in terms of the reduced variables, equations (I-6), and the reduced impact parameter,

$$b^* = b/\sigma \qquad \text{(I-13)},$$

we have,

$$\Theta(b^*,E^*) = \pi - 2b^* \int_{r_m^*}^{\infty} \frac{dr^*}{(r^*)^2} \left[1 - \frac{V^*(r^*)}{E^*} - \left(\frac{b^*}{r^*}\right)^2\right]^{-\frac{1}{2}} \qquad \text{(I-14)}$$

and

$$Q^{\ell *}(E^*) = 2\left[1 - \frac{1}{2}\left(\frac{1+(-1)^{\ell}}{1+\ell}\right)\right]^{-1} \int_0^{\infty} \left[1-\cos^{\ell}(\Theta(b^*,E^*))\right] b^*db^* \qquad \text{(I-15)}.$$

Quantal

From the Heisenberg uncertainty principle[5],

$$\Delta x\, \Delta p \gtrsim \hbar \qquad \text{(I-16-a)}$$

$$\Delta\, \theta\, \Delta\ell \gtrsim \hbar \qquad \text{(I-16-b)}$$

it is evident that a well defined trajectory or scattering angle is not feasible in the quantum theory of scattering. As a starting point we consider the time independent Schrodinger equation[8] for a spherically symmetric potential,

$$\left[\vec{\nabla}^2 + k^2 - U(r)\right]\Psi(r,\theta) = 0 \quad , \tag{I-17-a}$$

where $\Psi(\vec{r})$ is the time independent wave function, k is the wave number and

$$U(r) = \frac{2\mu}{\hbar 2} V(r) \quad , \tag{I-17-b}$$

with the restriction that $\Psi(\vec{r})$ be continuous for all r and the boundary conditions

$$\Psi(o) = 0 \; * \quad , \tag{I-17-c}$$

$$\Psi(r,\theta) \underset{r\to\infty}{\sim} e^{i\vec{k}\cdot\vec{r}} + f(\theta)\frac{e^{ikr}}{r} \quad . \tag{I-17-d}$$

The right hand side of equation (I-17-d) represents an incoming plane wave, $e^{i\vec{k}\cdot\vec{r}}$, and an outgoing spherical wave where $f(\theta)$, known as the scattering amplitude, contains the detailed information about the collision, i.e., the angular distribution of scattered particles in the center of mass system.

**(a) We assume $V(r)\to+\infty$ as $r\to 0$ and $V(r)\to 0$ faster than r^{-2} as $r\to\infty$.*

If we consider an incident beam of plane waves under the effect of an interaction $V(r)$, we can define a probability per unit area of the incident beam that a particle will be scattered into a solid angle, $d\Omega(\theta,\phi)$, as

$$\sigma(\theta,\phi)d\Omega(\theta,\phi) = \frac{\text{Number of particles scattered into } d\Omega(\theta,\phi) \text{ per second}}{\text{Number of incident particles per unit area per second}} \qquad \text{(I-18)}$$

where $\sigma(\theta,\phi)$ is called the differential cross section. For an incoming beam of plane waves we find that the incoming particle flux is given by

$$I = \hbar k/\mu \qquad \text{(I-19-a)},$$

while for the scattered beam at large r

$$I_s(\theta,\phi) = \frac{\hbar k}{\mu r^2}|f(\theta)|^2 + 0\left(\frac{1}{r^3}\right) \qquad \text{(I-19-b)}$$

and the number of particles per second scattered into a solid angle $d\Omega(\theta,\phi)$ is

$$I_s(\theta,\phi)r^2 d\Omega(\theta,\phi) = \frac{\hbar k}{\mu}|f(\theta)|^2 \sin\theta d\theta d\phi \qquad \text{(I-19-c)}.$$

Using equations (I-19) in (I-18) we obtain for the differential cross section

$$\sigma(\theta,\phi)\ d\Omega(\theta,\phi) = |f(\theta)|^2\ d\Omega(\theta,\phi) \qquad \text{(I-20)}.$$

The total cross section and transport cross sections are then easily defined by weighted integrals of (I-20);

$$Q_{total}(E) \equiv 2\pi \int_0^{\pi} |f(\theta)|^2 \sin\theta d\theta \qquad \text{(I-21-a)}$$

$$Q^{\ell}(E) \equiv 2\pi \int_0^{\pi} (1-\cos^{\ell}\theta) |f(\theta)|^2 \sin\theta d\theta \qquad \text{(I-21-b)}$$

Thus the calculation of the quantal cross sections, equations (I-21), reduces to the determination of the scattering amplitude $f(\theta)$.

For spherically symmetric potentials, the method of partial waves has been successfully used to determine $f(\theta)$ and the cross sections, equations (I-21).[9-10] This method of solution of the Schrodinger equation is based on expanding the time independent wave function in a series of Legendre Polynomials,

$$\Psi(r,\theta) = \sum_{\ell=0}^{\infty} \frac{u_{\ell}(r)}{kr} P_{\ell}(\cos\theta) \qquad \text{(I-22).}$$

Substituting equation (I-22) into (I-17-a), multiplying by $P_{\ell}'(\cos\theta)$, and integrating over θ by using the orthogonality condition for the Legendre polynomials we obtain the radial equation for $u_{\ell}(r)$,

$$\left[\frac{d^2}{dr^2} - \frac{\ell(\ell+1)}{r^2} - U(r) + k^2\right] u_{\ell}(r) = 0 \qquad \text{(I-23-a)}$$

The asymptotic form of equation (I-23-a) for large r is

$$\left[\frac{d^2}{dr^2} - \frac{\ell(\ell+1)}{r^2} + k^2\right] w_\ell(r) = 0 \qquad \text{(I-23-b)}$$

which has as its solution

$$w_\ell(r) = A_\ell F_\ell(kr) + B_\ell G_\ell(kr) \quad , \qquad \text{(I-24-a)}$$

a linear combination of the regular and irregular Recatti-Bessel functions. These functions are related to the spherical Bessel and Neumann functions, in terms of which equation (I-24-a) becomes

$$w_\ell(r) = kr\left[A_\ell j_\ell(kr) + B_\ell n_\ell(kr)\right] \qquad \text{(I-24-b)}$$

and, using the asymptotic forms of these functions, we have,

$$w_\ell(r) = A_\ell \sin\left[kr - \frac{\pi\ell}{2}\right] + B_\ell \cos\left[kr - \frac{\pi\ell}{2}\right] \qquad \text{(I-24-c)}.$$

We now define,

$$\eta_\ell \equiv \tan^{-1}\left[B_\ell/A_\ell\right] \qquad \text{(I-25-a)}$$

such that

$$A_\ell = \cos\eta_\ell \qquad \text{(I-25-b)}$$

and

$$B_\ell = \sin \eta_\ell \qquad \text{(I-25-c)},$$

and using equations (I-25) in (I-24-e) we have,

$$w_\ell(r) = \sin\left[kr - \frac{\pi\ell}{2} + \eta_\ell\right] \qquad \text{(I-26)},$$

where η_ℓ is the phase shift. If we now expand the right hand side of (I-17-d) in a series of Legendre Polynomials and equate the result to the asymptotic form of equation (I-22), using (I-26), we obtain finally

$$f(\theta) = \sum_{\ell=0}^{\infty} \frac{1}{2ik}\left[e^{2i\eta_\ell}-1\right] (2\ell+1)\ P_\ell(\cos\theta) \qquad \text{(I-27)}.$$

Equation (I-27) can now be used in equations (I-21), the resulting integrations being performed by using the recursion and orthogonality relations for the Legendre polynomials, to obtain the total and transport cross sections. A general relation for the quantum transport cross sections has been derived[11], but due to its complexity only the total cross section and the transport cross sections for $\ell = 1$ and $\ell = 2$ will be reproduced here;[10]

$$Q_{total}(E) = \frac{4\pi}{k^2} \sum_{\ell=0}^{\infty} (2\ell+1)\ \sin^2(\eta_\ell) \qquad \text{(I-28-a)}$$

$$Q^{(1)}(E) = \frac{4\pi}{k^2} \sum_{\ell=0}^{\infty} (\ell+1)\ \sin^2(\eta_\ell-\eta_{\ell+1}) \qquad \text{(I-28-b)}$$

$$Q^{(2)}(E) = \frac{4\pi}{k^2} \sum_{\ell=0}^{\infty} \frac{(\ell+1)(\ell+2)}{(2\ell+3)} \sin^2(\eta_\ell - \eta_{\ell+2}) \qquad \text{(I-28-c)}.$$

The resulting diffusion cross section, equation (I-28-b), may now be used in equations (I-8) and (I-9) to obtain a reduced cross section and collision integral, and finally a zero field reduced mobility.

Description of Numerical Calculations

Classical

Just as the classical theory of scattering is well developed, so are the numerical techniques required to evaluate the classical deflection angle and cross sections. O'Hara and Smith[12] have in fact developed a comprehensive computer code to evaluate not only the transport cross sections, but also the corresponding collision integrals. The heart of this code is the Clenshaw-Curtiss[13] Quadrature, which makes possible the efficient evaluation of the numerous integrals necessary to obtain even a single collision integral. A change of variables in the integral of interest is made such that the integral becomes,

$$I = \int_{-1}^{1} f(x)dx \qquad \text{(I-29)}$$

where f(x) is continuous on (-1,1). The integrand f(x) is then expanded in a series of Chebyshev polynomials, and the series is integrated term by term to give us the desired quadrature. The advantages of this method are[14]; 1) very good accuracy is obtained with relatively few abscissae, 2) the number of abscissae can be doubled without

discarding previous calculations, 3) a reliable error estimate can be easily computed, and 4) the weights and abscissae are simple to compute for any number of abscissae. As this code has been extensively tested and was readily accessible, it was used to obtain all classical collision integrals evaluated.

Quantal

Phase shifts. In the section above, we discussed the problem of quantum scattering and concluded that it is necessary to solve the radial equation,

$$\left[\frac{d^2}{dr^2} - \frac{\ell(\ell+1)}{r^2} - U(r) + k^2\right] u_\ell(r) = 0 \qquad \text{(I-30-a)}$$

with the boundary conditions,

$$u_\ell(0) = 0 \qquad \text{(I-30-b)}$$

$$u_\ell(r) \xrightarrow{r\to\infty} w_\ell(r) = kr\left[A_\ell j_\ell(kr) + B_\ell n_\ell(kr)\right] \qquad \text{(I-30-c)},$$

for a physical interaction, U(r). We will solve these equations by numerically integrating the radial equation, making use of the first boundary condition to start the procedure at small r, and matching the numerical solution to the asymptotic one at large r to evaluate the coefficients A_ℓ and B_ℓ.

There exists a large number of techniques for the solution of linear second-order differential equations[15], but the method of Numerov[16-18] is well adapted to equations of the form of (I-30-a). If we consider the relationship between the second order central difference operator δ^2 and the second order differential operator D^2 where

$$\delta^2 y(x) \equiv y(x+h) - 2y(x) + y(x-h) \tag{I-31-a}$$

$$D^2 y(x) \equiv y''(x) = \frac{d^2 y(x)}{dx^2} \tag{I-31-b}$$

we obtain[16],

$$\delta^2 y(x) = h^2 \left[1 + \frac{1}{12}\delta^2 + O(h^6)\right] y''(x) \tag{I-31-c}.$$

Noting that equation (I-30-a) can be written in the form,

$$y''(x) = F(x)y(x) \tag{I-32}$$

and using this result in (I-31-c), retaining terms to order h^4, we obtain

$$y(x+h)-2y(x)+y(x-h) = h^2\left[F(x)y(x)+\frac{1}{12}(F(x+h)y(x+h) - 2F(x)y(x) + F(x-h)y(x-h))\right] \tag{I-33-a}.$$

Using the notation,

$$x_n = x_o + nh \qquad \text{(I-33-b)}$$

$$f(x_n) = f_n \qquad \text{(I-33-c)}$$

where x_o is the starting point of the procedure, we have,

$$y_{n+1} - 2y_n + y_{n-1} = \frac{h^2}{12}\left[F_{n+1}\, y_{n+1} + 10F_n y_n + F_{n-1} y_{n-1}\right] \qquad \text{(I-33-d)}$$

or

$$\left[1-\frac{h^2}{12} F_{n+1}\right] y_{n+1} = h^2 F_n y_n + 2\left[1-\frac{h^2}{12} F_n\right] y_n - \left[1-\frac{h^2}{12} F_{n-1}\right] y_{n-1} \qquad \text{(I-34-a)}.$$

Defining

$$Y_n \equiv \left[1 - \frac{h^2}{12} F_n\right] y_n \qquad \text{(I-34-b)},$$

we finally obtain

$$Y_{n+1} = h^2 F_n y_n + 2Y_n - Y_{n-1} \qquad \text{(I-34-c)},$$

the Numerov integrator.

To start the integration procedure, we choose a point r_o such that the effective potential $V_{eff}(r_o) = V(r_o) + \frac{\ell(\ell+1)}{r_o^2}$ is much larger

than the relative energy of the colliding particles, $E = k^2/2\mu$, in order that we may approximate the wave function at r_o by,

$$u_\ell(r_o) \equiv u_\ell^{(o)} = 0 \qquad \text{(I-35-a)}$$

and at $r_o + h$, where h is the step size, by

$$u_\ell(r_o+h) \equiv u_\ell^{(1)} = h^{\ell+1} \qquad \text{(I-35-b)}.$$

Equation (I-34-c) is then used to obtain the radial solution at successive points, $r_j = r_o + jh$, until an r such that the V_{eff} (r) is small compared to the relative energy is reached. When this "asymptotic region" is reached the second boundary condition, equation (I-30-c), is applied at two successive values of r

$$u_\ell(r) = kr\left[A_\ell j_\ell(kr) + B_\ell n_\ell(kr)\right] \qquad \text{(I-36-a)}$$

$$u_\ell(r+h) = k(r+h)\left[A_\ell j_\ell(k(r+h))\right] + B_\ell n_\ell\left[(k(r+h))\right] \qquad \text{(I-36-b)},$$

and from these conditions the coefficients A_ℓ and B_ℓ and thus the phase shift

$$\eta_\ell = \tan^{-1}(B_\ell/A_\ell) \qquad \text{(I-36-c)},$$

are determined. The phase shifts determined in this manner will change as the integration procedure is continued, but as V_{eff} (r) "dies out" the phase shift will converge. The criteria for stopping the

radial integration will be that two successive evaluations of the phase shift must agree to within a small number ε. In order to streamline this convergence somewhat the phase shift will only be evaluated when the radial solution goes thru a zero. This condition is arbitrary, i.e., it could be replaced the condition that convergence be checked at each extrema in the radial solution, etc., but it eliminates the necessity of calculating the phase shift for every pair of points, r and r+h, in the asymptotic region.

JWKB Correction to Quantal Phase Shift. The procedure described above for obtaining the quantal phase shift totally ignores the effects of the long range part of the interaction beyond the point where the phase shift converges. Admittedly the contribution from this region will be small for any single phase shift, but when the effect is summed over several hundred angular momentum values, the overall effect can be substantial.

The quantal cross sections are weighted sums of the sine squared of the phase shifts or phase shift differences (equations I-28). Taking into account the additive JWKB correction to the phase shift, the argument of the sine function can be written as the sum of a quantal term and a correction term;

$$\Delta_\ell = \Delta_\ell^q + \Delta_\ell^c \quad . \tag{I-37}$$

Expanding $\sin^2(\Delta_\ell^q + \Delta_\ell^c)$ we have,

$$\sin^2(\Delta^q+\Delta^c) = \sin^2\Delta^q_\ell\cos^2\Delta^c_\ell+\cos^2\Delta^q_\ell\sin^2\Delta^c_\ell+2\sin\Delta^q_\ell\cos\Delta^q_\ell\sin\Delta^c_\ell\cos\Delta^c_\ell \quad \text{(I-38-a)}$$

or,

$$\sin^2(\Delta^q_\ell+\Delta^c_\ell) = \sin^2\Delta^q_\ell\left[1-\frac{(\Delta^c_\ell)^2}{2!}+\ldots\right]^2 + \cos^2\Delta^q_\ell\left[\Delta^c_\ell-\frac{(\Delta^c_\ell)^3}{3!}+\ldots\right]^2$$

$$+ 2\sin\Delta^q_\ell\cos\Delta^q_\ell\left[\Delta^c_\ell-\frac{(\Delta^c_\ell)^3}{3!}+\ldots\right]\left[1-\frac{(\Delta^c_\ell)^2}{2!}+\ldots\right] \quad \text{(I-38-b)}$$

and noting that Δ^c_ℓ is small we finally obtain,

$$\sin^2(\Delta^q_\ell+\Delta^c_\ell) = \sin^2\Delta^q_\ell + \Delta^c_\ell\sin(2\Delta^q_\ell) + O\left[(\Delta^c_\ell)^2\right] \quad \text{(I-39)}$$

Thus, the effect of the correction term not only depends on its value, but also on the value of the quantal phase shift.

As a means of economically calculating this correction to the quantal phase shift, we have used a JWKB approximation as suggested by Dickinson[10]. The JWKB approximation to the phase shift is[19],

$$\eta_\ell^{JWKB} = k\int_{r_m}^{\infty}\left[1-\frac{V(r)}{E}-\frac{b^2}{r^2}\right]^{1/2}dr - k\int_b^{\infty}\left[1-\frac{b^2}{r^2}\right]^{1/2}dr \quad \text{(I-40)}$$

where,

$$b \equiv \frac{\ell+1/2}{k}$$

and r_m is the outer most zero of, $1 - V(r)/E - b^2/r^2$. Using equation (I-40) we can write the JWKB phase shift due to the long range interaction beyond r_o, the point at which the numerical integration of the radial equation is stopped as

$$\delta_\ell^{JWKB} = k\int_{r_o}^{\infty} \left\{\left[1 - \frac{V(r)}{E} - \frac{b^2}{r^2}\right]^{1/2} - \left[1 - \frac{b^2}{r^2}\right]^{1/2}\right\} dr \qquad \text{(I-41)}.$$

As r becomes large, an ion-neutral potential will approach a pure ion-induced dipole interaction,

$$V(r) \xrightarrow{r\to\infty} -\frac{\alpha e^2}{2r^4} \qquad \text{(I-42)}$$

where α is the polarizability of the neutral species. If we assume that beyond r_o the only appreciable portion of the ion-neutral interaction is the "polarization tail", we can use equation (I-42) in (I-41) to obtain the desired correction to the phase shift as,

$$\delta_\ell^{JWKB} = k\left\{\left[r_o^2-b^2\right]^{1/2} - \left[r_o^2-b^2 + q^4/r_o^2\right]^{1/2} + b\,\sin^{-1}\left(\frac{b}{r_o}\right) - \left(\frac{B^2-A^2}{A}\right) F(\nu,t) - (2A)\,E(\nu,t)\right\}, \quad b^4 \geq 4q^4 \qquad \text{(I-43-a)}$$

$$\delta_\ell^{JWKB} = k\left\{\left[r_o^2-b^2\right]^{1/2} - \cos\beta\left[r_o^2-b^2 + q^4/r_o^2\right]^{1/2} + b\,\sin^{-1}\left(\frac{b}{r_o}\right) + 2q\left[(1-x^2)F(\beta,x) - E(\beta,x)\right]\right\}, \quad b^4 \leq 4q^4 \qquad \text{(I-43-b)}$$

where,

$$b = \frac{\ell + 1/2}{k} \tag{I-43-c}$$

$$q^4 = \frac{\alpha}{2E} \tag{I-43-d}$$

$$A = \frac{1}{\sqrt{2}}\left[b^2 + \sqrt{b^4 - 4q^4}\right]^{1/2} \tag{I-43-e}$$

$$B = \frac{1}{\sqrt{2}}\left[b^2 - \sqrt{b^4 - 4q^4}\right]^{1/2} \tag{I-43-f}$$

$$\nu = \sin^{-1}\left(\frac{A}{r_o}\right) \tag{I-43-g}$$

$$t = B/A \tag{I-43-h}$$

$$\beta = \cos^{-1}\left(\frac{r_o^2 - q^2}{r_o^2 + q^2}\right) \tag{I-43-i}$$

$$x = \left[\frac{b^2 + 2q^2}{4q^2}\right]^{1/2} \tag{I-43-j}$$

and the functions F and E are the incomplete elliptic integrals of the first and second kind respectively. We note here a misprint in the work of Dickinson[10], in that the arguments of the elliptic integrals in his equation (19), corresponding to (I-43-b) above, are in reverse order to the convention of Byrd and Friedman[20], while his equation (18) agrees with this convention.

Cross Sections. As the corrected phase shifts were evaluated, their contribution to the sums of equations (I-28) was determined. This process is straightforward and need not be discussed here.

In general, the phase shift sum for the elastic cross section was found to converge much slower than the corresponding diffusion and viscosity sums. This is to be expected since the latter sums depends on the sine of phase shift difference, and for large angular momenta the phase shift is a slowly varying function of ℓ. For low energies, as few as 30 to 50 phase shifts were required to obtain the desired accuracy while up to 200 were necessary at the highest energies considered. The ratio of the partial cross section to the sum of partial cross sections was used as a check on the accuracy of the sums. In the worst case observed this ratio was less than 10^{-2} for the elastic cross section and less than 10^{-4} for the diffusion and viscosity cross sections, but in general the accuracy achieved for the sums was very much better than the worst case.

Collision Integrals. To insure the accuracy of the collision integrals, two separate methods were used in their calculation. In the first method, a cubic spline fit of the log of the diffusion cross section versus the log of the energy was used to interpolate values of the cross section for a Simpson's rule integration. The maxima and minima of the log $(Q^{(1)})$ vs. log (E) curve were found and the integration was divided into integrals from one extrema to the next, each being evaluated with 0.1% numerical accuracy. In the second method, a cubic spline fit of $Q^{(1)}$ vs. E was used to carry out the necessary integration in closed form. The resulting integral is a sum,

$$I = \sum_{i=1}^{N} \left\{ \int_{Ei}^{E_{i+1}} dE\ e^{-E/kT} E^2 \sum_{j=1}^{4} A_j E^{j-1} \right\} \qquad \text{(I-44)}$$

where $N + 1$ is the number of cross sections, E_i is the energy at which the i^{th} cross section was evaluated, and the A_j's are the coefficients of the spline fit. The collision integrals obtained by these two methods agree to at least three significant digits for all cases.

Over the temperature range $1°K \leq T \leq 1000°K$, the contributions from the highest and lowest energy regions are much smaller than the 0.1% numerical accuracy of the calculation such that the error introduced by the transition from an infinite integral to a finite one can be assumed to be negligible.

CHAPTER II

RESULTS AND DISCUSSION

Ion-Rare Gas Interaction Potentials

The various calculations described in Chapter I all ultimately depend on the ability to efficiently calculate the interaction potential, V(R), over a wide range of ion-atom separations, R. A large number of ion-atom interaction potentials now exist in the literature[9, 21-32]* but the majority of these are reported as tables of energy versus ion-atom separation** which must be approximated by some function f(R) before they can be used. Although this process is a simple exercise in functional or polynomial approximation, a short discussion of the types of approximating functions used and a tabulation of results will be given.

Functional Forms

The common characteristics of all ion-neutral interactions are; 1) a short range repulsive core, 2) an attractive potential well, and 3) a long range ($-1/r^4$) behavior arising from the ion-induced dipole interaction. In general, tabulations of interaction potentials are limited to the potential well, but our knowledge of the behavior of the ion-neutral interaction in the neighborhood of the repulsive core

This list is by no means exhaustive.

***Exceptions include the proton-rare gas interactions of refs. 22 and 23.*

and of the attractive polarization tail enables us to choose appropriate model functions for these regions and then insure a smooth transition from one region to the next.

The approximation of the well regions for the interactions considered here[9, 21-25, 27], was carried out by one of two basic methods. A cubic interpolating polynomial was used to fit the proton-helium and proton-neon interactions of Peyerimhoff[21], while a least squares fit of the tabulated interaction was used for ion rare gas interactions of Catlow et al.[9], Klingbeil[24], Rich et al.[25], and Gordon et al.[27]. The functions used for the least squares fits will be presented later, with the corresponding interactions.

Proton-Rare Gas Interactions

Weise Interactions*. Of all the interactions considered here, only this set is presented in the literature in a functional form. They were obtained by assuming a model function for the interaction and then adjusting the parameters until the differential cross section calculated using this model matched the corresponding experimental cross section. Two sets of functions using different model potentials were presented by Weise et al.[22] and Mittmann et al.,[23], but only the set used in this calculation will be considered here. The model function used for the Weise interactions is

$$V_1(R) = \varepsilon \left(\exp(2A_1A_2(1-\rho)) - 2 \exp(A_1A_2(1-\rho))\right.$$

*Henceforth the Weise et al.[22] and Mittmann et al.[23] interactions will be referred to as the Weise interactions for the sake of brevity.

Where, $\rho = R/Rmin$

$$A_2 = 1, \ \rho < 1 \qquad \text{(II-1)}$$

$$A_2 \neq 1, \ \rho \geq 1.$$

As noted by the authors, the Weise interactions do not have the proper long range behavior, and, as discussed in (II-1-A), it was necessary to insure this behavior by restricting the use of equation (II-1) to R less than some R_α, and using the function,

$$V_2(R) = B_1 \exp(-B_2 R) - 1/2\alpha R^{-4} \qquad \text{(II-2)}$$

for $R > R\alpha$.

The parameters used in equations (II-1) and (II-2) are given in Table I.

Peyerimhoff Interactions. The H^+ - He and H^+ - Ne interactions of Peyerimhoff[21] were obtained from a Hartree-Fock-Roothaan calculation, the H^+ - He potential having been used previously in a mobility calculation[10]. As noted above, a cubic interpolating polynomial was used to fit Peyerimhoff's interactions for $R_A \leq R \leq R_B$ where R_A and R_B are the lower and upper limits of the tabulated data while outside this region the functions,

$$V_1(R) = A_1 R^{-12} + A_2 R^{-6} \qquad R < R_A$$

$$V_3(R) = C_1 \exp(-C_2 R) - 1/2\alpha R^{-4} \qquad R > R_B \qquad \text{(II-3)}$$

Table I. The Weise et al. Interactions.

	A_1	A_2	ε	R_{min}	B_1	B_2	R_α	α
H^+ - He	2.2	.85	.07350	1.455	-5.715E+2	2.817	5.1	1.384
H^+ - Ne	2.68	.85	.08379	1.871	-2.798E+3	2.805	5.6	2.666
H^+ - Ar	2.5	.86	.14847	2.476	-5.478E+5	2.423	8.9	11.067
H^+ - Kr	2.5	.80	.16354	2.778	-5.608E+7	2.326	11.6	16.736

were used. The A's and C's were determined by requiring that the interactions and their 1st derivatives be continuous at R_A and R_B respectively. Their values are given in Table II along with those of R_A and R_B.

Klingbeil and Rich et al. Interactions. The H^+ - Ar interaction of Klingbeil[24] and the H^+ - Kr interaction of Rich et al.[25] are the results of a procedure in which differential scattering data is inverted to obtain an interaction potential. A least squares fit of the tabulated interactions to the function

$$V_2(R) = B_1 \exp(-B_2R) + B_3R^{-6} + B_4R^{-4}, \quad R_A \leq R \leq R_B \qquad \text{(II-4)}$$

was made, where R_A and R_B are again the lower and upper limits of the tabulated data. In the regions $R < R_A$ and $R > R_B$, the interactions were approximated in a manner identical to that used for the Peyerimhoff interactions. The parameters used in equations (II-3) and (II-4) are presented in Table II along with values of R_A and R_B.

Alkalai Ion-Rare Gas Interactions

Catlow et al. Interactions. The Li^+ - He interaction has been investigated by a number of authors[9, 32, 33], and several ab initio Hartree Fock calculations exist for this system[9, 31, 34], due to its relative simplicity, i.e., it is an ion-neutral system with only three electrons. A least square fit of the ab initio interaction of Catlow et al.[9] was made and mated to appropriate long and short range model functions as discussed earlier. The resulting approximating function is;

Table II. Proton-Rare Gas Interactions of Peyerimhoff[24] (H^+ - He, Ne), Klingbeil (H^+ - Ar), and Rich et al. (H^+ - Kr).

	A_1	A_2	R_A	B_1	B_2	B_3	B_4	R_B	C_1	C_2	α
He	.07203	.07137	1.0	--	--	--	--	4.0	-.7784	1.678	1.384
Ne	3.974	-.6101	1.35	--	--	--	--	4.0	-17.34	2.279	2.666
Ar	105.82	-3.664	1.686	62.78	2.187	20.41	-19.56	4.898	-.6601	.6992	11.067
Kr	6.45E+3	-39.77	2.269	-3.37E+3	3.681	385.76	-52.37	6.0	-.7372	.5595	16.738

$$V_1(R) = (3.476 \times 10^{-7})R^{-12} + 16.93 \exp(-2.6306R),\ R < 1.29,$$

$$V_2(R) = 24.69 \exp(-2.6325R) - .7152R^{-4},\ 1.29 \leq R \leq 8.0, \qquad \text{(II-5)}$$

$$V_3(R) = -2.923 \times 10^{-4} \exp(-.4933R) - .692R^{-4},\ R > 8.0.$$

Gordon-Waldman Interactions. The ion neutral interactions of Gordon and Waldman[27] were calculated using an electron-gas Drude-model[26] in which the atoms are treated as three-dimensional harmonic oscillators. Due to the simplicity of the calculations required by this model, "the computer time spent by the calculation is insignificant"[26], and the authors have produced a large number of interactions over a wide range of internuclear separations. From this collection of interaction potentials the nine systems, Li^+ - (He, Ne, Ar), Na^+ - (He, Ne, Ar), and K^+ -(He, Ne, Ar) were chosen for consideration and fit by a least squares technique to a model function suggested by Weise et al.[22-23] This model function has the form,

$$F(\rho) = (G(\rho)\ (\alpha_1 + G(\rho)\ (\alpha_2 + \alpha_3 G(\rho)))H(\rho) - \varepsilon \qquad \text{(II-6)}$$

where,

$$G(\rho) = \frac{M}{N-M}\left(\rho^N - \left(\frac{N}{M}\right)\rho^M\right) + 1,\ N > M, \qquad \text{(II-7)}$$

$$H(\rho) = \frac{1}{(1 + \rho^L)}\ , \qquad \text{(II-8)}$$

$$\rho = R_{min}/R\ , \qquad \text{(II-9)}$$

and $\varepsilon = \alpha_1 + \alpha_2 + \alpha_3$, (II-10)

and the properties,

$$V(\rho) \to +\infty \text{ as } \rho \to 0 \quad ,$$

$$V(\rho) \to 0 \text{ as } \rho \to \infty \quad , \qquad \text{(II-11)}$$

$$V(1) = -\varepsilon \quad ,$$

$$V'(1) = 0 \quad ,$$

i.e., all the general characteristics desired for an ion-neutral potential. Despite its very general appearance, large number of independent parameters (7), and desirable properties, it was necessary to divide the tabulated interactions into four separate regions as depicted in Figure 2. The first and second regions were separated at $R = R_A$, where $V(R_A)$ is well up on the repulsive core, the second and third at R_B, where $V(R_B)$ was in the vicinity of the crossing point, and the third and fourth at R_C, where the interaction potential was approximately equal to the polarization interaction for $R>R_C$. The resulting interaction potentials have the form,

$$V_1(R) = F(R) + A_1\left(\frac{R}{R_A}\right)^{A_2} \quad , \qquad R<R_A,$$

$$V_2(R) = F(R), \qquad R_A \leq R \leq R_B,$$

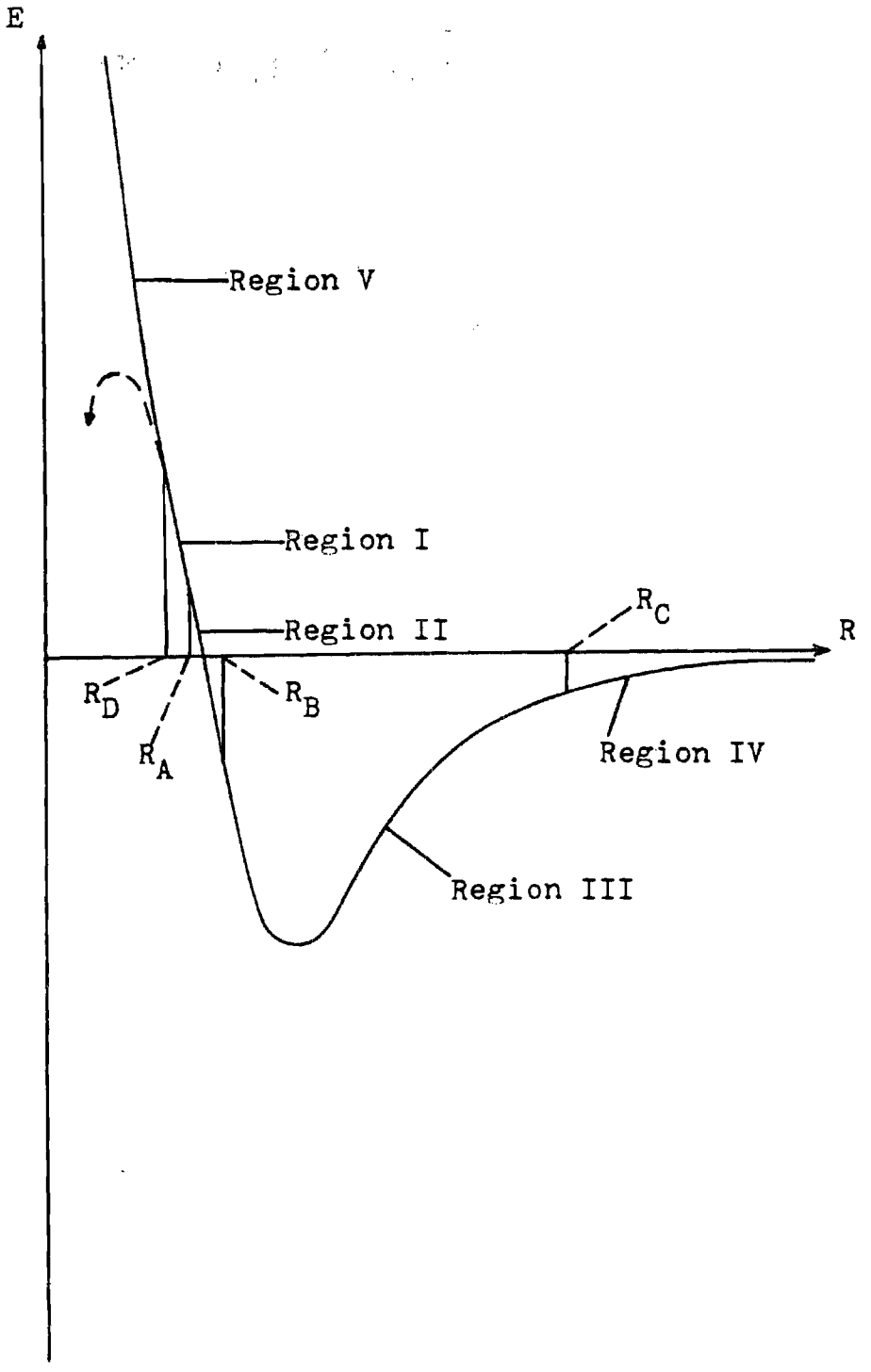

Figure 2. A Typical Ion-Neutral Interaction Divided into Regions as for the Gordon-Waldman[27] Interactions.

$$V_3(R) = F(R), \qquad R_B \leq R \leq R_C,$$

$$V_4(R) = B_1 \exp(B_2R) + B_3R^{-6} - 1/2\alpha R^{-4} + B_4 \exp(B_5R), \; R>R_C.$$

The parameters A_1 and A_2 were determined by the condition that V_1 and V_2, and their derivatives be equal at $R = R_A$, the parameters B_1 - B_3 are the results of a least squares fit, B_4 and B_5 were determined by matching V_3, V_4, and their derivatives at $R = R_C$ and R_A, R_B, and R_C were chosen to provide the smoothest possible transition from one region to the next. It was found that for the systems Li^+ - Ne, Ar and Na^+ - He, Ne, the above procedure broke down for very small R and the resulting interaction approached - ∞ rather than + ∞ as $R \to 0$. This was remedied by the addition of a fifth region and the function

$$V_5(R) = C_1 \exp(C_2R) + C_3R^{-8}, \; R < R_D$$

where C_1 and C_2 were determined by matching V_1, V_5, and their derivatives at R_D, and C_3 was chosen to obtain the best approximation of the tabulated interaction for small R. The values of all parameters defined above are given in Tables III-a through e. This procedure is a bit cumbersome, but the approximating functions derived from it generally match the Gordon potentials to at least three significant places. Admittedly, a simpler form for the potential could have been used, but the reproduction of the interactions would not have been as faithful in such a case.

Table III-a. Parameters for the Gordon-Waldman Interactions, Region I.

	α_1	α_2	α_3	R_{min}	L	M	N	R	A_1	A_2
Li^+-He	1.289E-2	-7.689E-5	2.146E-7	4.950	-2.445	1.15	3.725	1.755	1.799E-4	323.42
Li^+-Ne	1.238E-2	1.954E-3	-5.63E-5	5.0	- .25	1.7	3.5	2.255	8.856E-5	429.72
Li^+-Ar	2.552E-2	5.928E-4	-1.208E-5	5.23	- .25	2.2	4.0	3.003	4.663E-5	988.78
K^+-He	1.215E-2	-7.55E-5	2.404E-7	6.5003	- .95	1.8	4.0	3.7	4.767E-4	39.528
K^+-Ne	3.262E-2	-2.476E-4	1.049E-6	6.0425	-2.5	2.0	4.0	3.39	2.269E-3	32.771
K^+-Ar	1.552E-2	-1.023E-4	4.779E-7	6.733	-3.4	2.2	5.01	4.051	2.476E-4	43.657
Na^+-He	8.006E-3	2.266E-4	-3.864E-6	5.75	- .8	1.9	3.95	3.59	5.924E-4	32.901
Na^+-Ne	1.584E-2	8.067E-4	-1.047E-5	5.743	- .478	1.99	3.95	3.412	9.487E-5	288.41
Na^+-Ar	4.373E-2	-2.454E-4	6.304E-7	5.989	- .85	2.1	4.35	3.75	5.999E-3	17.928

Table III-b. Parameters for the Gordon-Waldman Interactions, Region II.

	α_1	α_2	α_3	R_{min}	L	M	N	R_A	R_B
Li^+-He	9.903E-3	4.765E-4	-1.589E-5	5.08	-1.01	1.15	3.684	1.755	2.8
Li^+-Ne	5.182E-3	3.475E-3	-1.462E-4	1.685	- .25	1.7	3.5	2.255	3.035
Li^+-Ar	1.303E-2	3.696E-3	-1.768E-4	5.174	- .25	2.2	4.0	3.003	3.62
K^+-He	1.574E-3	7.005E-4	-3.049E-5	7.088	- .95	1.8	4.0	3.7	4.236
K^+-Ne	2.996E-3	1.149E-3	-4.18E-5	6.986	-2.5	2.0	4.0	3.39	4.393
K^+-Ar	6.072E-3	8.726E-4	-4.827E-5	7.01025	-3.4	2.2	5.01	4.051	4.713
Na^+-He	-1.566E-4	3.079E-6	-5.834E-9	11.7515	- .8	1.9	3.95	3.59	4.35
Na^+-Ne	-1.115E-3	4.077E-3	-2.899E-4	5.819	- .478	1.99	3.95	3.412	4.21
Na^+-Ar	2.545E-3	5.357E-3	-4.315E-4	6.34045	- .85	2.1	4.35	3.75	4.65

Table III-c. Parameters for the Gordon-Waldman Interactions, Region III.

	α_1	α_2	α_3	ϵ	R_{min}	L	M	N	R_B	R_C
Li^+-He	2.662E-3	-7.927E-5	3.932E-6	2.587E-3	3.6327	3.55	7.21	9.715	2.8	6.0
Li^+-Ne	4.665E-3	-1.5E-4	1.627E-5	4.531E-3	3.716	3.6	7.027	10.0	3.035	6.0
Li^+-Ar	9.664E-3	3.673E-3	-2.015E-3	1.132E-2	4.15575	3.379	6.948	9.9	3.62	5.8
K^+-He	8.175E-4	-6.174E-6	9.236E-8	8.115E-4	5.429	4.3	8.75	12.46	4.236	6.9
K^+-Ne	1.457E-3	-1.123E-5	2.202E-7	1.446E-3	5.534	4.05	8.9	12.7	4.393	7.45
K^+-Ar	4.151E-3	-6.299E-5	1.636E-6	4.09E-3	5.894	4.025	8.36	11.4	4.713	6.5
Na^+-He	1.294E-03	-3.382E-5	1.949E-5	1.280E-3	4.5641	3.925	7.25	12.71	4.35	6.27
Na^+-Ne	2.535E-3	-4.31E-5	-5.123E-7	2.491E-3	4.5902	3.7576	7.4825	12.09225	4.21	6.6
Na^+-Ar	5.686E-3	1.068E-3	-8.462E-4	5.908E-3	5.1314	3.426	7.6192	11.263	4.65	6.62

Table III-d. Parameters for the Gordon-Waldman Interactions, Region IV.

	B_1	B_2	B_3	B_4	B_5	α	R_C
Li^+-He	-2.21269	- .87596	- .13376	2.21382	- .87624	1.384	6.0
Li^+-Ne	-1.885E-3	- .8274	- .18992	-1.420E+2	-3.10534	2.667	6.0
Li^+-Ar	6.609E+2	-2.6532	- 5.04464	48.241	-2.6871	11.0673	5.8
K^+-He	-5.566E-2	-1.13719	- 6.92581	3.007E-2	-1.3149	1.384	6.9
K^+-Ne	3.077E-4	- .42542	-19.66174	-3.169E+9	-4.74321	2.667	7.45
K^+-Ar	-6.61E-4	- .35866	-46.7269	6.846E+5	-3.31376	11.0673	6.5
Na^+-He	6.256E-3	-1.14325	- 3.09332	-3.6741	-2.5598	1.384	6.27
Na^+-Ne	-8.118E-3	-1.0816	- 5.06948	-1.2826E-3	- .54198	2.667	6.6
Na^+-Ar	2.219E+5	-3.3265	-19.05964	2.247E-2	-1.27089	11.0673	6.62

Table III-e. Parameters for the Gordon-Waldman Interactions, Region V.

	R_o	C_1	C_2	C_3
Li^+-Ne	2.0	49.3188	-2.684	.02
Li^+-Ar	2.0	7.9221	-4.663E-5	3.4
Na^+-He	2.0	2.02995	- .9295	1.9
Na^+-Ne	2.0	14.3778	-1.3898	6.8

Phase Shifts

Comparison with Published Data

The phase shifts were calculated in the manner described in Chapter I, being basically quantal with a JWKB correction for the long range portion of the interaction. The phase shift routine was checked in two ways. First a comparison of our calculated phase shifts for the scattering of electrons and positrons by atomic hydrogen was made with the tabulated values of Bransden[4]. We then calculated the Boltzman sum phase shift

$$G_B^- = \sum_{\ell=0}^{\infty} (2\ell+1)\ \delta_\ell \qquad \text{(II-12)}$$

for an attractive static screened coulomb interaction,

$$V(r) = \frac{-e^{-r/\lambda_D}}{r}$$

where λ_D is the Debye screening length, and compared our results with the very accurate results of Rodgers[35]. As can be seen in Tables IV-a and b, our phase shifts agree quite well with those of Bransden. From Table V, we note that at low k where only a few phase shifts are involved in the sum, our results agree with those of Rodgers to four or five significant places but as k increases, and more phase shifts become involved in the sum, our agreement drops to two significant digits. We wish to note that neither of these calculations included the JWKB correction described above.

Table IV-a. Positron-Hydrogen Atom (Tolerance for Convergence of Phase Shifts is 10^{-4})

k	0^+		1^+		2^+	
	Bransden	W.F.M.	Bransden	W.F.M.	Bransden	W.F.M.
.1	-.058	-.058				
.2	-.1145	-.1146	-.0017	-.0018		
.3	-.1680	-.1683	-.0055	-.0056		
.4	-.2181	-.2181	-.0121	-.0121	-.0005	-.0005
.5	-.2640	-.2636	-.02	-.021	-.0013	-.0013
.6	-.3043	-.3042	-.0322	-.0322	-.0028	-.0028
.8	-.3713	-.3712	-.0584	-.0583	-.0082	-.0082

Table IV-b. Electron-Hydrogen Atom (Tolerance for Convergence of Phase Shifts if 10^{-4})

k	0^-		1^-		2^-	
	Bransden	W.F.M.	Bransden	W.F.M.	Bransden	W.F.M.
.1	.721	.7201	.0003	.0002		
.2	.9731	.971	.0021	.002		
.3	1.0458	1.0445	.0066	.0066		
.4	1.0575	1.0567	.0147	.0146	.0005	.0005
.5	1.0448	1.044	.026	.0259	.0014	.0014
.6	1.0210	1.02	.0406	.0404	.003	.0029
.8	.9633	.9628	.0752	.075	.0087	.0086

Table V. $\lambda_D = 1.0$

k	$G_B^- = \sum_\ell (2\ell+1)\ \delta_\ell(k)$ in π radians	
	Rodgers	W.F.M.
10^{-4}	.99974	.99974
10^{-3}	.99743	.99748
10^{-2}	.974332	.97485
4.7×10^{-2}	.88309	.88532
10^{-1}	.77438	.77794
1.5×10^{-1}	.69958	.70342
4.7×10^{-1}	.56872	.57135
8.3×10^{-1}	.68482	.68694
1.0	.76827	.7703

We have also attempted to compare our results for the Li^+ - He and H^+ - He systems with similar results of Catlow et al.[9] and Dickinson[10] for the same systems, respectively. Catlow et al. have plotted their phase shifts for several values of k, and to the accuracy with which we could read their graphs, our phase shifts agree with theirs. Dickinson has, for low k, fit his S wave phase shifts to the expression,

$$\delta_o(k) = 12\,\pi - 31.5\,k \qquad \text{(II-13)}$$

which is in general agreement with our results. For the Peyerimhoff potential, also used by Dickinson, we obtain $\delta_o = 37.469$ radians at $k = 6 \times 10^{-3}$ a.u. compared with $\delta_o = 37.51$ radians calculated using equation (II-13).

We have, therefore, tested our phase shift routine for several totally different interactions and are satisfied as to the accuracy of our subsequent results, which have all been calculated to a convergence tolerance of 10^{-3} radians.

Ion-Neutral Phase Shifts

Consideration of the relationship between the scattering phase shift as a function of angular momentum and the effective interaction potential can yield valuable insight into the phase shift treatment of the scattering problem. The parallel consideration of the phase shift for a given angular momentum as a function of energy is also enlightening but will not be treated here (see, for instance, Child[6]).

As a starting point, we note that attractive interactions will produce positive phase shifts and repulsive interactions negative phase shifts, as illustrated by the positron-hydrogen and electron-hydrogen phase shifts of Tables IV. For an ion-neutral interaction with both attractive and repulsive branches, the sign of the phase shift will depend on which branch of the interaction is dominant (see Figures 3-7).

For large angular momenta, the phase shift will approach zero, corresponding to the diminished effect of the interaction at large impact parameter. The phase shift will always approach zero through positive values, however, due to the long range polarization (attractive) interaction, characteristic of ion-neutral interactions. At high energy, the repulsive branch of the interaction will dominate the S-wave scattering, resulting in a negative S-wave phase shift. Since the phase shift must approach zero for large angular momenta through positive values, there must exist a maximum in the phase shift versus ℓ. This maxima can be related semiclassically to the forward glory found in classical scattering[41]. In addition to the maximum in the phase shift, there also exists an inflection point, to the right of the maximum, where the phase shift begins to flatten out as it approaches zero. This inflection also has a semiclassical link to a classical scattering phenomena, rainbow scattering[41]. With decreasing energy, the S-wave phase shift increases, becoming positive as the attractive portion of the interaction becomes dominant. The presence of the maximum and inflection point in the phase shift persists, however, to very low energies.

As the energy is decreased, discontinuities appear in the phase shift. These discontinuities are very close to π radians and are related

Table VI. Li^+ - He Phase Shifts

ℓ	$(2\mu V_{eff}(max))^{1/2}$	Phase Shifts (π radians) k = .0096	k = .1	k = .5	k = 1.0	k = 4.0
0		7.133	6.296	4.432	3.022	-1.811
1	1.25E-2	7.030	6.593	4.847	3.464	-1.336
2	3.75E-2	(*) 6.006	6.653	5.175	3.849	-0.885
3	7.50E-2	6.002	6.316	5.412	4.174	-0.459
4	1.25E-1	5.001	6.086	5.551	4.438	-0.058
5	1.87E-1	5.000	(*)5.054	5.583	4.638	0.318
6	2.61E-1	5.000	5.031	5.491	4.769	0.669
7	3.48E-1	4.000	4.020	5.259	4.826	0.994
8	4.46E-1	4.000	4.013	4.644	4.803	1.293
9	5.56E-1	3.000	3.010	4.298	4.693	1.565
10	6.78E-1	3.000	3.007	(*)3.205	4.470	1.810
11	8.12E-1	2.000	2.005	3.147	4.045	2.028
12	9.59E-1	2.000	2.004	2.111	3.575	2.217
13	1.119	2.000	2.003	2.086	(*)2.436	2.376
14	1.291	1.000	1.003	1.068	2.315	2.504
15	1.475	1.000	1.002	1.055	1.245	2.600
16	1.672	-----	0.002	1.046	1.196	2.663
17	1.882	-----	0.002	0.038	0.161	2.690
18	2.106	-----	0.001	0.032	0.134	2.677
19	2.345	-----	0.001	0.027	0.113	2.623
20	2.602	-----	0.001	0.023	0.097	2.524
21	2.886	-----	0.001	0.020	0.083	2.318

(*)First discontinuity in the Phase Shift; $k < (2\mu V_{eff}(max))^{1/2}$.

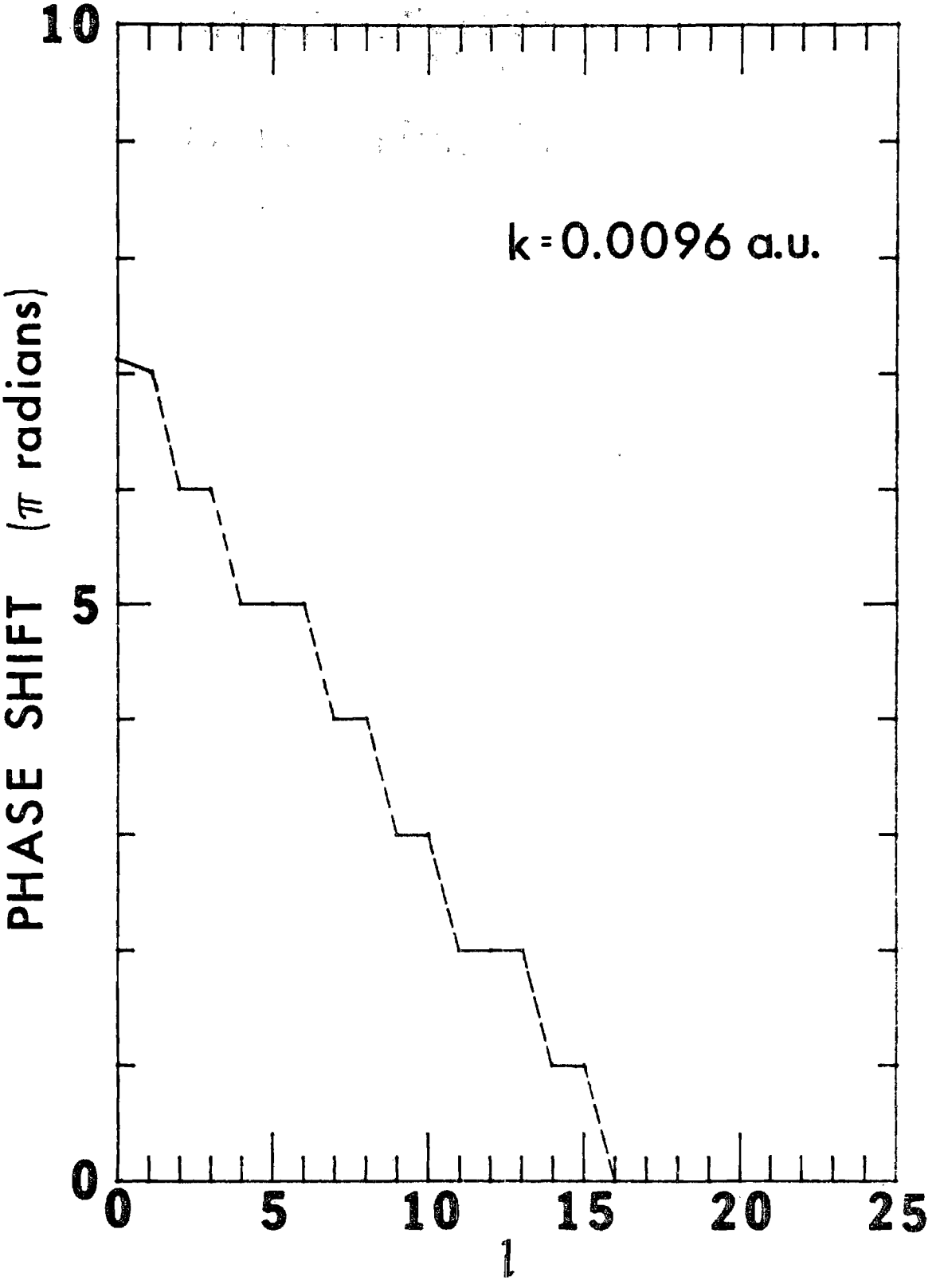

Figure 3. Li^+ - He Phase Shifts (k = 0.00962 a.u.).

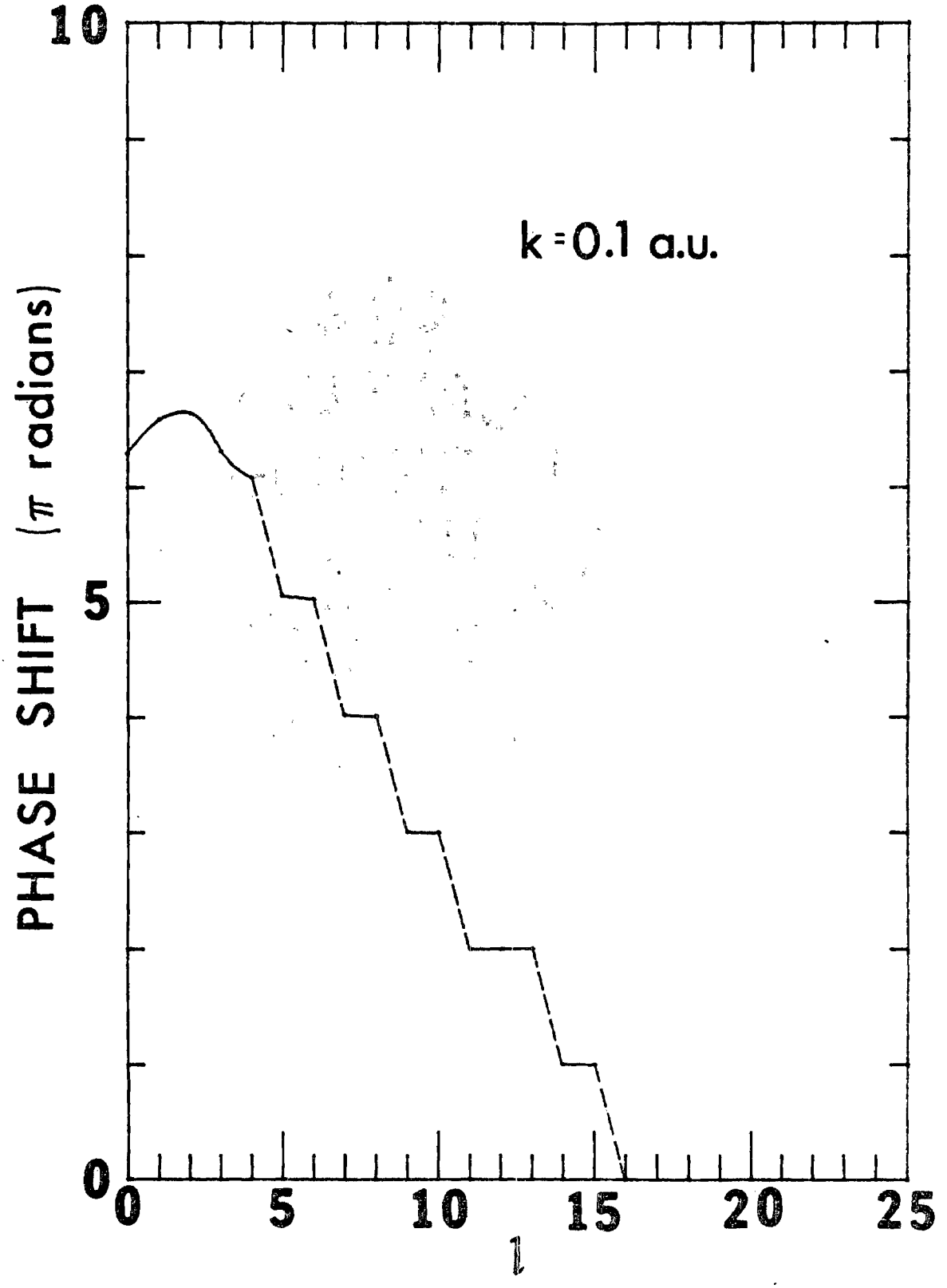

Figure 4. Li^+ - He Phase Shifts (k = 0.1 a.u.).

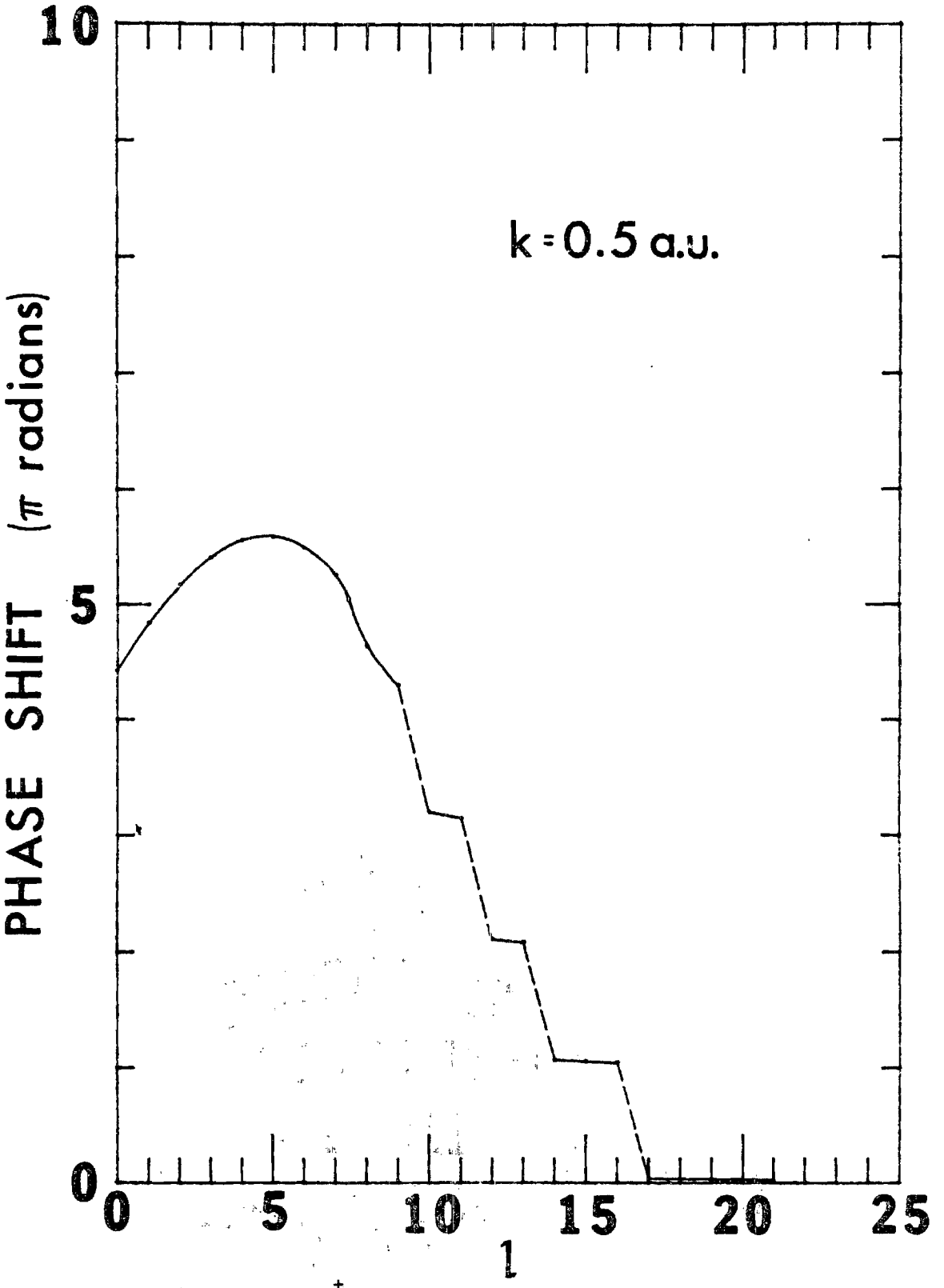

Figure 5. Li^+ - He Phase Shifts (k = 0.5 a.u.).

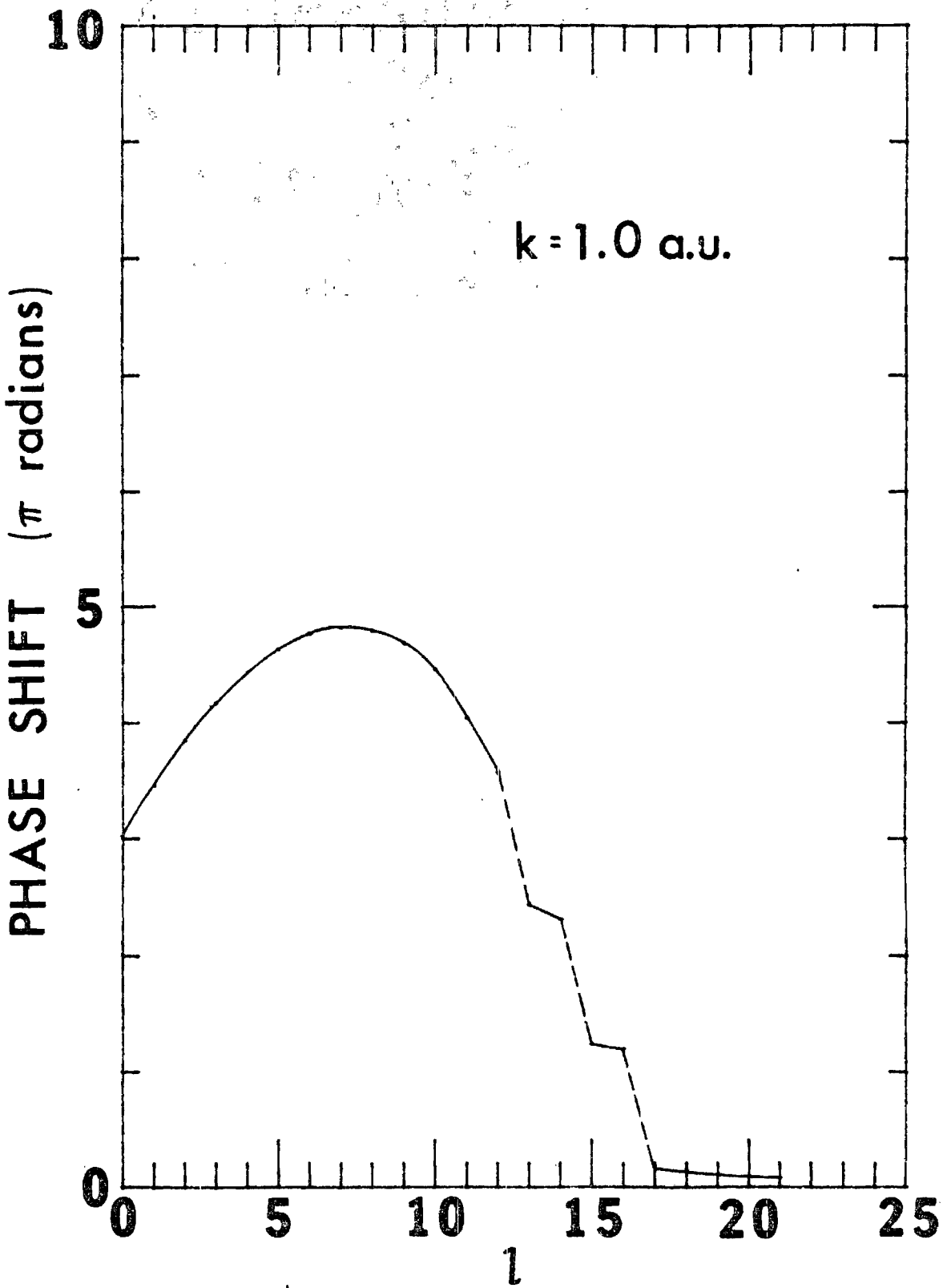

Figure 6. Li^+ - He Phase Shifts (k = 1.0 a.u.).

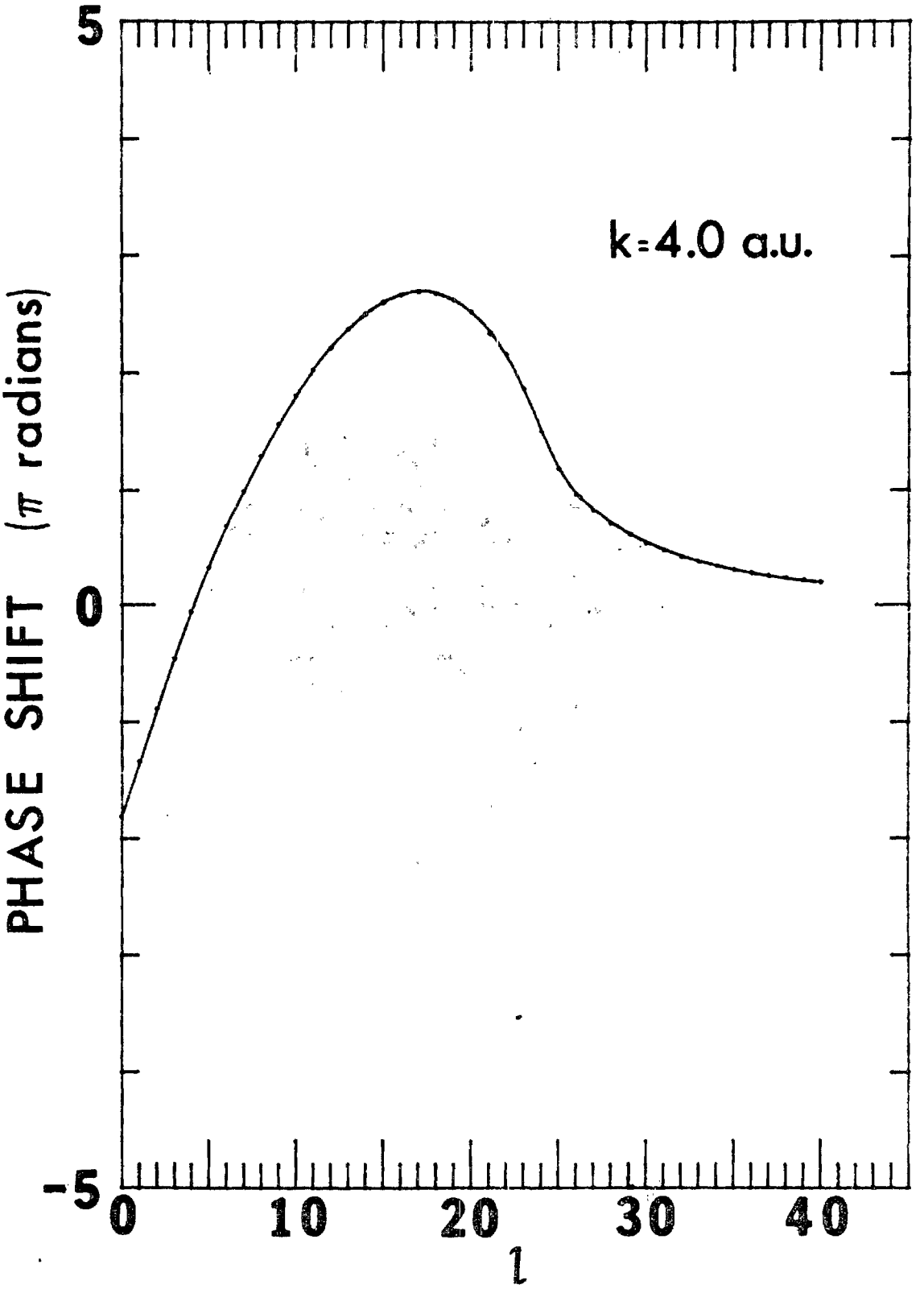

Figure 7. Li^+ - He Phase Shifts (k = 4.0 a.u.).

to the existence of virtual states in the effective potential[42]. The effect of increasing the angular momentum by one unit is to produce a narrower and shallower well in the effective potential which, in turn, may reduce the number of nodes in the wave function, in the well region, by one, thus introducing a discontinuity of π in the phase shift. From Table VI, we see that no discontinuities of π occur in the phase shift until the relative energy lies below a maximum in the effective potential, making resonant tunneling to a virtual state possible. Indeed, if the relative energy is higher than the maximum in the effective potential for all ℓ as for k = 4.0 a.u. (no maxima occur for $\ell > 21$), there are no discontinuities of π in the phase shift.

As an illustration of the general characteristics of ion-neutral phase shifts, the data in Table VI is displayed in Figures 3-7.

Cross Sections

The general behavior of quantum mechanical cross sections and their relationship to the corresponding classical ones has been discussed in great detail in the literature for a Lennard-Jones interaction[36-38]. These studies were conducted as a function of the reduced de Broglie wavelength of the system

$$\Lambda^* = \frac{h}{\sigma \sqrt{2\mu\varepsilon}} \qquad \text{(II-14)}$$

(where h is Planck's constant, μ the reduced mass, and σ and ε the hard-core radius and well depth of the Lennard-Jones potential), the result being to effectively vary the degree to which the system could be

considered "quantal", e.g., $\Lambda^* = 0$ corresponds to a purely classical system while $\Lambda^* = 2.67$ is the reduced de Broglie wavelength of the strongly quantal helium system. Our results are in good qualitative agreement with these studies.

As a first step we shall consider the general behavior of classical and quantal cross sections, using our results for the Li^+ - He interaction of Catlow et al.[9] and the H^+ - He interaction of Weise et al.[22] as examples. We will then discuss our results for the H^+ - rare gas systems and attempt to point out the effects of differences in interactions for a given system on the diffusion cross section. The set of cross sections which we shall use in our discussion are shown in Figures 8 and 9, where they are referenced to low energy asymptotic cross sections (dashed lines), calculated using the assumption that for low energies, only the long range polarization tail will significantly affect the scattered particle. The Schiff-Laudau-Lifshitz approximation,

$$Q_{SLL}^{(E)} = 11.373 \left[\frac{\alpha\mu}{2k}\right]^{2/3} \qquad \text{(II-15)}$$

is the result of this assumption for the elastic cross section, while we have chosen the classical result,

$$Q_{Cl}^{(D)} = \frac{2.21}{k}\sqrt{\alpha\mu} \qquad \text{(II-16)}$$

for the diffusion cross sections while noting that other approximation[1, 32] lead to slightly different results.

Classical Cross Sections

The divergence of the classical elastic cross section as a result of a finite scattering angle for large impact parameter does not carry over into the classical transport cross sections due to the suppression of small angle contributions by the characteristic $(1 - \cos^{\ell}\Theta)$ factor. We have found, in fact, that the classical transport cross sections, while unable to reproduce all the details of the correct quantum mechanical cross sections, can yield useful and surprisingly accurate results, particularly in the case of small Λ^* as predicted by Munn et al.[36]

At low energies, orbiting, arising from the attractive potential well and long range polarization tail, is the dominant feature of the classical transport cross section for ion-neutral systems[1]. In Figures 8 and 9, the classical diffusion cross section is plotted along with the results obtained from equation (II-16) for the Li^+ - He and H^+ - He systems, respectively. These results are indistinguishable for very small relative energies, showing the validity of the approximation leading to (II-16). As the relative momentum of the particles is increased, the influence of the potential well is observed as a deviation of the classical diffusion cross section above or below the low energy asymptote depending on whether the true interaction is stronger than the polarization interaction, as in the case of H^+ - He, or weaker, as in the Li^+ - He case, in the region of transition from the potential well to the long range tail.

Shifting our attention to higher relative momenta, the orbiting limit, $k = 2.886$ a.u. and $k = 6.451$ a.u. for the Li^+ - He and H^+ - He,

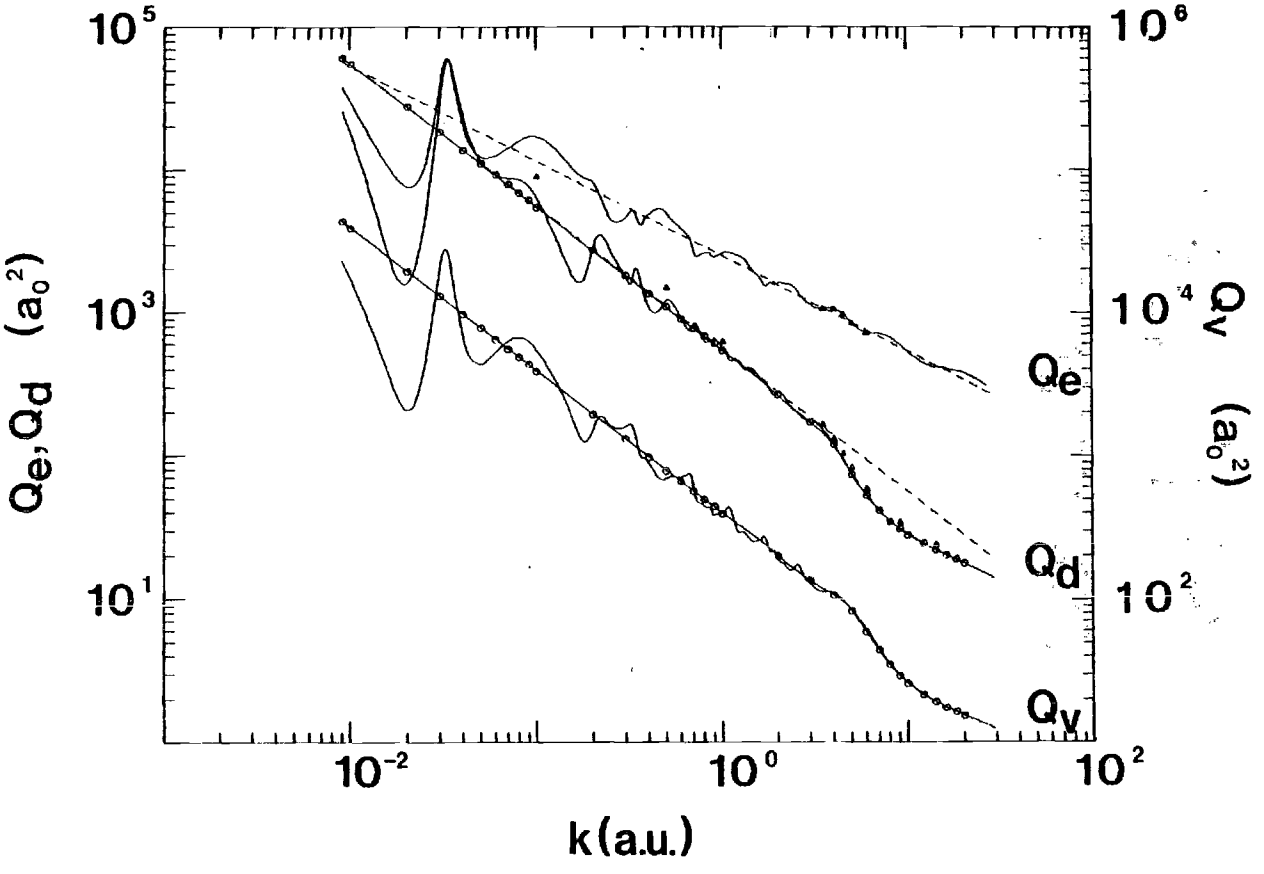

Figure 8. Li^+ - He Cross Sections; quantal (——), classical (-o-o-), asymptotic (----), and calculated values of Catlow et al.[9] (▲).

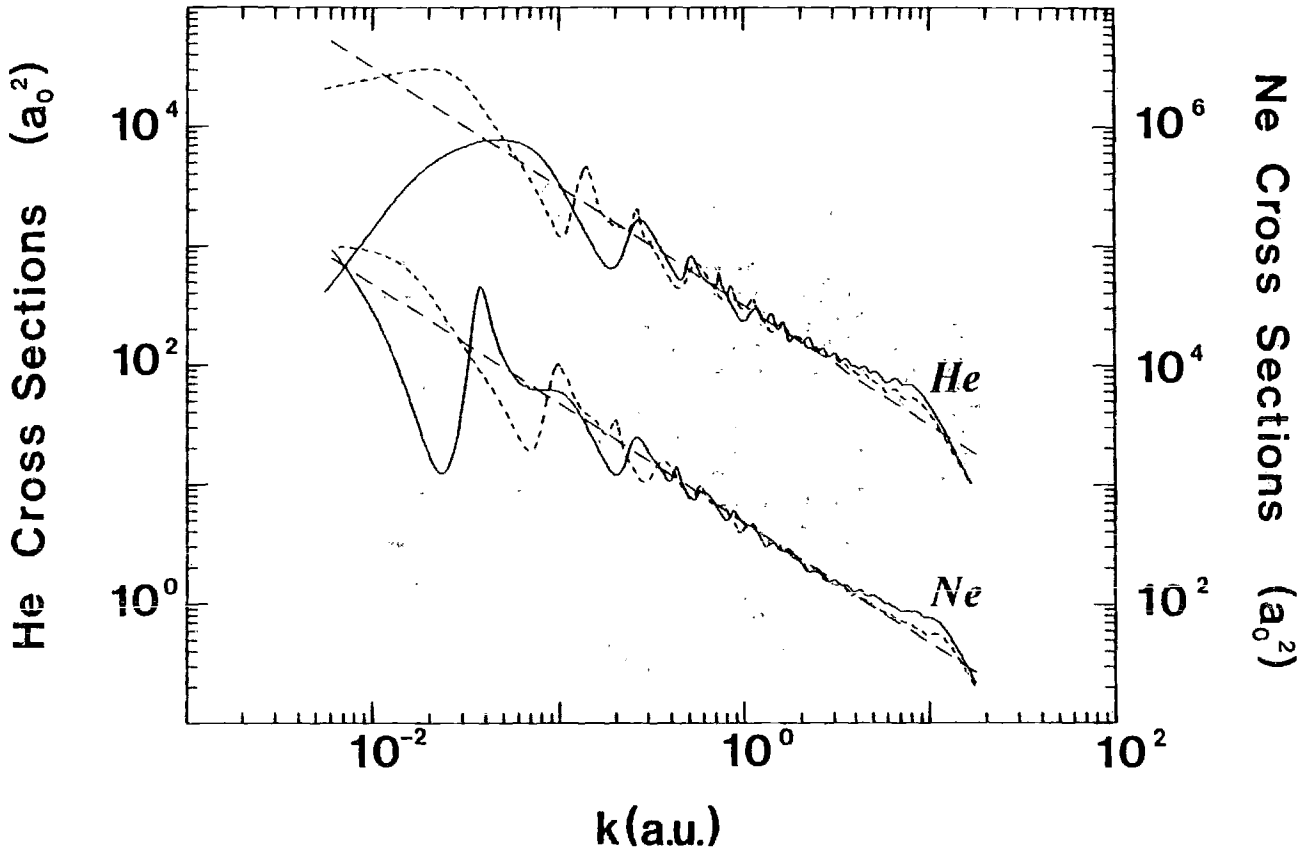

Figure 9. H^+ - He Cross Sections (Weise interaction); quantal (——), classical (-o-o-), and asymptotic (----).

respectively, is reached. This limit marks the transition from a discontinuity in the scattering angle as a function of impact parameter, orbiting, to a minimum in the scattering angle, the rainbow angle. Rainbow scattering results in an infinite differential cross section which "can have a large or small effect on the transport cross sections depending on the angle at which it occurs, because of the weighting factors $(1 - \cos^{\ell}\Theta)$."[36] The rainbow angle is always negative, having its largest negative value just above the orbiting limit and decreasing rapidly in magnitude toward zero with increasing relative energy. "The net result is an undulatory behavior in the transport cross sections until the energy is high enough that the rainbow becomes less than π and continues to decrease as E is increased, whereby the $(1 - \cos^{\ell}\Theta)$ factors quickly damp out the undulation."[36] This general behavior is observed in Figure 8 as a gentle undulation in the diffusion and viscosity cross sections above the Li^+ - He orbiting limit, k = 2.886 a.u., and dramatically in Figure 9 as sharp undulations in the transport cross sections just above the orbiting limit, k = 6.451 a.u., followed by a rapid decrease in the cross sections as the high energy, small scattering angle, regime is reached.

Quantal Cross Sections (Li^+ - He and H^+ - He)

Unlike the classical case, both the quantal elastic and transport cross sections are finite for all physical interactions with the exception of the coulomb potential, for which classical and quantum mechanics yield the same divergent elastic cross section. The finiteness of the quantal elastic cross section can be explained by noting that, for large impact parameters, the deviation of the trajectory of the

scattered particle from a straight line will be smaller than the uncertainty in its original direction of motion. Under these circumstances, it is impossible to detect the occurrence of a scattering event, i.e., the contribution to the total cross section from large impact parameters will be zero, alleviating the problems encountered in classical scattering theory.

The characteristic low energy oscillations of the quantal cross sections about the classical in Figures 8 and 9 are a result of the discrete nature of the quantal angular momentum. At very low energies, these oscillations can be very rapid and quite large due to the small number of terms involved in the phase shift sum and the 1/E dependence of the cross section. As energy is increased, these oscillations will decrease in magnitude and frequency until, as larger and larger numbers of terms contribute to the phase shift sum, the quantal and classical transport cross sections will become indistinguishable, as shown by Mott and Massey[42]. Munn et al.[37] have noted that the agreement, "in the mean", at low energy between classical and quantal transport cross sections is dependent on the reduced de Broglie wavelength of the system. Both the Li^+ - He and H^+ - He systems have small de Broglie wavelengths, $\Lambda^* \gtrsim .44$, and show very good agreement between classical and quantal results as compared with the results of Munn et al.[36] and Imam-Rahajoe et al.[38] for Lennard-Jones potentials and larger Λ^*.

As in classical scattering, orbiting plays an important role in the behavior of the low energy cross section, however, quantal orbiting is modified by the discrete nature of the angular momentum, as mentioned previously, and by barrier penetration. This latter phenomena

removes discontinuities associated with the maximum in the effective potential found in semi-classical treatments, and affects the size, shape, and location of the oribiting oscillations.[37] Barrier penetration can also result in the absence of a peak which would be expected from a semi-classical analysis.[37]

Superimposed on this structure are oscillations arising from the quantal analogue of glory scattering. The classical deflection function can be related to semiclassical phase shift by the relation,

$$\chi(b) = \frac{2}{k}\frac{d\delta}{db} = 2\frac{d\delta}{d\ell}$$

where b is the impact parameter, k the wave number, and ℓ the angular momentum. Thus, a slope of 0 or $\pm\frac{\pi}{2}$ in the semi-classical phase shift versus ℓ would correspond to a scattering angle of zero or π, a forward or backward glory. Treating the quantal phase shift versus angular momentum as a continuous quantity, despite its true discrete nature, analogous behavior is observed. The effect of glory scattering on the elastic cross section is dependent on the value of the phase shift in the vicinity of the glory.

In the case of a forward glory, since the phase shift varies slowly with ℓ, several terms in the phase shift sum may make approximately the same contribution. As the phase shift in the vicinity of the glory changes through odd and even multiples of $\frac{\pi}{2}$ with increasing energy, these contributions can become either very large or quite small. The result is an undulation of the elastic cross section versus energy. The effect of a forward glory on the transport cross sections will be quite

small since the transport cross sections depend only on phase shift differences.

As the relative energy is increased above the orbiting limit, the repulsive branch of the interaction becomes more important, and the phase shift becomes negative for small angular momentum. The attractive nature of the effective potential for low ℓ is reflected, however, in a positive maximum in the phase shift versus ℓ. This maximum (forward glory) decreases in value but broadens as energy increases. As before, the elastic cross section undulates as the broad maximum passes through odd and even multiples of $\frac{\pi}{2}$. The transport cross sections also exhibit gentle undulations in this region, however, these rapidly die out as the phase shift differences decrease.

Rare Gas Diffusion Cross Sections

A detailed comparison of the proton-rare gas diffusion cross sections, shown in Figures 10 and 11, for each pair of interactions is difficult, at least, due to their complex structure. Similarities are observed in the low energy oscillations, but no one to one correspondence can be made. In fact, the long range interactions, which dominate the low energy-small angular momentum (ℓ = 1 or 2) scattering, are identical for each pair of interactions leading to identical maxima in their effective potentials. The differences in the cross sections must then arise from detailed variations of the interactions in the vicinity of the potential well. These variations in the well region are observed most dramatically, however, for energies near the orbiting limit, (k = 1 - 20 a.u.). From Figure 12 we see that the interactions of Weise et al.[22] for H^+ - He and H^+ - Ne systems are more attractive than

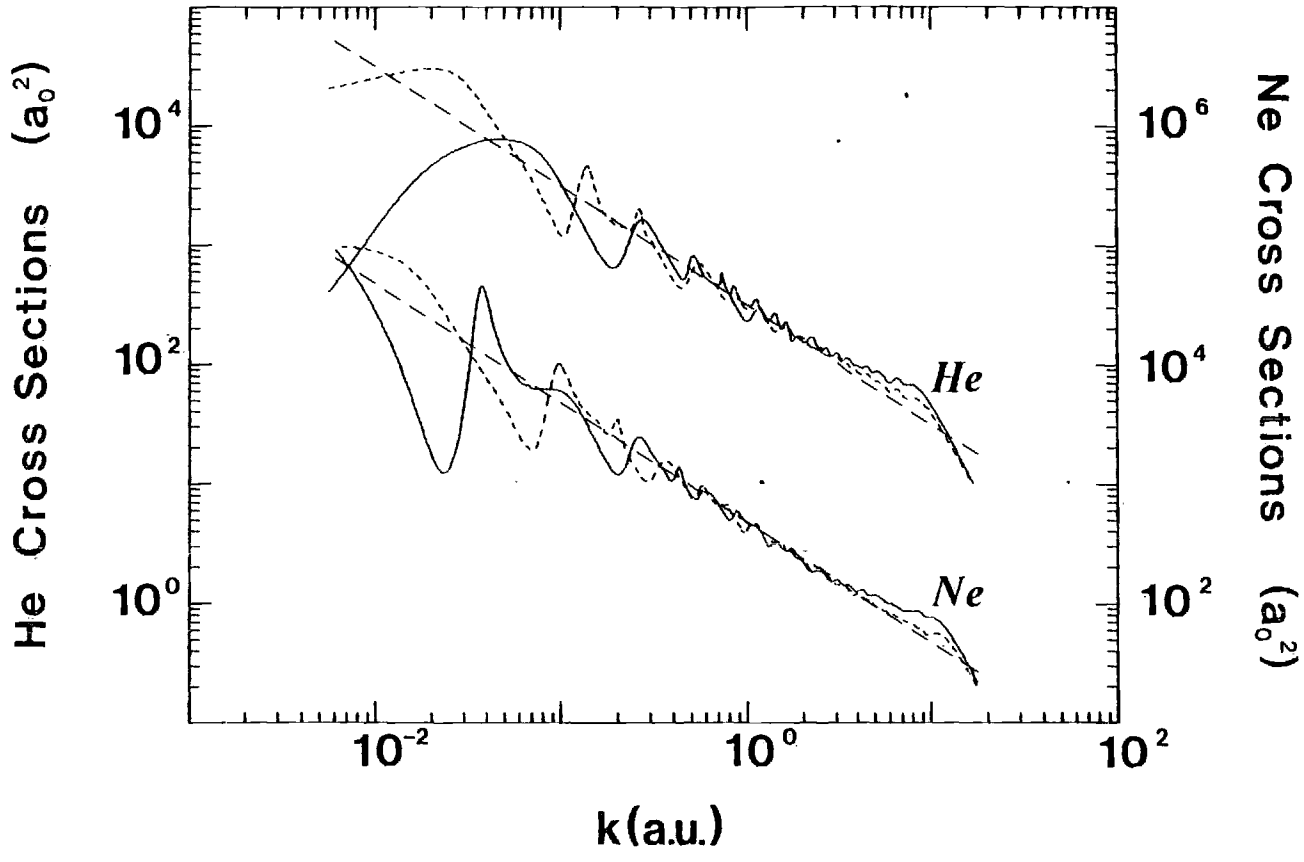

Figure 10. H^+ - (He, Ne) Quantal Diffusion Cross Sections; Weise interactions (——), Peyerimhoff interactions (----), and asymptotic (— — —).

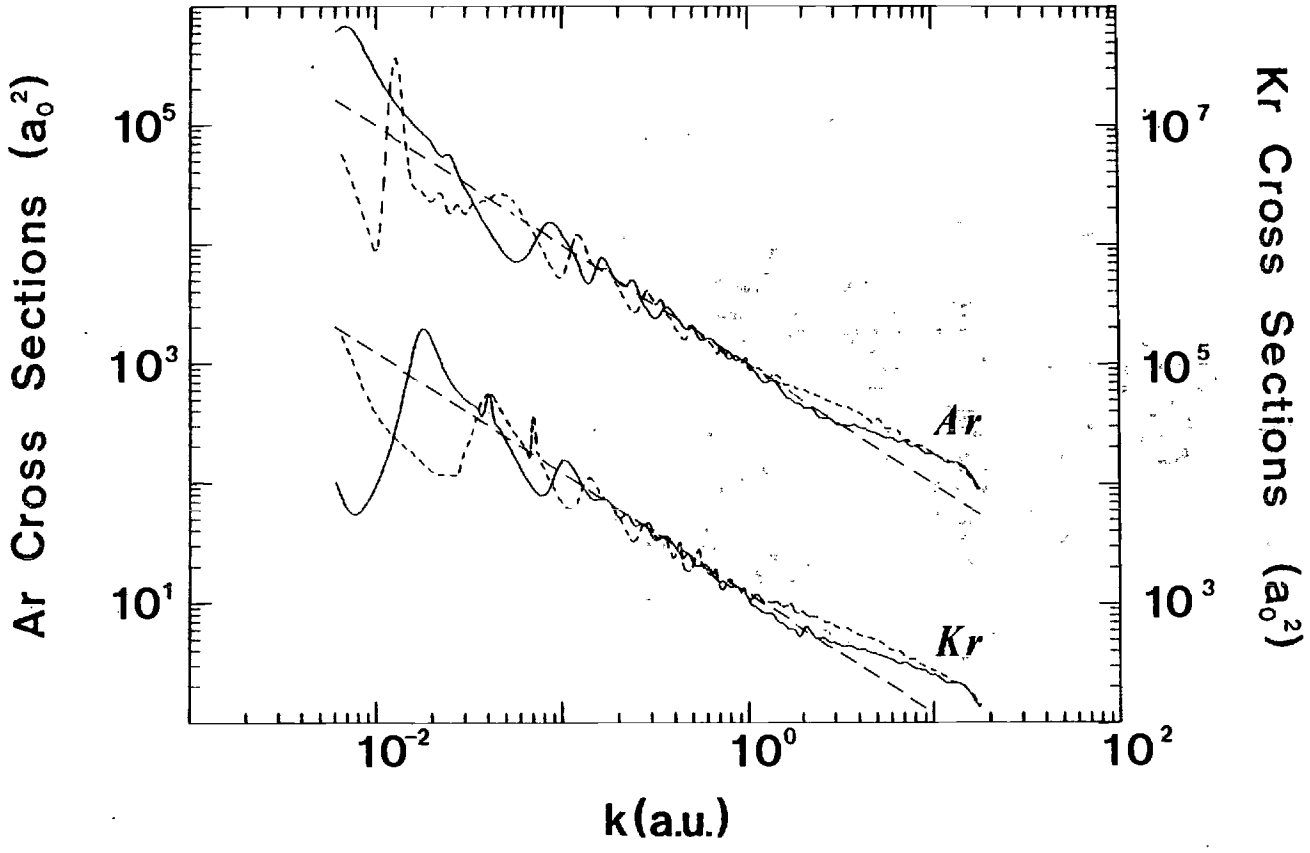

Figure 11. H^+ - (Ar, Kr) Quantal Diffusion Cross Sections; Weise interactions (——), Klingbeil and Rich et al. interactions (----), asymptotic (— — —).

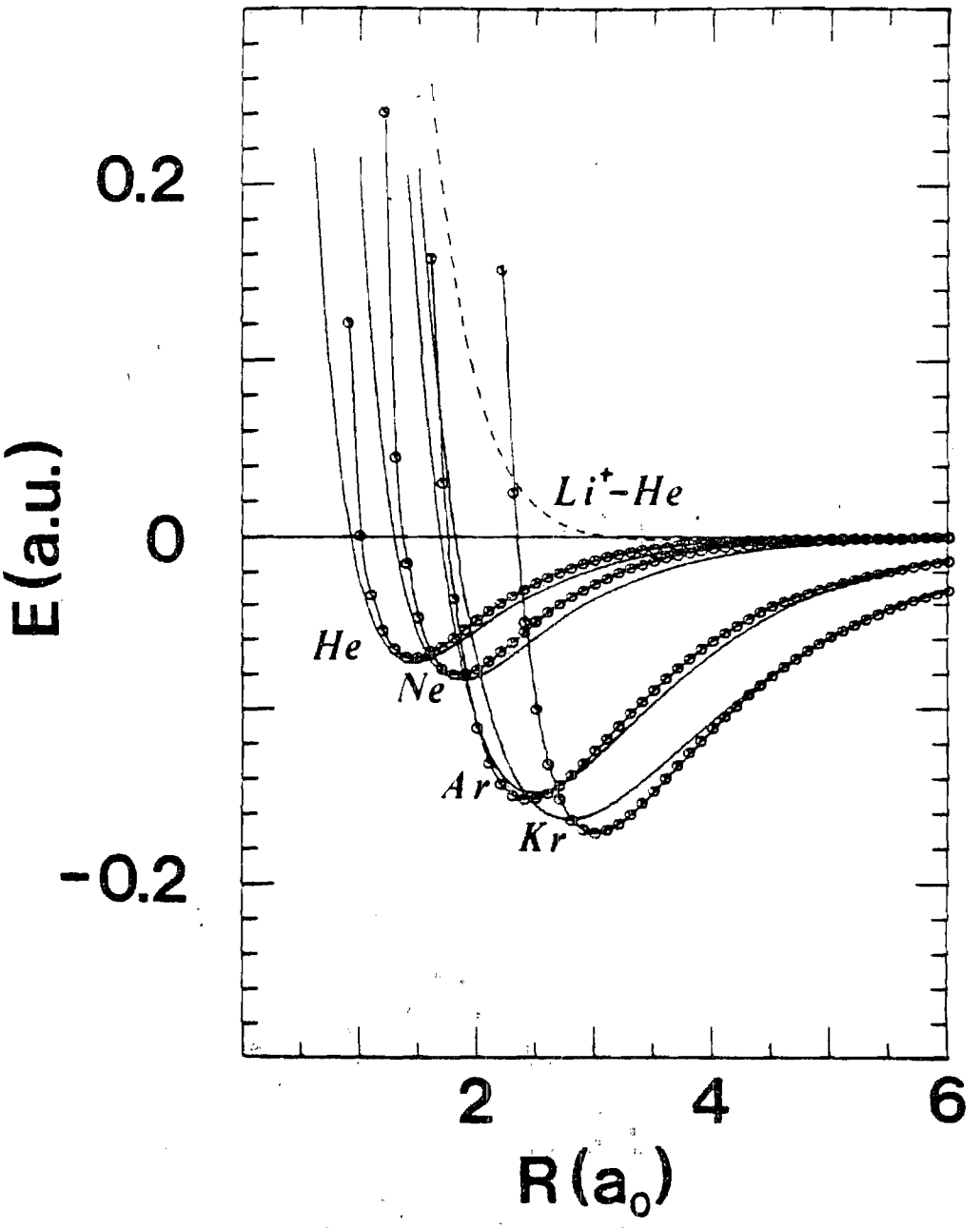

Figure 12. H^+ - Rare Gas and Li^+ - He interactions; Weise interactions[22,23] (——), Peyerimhoff[21], Klingbeil[24], and Rich et al.[25] interactions (—o o—), and Catlow et al.[9] interaction (----).

those of Peyerimhoff[21] in the well region, leading to a higher cross section (as expected) in the range k = 3 - 20 a.u. in Figure 5. Similar observations can be made in the cases of the H^+ - Ar and H^+ - Kr systems for although the Weise el al.[22] interactions are slightly deeper than their counterparts, they are narrower over the well region and thus exert their influence over a smaller range of r. The results are cross sections which lie below those obtained for the Klingbeil and Rich et al. interactions in the energy region dominated by the potential well.

In all cases, the cross sections tend to converge at high energy despite large differences in repulsive cores. This is reconciled by recalling that large numbers of terms will contribute to the phase shift sum at high energy and noting that the centrifugal barrier will rapidly mask any variations in interactions.

Mobilities

Carrying out the procedures outlined in Chapter I, we have calculated the quantal and classical collision integrals and mobilities for the eight proton-rare gas interactions of Weise et al.[22, 23] (H^+ - He, Ne, Ar, Kr), Peyerimhoff[21] (H^+ - He, Ne), Klingbeil[24] (H^+ - Ar), and Rich et al.[25] (H^+ - Kr), and for the Li^+ - He "Catlow potential".[9] In addition, the nine interactions of Gordon and Waldman[27], (Li^+, Na^+, K^+ - He, Ne, Ar) were used in a classical calculation, quantal results being obtained for the K^+ - He and K^+ - Ne systems only. In view of the good agreement between the quantal and classical results for the three alkalai ion-neutral systems considered (Li^+ - He, K^+ - He, K^+ - Ne), full quantal calculations for the remaining systems were deemed unnecessary.[43, 44]

H^+ - Rare Gas

The averaging procedure which produces the collision integral (equation (I-2)) effectively "samples" the collision cross section through the weighting function, $(\frac{E}{kT})^2 e^{-E/kT}$ which has its maximum value at E = 2kT. For low temperatures the weighting function will be very narrow and confined to low energies, while as the temperature is increased the maximum will shift to higher energies and the distribution will broaden. Thus, the large low energies oscillations in the diffusion cross section may propagate into the collision integral, and hence the mobility, when the width of weighting function is comparable to the wavelength of the oscillation. At higher temperatures, the broadened weighting function will "sample" several such oscillations, which will tend to cancel one another, and produce a smooth average. This averaging procedure is simply a reflection of the transition to the region where the classical approximation is valid, and importance of the individual oscillations in the cross section becomes secondary to their average value.

This transition is readily apparent in the quantal mobilities for the H^+ - He and H^+ - Ne systems, Figure 13 and Table VII. The quantal mobilities oscillate about the classical at low temperatures, but the oscillations quickly die out as the temperature is increased. The maximum at T = 8°K in the H^+ - He mobility calculated from the Peyerimhoff interaction (dashed line) can be related to a minimum in the diffusion cross section at $k \lesssim 0.4$ a.u. while the maximum in its counterpart, from the Weise et al. potential, at T = 40°K (solid line) can be related to a minimum in the corresponding cross section at

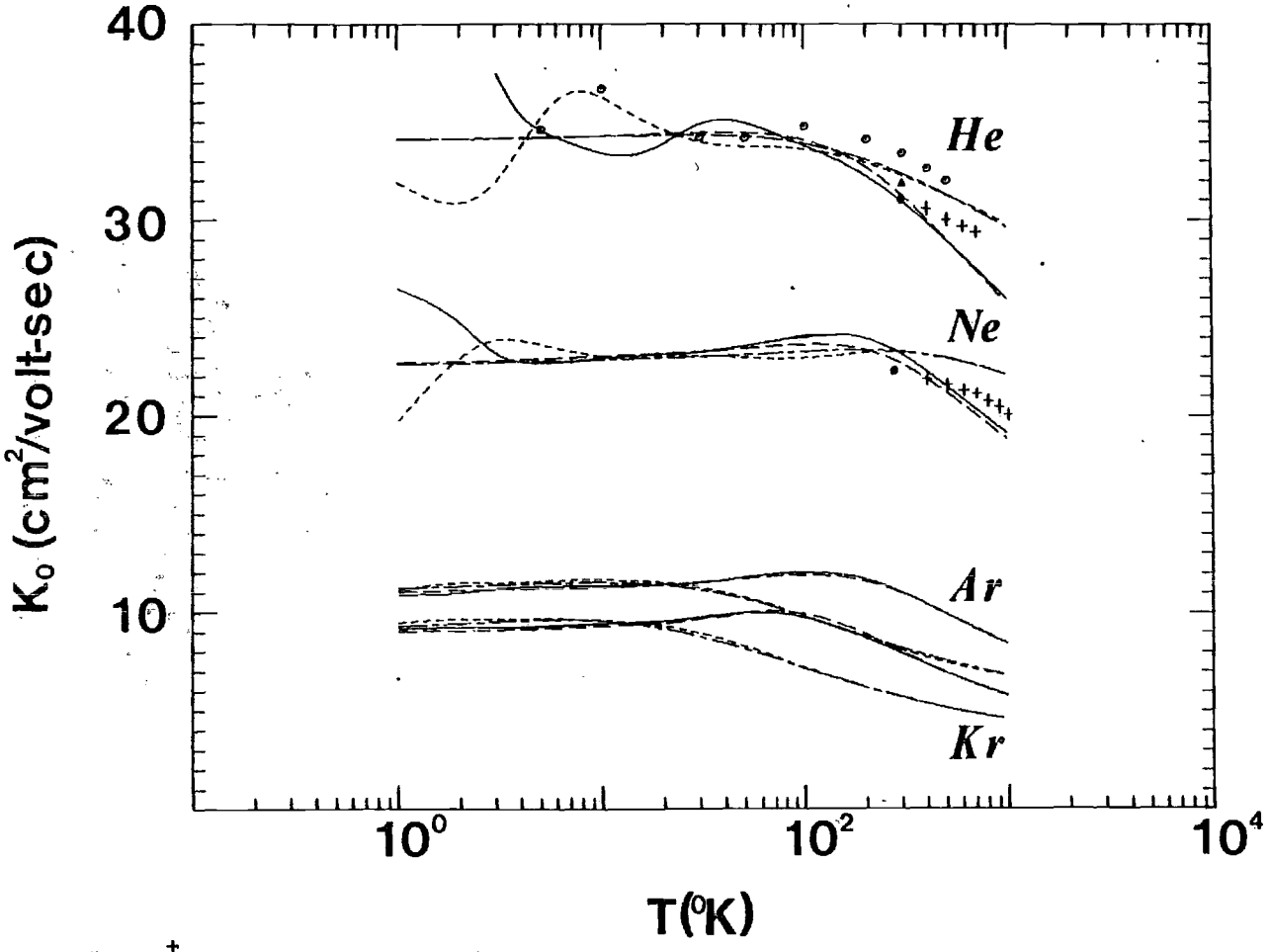

Figure 13. H^+ - Rare Gas Zero Field Reduced Mobilities. Weise interactions; quantal (——) and classical (— — —). Peyerimhoff, Klingbeil, and Rich et al. interactions; quantal (----) and classical (— - —). Points; calculated (Dickinson[10], ⊙), derived (Ellis et al.[48], +), and experimental (McFarland et al.[45], ♦ ; Orient[46], ▲; Orient[47], ●).

Table VII. H^+ - He Mobilities

	Mobility (cm^2/volt - sec)					
	Classical		Quantal		Experiment	
T	Peyerimhoff	Weise et al.	Peyerimhoff	Weise et al.	Derived (48)	Measured
1	34.13	34.09	31.91	48.46		
5	34.22	34.18	35.18	34.55		
10	34.26	34.27	36.25	33.38		
25	34.32	34.42	34.20	34.49		
50	34.25	34.45	33.73	34.93		
100	33.88	34.06	33.57	33.76		
150	33.46	33.42	33.27	32.93		
200	33.07	32.69	32.91	32.19		
250	32.70	31.95	32.57	31.51		31.0 (297°K)
300	32.37	31.25	32.24	30.88		31.8
350	32.06	30.60	31.95	30.31	30.9	
400	31.78	30.01	31.69	29.78	30.6	
500	31.28	28.97	31.25	28.87	30.0	
600	30.85	28.10	30.88	28.09	29.7	
700	30.46	27.39	30.55	27.43		
1000	29.56	25.72	29.77	25.85		

$k \gtrsim 0.9$ a.u. Also displayed in this diagram are several points taken from a calculation by Dickinson[10], using an interaction also based on the work of Peyerimhoff, and various experimental values[45-48]. The present work agrees quite well with the low temperature values of Dickinson, but shows a marked disagreement above 100°K, in particular, we do not find the peak at 110°K pointed out by Dickinson. This was a point of much concern, but after a close scrutiny of the cross section in the region around k = 1.5 a.u. and a comparison of the oscillation in question to the weighting function, $(\frac{E}{kT})^2 e^{-E/kT}$, centered at T = 110°K, we have concluded that; 1) the wavelength of the oscillations in the cross section near k = 1.5 a.u. is small compared to the extent of the weighting function, and 2) the size of the neighboring maxima is sufficient to cancel the minima at k = 1.5 a.u. Although our interaction and that of Dickinson are both based on the work of Peyerimhoff, they are not identical, possibly explaining the observed discrepancy in mobilities. We do note, however, that while neither the Weise et al. nor Peyerimhoff interaction yields a mobility in close agreement with experiment, our curves do lie closer to the measured values than that of Dickinson.

As we move on to the H^+ - Ne, H^+ - Ar, and H^+ - Kr systems (Figures 10 and 11, and Tables VIII-X), we find progressively higher reduced masses, smaller reduced de Broglie wavelength, and better agreement at lower temperature between the quantal and classical mobilities. The result of the increased reduced mass is to broaden the weighting function and make the averaging procedure more effective at lower temperatures, thus tending to accelerate the convergence of the

Table VIII. H^+ - Ne Mobilities

T	Mobility (cm^2/volt - sec) Classical Peyerimhoff	Classical Weise et al.	Quantal Peyerimhoff	Quantal Weise et al.	Experiment Derived (48)	Experiment Measured
1	22.64	22.72	19.74	26.48		
5	22.76	22.90	23.60	22.65		
10	22.84	23.03	22.99	22.92		
25	22.97	23.23	23.05	23.17		
50	23.11	23.44	22.94	23.57		
100	23.27	23.64	22.93	24.06		
150	23.34	23.57	23.11	24.14		
200	23.35	23.33	23.22	23.93		
250	23.32	23.00	23.25	23.56		
300	23.27	22.63	23.22	23.13		22.3 (273°K)
350	23.20	22.25	23.16	22.69	22.1	
400	23.12	21.88	23.08	22.26	21.9	
500	22.94	21.17	22.90	21.50	21.6	
600	22.75	20.55	22.72	20.86	21.3	
800	22.38	19.54	22.36	19.84	20.8	
1000	22.03	18.75	22.04	19.07	20.1	

Table IX. H^+ - Ar Mobilities

	Mobility (cm^2/volt - sec)			
	Classical		Quantal	
T	Klingbeil	Weise, et al.	Klingbeil	Weise, et al.
1	11.25	11.06	11.14	10.89
5	11.48	11.20	11.59	11.27
10	11.52	11.26	11.66	11.32
25	11.24	11.45	11.36	11.44
50	10.64	11.72	10.72	11.77
100	9.74	11.90	9.75	12.03
150	9.16	11.78	9.11	11.92
200	8.74	11.54	8.66	11.65
250	8.42	11.25	8.32	11.32
300	8.17	10.95	8.06	10.98
350	7.96	10.66	7.86	10.67
400	7.79	10.38	7.68	10.37
500	7.52	9.90	7.42	9.87
750	7.07	8.99	7.00	8.96
1000	6.80	8.39	6.76	8.37

Table X. H^+ - Kr Mobilities

T	Mobility (cm^2/volt - sec) Classical Rich et al.	Classical Weise et al.	Quantal Rich et al.	Quantal Weise et al.
1	9.30	9.00	9.50	9.14
5	9.61	9.16	9.66	9.23
10	9.54	9.27	9.50	9.37
25	8.93	9.54	8.09	9.60
50	8.10	9.96	7.12	9.95
100	7.12	9.90	6.68	9.70
150	6.55	9.38	6.35	9.14
200	6.17	8.84	6.07	8.64
250	5.89	8.37	5.83	8.21
300	5.67	7.97	5.64	7.86
350	5.50	7.64	5.47	7.56
400	5.36	7.35	5.34	7.30
500	5.13	6.90	5.12	6.89
750	4.77	6.17	4.77	6.21
1000	4.56	5.73	4.57	5.78

classical and quantal approximations, as anticipated from the decreasing reduced de Broglie wavelength. Significant quantal deviations are present in the H^+ - Ne mobilities up to T = 10°K, but only small deviations (1-2%) are observed in the H^+ - Ar and H^+ - Kr mobilities down to T = 1°K.

As a final note, we point out the sensitivity of the mobility to differences in the pairs of interactions. This sensitivity is the basis of the direct determination method of Viehland and Mason[43] for inverting experimental mobility data to obtain ion neutral interactions.

Li^+ - He Mobility

The Catlow[9] potential has been the subject of an extensive study[33, 44] with the goal of using experimental mobilities as a means of testing theoretical ion-neutral interactions, (see Appendix A)*. This study was made possible by the work of Viehland and Mason[49] which linked the mobility as a function of the gas temperature to the mobility as a function of E/N, electric field divided by number density, the basic experimental variable.

The Li^+ - He system is well adpated to this type of study due to the exceptional agreement found between the classically and quantally calculated mobilities, less than 1% down to 3°K, see Figure 14 and Table XI. Referring to the Li^+ - He diffusion cross section (Figure 8) we find that above $k \gtrsim .5$ a.u. ($T \gtrsim 4.3$°K) oscillations are small, differing from the classical value by less than 1%. Coupling this behavior with the relatively large reduced mass of this system (2.54 a.u. as opposed to .805 a.u. for the H^+ - He system) which enhances the averaging

*Appendix A is a reprint of reference 33.

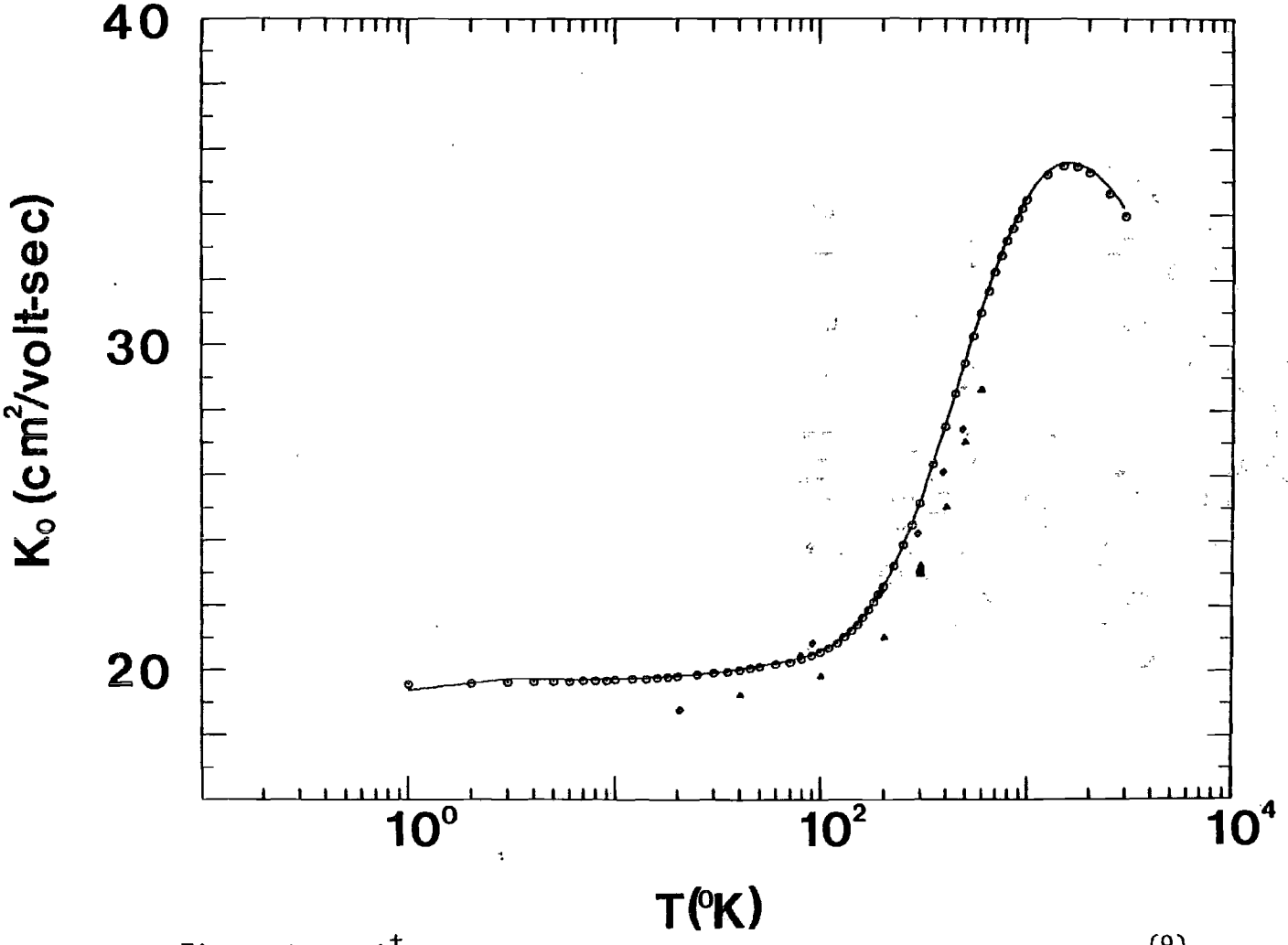

Figure 14. Li^+ - He Zero Field Reduced Mobilities; Catlow et al.[9] interactions quantal (——) and classical (o), tabulated values of Catlow et al.[9] (▲), experimental values of Akridge et al.[51] (■) and Hoselitz[52] (◇).

Table XI. Li^+ - He Mobilities.
(Catlow[9] Interaction)

T	Mobility (cm^2/volt - sec) Classical	Quantal	Experiment Derived[48]	Measured[50]
1	19.55	19.38		
5	19.64	19.71		
10	19.68	19.72		
25	19.84	19.85		
50	20.08	20.12		
100	20.55	20.60		
150	21.41	21.46		
200	22.57	22.64		
250	23.84	23.94		
300	25.13	25.23	22.9	23.1
350	26.34	26.47		
400	27.47	27.61	25.0	
500	29.43	29.59	26.4	
600	30.99	31.16	27.5	
800	33.18	33.33	29.1	
1000	34.44	34.57	30.2	
1500	35.47	35.58	31.9	
2000	35.26	35.36	32.5	
3000	33.93	34.11	32.6	
5000	31.43		32.0	
10000	27.93		30.1	
15000	26.19		28.4	
20000	25.16		26.9	
25000	24.50		24.6	

procedure, it is not difficult to see that to an excellent approximation the quantal effects can be ignored for this system. A similar result is found[44]* for the Li^+ - He potential of Hariharan and Staemmler.[31]

Since much effort was directed toward accurately reproducing the Catlow potential (Section II-1), we were quite disturbed at finding that our diffusion cross section lies below the values of Catlow et al.[9] at all energies, resulting in a mobility which is 5-7% higher than that of Catlow et al. at all temperatures. Assuming that their interaction was faithfully reproduced and that our calculations are accurate, comparison with the experimental data of Akridge et al.[50] would lead us to believe that the Catlow interaction is too "weak" in the region of the potential well and too repulsive in the region of the core (see Appendix A). The interaction of Gatland et al.[44], produced by inversion of mobility data, and the interaction of Hariharan and Staemmler tend to support the first conclusion while the latter is supported by the beam scattering data of Inouye and Kita[51], see Figure 15.

Alkali Ion-Rare Gas Mobilities

It was originally intended that both classical and quantal calculations should be made for the nine alkali ion-neutral combinations, (Li^+, Na^+, K^+ - He, Ne, AR), for which the interactions of Gordon and Waldman[27] are available, but these calculations were carried out only for the K^+ - He and K^+ - Ne systems. The small differences found between classical and quantal values for these systems (see Tables XII and XIII) and for the Li^+ - He "Catlow interaction", differences often

*A preprint of this reference is contained in Appendix B.

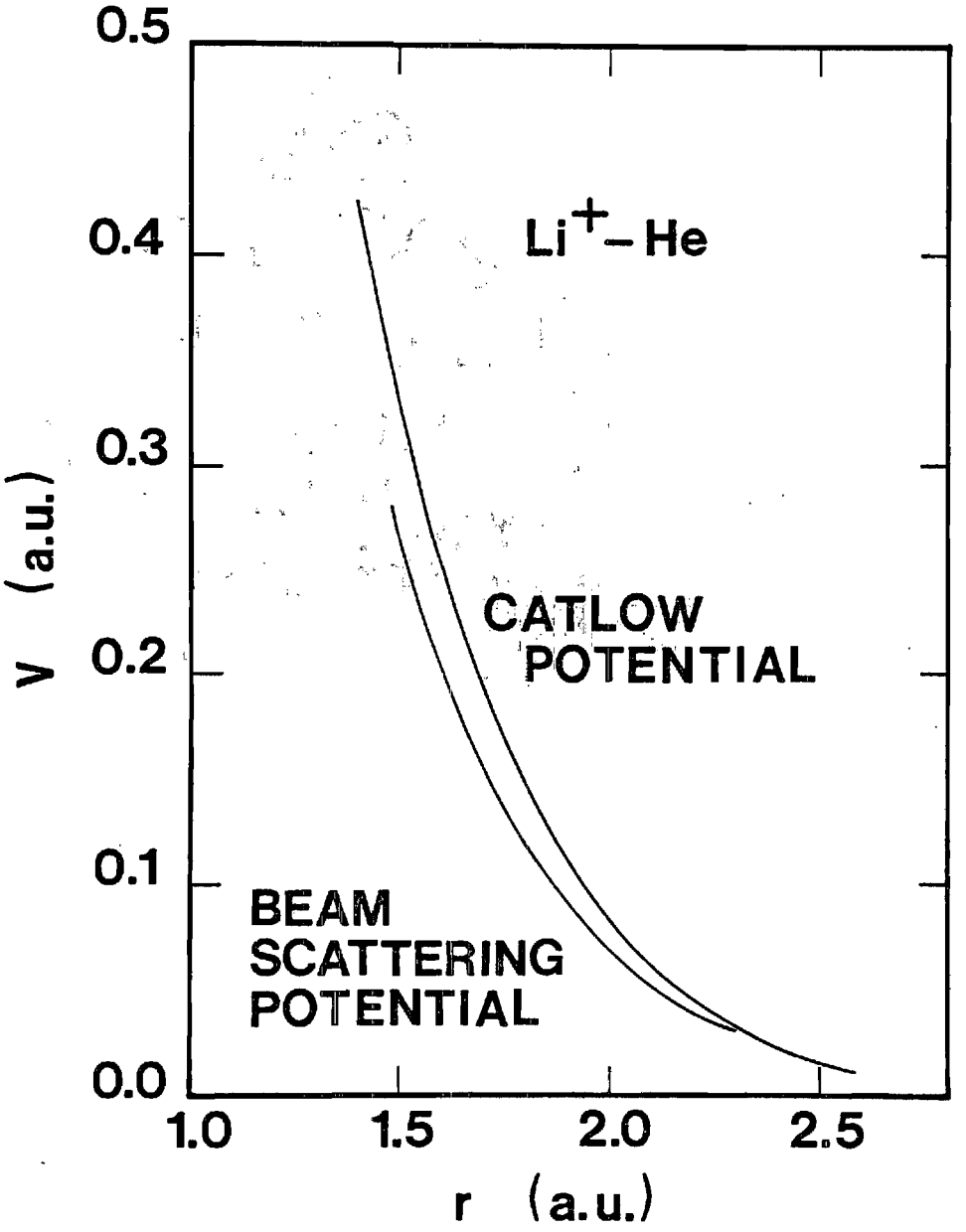

Figure 15. Comparison of the Short Range Interaction of Inouye and Kita[51] Derived from Beam Scattering Data to the Short Range Portion of the "Catlow" Potential[9].

Table XII. K^+ - He Mobilities

T	Mobility (cm^2/volt - sec) Classical	Quantal	Experiment Derived[48]
20	17.16	17.12	
50	17.39	17.22	
100	18.39	18.33	
150	19.44	19.51	
200	20.20	20.32	
250	20.65	20.81	
300	20.89	21.04	21.5
400	20.90	21.05	21.8
500	20.61	20.77	21.7
600	20.22	20.36	21.6
800	19.35	19.47	21.1
1000	18.54	18.65	20.5
1200	-----	-----	20.0
1500	16.92	17.02	19.3
2000	15.78	15.87	18.2
2500	14.92		17.3
3000	14.25		16.6
4000	13.28		15.3
5000	12.59		14.4
6000	12.08		13.7
8000	11.36		
10000	10.87		

Table XIII. K^+ - Ne Mobilities

T	Mobility (cm^2/volt - sec) Classical	Quantal	Experiment Derived[48]
20	6.43	6.43	
50	6.47	6.51	
100	6.56	6.61	
150	6.76	6.81	
200	6.99	7.04	
250	7.21	7.26	
300	7.41	7.44	7.43
400	7.65	7.69	7.62
500	7.77	7.81	7.75
600	7.80	7.86	7.82
800	7.72		7.84
1000	7.56		7.78
1200	----		7.69
1500	7.08		7.53
2000	6.65		7.25
2500	6.31		6.98
3000	6.02		6.72
4000	5.58		6.28
5000	5.26		5.94
6000	5.01		5.70
8000	4.64		5.40

on the order of the numerical accuracy of the calculation, led us to conclude that only the classical mobilities should be calculated for the remaining seven combinations. As these systems all have relatively large reduced mass and small reduced de Broglie wavelength (see Table XIV), the agreement found between classical and quantal calculation should not be unexpected.

Parametric studies of the correlation between the mobility as a function of temperature and the interaction from which the data was calculated[1, 43, 53]* have provided results useful in the study of ion-neutral interactions. From the discussion of these results by Gatland et al.[43] we draw the following conclusions;

1) "The low temperature mobility is dominated by the long-range attractive polarization interaction and the high temperature mobility by the short range repulsion."

2) At some intermediate energy, where the short range repulsive and long range attractive interactions serve to cancel each other, there will be a reduced cross section and thus a maximum in the mobility.

3) This maximum "is dominated by collisions in which the characteristic ion-neutral interaction distance corresponds roughly to the value $r \tilde{\sim} \sigma$, where $V(\sigma) = 0$, or to $r \tilde{\sim} r_m$, where r_m is the position of the potential minimum."

4) The height and breadth of the maximum in the mobility will generally vary inversely to the "hardness" of the repulsive core of the interaction, i.e., a "hard", short range interaction will result in a

*A reprint of reference 53 is contained in Appendix C.

Table XIV. Reduced de Broglie Wavelengths.

		σ (a.u.)	μ (a.u.)	ε (a.u.)	Λ*
H^+ - He	Peyerimhoff	1.0	1466.945	.0714	.434
H^+ - He	Weise et al.	0.92	1466.945	.0735	.465
H^+ - Ne	Peyerimhoff	1.37	1748.779	.0813	.272
H^+ - Ne	Weise et al.	1.3	1748.779	.0838	.282
H^+ - Ar	Klingbeil	1.739	1790.085	.1533	.154
H^+ - Ar	Weise et al.	1.68	1790.085	.1485	.162
H^+ - Kr	Doverspike et al.	2.34	1814.302	.1714	.108
H^+ - Kr	Weise et al.	1.82	1814.302	.1635	.142
Li^+ - He	Catlow	3.0305	4627.761	2.363E-3	.4433
Li^+ - He	Waldman & Gordon	3.054	4627.761	2.587E-3	.4205
Li^+ - Ne	Waldman & Gordon	3.13	9413.92	4.531E-3	.2173
Li^+ - Ar	Waldman & Gordon	3.475	10749.125	1.132E-2	.1159
Na^+ - He	Waldman & Gordon	3.936	6214.210	1.280E-3	.4002
Na^+ - Ne	Waldman & Gordon	3.964	19584.824	2.491E-3	.1605
Na^+ - Ar	Waldman & Gordon	4.402	26409.542	5.908E-3	.0808
K^+ - He	Waldman & Gordon	4.737	6617.015	8.115E-3	.4048
K^+ - Ne	Waldman & Gordon	4.846	24235.003	1.446E-3	.1549
K^+ - Ar	Waldman & Gordon	5.084	35626.324	4.09E-3	.0724

small maximum while a "softer", longer range repulsion will produce a higher and broader maximum.

5) Addition of attractive terms to the interaction, e.g., an ion-induced quadropole (inverse r to the sixth) interaction, will serve to reduce the maximum in the mobility.

6) In the limit of high temperatures, where the repulsive portion of the interaction is dominant, the mobility will decrease as $T^{-(1/2)+(2/m)}$ where m is the exponent of (1/r) in the repulsive term of the interaction[1].

As an example of the use of these conclusions, consider the experimental and calculated mobilities of the K^+ - He system in Figure 16. To the right of the maximum the calculated mobility lies below the measured, but has approximately the same temperature dependence. This would indicate that the repulsive portion of the Waldman-Gordon interaction has approximately the correct slope, but is uniformly too strong, resulting in a cross section which is too large. The maxima in the calculated and measured mobilities occur at approximately the same temperature indicating that the minimum of the Waldman-Gordon interaction occurs at approximately the correct position, however, the calculated mobility lies below the measured value. This could easily result from the error in the repulsive core with no additional error in the well depth, but in the absence of information to the left of the maximum, such a conclusion is impossible.

The results of the remaining calculations are presented in Tables XV-XVII and Figures 16 through 24* along with experimental mobilities. Analysis similar to that presented for the K^+ - He system is possible for these systems[43], however, in general the mobilities calculated from the Waldman-Gordon interactions are in good agreement with experiment leading us to conclude that these interactions are good representations of the true ion-neutral interactions.

Conclusions

At low relative impact energies, the classical transport cross sections serve as a "mean" about which their quantal couterparts will oscillate. These oscillations decrease in amplitude and frequency with increasing relative energy until, above the orbiting limit, the quantal and classical cross sections become indistinguishable. While unable to reproduce the details of the correct quantum mechanical cross sections, the classical cross sections can yield useful and surprisingly accurate results, particularly in the case of small Λ^* as predicted by Munn et al.[36]

For most of the systems considered, the oscillations evident in the quantal diffusion cross sections were effectively averaged out in the calculation of the collision integrals. However, for the systems with very small reduced mass, H^+ - (He, Ne, Ar, Kr), quantal effects can be observed in the mobility. The magnitude of these effects and the temperature at which they are observed, decrease with increasing reduced

*In Figures 16-24, the mobilities are referenced to K_{pol}, the zero field reduced mobility arrived at using only the polarization interaction, $K_{pol} = 36.03/\ \alpha\mu\ cm^2/volt\text{-}sec$ (μ in a.m.u.), or $K_{pol} = 1538.29/\ \alpha\mu\ cm^2/volt\text{-}sec$ (μ in a.u.).

Table XV. K^+ - Ar Mobilities.

T	Mobility (cm^2/volt - sec) Theory Classical	Experiment Derived[48]
20	2.54	
50	2.56	
100	2.58	
150	2.61	
200	2.63	
250	2.66	
300	2.70	2.67
400	2.80	2.74
500	2.90	2.85
600	2.99	2.96
800	3.16	3.09
1000	3.28	3.18
1500	3.45	3.29
2000	3.48	3.32
3000	3.41	3.24
4000	3.29	3.18
5000	3.17	3.10
6000	3.07	3.03
8000	2.89	2.90
10000	2.76	2.79
12000	2.52	2.57
20000	2.38	2.41

Table XVI. Li^+ (He, Ne, Ar) Mobilities.

	Mobility (cm^2/volt - sec)					
	Li^+ - He		Li^+ - Ne		Li^+ - Ar	
T	Theory (Classical)	Experiment (Derived (48))	Theory (Classical	Experiment (Derived (48))	Theory (Classical	Experiment (Derived (48))
20	20.06		10.09		4.58	
50	20.35		10.23		4.62	
100	20.73		10.38		4.66	
150	21.34		10.49		4.69	
200	22.21		10.62		4.72	
250	23.22		10.80		4.74	
300	24.25	22.9	11.03	10.6	4.76	4.59
400	26.27	25.0	11.58	11.4	4.80	4.64
500	27.96	26.4	12.17	12.0	4.85	4.72
600	29.37	27.5	12.74	12.5	4.92	4.82
800	31.35	29.1	13.80	13.2	5.11	5.04
1000	32.53	30.2	14.64	13.7	5.33	5.26
1500	33.55	31.9	16.00	14.5	5.91	5.71
2000	33.38	32.5	16.59	14.9	6.45	6.08
3000	32.17	32.6	16.79	15.2	7.24	6.60
4000	30.94	32.4	16.50	15.1	7.72	6.86
5000	29.89	32.0	16.09	15.0	7.99	7.03
6000	29.00	31.6	15.67	14.8	8.14	7.15
8000	27.65	30.9	14.93	14.4	8.20	7.29
10000	26.68	30.1	14.33	14.1	8.15	7.31
15000	25.17	28.4	13.25	13.5	7.86	7.15
20000	24.32	26.9	12.55		7.57	6.91
25000	23.81	24.6	12.05		7.33	

Table XVII. Na^+ - (He, Ne, Ar) Mobilities.

	Mobility (cm^2/volt - sec)					
	Na^+ - He		Na^+ - Ne		Na^+ - Ar	
T	Theory	Experiment	Theory	Experiment	Theory	Experiment
20	17.59		7.00		2.96	
50	17.92		7.05		2.99	
100	18.75		7.13		3.03	
150	19.95		7.26		3.06	
200	21.10		7.46		3.08	
250	22.10		7.71		3.10	
300	22.89	22.6	7.96	8.16	3.13	3.07
400	23.92	24.0	8.44	8.69	3.20	3.15
500	24.43	24.7	8.83	9.02	3.30	3.23
600	24.58	25.2	9.14	9.23	3.40	3.31
800	24.40	25.8	9.53	9.48	3.60	3.46
1000	23.88	26.0	9.72	9.61	3.80	----
1500	22.42	25.6	9.72	9.64	4.13	3.84
2000	21.14	25.0	9.46	9.53	4.32	3.99
3000	19.28	23.7	8.85	9.22	4.44	4.13
4000	18.00	22.5	8.33	8.90	4.40	4.17
5000	17.08	21.4	7.91	8.58	4.32	4.15
6000	16.37	20.5	7.56	8.29	4.21	4.10
8000	15.34	19.1	7.04	7.77	4.01	3.99
10000	14.63	18.0	6.65	7.32	3.84	3.89

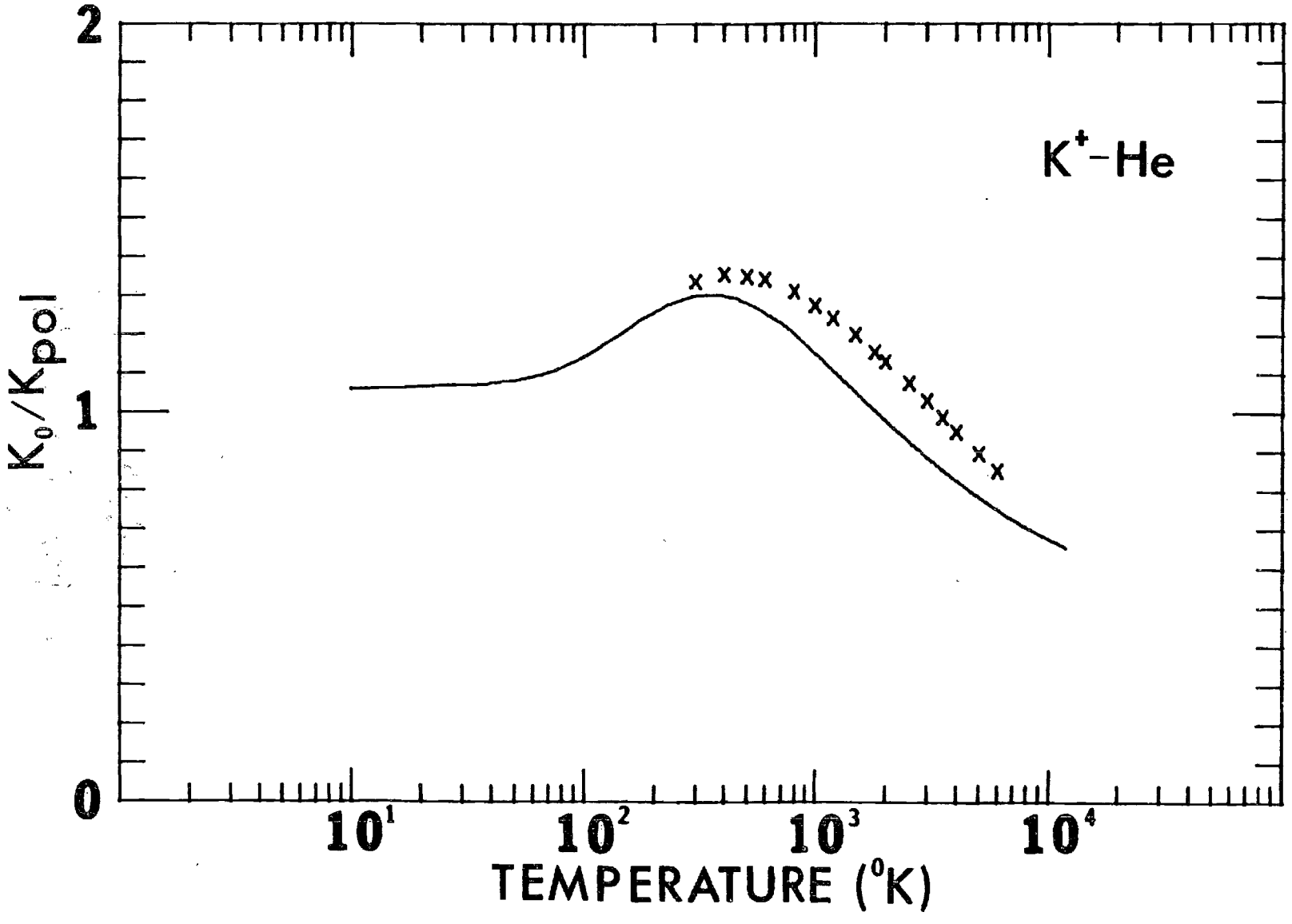

Figure 16. K^+ - He Mobilities.

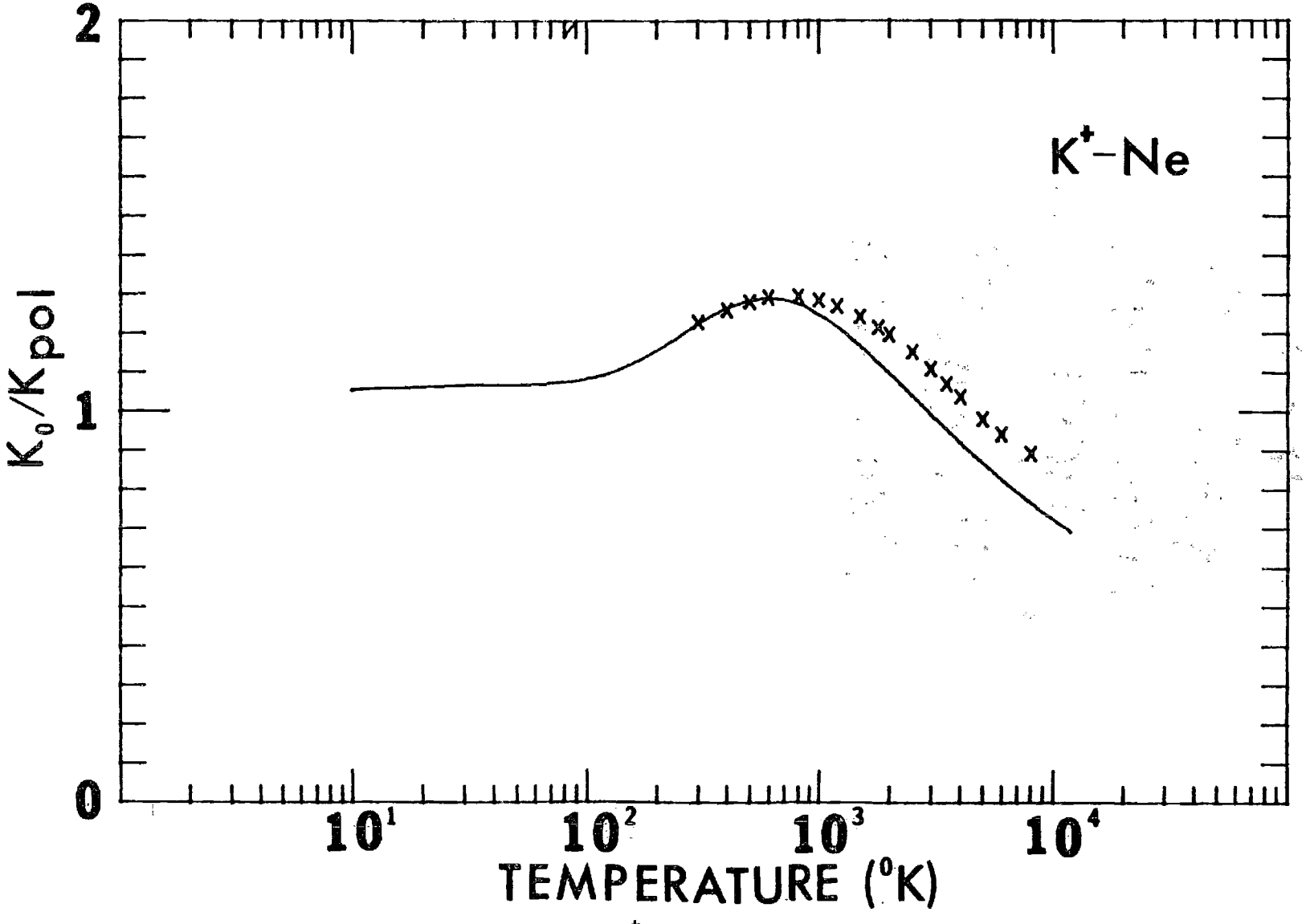

Figure 17. K^+ - Ne Mobilities.

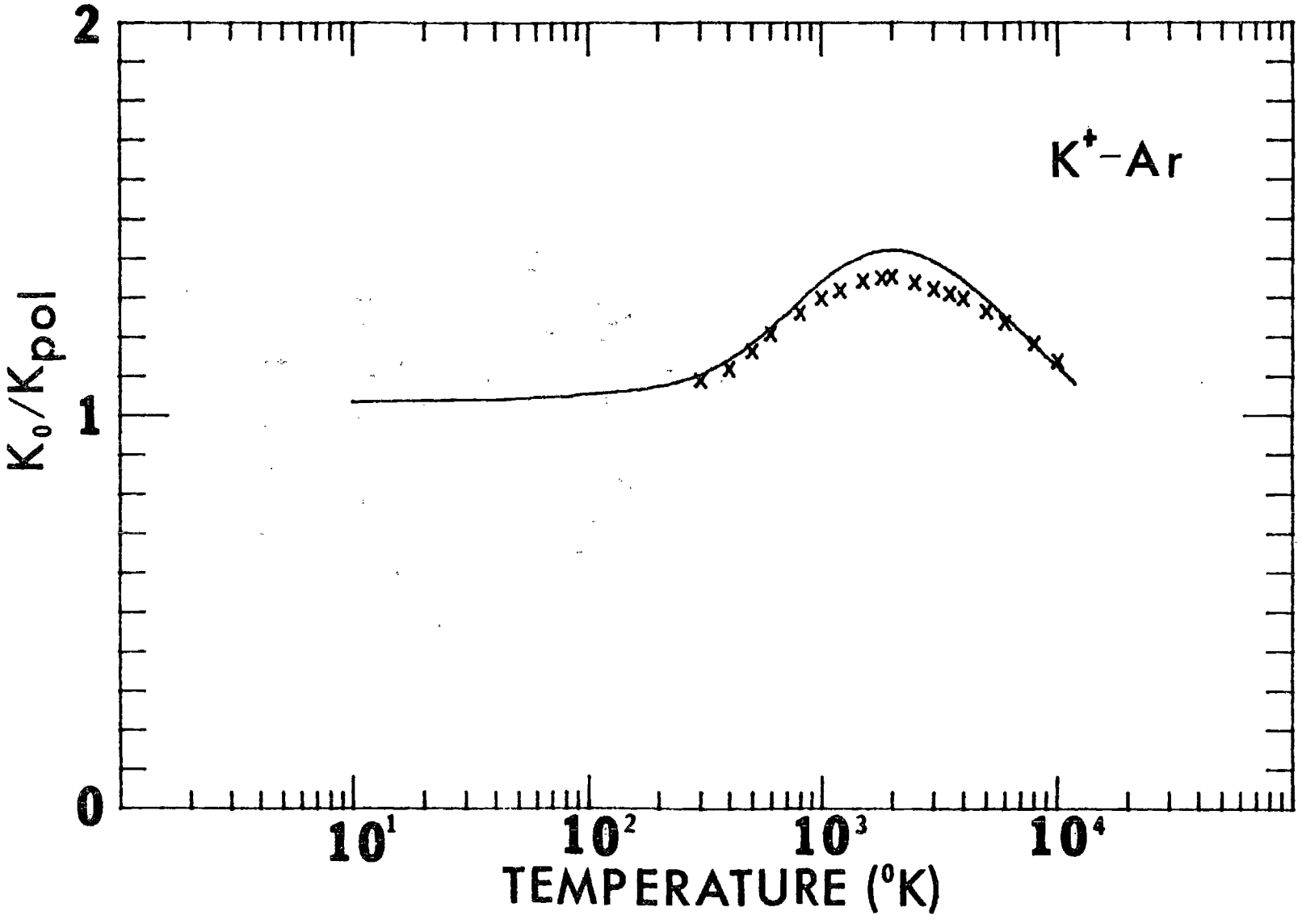

Figure 18. K^+ - Ar Mobilities.

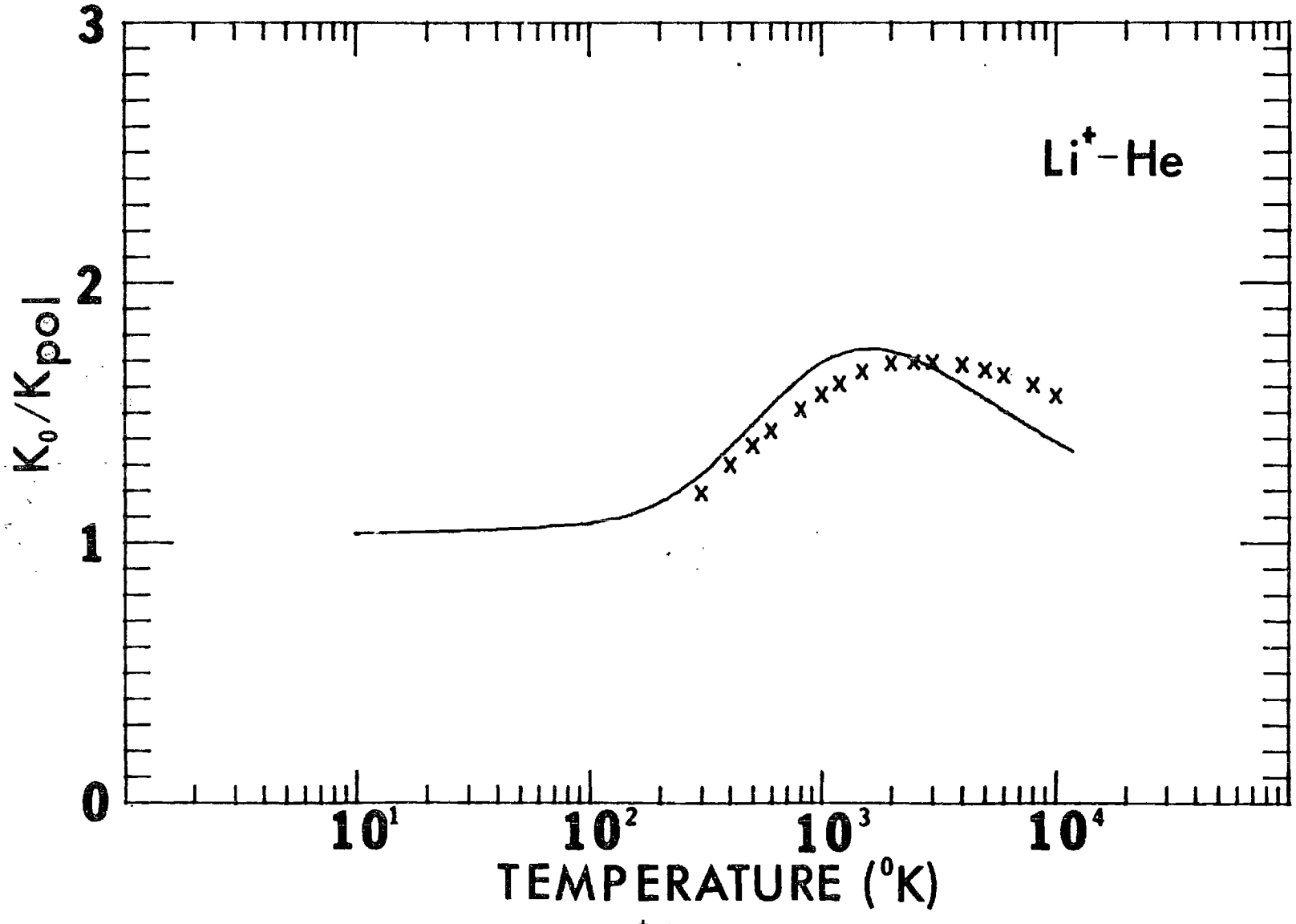

Figure 19. Li^+ - He Mobilities.

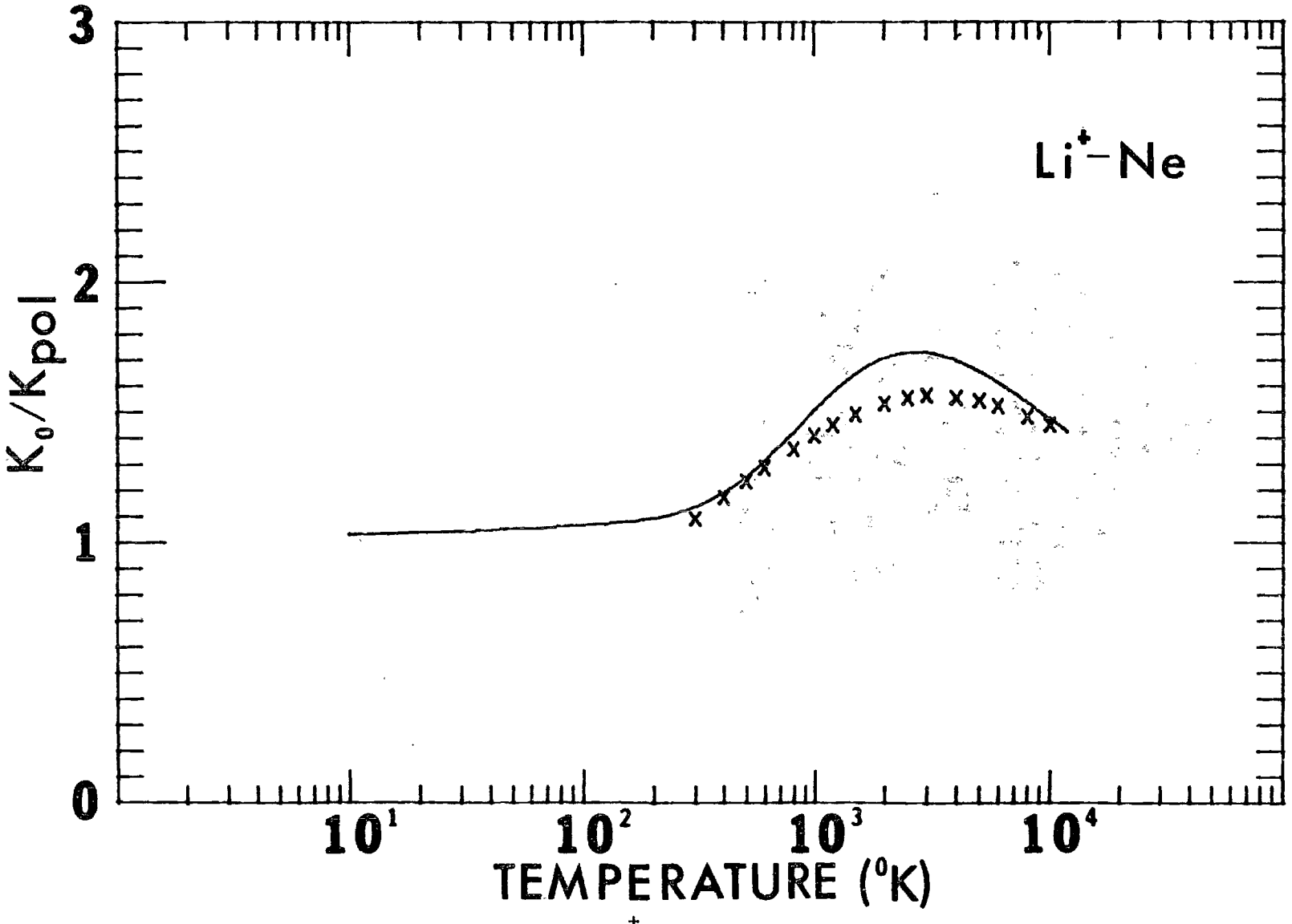

Figure 20. Li^+ - Ne Mobilities.

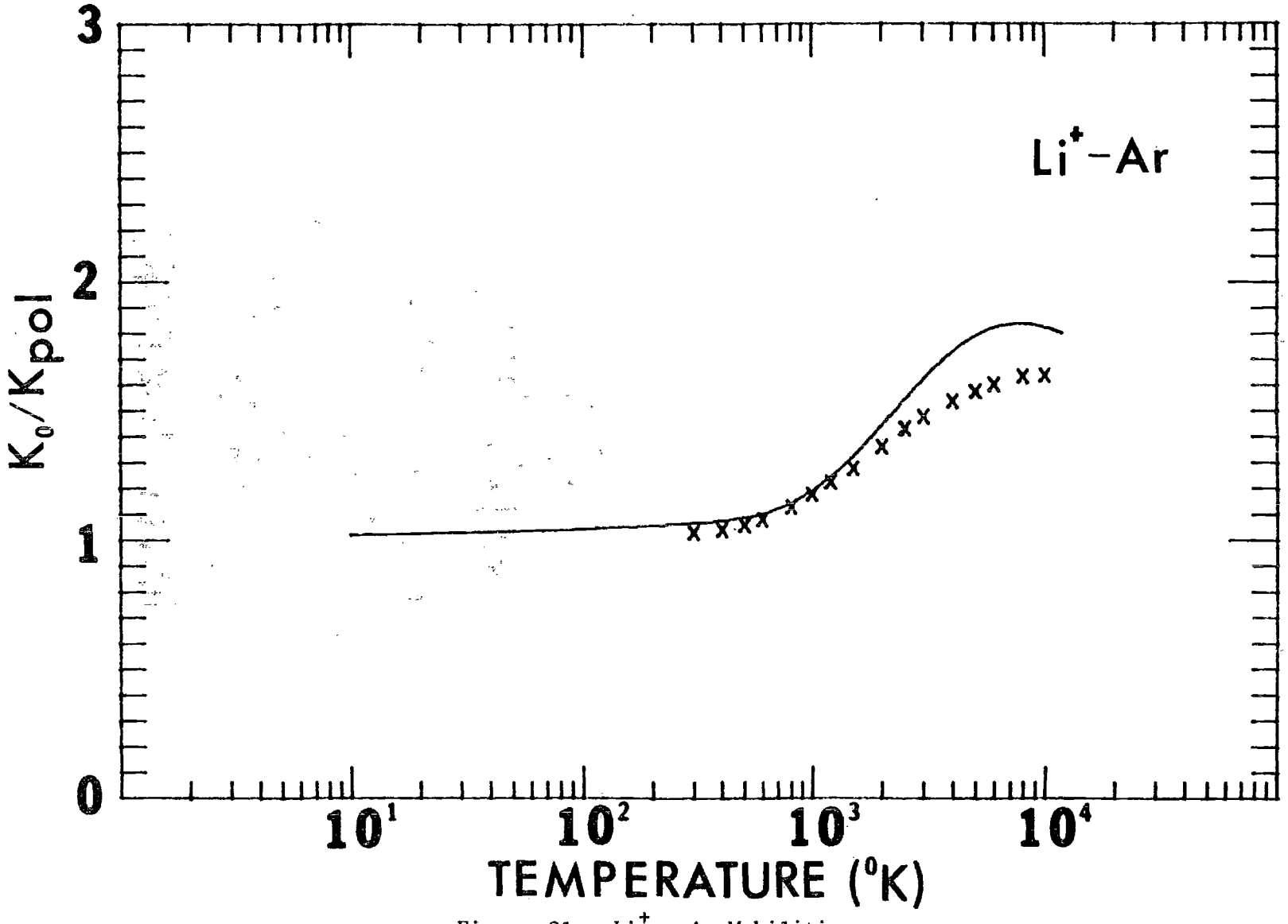

Figure 21. Li^+ - Ar Mobilities.

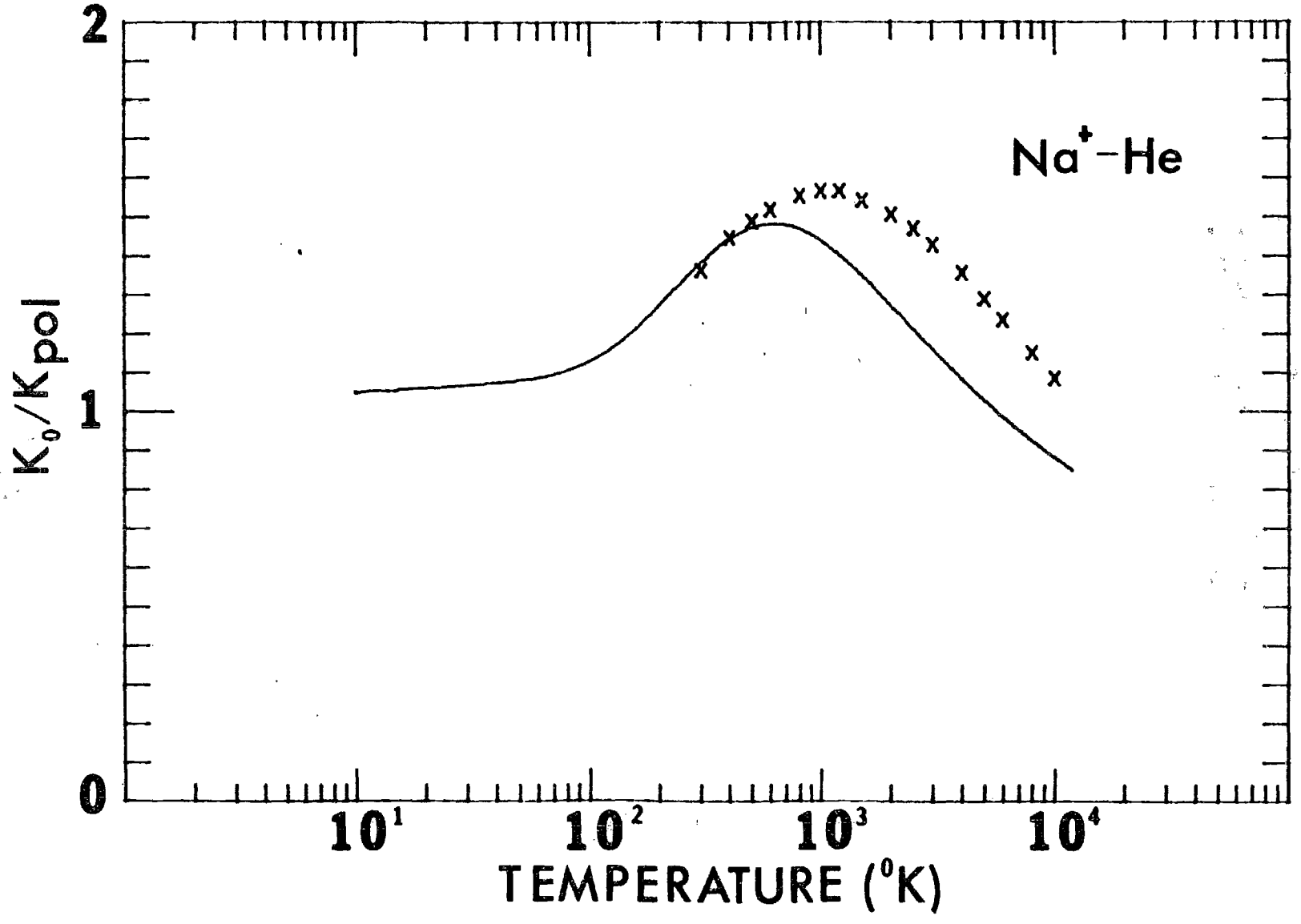

Figure 22. Na^+ - He Mobilities.

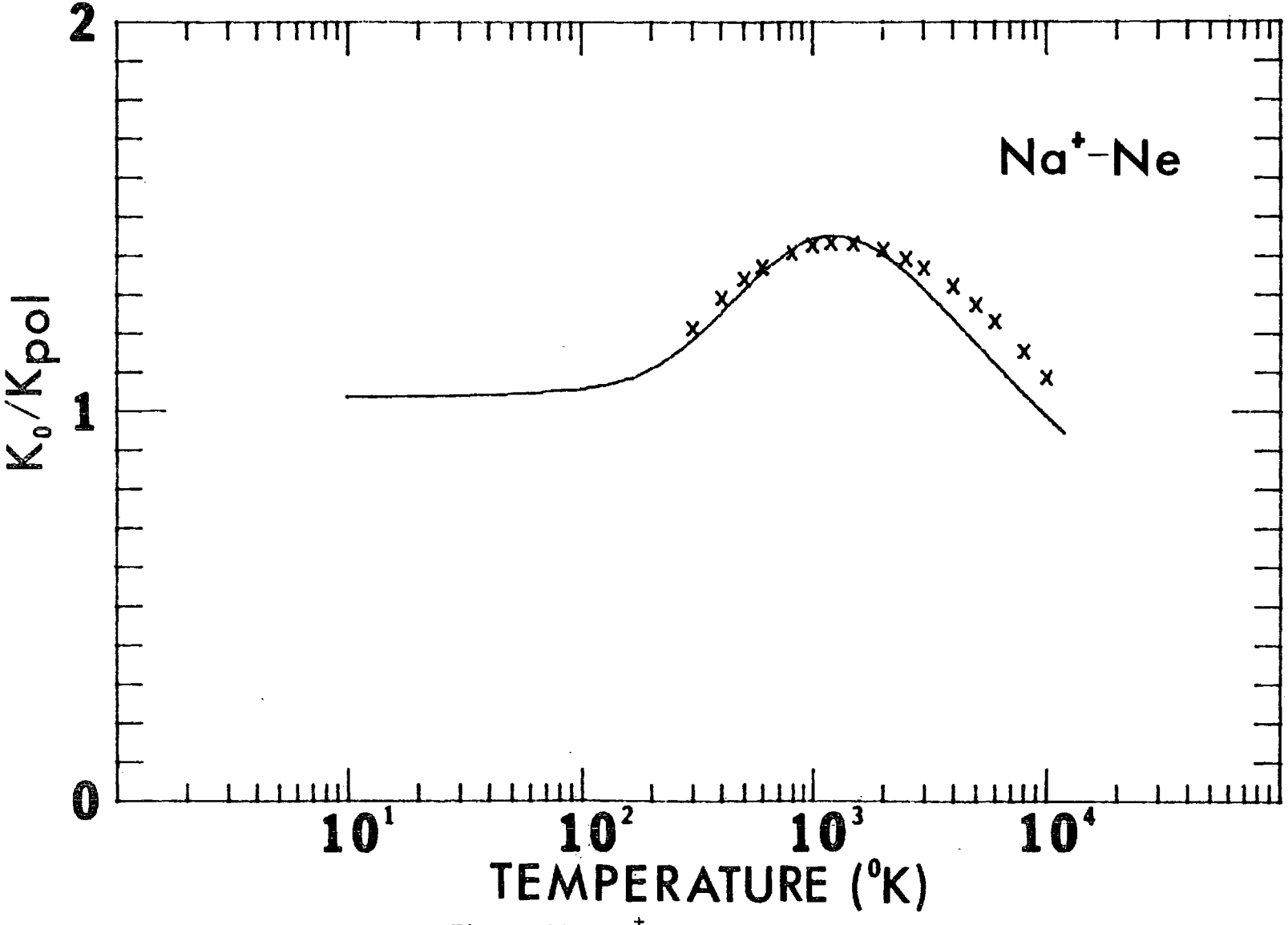

Figure 23. Na^+ - Ne Mobilities.

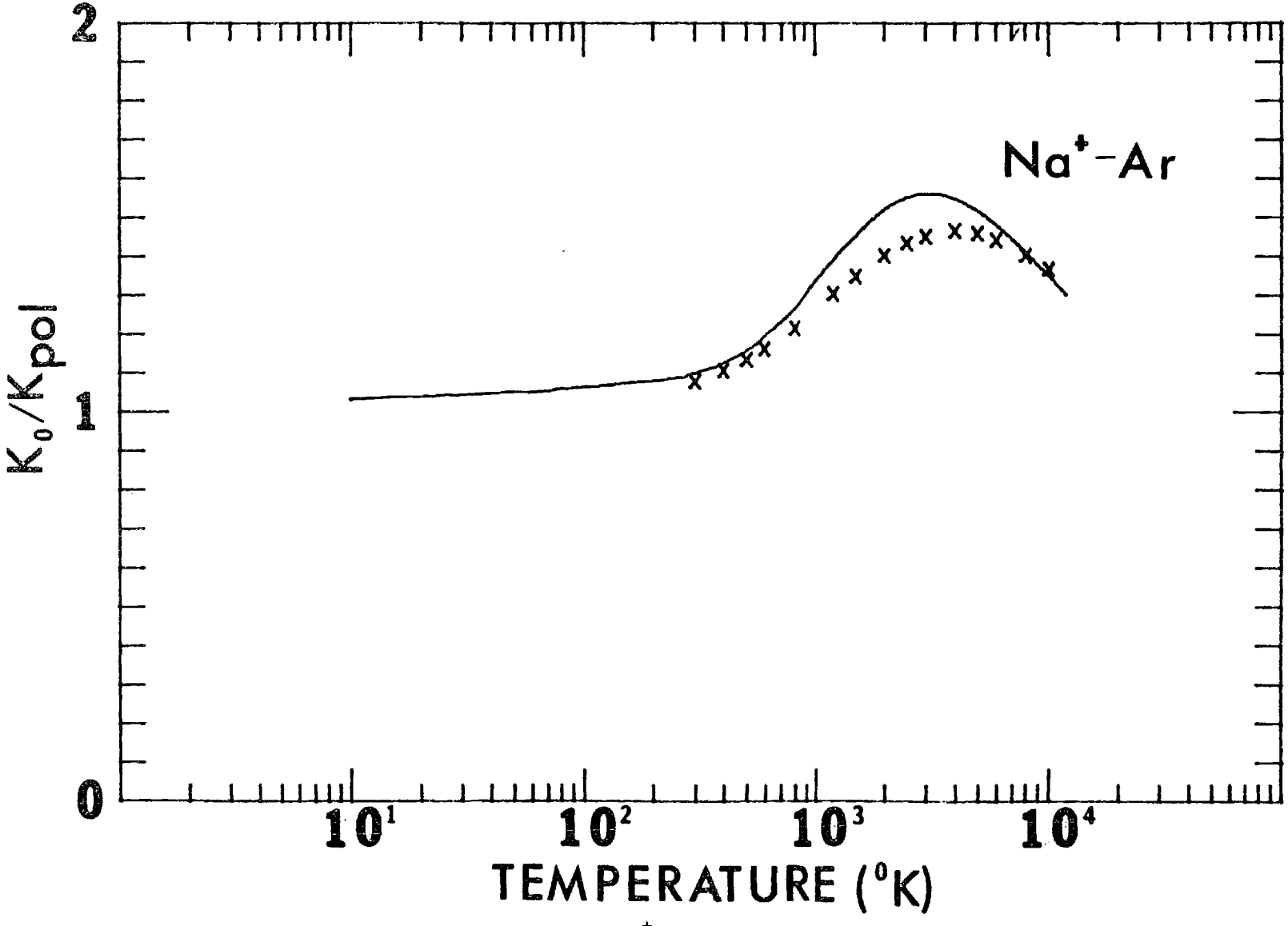

Figure 24. Na^+ - Ar Mobilities.

mass. For all of the other systems considered, quantal and classical calculations agreed remarkably well. It is to be noted that the reduced de Broglie wavelength, Λ^*, was less than 0.5 for all of these ion-rare gas combinations, which thus qualifies them as "classical molecules" under the criteria established by Munn et al.[36].

The ability of an interaction potential to reproduce measured zero field mobilities is a good test of the interaction over a wide range of ion-neutral separations. In the case of the Catlow[9] interaction (Li^+ - He), discrepancies between calculated and measured mobilities lead us to the conclusion that the Catlow interaction is too weak in the region of the potential well and too repulsive in the neighborhood of the core. Similarly, discrepancies between experimental mobilities and those calculated from the interactions of Gordon and Waldman[27] can be interpreted as deficiencies in specific portions of their interaction potentials.

PART II

Excitation in Electron-Metastable Helium Collisions

CHAPTER III

EXCITATION IN ELECTRON-METASTABLE HELIUM COLLISIONS

Introduction

The Born Approximation

Even for very simple systems, the exact description of a scattering event can become quite difficult and expensive. Simplifying assumptions are therefore made in order to make the treatment of collisions feasible without the application of brute force techniques, e.g., the ab initio calculation of wave functions for the colliding system.

The simplest of these approximations, the Born series, has been used extensively and gives reliable results for large relative energies. As a starting point consider the Lippmann-Schwinger equation for the T-matrix operator,

$$T = V + VG_oT \qquad \text{(III-1)}$$

where V is the interaction and G_o is the free particle Green's operator.[54] An iterative solution may be constructed by repeatedly inserting this expression for T into the right-hand side of the equation to obtain

$$T = V + VG_oV + VG_oVG_oV + ... \qquad \text{(III-2)}$$

or,

$$T = V + \sum_{i=1}^{\infty} (VG_o)^i V \qquad \text{(III-3)}$$

which is known as the Born series. Alternately, we can consider the Lippman-Schwinger equation for the "incoming" or "outgoing" scattered wave function

$$\Psi_\alpha^\pm = \Phi_\alpha + G_o^\pm V \Psi_\alpha^\pm \qquad \text{(III-4)}$$

where Φ_α represents a plane wave and the free particle Green's operators $G_o^\pm$ are defined by

$$G_o^\pm \equiv \lim_{\varepsilon \to 0^+} \left[\frac{1}{E - H_o \pm i\varepsilon} \right] \qquad \text{(III-5)},$$

where H_o is the free particle Hamiltonian. Again seeking an iterative solution of the Lippman Schwinger equation, we obtain

$$\Psi_\alpha^\pm = \Phi_\alpha + \sum_{i=1}^{\infty} (G_o^\pm V)^i \Phi_\alpha \qquad \text{(III-6)},$$

the Born series for the scattered wave functions.

There is a difficulty, however, which arises in the application of the Born series. The 1st Born, or simply the Born approximation, involves only the first term on the right-hand side of equations (III-3 or 6), such that the T-matrix obtained is,

$$T_B = \langle \Phi_\beta | V | \Phi_\alpha \rangle \qquad \text{(III-7)},$$

where Φ_α and Φ_β are plane waves. Thus the 1st Born assumes that the form of the projectile wave function is not affected by the interaction with the target, although its momentum vector may be altered in direction and/or magnitude, i.e., $\vec{k}_\alpha \rightarrow \vec{k}_\beta$. This approximation improves with increasing relative energy, however, for low energies the Born cross section will generally exceed experimental values by a factor of two or three. In an attempt to overcome this problem, higher order terms in the Born series may be calculated, but this approach also leads to difficulty since; (1) for all but the weakest of interactions, the Born series will converge slowly if at all, and (2) the higher order Born terms increase rapidly in complexity making them very difficult to handle.

The Distorted Wave Born Approximation

An extension of the Born series arises when the potential, V, can be broken up into an interaction, V_A, for which the scattering problem can be solved exactly and an additional interaction, V_B, i.e.,

$$V = V_A + V_B \qquad \text{(III-8)}.$$

Again taking Φ_α to be a plane wave we define,

$$\chi_\alpha^\pm = \Phi_\alpha + G_o^\pm V_A \chi_\alpha^\pm = \left[1 + G_A^\pm V_A\right] \Phi_\alpha \qquad \text{(III-9)},$$

describing the scattering by V_A alone, where $G_o^{\pm}$ is again the free particle Green's operator and $G_A^{\pm}$ is defined by

$$G_A^{\pm} \equiv \lim_{\varepsilon \to o^+} \left[\frac{1}{E - H_o - V_A \pm i\varepsilon} \right] \qquad \text{(III-10)}.$$

Taking χ_α^+ as the incident state for the interaction V_B, we can write the full scattering solution, $\Psi_\alpha^{\pm}$, as

$$\Psi_\alpha^{\pm} = \chi_\alpha^{\pm} + G_A^{\pm} V_B \Psi_\alpha^{\pm} \qquad \text{(III-11)}.$$

Equivalent forms of equation (III-11) are

$$\Psi_\alpha^{\pm} = \left[1 + G^{\pm} V_B \right] \chi_\alpha^{\pm} \qquad \text{(III-12a)},$$

where

$$G^{\pm} \equiv \lim_{\varepsilon \to 0^+} \left[\frac{1}{E - H_o - V_A - V_b \pm i\varepsilon} \right] \qquad \text{(III-12b)},$$

or,

$$\Psi_\alpha^{\pm} = \left[1 + G^{\pm} (V_A + V_B) \right] Q_\alpha \qquad \text{(III-13)}.$$

Combining equations (III-9) and (III-12a), we obtain

$$\Psi_\alpha^{\pm} = \left[1 + G^{\pm}V_B\right]\left[1 + G_A^{\pm}V_A\right]\Phi_\alpha \qquad \text{(III-14)},$$

which shows explicitly that we are considering a plane wave which is influenced first by the interaction V_A and then by V_B.

The T-matrix for this situation can be shown to be[55]

$$T_{\beta\alpha} = \langle \Phi_\beta \mid V_A \mid \chi_\alpha^+ + \chi_\beta^- \mid V_B \mid \Psi_\alpha^+ \rangle \qquad \text{(III-15)}.$$

Substituting (III-12) into (III-15) and retaining terms through 1st order in V_B, we obtain the Distorted Wave Born Approximation,

$$T_{\beta\alpha}^{DWBA} = \langle \Phi_\beta \mid V_A \mid \chi_\alpha^+ + \chi_\beta^- \mid V_B \mid \chi_\alpha^+ \rangle \qquad \text{(III-16)}.$$

For applications of the DWBA and its extension to the multichannel problem, see Taylor[54] or Schiff[5].

The VPS* Approximation

It has been pointed out by Vainshtein et al.[56] that for electron-atom collisions the above approximations tend to focus on the attraction of the incident electron by the screened nucleus, while the interaction of primary importance in excitation and ionization is the repulsion between the incident and atomic electrons. These authors have presented an approach to electron-atom collisions in which this later interaction has been brought to the fore. It is our purpose here

L. Vainshtein, L. Presnyakov, and I. Sobel'man.

to briefly review their model, which has been tested for the case of the excitation of hydrogen by incident electrons with excellent results, and to then show its validity in the case of e^- - He collisions and to apply the VPS approximation to this system.

CHAPTER IV

REVIEW OF THE VPS APPROXIMATION

Basic Approximation

As a starting point for our discussion consider the Schroedinger equation for the collision of an electron and a hydrogen atom,

$$\left\{ \frac{1}{2}\nabla_1^2 + \frac{1}{2}\nabla_2^2 + \frac{1}{r_1} + \frac{1}{r_2} - \frac{1}{|\vec{r_2}-\vec{r_1}|} + E \right\} \Psi_o(\vec{r_1},\vec{r_2}) = 0 \qquad \text{(IV-1)}$$

where, $\vec{r_1}$ is the position vector of the atomic electron and $\vec{r_2}$ is the position vector of the incident electron. The wave function $\Psi_o(\vec{r_1},\vec{r_2})$ is the solution of (IV-1) satisfying the boundary condition,

$$\Psi_o(\vec{r_1},\vec{r_2}) \xrightarrow[r_2\to\infty]{} \Phi_o(\vec{r_1})e^{i\vec{k_o}\cdot\vec{r_2}} + \sum_m f_m(\theta,\phi)\Phi_m(\vec{r_1})\frac{e^{i\vec{k_m}\cdot\vec{r_2}}}{r_2} \qquad \text{(IV-2)}$$

where $\Phi_m(\vec{r_1})$ are the unperturbed atomic wave functions.

We now seek a solution, Ψ_o, of the form

$$\Psi_o(\vec{r_1},\vec{r_2}) = \Phi_o(\vec{r_1})\ g(\vec{r_1},\vec{r_2}) \qquad \text{(IV-3)}$$

where the function $g(\vec{r_1},\vec{r_2})$ will explicitly describe the interaction between the incident and atomic electrons in the field of the nucleus.

Substituting this function into equation (IV-1) we obtain

$$\Phi_o(\vec{r_1}) \left[\frac{1}{2} \nabla_1^2 + \frac{1}{2} \nabla_2^2 + \frac{1}{r_2} - \frac{1}{|\vec{r_2}-\vec{r_1}|} + \frac{k_o^2}{2} \right] g(\vec{r_1},\vec{r_2})$$

$$+ \vec{\nabla}_1 \Phi_o(\vec{r_1}) \vec{\nabla}_1 g(\vec{r_1},\vec{r_2}) = 0 \qquad \text{(IV-4)},$$

where we have used the fact that,

$$\left[\frac{1}{2} \nabla_1^2 + \frac{1}{r_1} + \varepsilon_o \right] \Phi_o(\vec{r_1}) = 0 \qquad \text{(IV-5)}.$$

Rearranging (IV-4) and introducing the variables,

$$\vec{R} \equiv \frac{1}{2} (\vec{r_2}+\vec{r_1}) \qquad \text{(IV-6)}$$

$$\vec{\rho} \equiv \frac{1}{2} (\vec{r_2}-\vec{r_1}) \qquad \text{(IV-7)}$$

which are the position vectors of the center of mass of the electrons with respect to the nucleus and the incident electron with respect to the center of mass respectively, we obtain,

$$\left[\frac{1}{2} \nabla_R^2 + \frac{1}{2} \nabla_\rho^2 + \frac{1}{R} - \frac{1}{\rho} + k_o^2 \right] g(\vec{\rho},\vec{R}) = \Phi g(\vec{\rho},\vec{R}) \qquad \text{(IV-8)}$$

where,

$$\Phi \equiv \frac{1}{R} - \frac{2}{|\vec{R}+\vec{\rho}|} - \vec{\nabla}_1 \ell n \Phi_o(\vec{r_1}) \left[\vec{\nabla}_R \ell n g(\vec{\rho},\vec{R}) - \vec{\nabla}_\rho \ell n g(\vec{\rho},\vec{R}) \right] \qquad \text{(IV-9)}$$

At this point, Vainshtein et al. introduce what they term their "principal assumption" and set Φ equal to zero making the function $g(\vec{\rho},\vec{R})$, the solution of the left hand side of equation (IV-8), i.e.,

$$\left[\frac{1}{2} \nabla_R^2 + \frac{1}{2} \nabla_\rho^2 + \frac{1}{R} - \frac{1}{\rho} + k_o^2 \right] g_o(\vec{\rho},\vec{R}) = 0 \qquad \text{(IV-10)}.$$

If we now introduce parabolic coordinates, the solution of (IV-10) can be easily found to be (see Schiff[5]),

$$g(\vec{\rho},\vec{R}) = N e^{ik_o^{\rightarrow} \cdot (\vec{R}+\vec{\rho})} F(i\nu,1,ik_o R - ik_o^{\rightarrow} \cdot \vec{R}) F(-i\nu,1,ik_o \rho - ik_o^{\rightarrow} \cdot \vec{\rho}) \qquad \text{(IV-11)}$$

where $\nu \equiv \frac{1}{k_o}$, the functions F are the confluent hypergeometric functions, and N is the normalization factor,

$$N = |\Gamma(1+i\nu)|^2 \qquad \text{(IV-12)}.$$

Using equations (IV-3) and (V-11), we obtain our solution,

$$\Psi_o(\vec{r_1},\vec{r_2}) = \Phi_o(\vec{r_1}) N e^{ik_o^{\rightarrow} \cdot (\vec{R}+\vec{\rho})} F(i\nu,1,ik_o R - ik_o^{\rightarrow} \cdot \vec{R})$$

$$F(-i\nu,1,ik_o \rho - ik_o^{\rightarrow} \cdot \vec{\rho}) \qquad \text{(IV-13)}$$

which we substitute into the expression for the cross section of the transition between states o and m,

$$\sigma_{om} = \frac{km}{4\pi^2 k_o} \int d\Omega(\theta,\phi) \left| \langle \Phi_m(\vec{r_1}) e^{i\vec{k_m}\cdot\vec{r_2}} | V(\vec{r_1},\vec{r_2}) | \Psi_o(\vec{r_1},\vec{r_2}) \rangle \right|^2 \quad \text{(IV-14)}$$

where,

$$V(\vec{r_1},\vec{r_2}) = \frac{1}{|\vec{r_2}-\vec{r_1}|} - \frac{1}{r_2} \quad \text{(IV-15).}$$

Consider now the matrix element

$$J \equiv \langle \Phi_m(\vec{r_1}) e^{i\vec{k_m}\cdot\vec{r_2}} | V(\vec{r_1},\vec{r_2}) | \Psi_o(\vec{r_1},\vec{r_2}) \rangle \quad \text{(IV-16)}$$

or, upon inserting (IV-13),

$$J = N \iint d\vec{r_1} d\vec{r_2} \Phi_m^*(\vec{r_1}) \Phi_o(\vec{r_1}) V(\vec{r_1},\vec{r_2}) e^{-i\vec{k_m}\cdot\vec{r_2}} e^{i\vec{k_o}\cdot(\vec{R}+\vec{\rho})}$$

$$F(i\nu,1,ik_oR-i\vec{k_o}\cdot\vec{R}) F(-i\nu,1,ik_o\rho-i\vec{k_o}\cdot\vec{\rho}) \quad \text{(IV-17).}$$

Vainshtein et al. note that the $1/r_2$ term in (IV-15) makes no contribution to this integral in the Born approximation and assume that such is the case here. Using this assumption along with the transformation,

$$d\vec{r}_1 d\vec{r}_2 = -\,8 d\vec{R} d\vec{\rho} \qquad \text{(IV-18)}$$

equation (IV-17) becomes,

$$J=-8N\int\int d\vec{R}d\vec{\rho}\,\Phi_m^*(\vec{r}_1)\Phi_o(\vec{r}_2)\,\frac{1}{2\rho}\,e^{-ik_m^{\rightarrow}\cdot(\vec{R}+\vec{\rho})}\,e^{ik_o^{\rightarrow}\cdot(\vec{R}+\vec{\rho})}$$

$$F(i\nu,1,ik_oR-ik_o^{\rightarrow}\cdot\vec{R})F(-i\nu,1,ik_o\rho-ik_o^{\rightarrow}\cdot\vec{\rho}) \qquad \text{(IV-19)}.$$

We now introduce the notation

$$F(\pm\nu,R) \equiv F(\pm i\nu,1,ik_oR-ik_o^{\rightarrow}\cdot\vec{R})$$

and the Fourier transform of the bound state wave functions,

$$\Phi_m^*(\vec{r}_1)\Phi_o(\vec{r}_1) = \frac{1}{(2\pi)^3}\int d\vec{t}\,e^{-i\vec{t}\cdot\vec{r}_1}\,\tilde{\Phi}(\vec{t}) \qquad \text{(IV-20-a)}$$

where,

$$\tilde{\Phi}(\vec{t}) \equiv \int d\vec{r}_1\,e^{i\vec{t}\cdot\vec{r}_1}\,\Phi_m^*(\vec{r}_1)\Phi_o(\vec{r}_1) \qquad \text{(IV-20-b)}$$

such that,

$$J = \frac{-8N}{(2\pi)^3} \iiint d\vec{R}d\vec{\rho}d\vec{t}\ e^{-i\vec{t}\cdot(\vec{R}-\vec{\rho})}\tilde{\Phi}(\vec{t})\ e^{i\vec{q}\cdot(\vec{R}+\vec{\rho})}$$

$$F_{(\nu,R)}\ \frac{F_{(-\nu,\rho)}}{2\rho} \qquad \text{(IV-21)}$$

where,

$$\vec{q} \equiv \vec{k_o} - \vec{k_m} \qquad \text{(IV-22)}.$$

Rearranging (IV-21) slightly, and making the change of variable,

$$\vec{S} \equiv \vec{q} - \vec{t}$$

this integral becomes,

$$J = \frac{8N}{(2\pi)^3} \iiint d\vec{R}d\vec{\rho}d\vec{S}\ e^{i\vec{S}\cdot\vec{R}}\tilde{\Phi}(\vec{q}-\vec{s})e^{i\vec{\rho}\cdot(2\vec{q}-\vec{S})}F(\nu,R)\frac{F(-\nu,\rho)}{2\rho} \qquad \text{(IV-23)}$$

The integral over $\vec{R}$,

$$J_1 \equiv \int d\vec{R}\ e^{i\vec{S}\cdot\vec{R}}\ F(\nu,R)$$

is sharply peaked about $\vec{S} = 0$ (the integral has an inverse S dependence), and the function $\tilde{\Phi}(\vec{q}-\vec{s})$ is assumed to be slowly varying near $\vec{S} = 0$, such that the error introduced by replacing $\tilde{\Phi}(\vec{q}-\vec{s})$ with $\tilde{\Phi}(\vec{q})$

in (IV-21) will be small. At this point, Vainshtein et al. introduce an approximation which has been the source of much controversy in the literature[57-60]. The authors contend that the replacement of $\vec{q}$ by $-\vec{q}$ in the term, $\exp[i\vec{\rho}\cdot(2\vec{q}-\vec{S})]$, will to some degree compensate for for the "over estimation of the contribution of the region $\vec{S} = \vec{q}$ in the integral over $\vec{S}$ space."[58] Using these approximations and noting that

$$\int d\vec{S} e^{i\vec{S}\cdot\vec{R}} \left\{ \frac{1}{(2\pi)^3} \int d\vec{\rho} e^{-i\vec{\rho}\cdot\vec{S}} \left[e^{-i2\vec{q}\cdot\vec{\rho}} \frac{F(-\nu,\rho)}{2\rho} \right] \right\} =$$

$$e^{-i2\vec{q}\cdot\vec{R}} \frac{F(-\nu,R)}{2R} \qquad \text{(IV-24)}$$

(IV-23) becomes,

$$J = 4N\tilde{Q}_{(\vec{q})} \int d\vec{R}\, e^{-i2\vec{q}\cdot\vec{R}} F(\nu,R) \frac{1}{R} F(-\nu,R) \qquad \text{(IV-25).}$$

This integral belongs to the class of integrals,

$$I = \int d\vec{r}\, e^{-\lambda r} \frac{e^{i\vec{S}\cdot\vec{r}}}{r} F(ia_1,1,ip_1 r - i\vec{p}_1\cdot\vec{r})$$

$$F(ia_2,1,ip_2 r + i\vec{p}_2\cdot\vec{r}) \qquad \text{(IV-26)}$$

which has been treated by Nordsieck[61], who gives as the result,

$$I = \frac{2\pi}{\alpha} e^{-\pi a_1} \left(\frac{\alpha}{\gamma}\right)^{ia_1} \left(\frac{\gamma+\delta}{\gamma}\right)^{-ia_2} F\left(1-ia_1, ia_2 1, \frac{\alpha\delta-\beta\gamma}{\alpha(\gamma+\delta)}\right) \qquad \text{(IV-27)}$$

where F is now the hypergeometric function and where

$$\alpha \equiv \frac{1}{2}\left(S^2+\lambda^2\right) \quad ,$$

$$\beta \equiv \vec{p_2}\cdot\vec{S} - i\lambda p_2 \quad ,$$

$$\gamma \equiv \vec{p_1}\cdot\vec{S} + i\lambda p_1 - \alpha \ ,$$

and

$$\delta \equiv p_1 p_2 + \vec{p_1}\cdot\vec{p_2} - \beta.$$

Using these results, (IV-26) can be found to yield,

$$J = 4N\tilde{\Phi}_{(\vec{q})} \left[\frac{\pi}{q^2} e^{-\pi\nu}(-1)^{i\nu} F(i\nu,-i\nu,1,x)\right] \qquad \text{(IV-28)}$$

where,

$$x \equiv \left[\frac{\vec{k_o}\cdot\vec{q}}{\vec{k_o}\cdot\vec{q}+q^2}\right]^2 = \left[\frac{2\Delta\varepsilon+q^2}{2\Delta\varepsilon+3q^2}\right]^2 \qquad \text{(IV-29)}$$

and $\Delta\varepsilon$ is the excitation energy,

$$\Delta\varepsilon \equiv \frac{1}{2}\,(k_o^2 - k_m^2) \qquad \text{(IV-30)}$$

Rewriting the normalization factor, N, in the alternate form,

$$N = N^* = \left|\Gamma(1+i\nu)\right|^2 = \frac{\pi\nu}{\sinh \pi\nu} \qquad \text{(IV-31)},$$

and making use of the complex conjugate of (IV-28),

$$J^* = 4N^*\,\tilde{\Phi}^*_{(\vec{q})}\,\left[\frac{\pi}{q^2}\; e^{\pi\nu}(-1)^{-i\nu}F(-i\nu,i\nu,1,x)\right] \qquad \text{(IV-32)},$$

we obtain from equation (IV-14),

$$\sigma_{om} = \frac{k_m}{4\pi^2 k_o}\int d\Omega(\theta,\phi)\;\frac{16\pi^2}{q^4}\left|\tilde{\Phi}_{(\vec{q})}\right|^2\left[f_{(\nu,x)}\right]^2 \qquad \text{(IV-33)},$$

where,

$$f(\nu,x) = \frac{\pi\nu}{\sinh \pi\nu}\; F(i\nu,-i\nu,1,x) \qquad \text{(IV-34)},$$

We now make use of equation (IV-20-b)

$$\tilde{\Phi}_{(\vec{q})} = \int d\vec{r_1}\;\Phi^*_m(\vec{r_1})\;\; e^{i\vec{q}\cdot\vec{r_1}}\;\Phi_o(r_1) \equiv \langle_m|e^{i\vec{q}\cdot\vec{r_1}}|0\rangle_{\vec{r_1}}$$

and the identity,

$$q^2 = k_o^2 + k_m^2 - 2k_o k_m \cos\theta \qquad \text{(IV-35)}$$

to obtain the VPS approximation for the excitation cross section,

$$\sigma_{om} = \frac{8\pi}{k_o^2} \int_{k_o-k_m}^{k_o+k_m} \frac{dq}{q^3} \left|\langle m| e^{i\vec{q}\cdot\vec{r}_1} |0\rangle_{\vec{r}_1}\right|^2 [f_{(\nu,x)}]^2 \qquad \text{(IV-36)},$$

where x is defined by equation (IV-29).

Equation (IV-36) is simply the Born approximation with the addition of a multiplicative factor, $[f(\nu,x)]^2$ in the integrand, which is very small for $k_o << 1$ and approaches one asymptotically with increasing k_o. Thus, the VPS approximation gives a result which lies below the Born cross section for small k_o and approaches it with increasing k_o, a fact which is qualitatively satisfying since the Born cross section is generally too high at low energies.

The reduction of the Born cross section is the direct result of having taken the electron-electron repulsion into account in writing the wave function for the scattered particle. In going from a plane wave to a Coulomb wave we have lowered the probability, for small k_o, of finding the incident electron near the atom, thus, reducing the probability of a transition occuring, i.e. the cross section. With increasing k_o, the Coulomb repulsion is gradually overcome, and the Born cross section is regained.

Effective Charge

Vainshtein et al. attempt to reduce the effect of the discarded portion of equation (IV-8), Q as defined by (IV-9), by introducing an effective charge in (IV-8) and then fixing the value of this effective charge in such a way as to cancel a portion of Q. They obtain as a result for the effective charge,

$$\zeta = \frac{k_o}{k_o+\sqrt{2\varepsilon_o}} \qquad \text{(IV-37)},$$

where ε_o is defined by equation (IV-5), and as a solution to (IV-10) with the inclusion of the effective charge, equation (IV-11) with

$$\nu \to \frac{\zeta}{k_o} = \frac{1}{k_o+\sqrt{2\varepsilon_o}} \qquad \text{(IV-38)}.$$

Exchange

Account is taken of the exchange of incident and atomic electrons by interchanging the roles of $\vec{r_1}$ and $\vec{r_2}$ in equation (IV-13) to obtain,

$$\Psi_o(\vec{r_2},\vec{r_1}) = \Phi_o(\vec{r_2})Ne^{ik_o\cdot(\vec{R}+\vec{\rho})}F(i\nu,1,ik_oR-ik_o\cdot\vec{R})$$

$$F(-i\nu,1,ik_o\rho-ik_o\cdot\vec{p}) \qquad \text{(IV-39)}$$

where,

$$\vec{\rho} \equiv -\vec{\rho} = \frac{1}{2}(\vec{r_1}-\vec{r_2}) \qquad \text{(IV-40)}.$$

Using (IV-39) in (IV-16), we obtain in place of (IV-16),

$$J_{ex}=N\int\int d\vec{r_1}d\vec{r_2}\Phi_m^*(\vec{r_1})\Phi_o(\vec{r_2})V(\vec{r_1},\vec{r_2})e^{-i\vec{k_m}\cdot\vec{r_2}}$$

$$xe^{ik_o\cdot(\vec{R}+\vec{\rho})}F(i\nu,1,ik_oR-ik_o\cdot\vec{R})F(-i\nu,1,ik_o\rho-ik_o\cdot\vec{\rho}) \qquad \text{(IV-41)}.$$

Using the Fourier transforms

$$\Phi_o(\vec{r_2}) = \frac{1}{(2\pi)^3}\int d\vec{S}\, e^{-i\vec{S}\cdot\vec{r_2}}\,\tilde{\Phi}_o(\vec{S}) \qquad \text{(IV-42-a)}$$

$$\Phi_m^*(\vec{r_1}) = \frac{1}{(2\pi)^3}\int d\vec{t}\, e^{-i\vec{t}\cdot\vec{r_1}}\,\tilde{\Phi}_m^*(\vec{t}) \qquad \text{(IV-42-b)}$$

and the transformation,

$$d\vec{r_1}d\vec{r_2} = -8d\vec{R}d\vec{\rho} \qquad \text{(IV-43)}$$

and again neglecting the core term in $V(\vec{r_1},\vec{r_2})$, equation (IV-41) becomes,

$$J_{ex} = \frac{-8N}{(2\pi)^6} \iiiint d\vec{R}d\vec{\rho}d\vec{S}dt\vec{\tilde{\Phi}}^{*}_{m}(\vec{t})\tilde{\Phi}_{o}(\vec{S})\ e^{i\vec{R}\cdot(\vec{q}-\vec{s}-\vec{t})}$$

$$x\ F(\nu,R)\ \frac{1}{2\rho}\ F(-\nu,\rho)\ e^{i\vec{\rho}\cdot(2\vec{k_o}-\vec{q}+\vec{s}-\vec{t})} \qquad \text{(IV-44)}.$$

As noted previously, the $\vec{R}$ integration is sharply peaked about $\vec{q} - \vec{s} - \vec{t} = 0$, therefore replacing $\tilde{\Phi}_o(\vec{s})$ by $\tilde{\Phi}_o(\vec{q} - \vec{t})$ we obtain

$$J_{ex} = \frac{-4N}{(2\pi)^6} \int d\vec{t}\tilde{\Phi}^{*}_{m}(\vec{t})\tilde{\Phi}_{o}(\vec{q}-\vec{t})\int d\vec{R}F(\nu,R)\, e^{i\vec{R}\cdot(\vec{q}-\vec{t})}$$

$$x\int d\vec{\rho}F(-\nu,\rho)\ \frac{1}{\rho}\ e^{i\vec{\rho}\cdot(2\vec{k_o}-\vec{q}-\vec{t})} \int d\vec{S}e^{i\vec{S}\cdot(\vec{\rho}-\vec{R})}\ ,$$

however,

$$\frac{1}{(2\pi)^3} \int d\vec{S}\ e^{i\vec{S}\cdot(\vec{\rho}-\vec{R})} = \delta(\vec{\rho}-\vec{R})$$

so we have,

$$J_{ex} = \frac{-4N}{(2\pi)^3} \int d\vec{t}\tilde{\Phi}^{*}_{m}(\vec{t})\tilde{\Phi}_{o}(\vec{q}-\vec{t})\int d\vec{R}F(\nu,R)\ \frac{1}{R}\ F(-\nu,R)$$

$$e^{i\vec{R}\cdot(2\vec{k_o}-2\vec{t})} \qquad \text{(IV-45)}.$$

Vainshtein et al. here assume that the major contribution to this integral arises from the small $\vec{t}$ such that the term $e^{-2i\vec{R}\cdot\vec{t}}$ may be neglected, decoupling the integrals. The $\vec{R}$ integral may be evaluated by the method of Nordsieck to give us,

$$\int d\vec{R}\ F(\nu,R)\ \frac{1}{R}\ F(-\nu,R)\, e^{i2\vec{k_o}\cdot\vec{R}} = \frac{\pi}{k_o^2}\ F(-i\nu,i\nu,1,\tfrac{1}{4}) \qquad \text{(IV-46)}$$

while the $\vec{t}$ integral yields upon expansion,

$$\int d\vec{t}\,\tilde{\Phi}_m^*(\vec{t})\tilde{\Phi}_o(\vec{q}-\vec{t}) = \iiint d\vec{t}\,dr_1^{\rightarrow}dr_2^{\rightarrow}\Phi_m^*(r_1^{\rightarrow})\Phi_o(r_2^{\rightarrow})e^{i\vec{q}\cdot r_2^{\rightarrow}}e^{i\vec{t}\cdot(r_1^{\rightarrow}-r_2^{\rightarrow})}$$

$$= \int dr_1^{\rightarrow}\Phi_m^*(r_1^{\rightarrow})\int dr_2^{\rightarrow}\Phi_o(r_2^{\rightarrow})e^{i\vec{q}\cdot r_2^{\rightarrow}}\int d\vec{t}\,e^{i\vec{t}\cdot(r_1^{\rightarrow}-r_2^{\rightarrow})}$$

$$= (2\pi)^3\int dr_1^{\rightarrow}\Phi_m^*(r_1^{\rightarrow})e^{i\vec{q}\cdot r_1^{\rightarrow}}\Phi_o(r_1^{\rightarrow})$$

or,

$$\int d\vec{t}\,\tilde{\Phi}_m^*(\vec{t})\tilde{\Phi}_o(\vec{q}-\vec{t}) = (2\pi)^3\langle m|e^{i\vec{q}\cdot r_1^{\rightarrow}}|0\rangle_{r_1^{\rightarrow}} \qquad \text{(IV-47)}.$$

As a result we have,

$$J_{ex} = \frac{-4N\pi}{k_o^2}\langle m|e^{i\vec{q}\cdot\vec{r}_1}|0\rangle_{r_1^{\rightarrow}}\ F(-i\nu,i\nu,1,\tfrac{1}{4}) \qquad \text{(IV-48)},$$

in agreement with Vainshtein et al.[56]

The Status of the VPS Approximation

As noted previously, portions of the VPS approximation have been the subject of a good deal of controversy in the literature.[57-60] The main source of criticism is the replacement of $2\vec{q}$ by $-2\vec{q}$ in equation (IV-23). Crothers and McCarrol[57] have noted that the formulation of the problem using the post wave function is formally equivalent to the treatment using the prior wave function, which leads to the VPS approximation, and makes the sign change of Vainshtein et al. unnecessary. This approach leads to a complex effective charge and a sharp maximum near threshold which in some cases may exceed the Born cross section by a factor of four or five. Both approaches appear to agree well with existing data (and each other) above 50eV although the VPS approximation is consistent with the data of Fite et al.[62-65] for the case $e^- + H(1S) \rightarrow e^- + H(2p)$ for all energies. Crothers[59] has also pointed out that the direct application of the method of Nordsieck[61] to (IV-23) gives a result which exceeds the Born cross section at all energies, perhaps justifying the contention of Vainshtein et al. that the replacement of $2\vec{q}$ by $-2\vec{q}$ somehow compensates for the error introduced in the peaking approximation.

Coleman[60] has reviewed both of these approaches and summarized the problems and objections discussed above. He also points out the questionable nature of the peaking approximation[66],

which is used in both forms of the approximation, but rather than make any judgement as to the overall usefulness of the approximation, he suggests that further investigation is in order.

CHAPTER V

EXTENSION OF THE VPS APPROXIMATION TO ELECTRON-METASTABLE HELIUM COLLISIONS

Basic Approximation

Having reviewed the VPS approximation in considerable detail, we will now consider the application of this method to e - He($2^{1,3}S$) collisions. The Schroedinger equation for this system is

$$\left\{ \sum_{j=1}^{3} \left[\frac{1}{2} \nabla_j^2 + \frac{2}{r_j} - \frac{1}{2} \sum_{i \neq j} \frac{1}{|\vec{r}_j - \vec{r}_i|} \right] + E \right\} \Psi_o(\vec{r}_1, \vec{r}_2, \vec{r}_3) = 0 \qquad \text{(V-1)}$$

where,

$$E \equiv \frac{1}{2} k_o^2 + \varepsilon \qquad \text{(V-2)}$$

and where,

$$\left\{ \sum_{j=1}^{2} \left[\frac{1}{2} \nabla_j^2 + \frac{2}{r_j} \right] - \frac{1}{|\vec{r}_2 - \vec{r}_1|} + \varepsilon \right\} \Phi_o(\vec{r}_1, \vec{r}_2) = 0 \qquad \text{(V-3)}$$

describes the metastable helium atom.

Since, for excitation, the interaction between the incident and excited electrons is of primary importance[56], we shall attempt to take this interaction into account in writing the wave function for the incident electron. We will view the excited helium atom as a core of charge one, consisting of the nucleus and the 1S orbital electron, and a single orbital electron. In this approximation, the Schroedinger equation for the outer orbital electron becomes,

$$\left\{ \frac{1}{2} \nabla_2^2 + \frac{1}{r_2} + \varepsilon' \right\} \Phi_o'(\vec{r}_2) = 0 \qquad \text{(V-4)}$$

while for the full system we have,

$$\left\{ \frac{1}{2} \nabla_2^2 + \frac{1}{2} \nabla_3^2 + \frac{1}{r_2} + \frac{1}{r_3} - \frac{1}{|\vec{r}_3 - \vec{r}_2|} + \frac{k_o^2}{2} + \varepsilon' \right\} \Psi_o'(\vec{r}_2, \vec{r}_3) = 0 \qquad \text{(V-5)}$$

where $\Psi_o'(\vec{r}_2, \vec{r}_3)$ must satisfy the scattering boundary condition,

$$\Psi_o'(\vec{r}_2, \vec{r}_3) \xrightarrow[r_3 \to \infty]{} \Phi_o'(\vec{r}_2)\, e^{i\vec{k}_o \cdot \vec{r}_3} + \sum_n f_n(\theta, \phi) \Phi_n'(\vec{r}_2) \frac{e^{ik_n r_3}}{r_3} \qquad \text{(V-6)}.$$

If we seek a solution of the form,

$$\Psi_o'(\vec{r}_2, \vec{r}_3) = \Phi_o'(\vec{r}_2) g(\vec{r}_2, \vec{r}_3) \qquad \text{(V-7)},$$

the problem is identical in form to equations (1-3) of Chapter IV, and we therefore have as our solution,

$$\Psi_o'(\vec{r}_2, \vec{r}_3) = \Phi_o'(\vec{r}_2) N e^{i\vec{k}_o \cdot (\vec{R} + \vec{\rho})} F(i\nu, 1, ik_o R - i\vec{k}_o \cdot \vec{R}) F(-i\nu, 1, ik_o \rho - i\vec{k}_o \cdot \vec{\rho}) \qquad \text{(V-8)}$$

where,
$$\vec{R} \equiv \frac{1}{2} (\vec{r}_3 + \vec{r}_2) \qquad \text{(V-9)},$$

$$\vec{\rho} \equiv \frac{1}{2} (\vec{r}_3 - \vec{r}_2) \qquad \text{(V-10)},$$

$$N \equiv |\Gamma(1 + i\nu)|^2 \qquad \text{(V-11)},$$

and
$$\nu \equiv 1/k_o \qquad \text{(V-12)},$$

as obtained in Chapter IV. Using equation (IV-36) we have for the excitation cross section,

$$\sigma_{on} = \frac{8\pi}{k_o^2} \int_{k_o-k_n}^{k_o+k_n} \frac{dq}{q^3} \left| \langle n|e^{i\vec{q}\cdot\vec{r}_2}|o\rangle_{\vec{r}_3} \right|^2 [f(\nu,x)]^2 \qquad \text{(V-13)}$$

where,

$$f(\nu,x) = \frac{\pi\nu}{\sinh \pi\nu} F(-i\nu,i\nu,1,x) \qquad \text{(V-14)}$$

and

$$x = \left[\frac{2\Delta\varepsilon + q^2}{2\Delta\varepsilon + 3q^2}\right]^2 \qquad \text{(V-15)},$$

as defined in Chapter IV.

The form factor for electron-helium collisions is given by,

$$F_{on}(\vec{q}) = \sum_{j=1}^{2} \left\{ \int\int d\vec{r}_1 \, d\vec{r}_2 \, \Phi_n^*(\vec{r}_1,\vec{r}_2) \, e^{i\vec{q}\cdot\vec{r}_j} \Phi_o(\vec{r}_1,\vec{r}_2) \right\} \qquad \text{(V-16)}.$$

If we approximate the initial and final helium wave functions by a product of single particle wave functions,

$$\Phi_o(\vec{r}_1,\vec{r}_2) = \Phi_{1S}(\vec{r}_1) \, \Phi_o'(\vec{r}_2) \qquad \text{(V-17-a)}$$

$$\Phi_n^*(\vec{r}_1,\vec{r}_2) = \Phi_{1S}^*(\vec{r}_1) \, \Phi_n'(\vec{r}_2) \qquad \text{(V-17-b)},$$

where the 1S orbital functions are assumed to be normalized to unity and the single particle wave functions for the outer electron are orthogonal for $n \neq o$, equation (V-16) becomes,

$$F_{on}(\vec{q}) \simeq \int d\vec{r}_2 \, \Phi_n^*(\vec{r}_2) \, e^{i\vec{q}\cdot\vec{r}_2} \Phi_o(\vec{r}_2)$$

or

$$F_{on}(\vec{q}) \simeq \langle n | e^{i\vec{q}\cdot\vec{r}_2} | 0 \rangle_{\vec{r}_2} \qquad \text{(V-18)}.$$

Substituting the helium form factor for the matrix element in (V-13) we obtain,

$$\sigma_{on} = \frac{8\pi}{k_o^2} \int_{k_o-k_n}^{k_o+k_n} \frac{dq}{q^3} |F_{on}(\vec{q})|^2 [f(\nu,x)]^2 \qquad \text{(V-19)}$$

or, introducing the generalized oscillator strength,

$$F_{on}(\vec{q}) = \frac{2(\varepsilon_n-\varepsilon_o)}{q^2} |F_{on}(\vec{q})|^2 \qquad \text{(V-20)},$$

$$\sigma_{on} = \frac{4\pi}{k_o^2(\varepsilon_n-\varepsilon_o)} \int_{k_o-k_n}^{k_o+k_n} \frac{dq}{q} F_{on}(\vec{q}) [f(\nu,x)]^2 \qquad \text{(V-21)}.$$

Effective Charge

The purpose of the introduction of an effective charge is to reduce the magnitude of the discarded portion of equation (V-5), (see Chapter IV). This equation and the portion which is discarded are

identical to their counterparts in the e - H system and we therefore conclude that, as before, the effective charge is given by

$$\zeta = \frac{k_o}{k_o + \sqrt{2\varepsilon}} \qquad \text{(V-22)}$$

where ε is defined by equation (V-3). With the inclusion of an effective charge, the solution of (V-5) is given by equation (V-8) - (V-12) with

$$\nu \to \frac{\zeta}{k_o} = \frac{1}{k_o + \sqrt{2\varepsilon}} \qquad \text{(V-23)}$$

in equation (V-12).

Exchange

Account of the exchange of incident and atomic electrons involves the inclusion of spin functions in the wave functions for the system.* The metastable He (1S, nℓ) atom has both an antisymmetric, singlet spin state and a symmetric, triplet spin state. The spin functions for the e - He ($n^{1,3}\ell$) systems can be obtained by combining the spin function for the incident electron with the singlet and triplet He (1S, 2S) spin functions[5]. For the e - He ($n^1\ell$) case the overall spin function is a partially-antisymmetric (the symmetry applies only to the atomic electrons), doublet spin state, while in the e - He ($n^3\ell$) case the overall spin function can be either a partially-symmetric, doublet spin

*A more detailed account is given in reference 67 (see Appendix D).

state or a symmetric, quartet spin state. The total wave functions for the system in the state α are given by,

$$\Psi_\alpha^S(1,2;3) = \frac{1}{\sqrt{3}} \sum_{1,2,3}^{\text{Cyclic}} \Phi_\alpha^S(1,2) F_\alpha(3) X_D^-(1,2;3) \qquad \text{(V-24-a)}$$

and,

$$\Psi_\alpha^T(1,2;3) = \frac{1}{\sqrt{3}} \sum_{1,2,3}^{\text{Cyclic}} \Phi_\alpha^T(1,2) F_\alpha(3) X_{Q,D}^+(1,2;3) \qquad \text{(V-24-b)}$$

where ϕ_α^S and ϕ_α^T are the symmetric and antisymmetric spatial wave functions for singlet and triplet helium, respectively, and $F_\alpha(3)$ is the spatial wave function for the incident electron. These wave functions are now antisymmetric with respect to the interchange of any two electrons.

With the inclusion of spin, the expression for the cross section for the transition between states 0 and n becomes,

$$\sigma_{on} = \frac{k_n}{4\pi^2 k_o} \int d\Omega(\theta,\phi) \Big|_{m_{s_1}} \sum_{m_{s_2}} \sum_{m_{s_3}} \sum \langle \Psi_n(1,2;3) | V(\vec{r}_1,\vec{r}_2,\vec{r}_3) | \Psi_o(1,2;3) \rangle \qquad \text{(V-25)}$$

Using equation (V-24-a) in (V-25) and carrying out the indicated sums, we obtain for the singlet-singlet cross section,

$$\sigma_{on}^{1,1} = \frac{k_n}{k_o} \int d\Omega(\theta,\phi) \left| f_{on}^S - g_{on}^S \right|^2 \qquad \text{(V-26-a)}$$

where f_{on}^S is the direct scattering amplitude for singlet-singlet transitions,

$$f^S_{on} = \frac{-1}{2\pi} \langle \Phi^S_n(1,2) F_n(3) | V | \Phi^S_o(1,2) F_o(3) \rangle \qquad \text{(V-26-b)}$$

and g^S_{on} is the corresponding exchange amplitude,

$$g^S_{on} = \frac{-1}{2\pi} \langle \Phi^S_n(3,2) F_n(1) | V | \Phi^S_o(1,2) F_o(3) \rangle \qquad \text{(V-26-c)}.$$

Similarly, using (V-24-b) in (V-25), we obtain the triplet-triplet cross section,

$$\sigma^{3,3}_{on} = \frac{k_n}{k_o} \int d\Omega(\theta,\phi) \left\{ \frac{1}{3} | f^T_{on} + g^T_{on} |^2 + \frac{2}{3} | f^T_{on} - g^T_{on} |^2 \right\} \qquad \text{(V-27-a)}$$

where f^T_{on} is the direct scattering amplitude for triplet-triplet transition,

$$f^T_{on} = \frac{-1}{2\pi} \langle \Phi^T_n(1,2) F_n(3) | V | \Phi^T_o(1,2) F_o(3) \rangle \qquad \text{(V-27-b)}$$

and g^T_{on} is the exchange amplitude,

$$g^T_{on} = \frac{-1}{2\pi} \langle \Phi^T_n(3,2) F_n(1) | V | \Phi^T_o(1,2) F_o(3) \rangle \qquad \text{(V-27-c)}.$$

Applying the VPS approximation to equations (V-26) and (V-27) and using equation (IV-35) we eventually obtain

$$\sigma^{1,1}_{on} = \frac{8\pi}{k_o^2} \int_{k_o - k_n}^{k_o + k_n} \frac{dq}{q^3} | F_{on}(\vec{q}) |^2 \left[f(\nu,x) - \frac{q^2}{2k_o^2} f(\nu,1/4) \right]^2 \qquad \text{(V-28-a)}$$

and

$$\sigma_{on}^{3,3} = \frac{8\pi}{k_o^2} \int_{k_o-k_n}^{k_o+k_n} \frac{dq}{q^3} |F_{on}(\vec{q})|^2 \left\{ [f(\nu,x)]^2 - \frac{q^2}{k_o^2} f(\nu,x) f(\nu,1/4) + \right. \quad \text{(V-28-b)}.$$

$$\left. \frac{3}{4} \frac{q^4}{k_o^4} [f(\nu,1/4)]^2 \right\}$$

As the energy of the incident electron is increased, $f(\nu,x) \to 1$ and equations (V-28) approach the result obtained by Ochkur[68]. Additionally we note that due to the $1/k_o^2$ dependence of the exchange amplitude, equations (V-28) also approaches (V-19) and thus the Born cross section at high energy.

Results and Discussion

Using the theory discussed above and the form factors computed by Kim and Inokuti,[69] the excitation cross sections for the processes

$$e^- + He(2^{1,3},S) \to e^- + He(n^{1,3},L) \qquad \text{(V-29)}$$

where $n^{1,3}L$ represents the states $2^{1,3}P$, $3^{1,3}S$, $3^{1,3}P$, $3^{1,3}D$, and $4^{1,3}P$, have been calculated as a function of incident electron energy E from threshold up to 500 eV. In Figures 25-a and 25-b we present the 2^1P and 3^1S cross sections calculated to within 1% accuracy, as for all our results, in the Born approximation, VPS approximation (equation V-21), VPS approximation with effective charge (equations V-21 and V-23), and VPS approximation with effective charge and exchange (equations V-28 and V-23). These curves exhibit the typical behavior of the VPS approximations, i.e., the VPS approximation gives a result lower than the Born

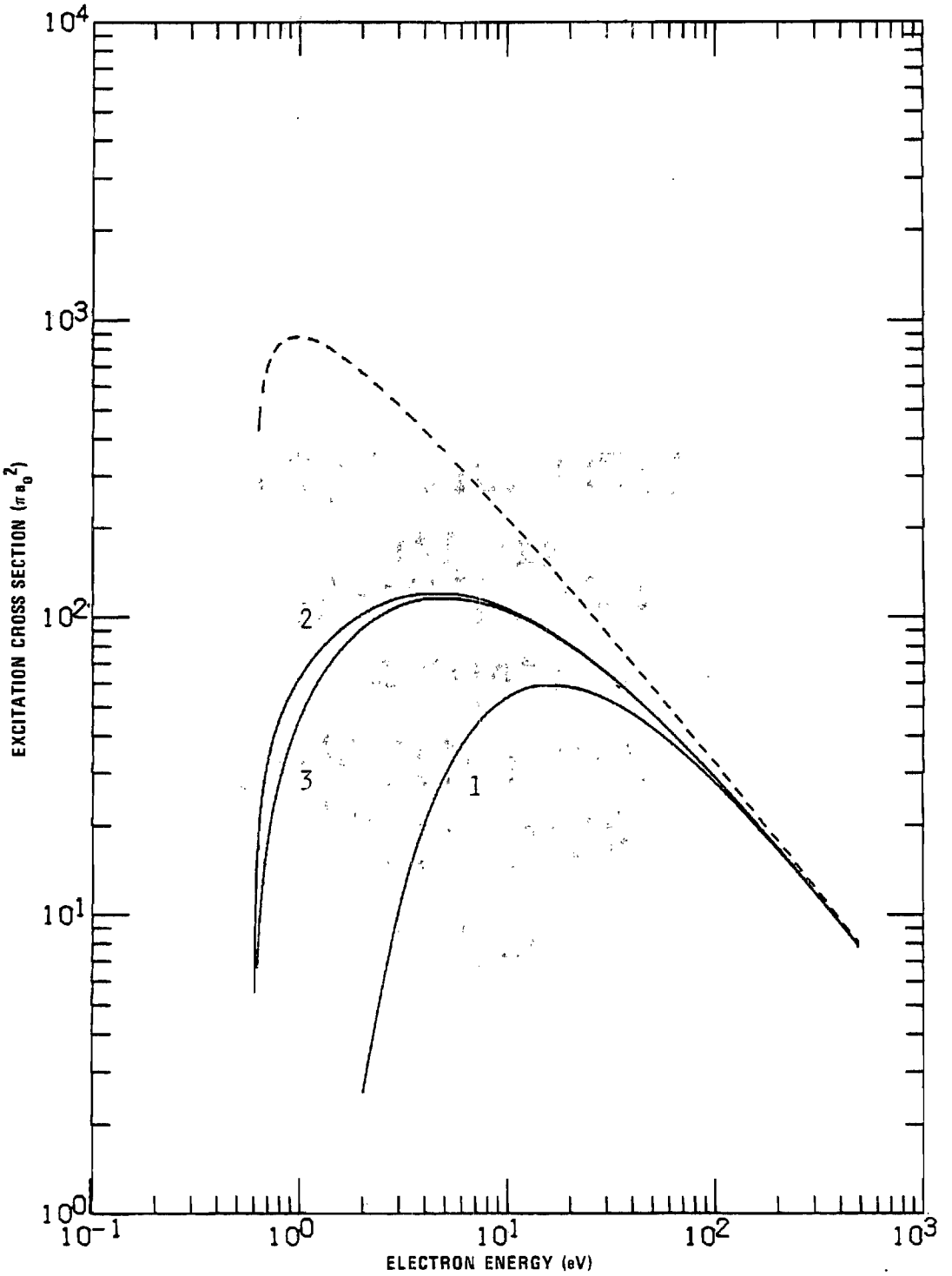

Figure 25-a. The e^- - He, 2^1S - 2^1P Excitation Cross Section; Born (----), VPS (curve 1), VPS with exchange (curve 2), and VPS with effective charge and exchange (curve 3).

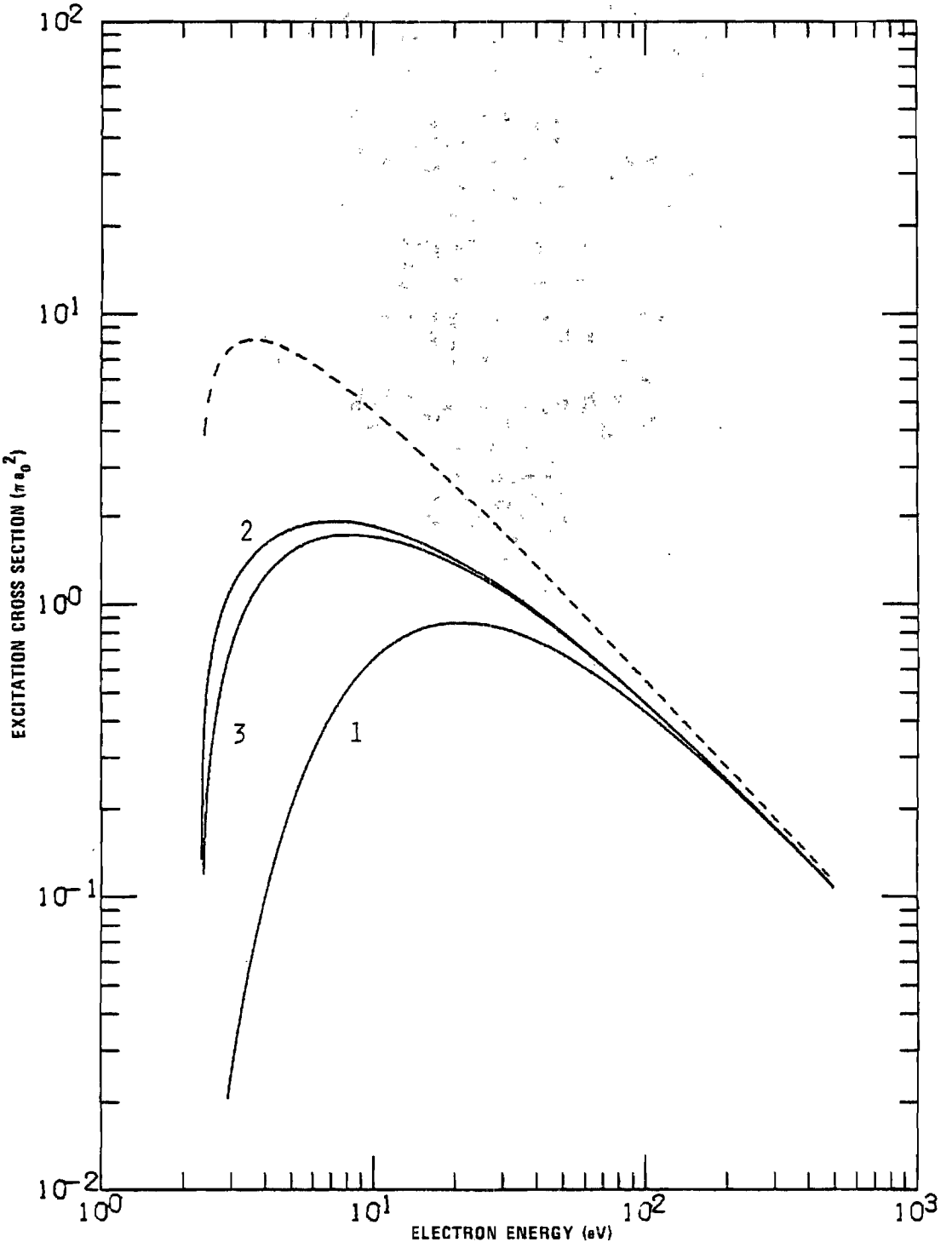

Figure 25-b. The e^- - He, 2^1S - 3^1S Excitation Cross Section; Born (----), VPS (curve 1), VPS with exchange (curve 2), and VPS with effective charge and exchange (curve 3).

cross section, the inclusion of effective charge raises the VPS cross section considerably (reflecting the incomplete screening of the nucleus), and the addition of exchange decreases this result slightly at low energies.

The excitation cross sections in the Born approximation and the VPS approximation with effective charge and exchange are presented in Figures 26, 27, and 28. We have included the close coupling results of Burke et al.[70] in Figure 26 for comparison. In general, these results lie between the VPS and Born approximations (although the agreement is quite good in the 2^3P case) indicating that the VPS may provide a lower bound to the actual cross section, in counterpoint to the Born approximation. In Figures 27 and 28, we note that the cross sections for the optically allowed $2^{1,3}S - 3^{1,3}P$ transitions are smaller than those for the optically forbidden $2^{1,3}S - 3^{1,3}S$, $3^{1,3}D$ transitions at low energies, although the allowed transitions dominate at high energies, as expected, due to their $E^{-1}\ell nE$ dependence. The dip in the 3^3P and 4^3P cross sections are a result of zeroes in the corresponding generalized oscillator strengths, however, Kim and Iuokuti[69] note that these effects may not appear in experimental cross sections due to effects not included in the first Born approximation.

In conclusion, we have obtained the cross section for the excitation of metastable helium by electron impact in two approximations. The Born approximation ignores the distortion of the wave function of the incoming electron, representing the relative motion of target and projectile by a plane wave, resulting in a cross section which is an upper bound to the true cross section. The VPS approximation acknowledges

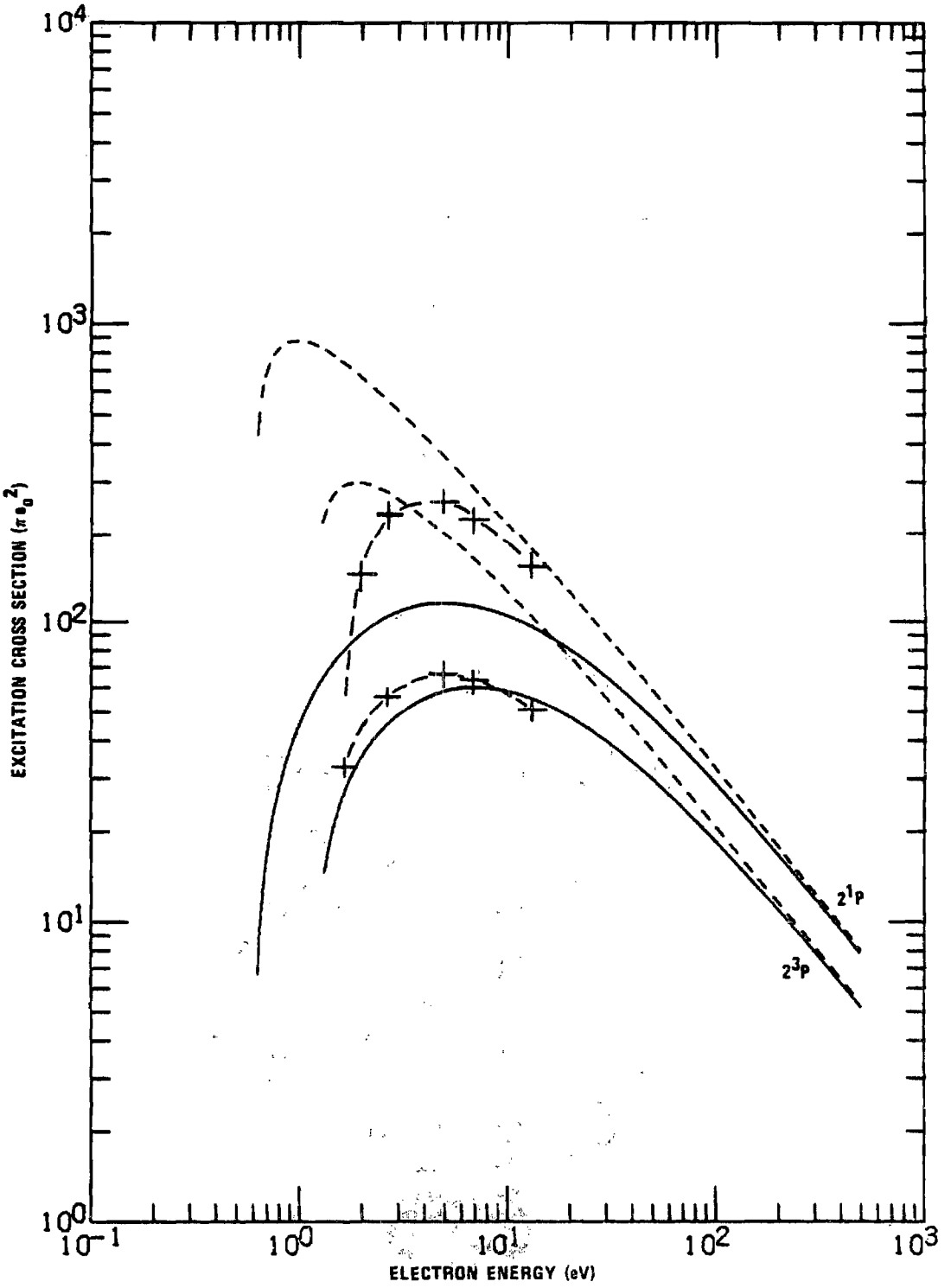

Figure 26. The e^- - He, $2^{1,3}S$ - $2^{1,3}P$ Excitation Cross Sections; Born (----), VPS with effective charge and exchange (——), and the close-coupling results of Burke et al.[70] (-x-x-).

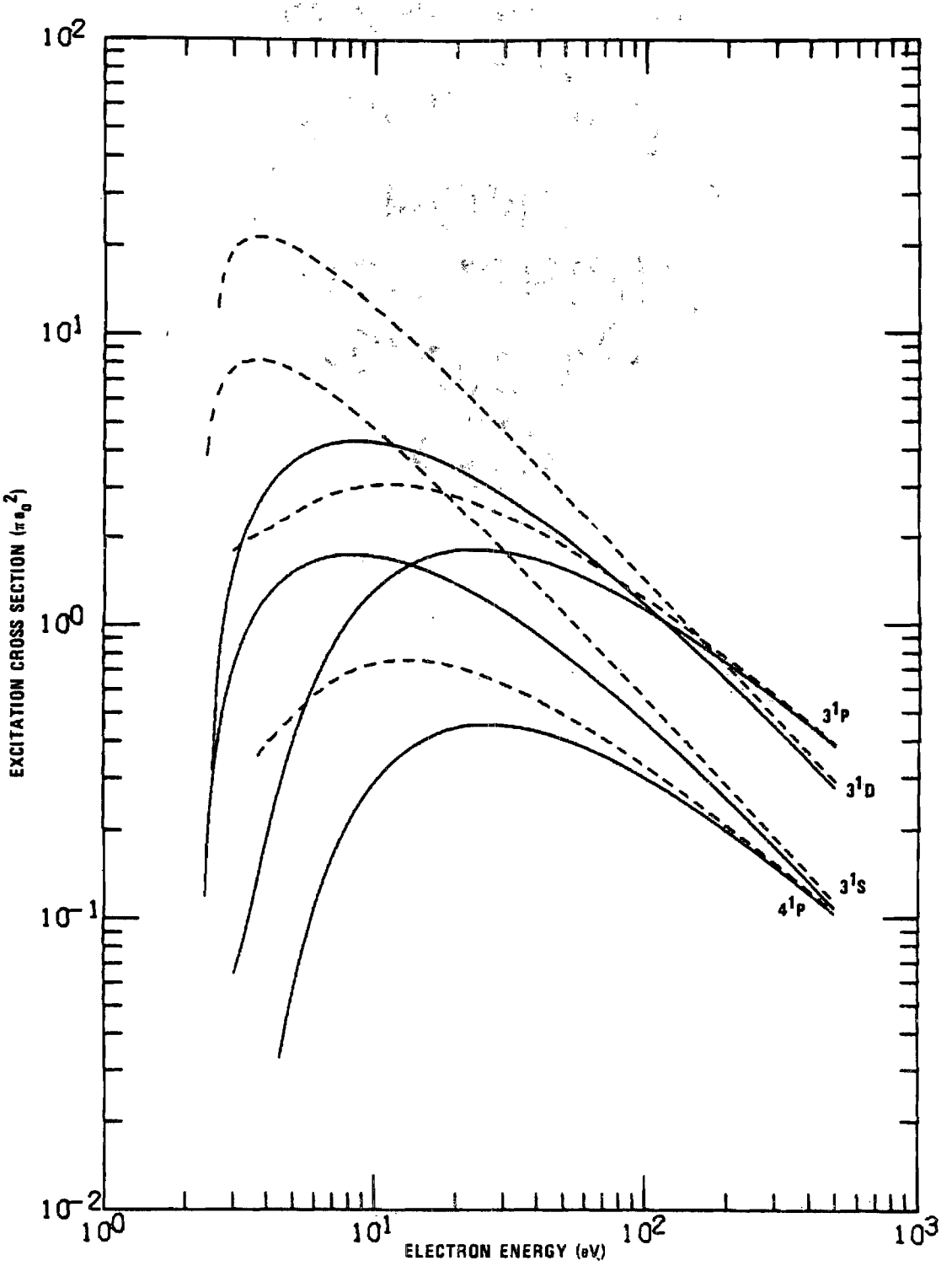

Figure 27. The e^- - He, Singlet-Singlet Excitation Cross Sections; Born (----) and VPS with effective charge and exchange (——).

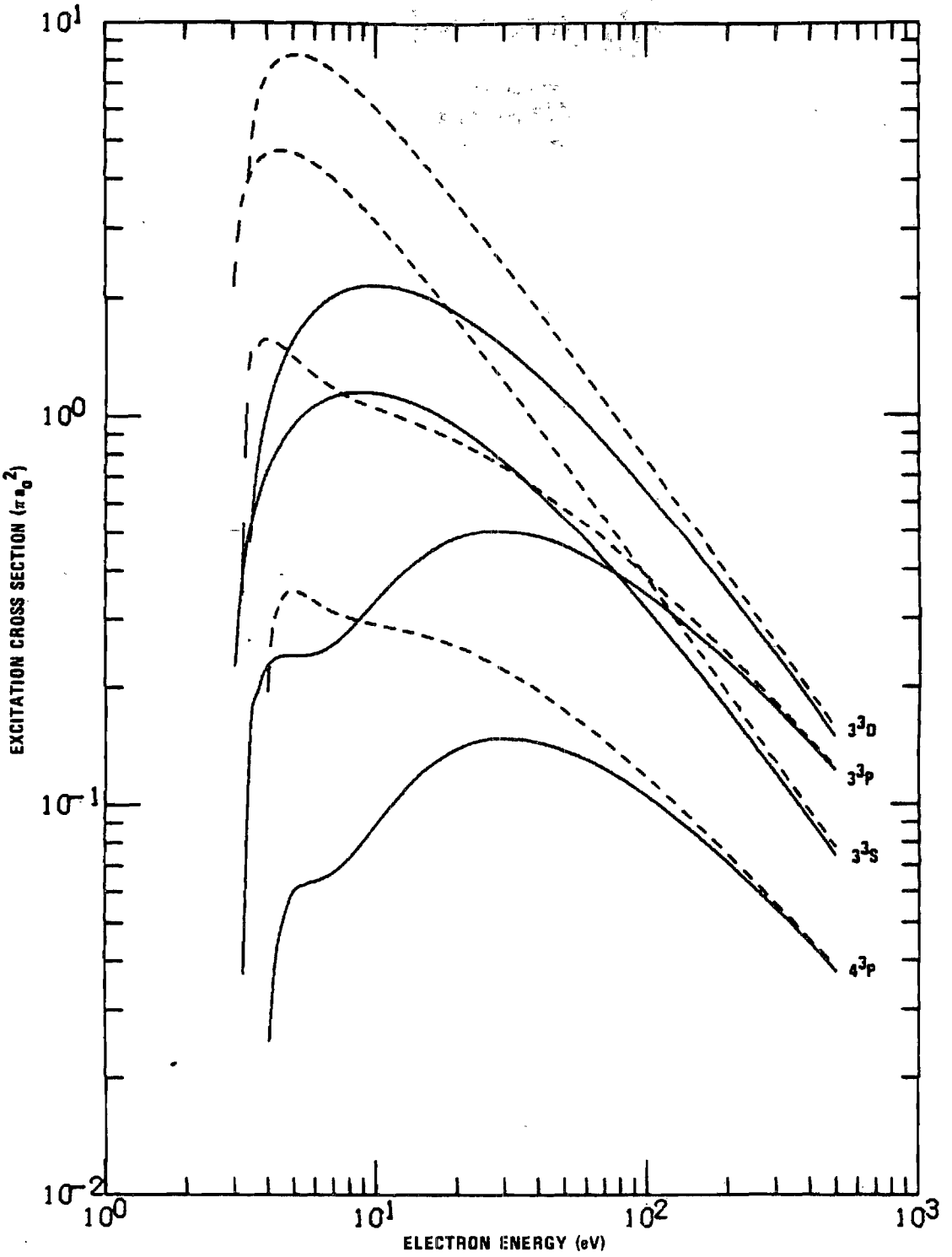

Figure 28. The e^- - He, Triplet-Triplet Excitation Cross Sections; Born (----) and VPS with effective charge and exchange (——).

the importances of the electron-electron repulsion in excitation and incorporates this effect into the wave function for the relative motion of target and projectile. This motion is represented as the interaction of the incident electron and an atomic electron and the motion of their center of mass in the field of a "core", consisting of the nucleus and the remaining orbital electrons. This approximation seems quite good for e - H collisions, as evidenced by the calculations of Vainshtein et al.[56], however in the absence of experimental data its validity is difficult to assess in the e - He case. Since the Born and VPS approximations correspond to two extremes in the representation of projectile-target relative motion, the curves in Figures 26, 27, and 28 may simply represent upper and lower bounds on the true cross sections for the excitation of metastable helium.

PART III

On the Use of the Massey-Mohr Approximation in Atomic Collisions: A Short Comment

CHAPTER VI

INTRODUCTION

Recently, a theoretical description of transitions in electron-atom and heavy particle collisions at intermediate energies has been introduced.[71] In the course of the development of his theory, Flannery has discussed the inclusion of simple approximations, among them the Born. We have subsequently found that the result obtained by Flannery is identical to one obtained by Massey and Mohr[72] in a somewhat different approach. We shall briefly indicate the authors' pertinent steps leading to their final results and demonstrate the equivalence of these results.

Method I; (Massey and Mohr[72])

The scattering of an incident electron by a target atom is described by the coupled equations,

$$[\nabla^2 + k_o^2]\, F_o\,(\vec{R}) = 2\mu \sum_n F_n\,(\vec{R})\, V_{no}\,(\vec{R}) \qquad \text{(VI-1-a)}$$

and

$$[\nabla^2 + k_m^2]\, F_m(\vec{R}) = 2\mu \sum_n F_n(\vec{R})\, V_{nm}\,(\vec{R}),\ m \neq 0 \qquad \text{(VI-1-b)}$$

where $F_o(\vec{R})$ is the wave function for the incident electron at position $\vec{R}$ with respect to the nucleus and μ is the reduced mass of the system. The interactions $V_{nm}(R)$ are defined by

$$V_{nm}(\vec{R}) = \int d\vec{r}\ \Psi_m^*(\vec{r})\ V(\vec{r},\vec{R})\ \Psi_n(\vec{r}) \qquad \text{(VI-2)}$$

where $\vec{r}$ represents the coordinates of the atomic electrons, $\Psi_m^*(\vec{r})$ and $\Psi_n(\vec{r})$ are the initial and final atomic wave functions, and

$$V(\vec{r},\vec{R}) \equiv V_o(\vec{R}) + \sum_{n=1}^{N} V_n(\vec{r}_n - \vec{R}) \qquad \text{(VI-3)}$$

where N is the number of atomic electrons. The first Born approximation is obtained by assuming that

$$F_o(\vec{R}) = e^{i\vec{k}_o \cdot \vec{R}} \qquad \text{(VI-4-a)}$$

and,

$$F_n(\vec{R}) = 0\ ,\ n \neq 0 \qquad \text{(VI-4-b)}$$

on the right hand side of equations (VI-1), which, subject to the usual scattering boundary conditions, have as solutions,

$$F_o(\vec{R}) = e^{i\vec{k}_o \cdot \vec{R}} - \frac{\mu}{2\pi} \int d\vec{R}' \frac{e^{ik_o|\vec{R}-\vec{R}'|}}{|\vec{R}-\vec{R}'|} V_{oo}(\vec{R}')\ e^{i\vec{k}_o \cdot \vec{R}'} \qquad \text{(VI-5-a)}$$

$$\text{and, } F_n(\vec{R}) = -\frac{\mu}{2\pi} \int d\vec{R}' \frac{e^{ik_n|\vec{R}-\vec{R}'|}}{|\vec{R}-\vec{R}'|} V_{on}(\vec{R}')\ e^{i\vec{k}_n \cdot \vec{R}'} \qquad \text{(VI-5-b)}$$

where,

$$-\frac{1}{4\pi}\frac{e^{ik|\vec{R}-\vec{R}'|}}{|\vec{R}-\vec{R}'|} \equiv G_o^+(\vec{R},\vec{R}') = \frac{1}{(2\pi)^3}\int d\vec{k}'\frac{e^{i\vec{k}'\cdot(\vec{R}-\vec{R}')}}{k^2-k'^2+i\varepsilon} \qquad \text{(VI-6)}$$

is the free particle Green's function satisfying the equation,

$$[\nabla^2 + k^2]\, G_o^+(\vec{R},\vec{R}') = \delta(\vec{R}-\vec{R}') \qquad \text{(VI-7)}.$$

The second Born approximation for the elastic case is obtained by using Equations (VI-5) in (VI-1-a) to yield,

$$[\nabla^2+k_o^2]F_o(\vec{R}) = 2\mu V_{oo}(\vec{R})e^{i\vec{k}_o\cdot\vec{R}} - \frac{\mu^2}{\pi}\sum_n V_{no}(\vec{R})\int d\vec{R}'\,\frac{e^{ik_n|\vec{R}-\vec{R}'|}}{|\vec{R}-\vec{R}'|} \qquad \text{(VI-8)}.$$

$$V_{on}(\vec{R}')\, e^{i\vec{k}_o\cdot\vec{R}'}$$

Restricting themselves to sufficiently high incident energies such that $k_n \simeq k_o$ for all n contributing significantly to the sum in (VI-8), and using the closure relationship for the atomic wave functions,

$$\sum_n \psi_n^*(\vec{r})\,\psi_n(\vec{r}') = \delta(\vec{r}-\vec{r}') \qquad \text{(VI-9)},$$

Massey and Mohr obtain in place of (VI-8),

$$[\nabla^2+k_o^2]\ F_o(\vec{R}) = 2\mu V_{oo}(\vec{R})e^{i\vec{k}_o\cdot\vec{R}} - \frac{\mu^2}{\pi}\iint d\vec{R}'d\vec{r}\ \frac{e^{ik_o|\vec{R}-\vec{R}'|}}{|\vec{R}-\vec{R}'|} \qquad \text{(VI-10)}.$$

$$V(\vec{R},\vec{r})\ V(\vec{R}',r)\ |\Psi_o(\vec{r})|^2\ e^{i\vec{k}_o\cdot\vec{R}'}$$

Rewriting this equation we obtain,

$$[\nabla^2+k_o^2]\ F_o(\vec{R}) = 2\mu\ \langle\Psi_o(\vec{r})|V(\vec{R},\vec{r})|\Psi_o(\vec{r})X_o^+(\vec{R},\vec{r})\rangle_{\vec{r}} \qquad \text{(VI-11)}$$

where we have introduced,

$$X_o^+(\vec{R},\vec{r}) \equiv e^{i\vec{k}_o\cdot\vec{R}} - \frac{2\mu}{4\pi}\int d\vec{R}'\ \frac{e^{ik_o|\vec{R}-\vec{R}'|}}{|\vec{R}-\vec{R}'|}\ V(\vec{R}',\vec{r})\ e^{i\vec{k}_o\cdot\vec{R}'} \qquad \text{(VI-12)}.$$

The solution to equation (VI-11) subject to the boundary condition

$$F_o(\vec{R}) \xrightarrow[R\to\infty]{} e^{i\vec{k}_o\cdot\vec{R}} + f(\theta,\phi)\ \frac{e^{ik_oR}}{R} \qquad \text{(VI-13)},$$

is

$$F_o(\vec{R}) = e^{i\vec{k}_o\cdot\vec{R}} - \frac{2\mu}{4\pi}\int d\vec{R}'\ \frac{e^{ik_o|\vec{R}-\vec{R}'|}}{|\vec{R}-\vec{R}'|}\langle\Psi_o(\vec{r})|V(\vec{R}',\vec{r})|\Psi_o(\vec{r}) \qquad \text{(VI-14)}.$$

$$X_o^+(\vec{R}',\vec{r})\rangle_{\vec{r}}$$

The asymptotic behavior of $F_o(R)$ is obtained by using the relation[40]

$$\frac{e^{ik_o|\vec{R}-\vec{R}'|}}{|\vec{R}-\vec{R}'|} \xrightarrow[R \to \infty]{} \frac{e^{ik_oR}}{R} e^{-i\vec{k}_o\cdot\vec{R}'} \qquad \text{(VI-15)},$$

giving us,

$$F_o(\vec{R}) = e^{i\vec{k}_o\cdot\vec{R}} + \frac{e^{ik_oR}}{R}\left[-\frac{\mu}{2\pi} \langle \Psi_o(\vec{r}) e^{i\vec{k}_o\cdot\vec{R}'} | V(\vec{R}',\vec{r}) \right. \qquad \text{(VI-16)}$$

$$\left. | \Psi_o(\vec{r}) X_o^+(\vec{R}',r) \rangle_{\vec{r},\vec{R}'} \right]$$

Comparing equations (VI-16) and (VI-13) we see that the scattering amplitude is given by

$$f(\theta,\phi) = -\frac{\mu}{2\pi} \Psi_o(\vec{r}) e^{i\vec{k}_o\cdot\vec{R}} | V(\vec{R},\vec{r}) | \Psi_o(\vec{r}) X_o^+(\vec{R},\vec{r}) \rangle_{\vec{r},\vec{R}} \qquad \text{(VI-17)}.$$

where, using (VI-6),

$$X_o^+(\vec{R},\vec{r}) - \Phi_{k_o}(\vec{R}) + \frac{2\mu}{(2\pi)^3} \int \frac{d\vec{k}_\alpha \, \Phi_{k_\alpha}(\vec{R}) \langle \Phi_{k_\alpha}(\vec{R}') | V(\vec{R}',\vec{r}) | \Phi_{k_\alpha}(\vec{R}') \rangle_{\vec{R}'}}{k_o^2 - k_\alpha^2 + i\varepsilon} \qquad \text{(VI-18)},$$

in which $\Phi_{k_o}(\vec{R})$ represents a plane wave.

The derivation presented above considers only elastic scattering, however, the inelastic case is equally straight forward, as shown by Rothenstein[73] and also leads eventually to equations (VI-12) or (VI-18).

Method II; (Flannery[71])

The formal solution for the scattering function, describing the collision of an incident projectile of coordinate $\vec{R}$ with a target atom having collective internal coordinates $\vec{r}$, is

$$\psi_i^+(\vec{r},\vec{R}) = \psi_i(\vec{r})e^{i\vec{k}_i\cdot\vec{R}} + \iint d\vec{r}'d\vec{R}'\ G_o^+(\vec{r},\vec{R};\vec{r}',\vec{R}')V(\vec{r}',\vec{R}')\ \psi_i^+(\vec{r}',\vec{R}') \quad \text{(VI-19)},$$

where,

$$G_o^+(\vec{r},\vec{R};\vec{r}',\vec{R}') = \frac{2\mu}{(2\pi)^3}\ S_n\ \Psi_n^*(\vec{r})\Psi_n(\vec{r}')\int d\vec{k}_\alpha\ \frac{e^{i\vec{k}_\alpha\cdot(\vec{R}-\vec{R}')}}{k_n^2-k_\alpha^2+i\varepsilon} \quad \text{(VI-20-a)},$$

or

$$G_o^+(\vec{r},\vec{R};\vec{r}',\vec{R}') = -\frac{2\mu}{4\pi}\ S_n\ \Psi_n^*(\vec{r})\Psi_n(\vec{r}')\ \frac{e^{ik_n|\vec{R}-\vec{R}'|}}{|\vec{R}-\vec{R}'|} \quad \text{(VI-20-b)}.$$

Making the approximation $k_n \simeq k_i$, which is good for sufficiently high impact energies, and using the closure relation, equation (VI-9), equation (VI-20-b) becomes,

$$G_o^+(\vec{r},\vec{R};\vec{r}',\vec{R}') = -\frac{2\mu}{4\pi}\ \frac{e^{ik_i|\vec{R}-\vec{R}'|}}{|\vec{R}-\vec{R}'|}\ \delta(\vec{r}-\vec{r}') \quad \text{(VI-21)}.$$

The $\vec{r}'$ integration in (VI-19) can be completed explicitly using (VI-21), giving us,

$$\Psi_i^+(\vec{r},\vec{R}) = \Psi_i(\vec{r})e^{i\vec{k}_i\cdot\vec{R}} - \frac{2\mu}{4\pi}\int d\vec{R}'\ \frac{e^{ik_i|\vec{R}-\vec{R}'|}}{|R-R'|}\ V(\vec{r},\vec{R}')\Psi_i^+(\vec{r},\vec{R}') \quad \text{(VI-22)}.$$

Flannery suggests the substitution,

$$\Psi_i^+(\vec{r},\vec{R}) = \Psi_i(\vec{r})\ X_i^+(\vec{r},\vec{R}) \tag{VI-23}$$

yielding,

$$X_i^+(\vec{r},\vec{R}) = e^{i\vec{k}_i\cdot\vec{R}} - \frac{2\mu}{4\pi}\int d\vec{R}' \frac{e^{ik_i|\vec{R}-\vec{R}'|}}{|\vec{R}-\vec{R}'|} V(\vec{r},\vec{R}')X_i^+(\vec{r},\vec{R}') \tag{VI-24},$$

which "describes the 'elastic' scattering of a 'fictitious' projectile of original wave number k_i by a 'fixed' multicenter electrostatic interaction $V(r,R)$."[71]

Using equation (VI-6) and

$$\phi_k(\vec{R}) \equiv e^{i\vec{k}\cdot\vec{R}}$$

equation (VI-24) can be written as,

$$X_i^+(\vec{r},\vec{R}) = \phi_{k_i}(\vec{R}) + \frac{2\mu}{(2\pi)^3}\int \frac{d\vec{k}_\alpha \phi_{k_\alpha}(\vec{R})}{k_i^2-k_\alpha^2+i\varepsilon} \langle\phi_{k_\alpha}(\vec{R}')|V(\vec{r},\vec{R}')| \tag{VI-25}.$$

$$X_i^+(\vec{r},\vec{R}')\rangle_{\vec{R}'}$$

If we now replace $X_i^+(\vec{r},\vec{R}')$ on the right hand side of this equation by $\phi_{k_i}(\vec{R}')$, we obtain, Flannery's equation (56),

$$X_i^+(\vec{r},\vec{R}) = \phi_{k_i}(\vec{R}) + \frac{2\mu}{(2\pi)^3}\int \frac{d\vec{k}_\alpha \phi_{k_\alpha}(\vec{R}) \langle\phi_{k_\alpha}(\vec{R}')|V(\vec{r},\vec{R}')|\phi_{k_i}(\vec{R}')\rangle\ \vec{R}'}{k_i^2-k_\alpha^2+i\varepsilon} \tag{VI-26}.$$

which is identical to the result obtained from the work of Massey and Mohr, equation (VI-18).

CONCLUSIONS

The discussion, presented above, of the work of Flannery and of Massey and Mohr is meant only to indicate the differences and similarities in their developments. Flannery began by attempting to solve the general scattering problem, used the Massey-Mohr approximation ($k_n \simeq k_i$) as a simplification, and then considered a Born approximation as one of several simple approximate solutions. Massey and Mohr, on the other hand, started with a Born approximation in mind and then used the approximation, $k_n \simeq k_i$, as a means of simplifying their result. Thus, it would appear that the Massey-Mohr approximation has a much more general application than envisioned by its creators, as shown by Flannery, whose result reduces to theirs in the Born approximation.

APPENDICES

APPENDIX A

TEST OF THE Li^+-He INTERACTION POTENTIAL

Test of the Li^+–He interaction potential*

W. F. Morrison, G. R. Akridge, H. W. Ellis, R. Y. Pai, and E. W. McDaniel

School of Physics, Georgia Institute of Technology, Atlanta, Georgia 30332

L. A. Viehland and E. A. Mason

Brown University, Providence, Rhode Island 02912

(Received 28 April 1975)

The mobility of Li^+ ions in He has been measured at a gas temperature of 300°K over a wide range of E/N, where E is the electric field intensity and N is the gas number density. A new theory of ion mobility is used to calculate from these data the standard Ω integral $\bar{\Omega}^{(1,1)}$ of kinetic theory for Li^+ in He over a range of effective gas temperature extending from 300 to 28 700°K. The *ab initio* quantum mechanical interaction potential for the Li^+–He system computed by Catlow *et al.* is also used to calculate $\bar{\Omega}^{(1,1)}$ as a function of T_{eff}. A comparison of the two sets of data serves as a test of the Catlow potential. The test is extended to still higher effective temperatures (up to 60 000°K) by comparison with values of $\bar{\Omega}^{(1,1)}$ computed from the short-range repulsive potential derived from Li^+ beam scattering experiments in helium. The Catlow potential reproduces the general features of the dependence of the "experimental" Ω integral on T_{eff} over the entire range of the test. However, significant discrepancies exist; they could be resolved by making substantial alterations in the Catlow potential in the region of short ion–atom separation distance and smaller adjustments in the region of the potential minimum.

In the last few years *ab initio* quantal calculations of the Li^+–He interaction potential which are in substantial agreement have been reported.[1,2] This "Catlow" potential has been tested by computing various quantities which depend upon it, such as the total and momentum-transfer elastic scattering cross sections, and comparing the theoretical results with the available experimental data. We report here a new kind of test of the Catlow potential, the first to cover a wide range of ion–atom separation distances using a single type of experimental data.

Our work is based on a recently developed theory of ion mobility.[3] The primary conditions required by the theory are that the ions be present only in trace amounts and that only binary, elastic ion–atom collisions occur; these conditions are always met in experimental measurements of Li^+ mobility in He. Unlike previous approaches,[4] this theory is not restricted to a specific ion–atom mass ratio or interaction potential and it applies at arbitrarily high values of E/N, the ratio of the electric field intensity to the gas number density. In first approximation the drift velocity v_d (related to the mobility K by $v_d = KE$) is given by

$$v_d = \frac{3}{8}\frac{eE}{N}\left(\frac{\pi}{2\mu k T_{eff}}\right)^{1/2}\frac{1}{\bar{\Omega}^{(1,1)}(T_{eff})}, \tag{1}$$

where e is the ion charge, μ is the ion–atom reduced mass, k is Boltzmann's constant, and where the effective temperature T_{eff} is given in terms of the gas temperature T and the atomic mass M by

$$T_{eff} = T(1 + Mv_d^2/3kT) . \tag{2}$$

Equation (1) shows that the ion–atom potential affects v_d only through the collision integral

$$\bar{\Omega}^{(1,1)}(T_{eff}) = \tfrac{1}{2}(kT_{eff})^{-3}\int_0^\infty \epsilon^2 Q^{(1)}(\epsilon)\exp(-\epsilon/kT_{eff})d\epsilon , \tag{3}$$

where $Q^{(1)}$ is the momentum-transfer (diffusion) cross section

$$Q^{(1)}(\epsilon) = 2\pi\int_0^\pi (1-\cos\theta)I(\theta)\sin\theta\, d\theta . \tag{4}$$

In these equations ϵ and θ are the kinetic energy and scattering angle for an ion–atom collision in the center-of-mass system, and $I(\theta)$ is the differential cross section for elastic scattering, a quantity which can be calculated from the ion–atom potential.[4] As a final note, both $\bar{\Omega}^{(1,1)}$ and $Q^{(1)}$ are equal to πd^2 for the collision of classical rigid spheres of diameter d.

The important feature of this new theory of ion mobility is that it shows that v_d depends only upon T_{eff}, so that variation of E/N at constant T in mobility measurements is equivalent to variation of T at constant E/N. This is important because much higher average ion energies can be achieved by operating at high values of E/N than can be obtained by heating the drift tube to the highest possible T. In summary, ion mobility measurements as a function of E/N at constant T can be used to obtain $\bar{\Omega}^{(1,1)}$ as a function of T_{eff} over a wide range of effective temperature, and these values can then be used to test the accuracy of an *ab initio* potential over a wide range of ion–atom separation.

The mobility of Li^+ ions (of mass 7 amu) moving in He at 300 °K has recently been measured over a wide range of E/N.[5] The accuracy of these measurements was 2%, except at the highest value of E/N, where the experimental error may be as high as ±5%. The average energy of the Li^+ ions ranged from 0.04 eV at the lowest value of E/N to 10.11 eV at the highest value. Using these data in Eqs. (1), (2) we have calculated $\bar{\Omega}^{(1,1)}$ as a function of T_{eff}, which ranged from 304 °K at the lowest value of E/N to 28 700 °K at the highest value. The results are plotted in Fig. 1, where the short-dash curve has been drawn through the many drift tube data points for $T_{eff} \leq 4650$ °K. (These data points have little scatter and only one is shown.) At large values of E/N (i.e., high T_{eff}), fewer data were collected because of the lower counting rates resulting from increased trans-

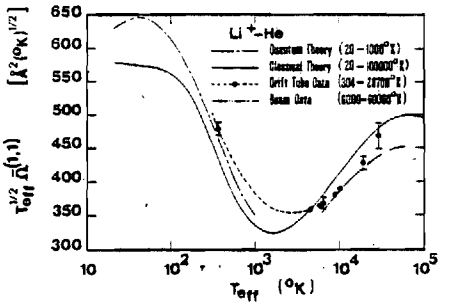

FIG. 1. $T_{\rm eff}^{1/2}\bar{\Omega}^{(1,1)}$ as a function of $T_{\rm eff}$. The curves labeled "Drift Tube Data" and "Beam Data" were obtained by analysis of experimental results, while those labeled "Classical Theory" and "Quantum Theory" were obtained by calculations based on the Catlow Potential. Many drift tube data were taken for $T_{\rm eff} \leq 4650\,^\circ$K; they are represented by the short-dash curve extending from 304 to 4650 °K. Above 4650 °K, drift tube data were taken at six values of $T_{\rm eff}$: 6030, 6800, 9070, 10 400, 19 500, and 28 700 °K. Data points are shown for these six temperatures. The error bars on the data points reflect only the experimental error associated with the drift velocity measurements. Additional error arises from the use of the first-order expression [Eq. (1)] rather than an exact expression for $\bar{\Omega}^{(1,1)}$ in terms of v_d.

verse diffusion in the drift tube. The data above about 4650 °K are insufficient in number to determine a curve, and are plotted as points. The point near 28 700 °K exhibits an especially large uncertainty. Here the small cross section for the Li^+–He system and the correspondingly small number of collisions are probably only marginally consistent with the swarm model used to analyze the experimental data, in spite of the very long ionic drift distance (up to 44 cm).

Because the ion mobility theory of Ref. 3 has been used only in its first approximation, the $\bar{\Omega}^{(1,1)}$ curve is more inaccurate than the 2% inaccuracy attributable to most of the mobility measurements. Based on the considerations given in Ref. 3, we estimate that, compared with the true results that would be obtained by using an infinite order approximation, the "Drift Tube Data" $\bar{\Omega}^{(1,1)}$ values shown in Fig. 1 are between 1.5% too low and 2.5% too high at temperatures near 300 °K and between 4% and 8% too high at high temperatures ($\gtrsim 10^4$ °K).

Li^+ beam scattering experiments with He targets[5] have led to the short-range, repulsive interaction potential

$$V(r) = 15.73\exp(-2.704\,r) \quad 1.47 < r < 2.29, \tag{5}$$

where the energy V and the separation distance r are expressed in atomic units (27.210 eV and 5.2917×10^{-9} cm, respectively). Using this potential and the tabulations available in the literature,[7] we have obtained the $\bar{\Omega}^{(1,1)}$ curve shown in Fig. 1 that is labeled "Beam Data." Since the potential (5) was claimed[6] to be accurate to 10%, the accuracy of this curve is 4%. Note that the $\bar{\Omega}^{(1,1)}$ curve can be valid only over a range of temperature (estimated[8] to be 6000–60 000 °K) because the potential (5) is restricted to a small range of Li^+–He separation. Comparison of the two sets of "experimental" $\bar{\Omega}^{(1,1)}$ data, one derived from ion mobility measurements and the other from beam scattering studies, shows them to be in excellent agreement over the range 10 000–20 000 °K.

In order to facilitate the theoretical calculation of $\bar{\Omega}^{(1,1)}$ from Eqs. (3), (4) we have fitted the Catlow potential by the expression

$$V(r) = \begin{cases} 16.93\exp(-2.6306r) + (3.476\times10^{-7})\,r^{-12} & r < 1.29\,, \\ 24.69\exp(-2.6325r) - 0.7152\,r^{-4} & 1.29 < r < 8\,, \\ -(2.923\times10^{-4})\exp(-0.4933r) - 0.692\,r^{-4} & r > 8\,, \end{cases} \tag{6}$$

in atomic units. A classical calculation of $\bar{\Omega}^{(1,1)}$ from this potential was made by using the Smith–O'Hara computer program.[9] The results, with a numerical accuracy of 0.1%, are shown in Fig. 1. The quantal calculation of $\bar{\Omega}^{(1,1)}$ from the potential (6) involved the evaluation of $Q^{(1)}$ by the phase-shift method according to the equation[10]

$$Q^{(1)}(\epsilon) = (4\pi/\kappa^2)\sum_{l=0}^{\infty}(l+1)\sin^2(\delta_l - \delta_{l+1})\,, \tag{7}$$

where δ_l is the lth order phase shift and κ is the wave number associated with ϵ. The phase shifts were evaluated by integration of the Schrödinger equation using a Numerov technique, the criterion for convergence being that two successive evaluations agree within 10^{-3} rad. The effect of the long-range polarization tail of the potential was taken into account[11] by using the JWKB approximation. The momentum-transfer cross section $Q^{(1)}$ is evaluated for κ in the range 10^{-3}–30 a.u., convergence being assumed when the ratio of the lth partial cross section to the sum was less than 10^{-5} for ten successive terms. In general, fewer than 100 phase shifts were required to achieve convergence, except at the highest energies where up to 200 were needed. The over-all numerical accuracy of the quantal $\bar{\Omega}^{(1,1)}$ calculations is 0.2%.

It should be noted from Fig. 1 that the classical and quantal $\bar{\Omega}^{(1,1)}$ curves computed from the Catlow potential are still distinguishable at 1000 °K. In way of contrast, He–He interaction potentials give indistinguishable results above room temperature. The enhanced persistence of the classical–quantal difference in ion–atom systems is a direct result of the presence of the long-range polarization tail of the potential, and is discussed in detail in the Appendix.

The ability of the Catlow potential, demonstrated in

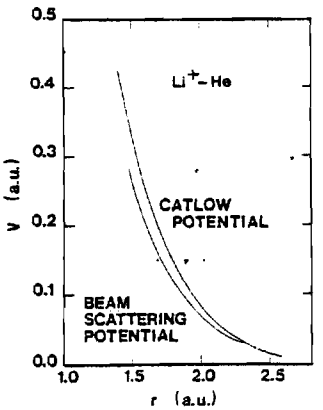

FIG. 2. The potential energy V as a function of the Li^+-He separation distance r in the region of small r. The "Beam Scattering" curve was obtained from Eq. (5), the "Catlow" curve from Eq. (6).

Fig. 1, to reproduce the general features of the "experimental" $\bar{\Omega}^{(1,1)}$ dependence on T_{eff} over the full range from 300–60 000° K is impressive. However, close examination reveals some problems, which will now be discussed.

Let us first compare the theoretical and experimental $\bar{\Omega}^{(1,1)}$ curves above 10 000° K. We note that in the range 10 000–20 000° K both sets of experimental data lie about 8% lower than the curve calculated from the Catlow potential. This discrepancy cannot be attributed to classical–quantal deviations in the theoretical curve; from the Appendix we estimate that such deviations should be less than 1% above 10 000° K. Next we note that between 20 000 and 60 000° K the discrepancy between the $\bar{\Omega}^{(1,1)}$ values calculated from the beam data and the Catlow potential persists at the level of 8%–10%. In this region above 20 000° K only a single drift tube measurement (of considerable uncertainty) was made, and little weight should be given to the $\bar{\Omega}^{(1,1)}$ value obtained from this measurement. Since both the magnitude and the direction of the 8%–10% discrepancy between the theoretical and experimental $\bar{\Omega}^{(1,1)}$ curves above 10 000° K conflict with the error limits for these curves previously discussed, we consider this discrepancy at high temperatures to be significant. It could be eliminated by making a substantial modification in the Catlow potential at small r. In Fig. 2 we have plotted $V(r)$ from Eqs. (5) and (6) in the region of small r, and it can be seen that the potentials differ by as much as 23%.

We next note from Fig. 1 that the theoretical and experimental $\bar{\Omega}^{(1,1)}$ curves show a slight discrepancy at 300° K. To be specific, using the quantal, theoretical value for $\bar{\Omega}^{(1,1)}$ (300° K) in Eq. (1) gives a value for the reduced mobility[4] of 23.78 cm^2/V-sec, which on the basis of the error analysis given previously should be too low (by no more than 0.5%, or 0.12 cm^2/V-sec). The experimental value[3] is 23.1 ± 0.5 cm^2/V-sec. We see therefore that the experimental and theoretical values do not lie within the combined error limits. We interpret this discrepancy as reflecting an inaccuracy in the Catlow potential in the region of the potential minimum.

In conclusion, we believe that this new test of the Catlow potential that we have presented indicates that this potential is inaccurate at short ion–atom separations, and may also be slightly inaccurate in the region of the potential minimum. Since the Li^+-He system has only four electrons and is one of the simplest systems to treat theoretically, and since the Catlow potential is the result of the most accurate calculations to date for this system, we conclude that experimental measurements still contain more detailed information about ion–atom interaction potentials than can readily be obtained from *ab initio* calculations.

APPENDIX

In the "intermediate" temperature region where quantal deviations from classical behavior are small, a semiclassical treatment of the scattering phase shifts leads to an expansion of the cross sections and collision integrals in powers of the square of Planck's constant.[12–14] For an inverse power potential of the form

$$V(r) = Cr^{-n}, \tag{A1}$$

the results become particularly simple;[15] dropping terms of the order of the fourth power of Planck's constant we find that

$$\bar{\Omega}^{(1,1)}_{\text{quantal}}(T) = \bar{\Omega}^{(1,1)}_{\text{classical}}(T)[1 + DT^{(2/n)-1}], \tag{A2}$$

where D is a constant. For atom–atom systems the potential behaves as r^{-6} at long range, so the percentage deviation of $\bar{\Omega}^{(1,1)}_{\text{quantal}}(T)$ from $\bar{\Omega}^{(1,1)}_{\text{classical}}(T)$ is proportional to $T^{-2/3}$. Similarly, the percentage error is proportional to $T^{-1/2}$ for ion–atom systems where the potential varies as r^{-4} at long range. Thus the temperature T' at which an ion–atom system exhibits the same percentage deviation as an atom–atom system (of comparable mass and similar potential) does at temperature T should be

$$T' \sim T^{4/3}. \tag{A3}$$

This suggests that the percentage error exhibited by He–He at $T = 300°$ K should be approximately equal to that exhibited by Li^+-He at 2000° K. Thus the classical–quantal differences discussed in the text for Li^+-He are not unexpected; they are a direct result of the long-range r^{-4} tail of the potential.

*Research supported by the Office of Naval Research and the National Science Foundation. Approved for public release; distribution unlimited.

[1]G. W. Catlow, M. R. C. McDowell, J. J. Kaufman, L. M. Sachs, and E. S. Chang, J. Phys. B 3, 833 (1970). The potential appearing in this paper and called by us the "Catlow" potential was actually calculated by J. J. Kaufman.
[2]M. Krauss, P. Maldonado and A. C. Wahl, J. Chem. Phys. 54, 4944 (1971).
[3]L. A. Viehland and E. A. Mason, Ann. Phys. (N.Y.) (in press).
[4]E. W. McDaniel and E. A. Mason, *The Mobility and Diffusion*

of Ions in Gases (Wiley, New York, 1973).
[5]G. R. Akridge, H. W. Ellis, R. Y. Pai, and E. W. McDaniel, J. Chem. Phys. 62, 4578 (1975).
[6]H. Inouye and S. Kita, J. Chem. Phys. 57, 1301 (1972).
[7]L. Monchick, Phys. Fluids 2, 695 (1959).
[8]J. O. Hirschfelder and M. A. Eliason, Ann. N.Y. Acad. Sci. 67, 451 (1957).
[9]H. O'Hara and F. J. Smith, Comp. Phys. Comm. 2, 47 (1971).
[10]E. W. McDaniel, *Collision Phenomena in Ionized Gases* (Wiley, New York, 1964), p. 443.
[11]A. S. Dickinson, J. Phys. B 1, 395 (1968).
[12]J. de Boer and R. B. Bird, Phys. Rev. 83, 1259 (1951).
[13]J. de Boer and R. B. Bird, Physica (Utr.) 20, 135 (1954).
[14]H. T. Wood and C. F. Curtiss, J. Chem. Phys. 41, 1167 (1964).
[15]J. O. Hirschfelder, C. F. Curtiss and R. B. Bird, *Molecular Theory of Gases and Liquids* (Wiley, New York, 1964), Ch. 10.

APPENDIX B

THE Li^+-He INTERACTION POTENTIAL

Reprinted from The Journal of CHEMICAL PHYSICS Vol. 66, No. 11 1 June 1977

The Li^+–He interaction potential*

I. R. Gatland, W. F. Morrison, H. W. Ellis, M. G. Thackston, and E. W. McDaniel

School of Physics, Georgia Institute of Technology, Atlanta, Georgia 30332

M. H. Alexander

Department of Chemistry, University of Maryland, College Park, Maryland 20742

L. A. Viehland and E. A. Mason

Brown University, Providence, Rhode Island 02912

(Received 8 February 1977)

New measurements of the mobility of Li^+ ions in He gas at 300°K are reported for a wide range of E/N, the ratio of the electric field strength to the gas number density. These data are used in conjunction with kinetic theory to test various Li^+–He interaction potentials over a wide range of separation distance. It is shown that the *ab initio* potential of Hariharan and Staemmler gives mobility values in excellent agreement with experiment at low and moderate E/N, but that significant discrepancies exist at high E/N. The mobility data are also directly inverted to give the Li^+–He interaction potential. This directly determined potential is in excellent agreement with the *ab initio* at intermediate and long range, but differs significantly in the short-range region. In the latter region, however, it is in agreement with the potential obtained by analysis of beam-scattering experiments.

I. INTRODUCTION

Recent developments[1] in the kinetic theory of ion motion in gases under the influence of arbitrarily large external electric fields now permit accurate calculations of ion mobilities for systems with centrally symmetric ion–neutral potentials when the potentials are available.[2] Such calculations allow mobility measurements to be used to obtain information on ion–neutral interactions. We report here a comprehensive study of one of the simplest systems to which this theory can be applied, the Li^+–He combination. This work refines and extends a previous study[3] of the Li^+–He system. In particular, five main features may be noted, as follows:

(1) New experimental measurements of the mobility of Li^+ in He have been carried out which extend the data to higher E/N (ratio of electric field strength to neutral gas number density) with considerable improvement in accuracy. Details are given in Sec. II.

(2) Quantum effects on the momentum-transfer and other transport collision integrals used in this work have been carefully investigated, since the earlier study[3] indicated the presence of unexpectedly large quantum deviations from classical behavior. The results are presented in Sec. III, where it is shown that the deviation is only about 1% at 3°K, and that quantum effects at thermal energies and above are insignificant.

(3) Convergence errors in the kinetic-theory formulas have been investigated and greatly reduced. The previous study[3] used only first-order kinetic theory, and the resulting convergence errors were estimated to range from −1.5% to +8% over the energy range of the mobility measurements. The present calculations have been carried to third-order kinetic-theory approximation, for which the convergence errors are estimated[4] to be less than the experimental uncertainty in the mobility measurements. In addition, comparison has been made with an independent calculation of mobilities for Li^+ in He by Lin and Bardsley[5] using a Monte Carlo method. Our calculations agree within 1%.

(4) New theoretical Li^+–He potentials have become available since the previous study,[3] which tested only the self-consistent-field (SCF) potential calculated by Catlow *et al.*[5] and by Krauss *et al.*[7] In particular, both a coupled electron pairs approximation (CEPA) potential[8] and an electron gas-Drude model (EGDM) potential[9] have been used to calculate mobilities in the present work, in addition to the older SCF potential. These calculations, which include the investigation of the kinetic-theory convergence errors, are described in Sec. IV.

(5) An iterative, direct-determination inversion procedure[10] has been used to obtain a potential which fits the mobility data. This new potential is very close to the CEPA potential of Hariharan and Staemmler except in the repulsive core above 0.1 eV, where it is about 15% lower than the theoretical potential but in good agreement with the results of beam experiments.[11] The direct determination of the potential from the mobility data is described in Sec. V.

II. EXPERIMENT

The reduced mobility of Li^+ ions (of mass 7 amu) in He gas was measured at 300 °K as a function of E/N. The instrument used was the Georgia Tech drift tube mass spectrometer, which has been described previously.[12,13] Swarms of Li^+ ions were allowed to drift through He gas along a variable drift distance which ranged from 25 to 44 cm. The mobility K (defined as v_d/E, the ratio of the drift velocity to the electric field strength) is inversely proportional to the number density of the neutral gas. The results were normalized to the number density at 0 °C and a pressure of 760 torr via the relation $K_0 = K(P/760)(273.16/T)$, where K_0 is the "reduced" mobility, P is the gas pressure in torr, and T is the gas temperature in °K. The neutral gas

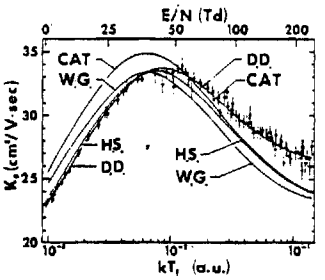

FIG. 1. The reduced mobility K_0 of Li^+ ions in He as a function of E/N and of the effective thermal collision energy kT_f, which is derived from the E/N and K_0 values using first order kinetic theory. The effective temperatures range from 300 °K ($kT_f = 10^{-2}$ a.u.) to 30 000 °K ($kT_f = 10^{-1}$ a.u.) with the mobility peak around 3000 °K ($kT_f = 10^{-2}$ a.u.). The points represent the experimental measurements, and the curves are calculated from various potentials as follows: CAT is the self-consistent field potential of Catlow *et al.* and Krauss *et al.* (Refs. 6 and 7), W. G. is the electron gas–Drude model potential of Waldman and Gordon (Ref. 9), H. S. is the coupled electron pair approximation of Hariharan and Staemmler (Ref. 8), and D. D. is our potential determined directly from the experimental data.

pressure used in the experiment varied, but was always less than 1 torr. The Li^+–He system presents experimental difficulties at these pressures owing to the rather small collision cross section. The present data, obtained with an improved Li^+ source, represent an improvement over measurements reported earlier[14] on the Li^+–He system. About 100 mobility runs were made, at E/N ranging from 2 to 230 Td (1 Td = 10^{-17} V-cm²); the average ion energy varied from thermal up to about 15 eV in the laboratory reference frame.

The major systematic error in the data occurs in the measurement of the neutral gas pressure, for which a capacitance manometer was used. Shortly before the data on Li^+–He were collected, this instrument was calibrated by carefully measuring the mobility of K^+ ions in N_2 gas at low values of E/N, and comparing this result with the accepted value of 2.54 cm²/V-sec. Sufficient data were then taken on Li^+ in He to establish a curve of reduced mobility as a function of E/N whose total error is believed not to exceed ±2% for $E/N \leq 75$ Td, ±3% for 75 Td < $E/N \leq 150$ Td, and ±4% for $E/N > 150$ Td. The experimental data are displayed as points in Fig. 1.

III. CLASSICAL-QUANTAL DEVIATIONS

Use of the kinetic theory of gaseous ion transport[1] requires the calculation of collision integrals and cross sections of the form

$$\Omega^{(l,s)}(T_{eff}) = [(s+1)!\,(k_B T_{eff})^{s+2}]^{-1} \times \int_0^\infty \exp(-\epsilon/k_B T_{eff})\,\epsilon^{s+1}\,Q^{(l)}(\epsilon)\,d\epsilon\,, \quad (1)$$

$$Q^{(l)}(\epsilon) = 2\pi\left[1 - \frac{1+(-1)^l}{2(l+1)}\right]^{-1} \int_0^\pi (1-\cos^l\theta)\,\sigma(\epsilon,\vartheta)\sin\vartheta\,d\vartheta, \quad (2)$$

where T_{eff} is an effective temperature discussed in the next section, k_B is Boltzmann's constant, ϵ and ϑ are the kinetic energy and scattering angle for an ion–neutral collision in the center-of-mass frame, and $\sigma(\epsilon,\vartheta)$ is the differential cross section for elastic scattering, a quantity that can be calculated either by classical or quantum mechanical methods from the ion–neutral interaction potential.[13] The normalization factors in Eqs. (1)–(2) have been chosen so that both $\Omega^{(1,s)}$ and $Q^{(1)}$ are equal to πd^2 for the collision of rigid spheres of diameter d.

Since quantal calculations of the collision integrals are much more difficult than classical calculations, it is important to investigate the conditions under which the quantal calculations can be dispensed with owing to negligible classical–quantal deviations. At very low temperatures, of course, classical calculations become quite inaccurate.[12] Furthermore, earlier calculations[3] suggested that classical–quantal deviations for an ion–atom system persisted to higher temperatures than would be the case for a comparable atom–atom system, owing possibly to the long-range r^{-4} tail. Such qualitative arguments shed little light, however, on the magnitude of the deviations for the Li^+–He system at thermal energies and above.

In Ref. 3 we reported classical–quantal deviations as large as 10%, a surprising result which we attempted to rationalize by a qualitative argument based on a supposed similarity of the He–He and Li^+–He interaction potentials. Re-examination of the calculations in Ref. 3 showed that the number of quantal cross sections used was insufficient to fully define the oscillations in $Q^{(1)}$ as ϵ varies. We have therefore recalculated $\Omega^{(1,1)}$ using the same SCF interaction potential,[6,7] an improved integration routine, and four times as many $Q^{(1)}$ values to be sure to include all oscillations. The result of this recalculation is that the quantal values of $\Omega^{(1,1)}$ now agree with the classical values within the combined accuracy of the numerical procedures down to 5 °K.

As a further check, we have calculated momentum-transfer cross sections $Q^{(1)}(\epsilon)$ for the Hariharan and Staemmler CEPA potential[8] using both classical and full quantal methods. The quantal phase shifts were calculated by the Gordon algorithm,[13] which is especially suited to long-range potentials. Calculations of $Q^{(1)}$ were carried out at 41 energies on a logarithmic scale over the energy range $10^{-6.5}$ a.u. (about 10^{-5} eV or 0.1 °K) to $10^{-2.5}$ a.u. (about 10^{-1} eV or 1000 °K). Below 10^{-5} a.u. (3 °K) the quantal results exhibit order-of-magnitude oscillations about the classical curve; above 10^{-5} a.u. the oscillations persist but differ from the classical values by at most 10%; above $10^{-3.5}$ a.u. (100 °K) the quantal and classical results agree to within 1%. Above the orbiting region ($\epsilon > 10^{-2.27}$ a.u. or 335 °K) the cross sections drop sharply away from the values given by a pure r^{-4} polarization potential, and the quantal and classical results become virtually identical.

TABLE I. Potential energy of Li^+–He as a function of internuclear separation (both in atomic units, i.e., 27.211 eV and 0.52917 Å) for three theoretical potentials,[6–8] for the potential obtained in this paper by directly inverting mobility data, and as obtained from beam-scattering experiments.[11]

Internuclear separation	EGDM[9] (Waldman and Gordon)	SCF[6,7] (Catlow *et al.*)	CEPA[8] (Hariharan and Staemmler)	Direct determination[a]	Beam exptl[11] (Inouye and Kita)
10.00	−0.000070		−0.000071	−0.000070	
9.00	−0.000107		−0.000109	−0.000110	
8.00	−0.000171	−0.000181	−0.000176	−0.000180	
7.00	−0.000294	−0.000298	−0.000306	−0.000310	
6.00	−0.000549	−0.000544	−0.000582	−0.000600	
5.50	−0.000775	−0.000765		−0.000850	
5.00	−0.001128	−0.001101	−0.001219	−0.001270	
4.50	−0.001640	−0.001591	−0.001775	−0.001810	
4.00	−0.002298	−0.002171	−0.002450	−0.002480	
3.75	−0.002520		−0.002703	−0.002710	
3.50	−0.002470	−0.002259	−0.002678	−0.002590	
3.25	−0.001700		−0.001983	−0.001910	
3.00	0.000697	0.000123	0.000160	0.000470	
2.75	0.007500			0.005660	
2.50	0.021000	0.016708	0.016043	0.015000	
2.25	0.045000	0.038786		0.032500	0.035847
2.00	0.092433	0.082306	0.080822	0.068000	0.070475
1.75	0.177505	0.166478	0.163689	0.129000	0.138554
1.50	0.322260	0.327374	0.322078	0.252700	0.272397
1.25	0.562430	0.632821	0.623772	0.483500	
1.00	0.964172	1.211805	1.199323	0.918500	
0.75		2.331407	2.216929	1.738300	
0.50		4.794386	4.780285	3.283500	

[a]Additional values at closer spacing are available on request to I. R. Gatland.

The quantum oscillations in $Q^{(1)}$ have a period, $\Delta \ln \epsilon$, of 0.5 or less and are centered on the classical curve, so they almost cancel in the subsequent integration for the collision integral. As a result the values of $\Omega^{(l,1)}$ calculated from the quantal and classical cross sections differ by less than 1% for values of T_{eff} above 3 °K. We conclude that quantum effects can be ignored in the present mobility calculations.

IV. MOBILITY CALCULATIONS AND THEORETICAL POTENTIALS

According to kinetic theory[1] the mobility K and drift velocity v_d of an atomic ion moving in trace amounts through a dilute gas of neutral atoms are given at all E/N and all neutral gas temperatures T by the expression

$$v_d = KE = \frac{3}{8}\frac{qE}{N}\left(\frac{m+M}{M}\right)^{1/2}\left(\frac{\pi}{2mk_B T_{eff}}\right)^{1/2}\frac{1+\alpha}{\Omega^{(1,1)}(T_{eff})}, \quad (3)$$

where q is the ion charge, and m and M are the ion and neutral masses, respectively. The term α, which is zero in first approximation, includes all of the higher kinetic-theory approximations, and depends in a complicated way on E/N, T, m, M and the ion-neutral potential. The effective temperature T_{eff} is given by

$$\tfrac{3}{2}k_B T_{eff} = \tfrac{3}{2}k_B T + \tfrac{1}{2}Mv_d^2(1+\beta), \quad (4)$$

where β is a correction term, similar to α, that is zero in first approximation. A computer program that calculates the classical mobility through the third kinetic-theory approximation, and that is designed to accept numerically tabulated potentials, has been described.[2] Since quantum effects are negligible for Li^+–He in the range of interest, as discussed in Sec. III, this program could be used directly. Further checks on computational accuracy are discussed below.

The three theoretical potentials used to calculate mobilities for comparison with the experimental data were the SCF result of Catlow *et al.*,[6] and Krauss *et al.*,[7] the CEPA result of Hariharan and Staemmler,[8] and the EGDM result of Waldman and Gordon.[9] Tabulations of the three potentials are included in Table I; they are seen to be quite similar, the most obvious differences being in a somewhat deeper minimum in the CEPA potential.

Two important checks on computational accuracy were made. The first merely tested the numerical accuracy of the computer program for calculating the collision integrals $\Omega^{(l,s)}$, by comparing collision integrals for the tabulated CEPA potential with collision integrals calculated by the computer program of O'Hara and Smith[10] using the analytical approximation to the CEPA potential suggested by Hariharan and Staemmler.[8] The discrepancies between the results of the two programs were less than 0.2%. The second, more crucial, check tested the accuracy of the kinetic-theory approximation scheme (i.e., the behavior of α and β). Previous calculations[2–4] have indicated that it is necessary to proceed to the third approximation to ensure that the calculated mobility has an accuracy of better than 3% even in unfavorable cases, but that for many real ion–atom

interactions the accuracy of the third approximation is better than 1%. A completely independent calculation of mobilities for Li^+ in He has been made by Lin and Bardsley[5] for the SCF potential,[6,7] using a Monte Carlo method rather than kinetic theory. Our third-order mobilities for this potential agree with theirs to within 1%.

It is thus almost certain that no errors as large as 1% appear in our calculated mobilities due to quantum effects on cross sections, numerical inaccuracies in computer programs, or convergence errors in the kinetic-theory formulas.

Third-order mobilities for the three theoretical potentials were calculated as a function of E/N or, equivalently, of an effective temperature $T_f = T_{\text{eff}}^{(1)}$, defined in terms of E/N and mobility by Eq. (4) with $\beta = 0$. The results are shown in Fig. 1 together with the experimental data. For $E/N < 40$ Td the curve for the CEPA potential is in nearly perfect agreement with the data, whereas the curves for the other two potentials are slightly too high. Above 50 Td all three curves fall below the mobility data, indicating that the short-range repulsive cores of the potentials are too large in magnitude.[2] The different slopes at large E/N further indicate that the repulsive cores are too steep.[2] These discrepancies are discussed in Sec. V. In view of the conceptual simplicity and relative computational ease of the EGDM theory, the result obtained by Waldman and Gordon[9] is quite impressive.

V. DIRECTLY DETERMINED POTENTIAL

Recently an iterative procedure has been developed[10] which allows the ion–neutral interaction to be directly determined from mobility data without the need to assume a functional form for the potential. We have applied this procedure to our smoothed mobility data for Li^+ in He, using the CEPA potential[8] to start the iteration. Model calculations show that the specific starting potential does not affect the final result,[10] but only determines the number of iterations needed for convergence. The present results converged after only two iterations, and the results are shown in Table I. The accuracy with which this directly determined potential reproduces the experimental mobility measurements is shown in Fig. 1. It should be noted that the directly determined potential is most accurate (± 5%) in the ion–neutral separation range 1.8–5.5 a.u. because the mobility data cover a finite range of E/N (0–230 Td) with a fixed gas temperature of 300 °K. We have extended this potential to larger separations in Table I by using the theoretical long-range polarization potential[13] $V(r) = -0.6925\, r^{-4}$, in a.u.; this extrapolation should be quite accurate. Our extrapolation to smaller separations becomes increasingly inaccurate below 1.8 a.u., however, because the mobility data are progressively less sensitive to this region of the potential.

At intermediate and large ion–neutral separations (i.e., $r > 2.6$ a.u.) our directly determined potential is in excellent agreement with the *ab initio* CEPA potential.[8] The two differ, however, at small separations; in fact, all three theoretical potentials have larger and steeper repulsive cores than the directly determined potential. We nevertheless believe the latter to be more accurate, for the reasons discussed in the following section.

VI. DISCUSSION

On the whole, agreement between theory and experiment is quite gratifying. The experimental mobilities have been extended in range and improved in accuracy, and the uncertainties in the kinetic-theory calculations have been reduced to 1% or less. The best *ab initio* potential, the CEPA result of Hariharan and Staemmler,[8] agrees well with the potential obtained by direct inversion of the mobility data, except in the region of the repulsive core. Even here the discrepancy is not great (about 15%), but it is real. Some independent experimental information on this region of the potential is available from the experiments of Inouye and Kita[11] on the scattering of Li^+ beams by He gas targets. They determined the potential between 1.47 and 2.29 a.u. within an estimated error of ± 10%; their results are given in Table I, where it is seen that the agreement with the directly determined potential is quite good. There may well be a systematic error in the CEPA calculations at small separations because calculated CEPA potentials for Li^+–H_2,[17] Li^+–N_2,[18] and Li^+–CO[19] have all been 10%–20% higher in the repulsive region than experimentally determined potentials. We conclude that the Li^+–He potential is probably given more accurately in the repulsive region by our directly determined potential from mobility data than by the *ab initio* CEPA calculations.

ACKNOWLEDGMENTS

We are grateful to Dr. S. L. Lin and Professor J. N. Bardsley for their cooperation in comparing Monte Carlo and kinetic-theory calculations, and to Professor R. G. Gordon and M. Waldman for making the results of their calculations available before publication.

*Research supported in part by the U. S. Army Research Office; the Atmospheric Sciences Section, National Science Foundation; and the Office of Naval Research. Approved for public release; distribution unlimited.

[1] L. A. Viehland and E. A. Mason, Ann. Phys. (NY) 91, 499 (1975).
[2] I. R. Gatland, L. A. Viehland, and E. A. Mason, J. Chem. Phys. 66, 537 (1977).
[3] W. F. Morrison, G. R. Akridge, H. W. Ellis, R. Y. Pai, E. W. McDaniel, L. A. Viehland, and E. A. Mason, J. Chem. Phys. 63, 2238 (1975).
[4] L. A. Viehland and E. A. Mason, Ann. Phys. (NY) (to be published).
[5] S. L. Lin and J. N. Bardsley, J. Chem. Phys. 66, 435 (1977).
[6] G. W. Catlow, M. R. C. McDowell, J. J. Kaufman, L. M. Sachs, and E. S. Chang, J. Phys. B 3, 833 (1970).
[7] M. Krauss, P. Maldonado, and A. C. Wahl, J. Chem. Phys. 54, 4944 (1971).
[8] P. C. Hariharan and V. Staemmler, Chem. Phys. 15, 409 (1976).

[9]M. Waldman and R. G. Gordon, J. Chem. Phys. (to be published).
[10]L. A. Viehland, M. M. Harrington, and E. A. Mason, Chem. Phys. 17, 433 (1976).
[11]H. Inouye and S. Kita, J. Chem. Phys. 57, 1301 (1972).
[12]G. M. Thomson, J. H. Schummers, D. R. James, E. Graham, I. R. Gatland, M. R. Flannery, and E. W. McDaniel, J. Chem. Phys. 58, 2404 (1973).
[13]E. W. McDaniel and E. A. Mason, *The Mobility and Diffusion of Ions in Gases* (Wiley, New York, 1973).
[14]G. R. Akridge, H. W. Ellis, R. Y. Pai, and E. W. McDaniel, J. Chem. Phys. 62, 4578 (1975).
[15]R. G. Gordon, J. Chem. Phys. 51, 14 (1969).
[16]H. O'Hara and F. J. Smith, Comput. Phys. Commun. 2, 47 (1971). See also P. D. Neufeld and R. A. Aziz, *ibid.* 3, 269 (1972).
[17]W. Kutzelnigg, V. Staemmler, and C. Hohneisel, Chem. Phys. 1, 27 (1973).
[18]V. Staemmler, Chem. Phys. 7, 17 (1975).
[19]V. Staemmler, Chem. Phys. 17, 187 (1976).

APPENDIX C

TABLES OF TRANSPORT COLLISION INTEGRALS FOR (n,6,4) ION-NEUTRAL POTENTIALS

ATOMIC DATA AND NUCLEAR DATA TABLES 16, 495-514 (1975)

TABLES OF TRANSPORT COLLISION INTEGRALS FOR (*n*, 6, 4) ION-NEUTRAL POTENTIALS*

L. A. VIEHLAND and E. A. MASON

Brown University
Providence, Rhode Island 02912

and

W. F. MORRISON and M. R. FLANNERY

School of Physics, Georgia Institute of Technology
Atlanta, Georgia 30332

Transport collision integrals are tabulated for the (*n*, 6, 4) model of ion-neutral-molecule interactions as functions of effective ion temperature for eight values of *n* and several values of a parameter γ that measures the relative strengths of the r^{-6} and r^{-4} attraction terms. The ions can have any charge and the neutral entities can be either atoms or spherically symmetric molecules. The accuracy of the calculations is estimated to be a few parts in 10^4. The tables can be used to estimate ion-neutral potentials by comparison with experimental ion mobility data or conversely can be used to estimate ion mobilities and diffusion coefficients as functions of gas temperature and electric field strength from fragmentary information.

*This work was supported in part by the U.S. Army Research Office

CONTENTS

INTRODUCTION

The prediction and interpretation of most phenomena involving ions in neutral gases, either atomic or molecular, depend on knowledge of the ion-neutral interaction potential. Since *ab initio* calculations are extremely difficult for most systems, the method usually employed to get the interaction potential is the careful analysis of accurate measurements of a property that depends on the potential in a well-established way. However, since a unique determination of the potential from a measured property is seldom possible, even in principle, a more indirect procedure is usually followed: A mathematical model containing a few parameters is chosen for the potential, and then the parameters are adjusted to obtain agreement with the measured property. Such models are ordinarily selected to reproduce various known asymptotic forms of the true potential and to behave in a qualitatively correct way in intermediate regions. A major step in such a procedure is the calculation of the experimental property from the potential model, a process which may require extensive numerical integration. This approach has a long and successful history for the determination of neutral-neutral potentials.[1-3] However, until recently the approach has been of very limited utility for ion-neutral potentials,[4] the reason being that the theory required measurements of ion mobility in weak electric fields as a function of temperature, and very few good experimental data were available.

Variation of the electric field in an ion mobility experiment has roughly the same effect as variation of the gas temperature; typically the average ion energy can be varied from the thermal value up to about 10 eV. It has long been realized that if mobility data covering such a wide range of ion energies could be analyzed accurately, information on the ion-neutral potential could be derived that would span a wide range of ion-neutral separation distances. The difficulty was that an accurate general mobility theory existed only for weak electric fields. Recently Viehland and Mason[5] have developed a rigorous kinetic theory of ion mobility that is applicable for electric fields of arbitrary strength, so it is now possible to determine ion-neutral potentials over an extensive range of separation distances by the traditional procedure of adjusting the parameters of potential models. The extensive numerical integrations required need to be done only once for a given form of potential. With suitable choices of dimensionless variables the results can be given as a set of numerical tables, so that future computational work is reduced to simple interpolation.

The present paper presents such numerical tables for a potential model that is expected to be a fair mimic of real ion-neutral interaction potentials. These tables can be used not only for the analysis of ion mobility measurements to find ion-neutral potentials but also for the converse problem of estimating ion mobilities and diffusion coefficients from fragmentary experimental and theoretical information.[4]

CALCULATIONS

Potential Model

The model chosen represents the potential $V(r)$ as the sum of one repulsion term and two attraction terms,

$$V(r) = \frac{B}{r^n} - \frac{C_6}{r^6} - \frac{C_4}{r^4}, \tag{1}$$

where n, B, C_6, and C_4 are constants. The inverse fourth power term accounts for the attraction between the charge on the ion and the dipole it induces in the polarizable neutral; for most real systems this attraction dominates the mobility at low temperatures and weak electric fields. The coefficient C_4 is often known rather accurately, since it is given by the simple expression

$$C_4 = \frac{1}{2}q^2\alpha, \tag{2}$$

where q is the ionic charge and α is the polarizability of the neutral entity. The inverse sixth power term accounts for the charge-induced quadrupole attraction plus the London dispersion attraction. The coefficient C_6 can often be calculated approximately[4] but is seldom known as accurately as C_4. The term B/r^n is an empirical representation of the short-range repulsion energy. Equation (1) makes no provision for the possibility of charge exchange between the ion and neutral.

It is convenient to rewrite Eq. (1) in the dimensionless form

$$V(r) = \frac{n\varepsilon}{n(3+\gamma) - 12(1+\gamma)} \times\left[\frac{12}{n}(1+\gamma)\left(\frac{r_m}{r}\right)^n - 4\gamma\left(\frac{r_m}{r}\right)^6 - 3(1-\gamma)\left(\frac{r_m}{r}\right)^4\right], \tag{3}$$

where ε and r_m are the depth and position, respectively, of the potential minimum and γ is a dimensionless parameter, ranging between 0 and 1, that measures the relative strengths of the r^{-6} and r^{-4} terms. This $(n, 6, 4)$ potential is a slight generalization of previously used models: the $(\infty, 4)$ model of Langevin[6] and Hassé,[7] the $(8, 4)$ model of Hassé and Cook,[8] and the $(12, 6, 4)$ model of Mason and Schamp.[9] Extensive tabulations are available[10-12] for the $(n, 6)$ model which has long been used for neutral-neutral interactions.

Mobility and Diffusion

To a good approximation the mobility K and drift velocity v_d can be represented at all temperatures and electric field strengths by[5]

$$KE \equiv v_d = \frac{3qE}{16N}\left(\frac{2\pi}{kT_{eff}}\right)^{1/2}\left(\frac{m+M}{mM}\right)^{1/2}\frac{1}{\bar{\Omega}^{(1,1)}(T_{eff})}, \tag{4}$$

where E is the field strength, q is the ion charge, N is the number density of the neutral gas, m is the ion mass, M is the neutral mass, and k is Boltzmann's constant. The effective temperature T_{eff} is given by

$$\frac{3}{2}kT_{eff} = \frac{3}{2}kT + \frac{1}{2}Mv_d^2, \tag{5}$$

in which T is the neutral gas temperature. All of the information on the ion-neutral potential is contained in the momentum-transfer collision integral $\bar{\Omega}^{(1,1)}$, which is a function of T_{eff}. The computation of $\bar{\Omega}^{(1,1)}$ and similar integrals for $(n, 6, 4)$ potentials is the focus of this paper.

Equations (4) and (5) are valid only for ions in pure neutral gases. The expressions for neutral gas mixtures, which are considerably more complex,[5,13] will not be given here. Since they involve the same kind of collision integral as is given here, the present tabulations can be used.

Since Eq. (4) is only a theoretical first approximation, some convergence error is involved in its use. The error depends in a complicated way on the ion-neutral potential and mass ratio and on the value of T_{eff}, but, as a rough rule, Eq. (4) can be expected to give mobilities that are too low by a few percent. More detailed error estimates are given by Viehland and Mason,[5] who also give expressions for higher approximations.

At low fields the diffusion coefficient D is related to the mobility by the familiar Einstein relation

$$D = (kT/q)K, \tag{6}$$

but at high fields D increases much more rapidly than K and becomes anisotropic. No completely satisfactory theory of ion diffusion at high fields yet exists. The following approximate formulas for the transverse and longitudinal components of the diffusion tensor are probably the best available at present:[14]

$$D_\perp \simeq (kT_\perp/q)K, \tag{7}$$

$$D_\parallel \simeq (kT_\parallel/q)K\left[1 + \frac{d\ln K}{d\ln(E/N)}\right], \tag{8}$$

where $D_\perp$ and $D_\parallel$ are the diffusion coefficients perpendicular and parallel to the field direction, respectively. The "temperatures" and the logarithmic derivative are

$$kT_\perp = kT + \frac{(m+M)A^*}{5m+3MA^*}Mv_d^2, \tag{9}$$

$$kT_\parallel = kT + \frac{5m - 2mA^* + MA^*}{5m+3MA^*}Mv_d^2, \tag{10}$$

$$1 + \frac{d\ln K}{d\ln(E/N)} = \left[1 + (6C^* - 5)\left(1 - \frac{T}{T_{eff}}\right)\right]^{-1}. \tag{11}$$

where A^* and C^* are dimensionless ratios of collision integrals. The resemblance of Eqs. (9) and (10) to Eq. (5) for T_{eff} is apparent; in fact,

$$T_{\text{eff}} = \frac{1}{3}(2T_\perp + T_\parallel). \tag{12}$$

Equations (7)–(11) can be used to calculate the diffusion coefficient but do not give results as accurate at high fields as does Eq. (4) for the mobility.

The Collision Integrals

The collision integral $\bar{\Omega}^{(1,1)}$ is the first of a family of integrals that arise in kinetic-theory calculations,

$$\bar{\Omega}^{(l,s)}(T) = [(s+1)!(kT)^{s+2}]^{-1}\int_0^\infty Q^{(l)}(E)e^{-E/kT}E^{s+1}dE, \tag{13}$$

where E is the relative energy of an ion-neutral collision (not to be confused with the field strength), and $Q^{(l)}(E)$ is a transport cross section, given classically by the equation

$$Q^{(l)}(E) = 2\pi\left[1 - \frac{1+(-1)^l}{2(1+l)}\right]^{-1}\int_0^\infty (1-\cos^l\theta)\,b\,db, \tag{14}$$

in which θ is the deflection angle in an ion-neutral collision of energy E and impact parameter b. The argument T of the collision integral in Eq. (13) can refer to the gas temperature, the effective temperature T_{eff}, or any temperature-like variable that arises in a particular problem. The normalization factors in Eqs. (13) and (14) were chosen so that all of the $\bar{\Omega}^{(l,s)}$ and $Q^{(l)}$ are equal to πd^2 for the collision of rigid spheres of diameter d. The deflection angle θ is calculated as a function of b and E from the classical equation of motion

$$\theta(b,E) = \pi - 2b\int_{r_0}^\infty \left[1 - \frac{b^2}{r^2} - \frac{V(r)}{E}\right]^{-1/2}\frac{dr}{r^2}, \tag{15}$$

where the distance of closest approach r_0 is the outermost root of

$$1 - \frac{b^2}{r_0^2} - \frac{V(r_0)}{E} = 0. \tag{16}$$

Thus three successive numerical integrations are required to obtain a collision integral. The integrations for $\theta(b,E)$ and $Q^{(l)}$ can be quite difficult because of singularities and other irregularities that can occur in their integrands. Considerable attention has been given to these integrations previously,[2-4,7-9] so little discussion is warranted here. We used the computer program developed by O'Hara and Smith.[15]

The numerical results finally give the dependent variable $\bar{\Omega}^{(l,s)}$ as a function of the independent variable T and of the four potential parameters ϵ, r_m, γ, and n. Dimensional analysis shows that two of the parameters can be absorbed into the two variables $\bar{\Omega}^{(l,s)}$ and T. Such a reduction is very convenient for purposes of numerical tabulation. It is conventional[2-4] to absorb r_m into $\bar{\Omega}^{(l,s)}$ and ϵ into T by the defining of dimensionless quantities

$$\Omega^{(l,s)*}(T^*,\gamma,n) = \bar{\Omega}^{(l,s)}(T,\epsilon,r_m,\gamma,n)/\pi r_m^2, \tag{17}$$

$$T^* = kT/\epsilon, \tag{18}$$

which are the basis of the present tabulations. The numerical methods used are believed[12] to give collision integrals accurate to 1 part in 10^4 for $T^* > 3$; the accuracy becomes progressively worse at lower T^*, reaching 1 part in 10^3 for $T^* < 1$. With a few exceptions, our results agree with previous calculations within mutual uncertainty.[4,8-12] The exceptions are F^* by Mason and Schamp[9] and all collision integrals by Lin and Hsu[11] below $T^* = 0.2$.

Our calculations are entirely classical. Quantum effects can be expected to cause deviations at low temperatures for light systems. Numerical calculations for the system Li^+-He show a quantum effect of about 9% at 100 °K, falling to about 4% at 1000 °K.[16] Heavier systems are expected to show smaller effects, since the quantum deviations decrease as μ^{-1}, where $\mu = mM/(m+M)$ is the reduced mass of the ion-neutral pair.[2]

Collision integrals higher than those tabulated can be generated by numerical differentiation and use of the recursion relation

$$\Omega^{(l,s+1)*} = \Omega^{(l,s)*}\left[1 + \frac{1}{s+2}\frac{d\ln\Omega^{(l,s)*}}{d\ln T^*}\right], \tag{19}$$

which can be obtained by differentiation of Eq. (13). This recursion relation can also be used to derive Eq. (11).

Tables I–IV give the collision integrals for various $(n, 6, 4)$ and $(n, 4)$ potentials. Table V gives the asymptotic forms of $\Omega^{(1,1)*}$ for $T^* \to 0$ and $T^* \to \infty$, as collected from various sources.[17-19] The asymptotic values of A^* and F^* in Tables I–IV come from the same sources. Table VI gives the values of T^* for which the first approximation to the mobility has a minimum or maximum. At these effective temperatures the mobility is independent of both gas temperature and field strength to first order, and the system behaves approximately as if the mean free time between collisions were a constant (the Maxwell model[4]).

Effect of Potential on Mobility

At low temperatures the mobility is dominated by the long-range polarization attraction, $-C_4/r^4$ of Eq. (1), so that the mobility approaches a constant nonzero

polarization limit as $T^* \rightarrow 0$. This polarization limit of the mobility is, at standard gas density,

$$K_{pol} = \frac{13.876}{\alpha^{1/2}} \left(\frac{m + M}{mM}\right)^{1/2} \text{cm}^2 V^{-1} \text{sec}^{-1}, \quad (20)$$

where α is the polarizability in Å^3 and the masses are in amu.

To show the effect of adding short-range repulsion, B/r^n of Eq. (1), we plot the ratio K/K_{pol} as a function of kT_{eff}/ϵ for three $(n, 4)$ potentials in Fig. 1, with $n = 8$, 12, 16. The addition of repulsion causes the mobility to rise with increasing temperature to a maximum and then decrease, eventually as $T_{eff}^{-(1/2)+(2/n)}$. The height of the maximum can be seen to depend strongly on the value of n, the steepness of the repulsion energy.

The effect of adding the attraction energy $-C_6/r^6$ to the potential is illustrated in Fig. 2, where K/K_{pol} is plotted as a function of kT_{eff}/ϵ for three (12, 6, 4) potentials, with $\gamma = 0$, 0.4, 0.8. The addition of r^{-6} attraction causes the height of the maximum in the mobility curve to decrease. Addition of sufficient r^{-6} energy causes a minimum to develop at lower temperatures, and further r^{-6} energy eventually suppresses both the maximum and the minimum.

The shape of a K versus T_{eff} curve thus contains useful information on the ion-neutral potential.

USE OF TABLES

The tables have two main purposes—the determination of ion-neutral potentials by analysis of mobility measurements and the estimation of mobilities (and diffusion coefficients) from fragmentary information. We consider the latter purpose first, since the calculations are simpler.

The simplest case arises when one is given an ion-neutral potential from some source and wishes to calculate the mobility. The first step is to fit the given potential with an $(n, 6, 4)$ model, for which four parameters are available. Since the coefficient C_4 is usually known, only three parameters are adjustable. It is probably best to choose two of them so that the well depth and minimum position, ϵ and r_m, respectively, of the potential are reproduced. The final parameter can be chosen to give a reasonable representation of the repulsive wall of the potential, such as requiring that the ratio σ/r_m be given correctly, where σ is the point at which the potential curve crosses the r-axis, $V(\sigma) = 0$. Alternatively, one might require that the coefficient C_6 be given correctly, if a reliable value is known. Methods for estimating C_6 are summarized in Ref. 4.

As an example, we consider the calculation of the mobility of K^+ ions in Ar from a potential given recently by Budenholzer et al.[20] These authors measured the total scattering cross section for a K^+ beam in Ar gas as a function of beam energy and fitted their results with an $(n, 6, 4)$ potential. They took the theoretical values,[4] $C_4 = 11.80$ eV Å^4 and $C_6 = 44.0$ eV Å^6, and adjusted the remaining two parameters of Eq. (1) to fit their measurements, obtaining $n = 9.6$ and $B = 3997$ eV Å$^{9.6}$; these parameter values correspond to $\sigma = 2.62$ Å, $r_m = 3.04$ Å, $\epsilon = 0.103$ eV, and $\gamma = 0.23$. The measure-

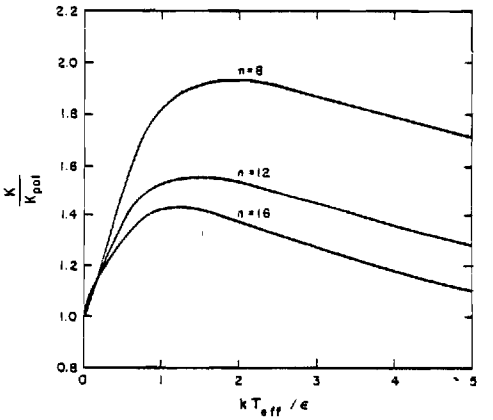

Fig. 1. Effect of short-range repulsion on mobility, as illustrated by a series of $(n, 4)$ potentials. The mobility is normalized by K_{pol}, the zero-temperature limit, and is plotted as a function of the dimensionless effective temperature

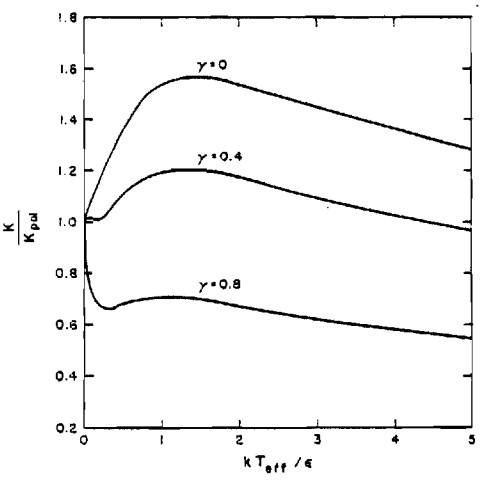

Fig. 2. Effect of additional r^{-6} attraction energy on mobility, as illustrated by a series of (12, 6, 4) potentials. The abscissa and ordinate are as in Fig. 1

ments were estimated to sample the potential over the range of $r = 2.4$ to 5.5 Å. From this information and the present tables it is straightforward to calculate the mobility as a function of effective temperature according to Eq. (4); because of the limitation upon the range of the potential, the mobility calculation is strictly valid only for effective temperatures less than about 2000 °K. The results are shown in Fig. 3, where they are compared with direct measurements of mobility.[21] The agreement is within about 12%. This is a useful accuracy but is poorer than the experimental uncertainty of about 2% in the measured mobilities. In this case the mobilities could be used to refine the potential.

A more common situation arises when only fragmentary information on the potential is available. Suppose the only direct information is one measurement of the mobility at 300 °K and one wishes to estimate K as a function of temperature and field strength. If C_4 and C_6 can be estimated, which is usually possible, then three pieces of information are available to determine a four-parameter potential. Clearly one guess has to be made. It is probably best to guess the value of n, which usually lies between 8 and 16 and for which analogy with similar systems is a useful guide. An estimate of the uncertainty involved can be obtained by choosing two values of n believed to bracket the most likely value and carrying through the calculations for both. Since examples of this sort are given in Ref. 4, we present no further details here, except to note that the calculated mobilities will be accurate within a few percent from 0 °K up to about 500 °K, after which the uncertainty grows rapidly because of the uncertainty in n, rising to about 10% at 700 °K.

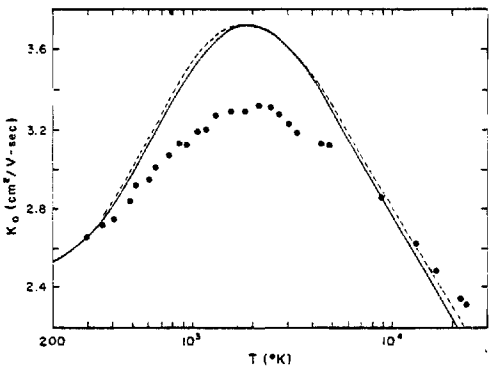

Fig. 3. Comparison of experimental mobilities with those calculated from an independently determined potential for K^+ ions in Ar gas: for a discussion, see the text. All results are given in terms of the reduced mobility K_0, referred to a standard gas density of 2.69×10^{19} molecules/cm³. The solid curve is the first kinetic-theory approximation of Eq. (4), and the dashed curve is the second approximation calculated according to the methods of Ref. 5

The inverse problem of determining the potential from mobility measurements is much more difficult. A unique inversion in the general case is impossible in principle.[22] Some assumption about the form of the potential must be made, such as the use of an $(n, 6, 4)$ model. Once such a model is assumed, the determination of its parameters by comparison of calculated and measured mobilities is essentially a problem in curve-fitting. There is a large literature on the subject for the analogous case of the transport coefficients of neutral gases,[1-3] which we cannot review here. For the specific case of ion mobilities, a simple but accurate graphical method has been described by Mason and Schamp.[9] Results from such graphical methods can be refined by various least-squares numerical procedures, if necessary.[12] There are other methods, still in a state of development, in which a starting potential is refined numerically without the need for an explicit assumption about its mathematical form.[23] Thus even if a particular ion-neutral potential cannot be accurately represented by an $(n, 6, 4)$ model, the present tables are still useful to furnish a starting potential for numerical refinement.

References

1. S. Chapman and T. G. Cowling, *The Mathematical Theory of Non-Uniform Gases*, 3rd ed., Cambridge University Press, London (1970)
2. J. O. Hirschfelder, C. F. Curtiss, and R. B. Bird, *Molecular Theory of Gases and Liquids*, John Wiley, New York (1964)
3. J. H. Ferziger and H. G. Kaper, *Mathematical Theory of Transport Processes in Gases*, North-Holland, Amsterdam (1972)
4. E. W. McDaniel and E. A. Mason, *The Mobility and Diffusion of Ions in Gases*, Chap. 6., John Wiley, New York (1973)
5. L. A. Viehland and E. A. Mason, Ann. Phys. (N.Y.) **91**, 499 (1975)
6. P. Langevin, Ann. Chim. Phys. **5**, 245 (1905). A translation is given by E. W. McDaniel, *Collision Phenomena in Ionized Gases*, Appendix II, John Wiley, New York (1964)
7. H. R. Hassé, Philos. Mag. **1**, 139 (1926)
8. H. R. Hassé and W. R. Cook, Philos. Mag. **12**, 554 (1931)
9. E. A. Mason and H. W. Schamp, Jr., Ann. Phys. (N.Y.) **4**, 233 (1958)

10. M. Klein and F. J. Smith, J. Res. Natl. Bur. Stds. A **72**, 359 (1968)
11. S. T. Lin and H. W. Hsu, J. Chem. Eng. Data **14**, 328 (1969). These results are incorrect below $T^* = 0.2$, where they exhibit significant differences not only from our work but also from the known asymptotes
12. M. Klein, H. J. M. Hanley, F. J. Smith, and P. Holland, "Tables of Collision Integrals and Second Virial Coefficients for the (n, 6, 8) Intermolecular Potential Function," U.S. National Bureau of Standards Report NSRDS-NBS 47 (1974)
13. J. H. Whealton, E. A. Mason, and R. E. Robson, Phys. Rev. A **9**, 1017 (1974)
14. L. A. Viehland and E. A. Mason, J. Chem. Phys. **63**, 2913 (1975); R. Y. Pai et al., J. Chem. Phys. **63**, 2916 (1975)
15. H. O'Hara and F. J. Smith, J. Comput. Phys. **5**, 328 (1970); Comput. Phys. Comm. **2**, 47 (1971)
16. W. F. Morrison et al., J. Chem. Phys. **63**, 2238 (1975)
17. L. Monchick and E. A. Mason, J. Chem. Phys. **35**, 1676 (1961)
18. L. D. Higgins and F. J. Smith, Mol. Phys. **14**, 399 (1968)
19. G. Heiche and E. A. Mason, J. Chem. Phys. **53**, 4687 (1970)
20. F. E. Budenholzer et al., Chem. Phys. Letters **33**, 245 (1975)
21. D. R. James et al., J. Chem. Phys. **58**, 3652 (1973)
22. J. Kestin and E. A. Mason, in *Transport Phenomena—1973* (J. Kestin, ed.) AIP Conf. Proc. No. 11, pp. 137–192, American Institute of Physics, New York (1973)
23. D. W. Gough, G. C. Maitland, and E. B. Smith, Mol. Phys. **24**, 151 (1972)

EXPLANATION OF TABLES

$\Omega^{(1,1)*}$	The momentum-transfer collision integral. Eqs. (13) and (17)
A^*	$\Omega^{(2,2)*}/\Omega^{(1,1)*}$
B^*	$[5\Omega^{(1,2)*} - 4\Omega^{(1,3)*}]/\Omega^{(1,1)*}$
C^*	$\Omega^{(1,2)*}/\Omega^{(1,1)*}$
E^*	$\Omega^{(2,3)*}/\Omega^{(2,2)*}$
F^*	$\Omega^{(3,3)*}/\Omega^{(1,1)*}$
T^*	The dimensionless temperature kT/ϵ, where ϵ is the well depth. See Eq. (18)
γ	The dimensionless parameter measuring the relative strengths of the r^{-3} and r^{-4} terms in the (n, 6, 4) potential. See Eq. (3). Note that $\gamma = 0$ in TABLE IV
n	The dimensionless parameter measuring the steepness of the repulsive term in the (n, 6, 4) potential. Eqs. (1) and (3)

TABLE I. Collision Integrals for (8, 6, 4) Potentials

	$\Omega^{(1,1)*}$						A^*					
T^*	$\gamma=0$	$\gamma=0.2$	$\gamma=0.4$	$\gamma=0.6$	$\gamma=0.8$	$\gamma=1.0$	$\gamma=0$	$\gamma=0.2$	$\gamma=0.4$	$\gamma=0.6$	$\gamma=0.8$	$\gamma=1.0$
0							0.8696	0.8696	0.8696	0.8696	0.8696	1.0058
0.01	20.157	18.726	16.992	14.844	12.123	8.6628	0.9010	0.9067	0.9145	0.9260	0.9451	0.9844
0.02	14.143	13.186	12.043	10.652	8.9385	6.8378	0.9081	0.9139	0.9216	0.9325	0.9498	0.9827
0.03	11.475	10.729	9.8441	8.7817	7.4943	5.9445	0.9137	0.9196	0.9272	0.9373	0.9531	0.9822
0.04	9.8838	9.2611	8.5293	7.6590	6.6162	5.3759	0.9186	0.9247	0.9320	0.9415	0.9561	0.9823
0.05	8.7970	8.2595	7.6303	6.8876	6.0065	4.9681	0.9231	0.9284	0.9362	0.9454	0.9590	0.9828
0.06	7.9968	7.5167	6.9631	6.3150	5.5501	4.6545	0.9269	0.9324	0.9405	0.9488	0.9616	0.9837
0.07	7.3733	6.9457	6.4463	5.8649	5.1897	4.4027	0.9307	0.9355	0.9432	0.9529	0.9642	0.9845
0.08	6.8748	6.4783	6.0272	5.5055	4.8943	4.1926	0.9336	0.9397	0.9469	0.9550	0.9675	0.9861
0.09	6.4555	6.0940	5.6796	5.2017	4.6511	4.0134	0.9384	0.9437	0.9508	0.9589	0.9693	0.9878
0.10	6.1001	5.7656	5.3825	4.9438	4.4403	3.8601	0.9435	0.9487	0.9551	0.9632	0.9728	0.9894
0.15	4.8459	4.6108	4.3437	4.0397	3.6925	3.2971	0.9795	0.9812	0.9841	0.9887	0.9944	1.0052
0.20	4.0340	3.8649	3.6714	3.4523	3.2011	2.9147	1.0180	1.0187	1.0182	1.0200	1.0224	1.0284
0.25	3.4475	3.3240	3.1791	3.0191	2.8324	2.6193	1.0502	1.0474	1.0484	1.0489	1.0497	1.0523
0.30	3.0039	2.9114	2.8024	2.6820	2.5412	2.3791	1.0748	1.0740	1.0712	1.0723	1.0721	1.0733
0.35	2.6589	2.5910	2.5046	2.4132	2.3049	2.1805	1.0921	1.0906	1.0888	1.0892	1.0887	1.0884
0.40	2.3832	2.3307	2.2663	2.1966	2.1104	2.0129	1.1055	1.1031	1.1005	1.0999	1.1004	1.1004
0.45	2.1639	2.1219	2.0691	2.0159	1.9499	1.8715	1.1121	1.1113	1.1096	1.1084	1.1078	1.1089
0.50	1.9832	1.9494	1.9085	1.8620	1.8124	1.7509	1.1172	1.1183	1.1146	1.1162	1.1134	1.1136
0.60	1.7055	1.6856	1.6579	1.6309	1.5971	1.5576	1.1226	1.1206	1.1199	1.1220	1.1207	1.1193
0.70	1.5058	1.4929	1.4747	1.4592	1.4359	1.4105	1.1236	1.1227	1.1221	1.1204	1.1213	1.1230
0.80	1.3563	1.3493	1.3366	1.3270	1.3136	1.2958	1.1238	1.1218	1.1216	1.1209	1.1197	1.1210
0.90	1.2407	1.2369	1.2307	1.2254	1.2158	1.2058	1.1219	1.1206	1.1195	1.1194	1.1193	1.1189
1.0	1.1501	1.1488	1.1449	1.1435	1.1387	1.1321	1.1200	1.1192	1.1187	1.1168	1.1178	1.1169
1.2	1.0158	1.0187	1.0195	1.0212	1.0215	1.0217	1.1176	1.1160	1.1156	1.1147	1.1141	1.1137
1.4	0.92242	0.92714	0.93104	0.93579	0.93906	0.94186	1.1163	1.1149	1.1137	1.1121	1.1119	1.1120
1.6	0.85449	0.86064	0.86578	0.87192	0.87767	0.88272	1.1154	1.1139	1.1132	1.1114	1.1103	1.1104
1.8	0.80239	0.80971	0.81617	0.82266	0.82993	0.83710	1.1156	1.1138	1.1129	1.1121	1.1101	1.1091
2.0	0.76122	0.76932	0.77682	0.78482	0.79174	0.80015	1.1167	1.1145	1.1131	1.1113	1.1111	1.1094
2.5	0.68849	0.69757	0.70637	0.71570	0.72495	0.73444	1.1194	1.1177	1.1160	1.1137	1.1119	1.1104
3.0	0.64058	0.65035	0.65979	0.66960	0.67960	0.68996	1.1227	1.1204	1.1188	1.1167	1.1146	1.1131
3.5	0.60601	0.61622	0.62625	0.63647	0.64681	0.65760	1.1264	1.1238	1.1218	1.1195	1.1176	1.1157
4.0	0.57962	0.59010	0.60043	0.61100	0.62172	0.63277	1.1298	1.1271	1.1251	1.1225	1.1203	1.1184
4.5	0.55861	0.56928	0.57978	0.59060	0.60156	0.61291	1.1329	1.1302	1.1280	1.1254	1.1230	1.1208
5.0	0.54134	0.55214	0.56281	0.57375	0.58488	0.59640	1.1357	1.1329	1.1306	1.1280	1.1256	1.1232
6.0	0.51426	0.52518	0.53608	0.54708	0.55851	0.57026	1.1404	1.1377	1.1352	1.1328	1.1300	1.1275
8.0	0.47700	0.48815	0.49930	0.51054	0.52200	0.53381	1.1474	1.1444	1.1418	1.1392	1.1367	1.1343
10.	0.45141	0.46263	0.47392	0.48520	0.49674	0.50868	1.1525	1.1494	1.1466	1.1441	1.1415	1.1390
20.	0.38377	0.39493	0.40615	0.41734	0.42877	0.44061	1.1652	1.1621	1.1591	1.1565	1.1541	1.1516
40.	0.32743	0.33822	0.34893	0.35972	0.37073	0.38213	1.1739	1.1709	1.1679	1.1653	1.1630	1.1607
60.	0.29820	0.30867	0.31898	0.32942	0.34007	0.35110	1.1776	1.1747	1.1718	1.1693	1.1670	1.1649
80.	0.27890	0.28912	0.29912	0.30928	0.31964	0.33036	1.1798	1.1769	1.1742	1.1718	1.1696	1.1675
100.	0.26472	0.27471	0.28448	0.29439	0.30450	0.31497	1.1812	1.1785	1.1759	1.1736	1.1714	1.1693
200.	0.22469	0.23392	0.24295	0.25204	0.26131	0.27090	1.1848	1.1823	1.1802	1.1782	1.1762	1.1744
400.	0.19026	0.19865	0.20691	0.21514	0.22351	0.23216	1.1873	1.1850	1.1833	1.1816	1.1799	1.1783
600.	0.17246	0.18036	0.18813	0.19585	0.20369	0.21180	1.1884	1.1862	1.1846	1.1830	1.1815	1.1801
800.	0.16080	0.16834	0.17577	0.18312	0.19060	0.19832	1.1890	1.1870	1.1854	1.1839	1.1825	1.1811
1000.	0.15228	0.15954	0.16669	0.17377	0.18096	0.18840	1.1894	1.1875	1.1859	1.1845	1.1831	1.1818
∞							1.1929	1.1929	1.1929	1.1929	1.1929	1.1929

See page 501 for Explanation of Tables

TABLE I. Collision Integrals for (8, 6, 4) Potentials

	B^*						C^*					
T^*	$\gamma=0$	$\gamma=0.2$	$\gamma=0.4$	$\gamma=0.6$	$\gamma=0.8$	$\gamma=1.0$	$\gamma=0$	$\gamma=0.2$	$\gamma=0.4$	$\gamma=0.6$	$\gamma=0.8$	$\gamma=1.0$
0	1.2500	1.2500	1.2500	1.2500	1.2500	1.1852	0.8333	0.8333	0.8333	0.8333	0.8333	0.8889
0.01	1.2547	1.2524	1.2485	1.2411	1.2258	1.1892	0.8303	0.8317	0.8343	0.8396	0.8521	0.8868
0.02	1.2573	1.2543	1.2493	1.2406	1.2245	1.1923	0.8288	0.8309	0.8344	0.8411	0.8547	0.8855
0.03	1.2592	1.2560	1.2505	1.2412	1.2251	1.1955	0.8275	0.8300	0.8341	0.8415	0.8555	0.8842
0.04	1.2601	1.2569	1.2514	1.2420	1.2265	1.1987	0.8265	0.8292	0.8337	0.8415	0.8557	0.8828
0.05	1.2602	1.2563	1.2527	1.2428	1.2275	1.2016	0.8257	0.8284	0.8334	0.8413	0.8555	0.8815
0.06	1.2602	1.2579	1.2528	1.2433	1.2288	1.2045	0.8252	0.8284	0.8331	0.8410	0.8553	0.8801
0.07	1.2623	1.2595	1.2527	1.2460	1.2291	1.2069	0.8247	0.8275	0.8325	0.8414	0.8546	0.8789
0.08	1.2704	1.2648	1.2564	1.2458	1.2340	1.2091	0.8235	0.8271	0.8321	0.8402	0.8549	0.8775
0.09	1.2801	1.2721	1.2626	1.2507	1.2348	1.2148	0.8220	0.8256	0.8311	0.8398	0.8533	0.8768
0.10	1.2917	1.2820	1.2711	1.2581	1.2407	1.2173	0.8195	0.8236	0.8298	0.8389	0.8525	0.8748
0.15	1.3530	1.3399	1.3256	1.3071	1.2845	1.2578	0.7989	0.8060	0.8148	0.8265	0.8422	0.8644
0.20	1.3864	1.3768	1.3630	1.3474	1.3283	1.3026	0.7752	0.7841	0.7945	0.8082	0.8256	0.8485
0.25	1.3937	1.3878	1.3787	1.3673	1.3507	1.3306	0.7554	0.7652	0.7763	0.7909	0.8089	0.8314
0.30	1.3868	1.3825	1.3756	1.3714	1.3605	1.3462	0.7414	0.7512	0.7619	0.7774	0.7950	0.8174
0.35	1.3752	1.3694	1.3672	1.3624	1.3583	1.3506	0.7323	0.7411	0.7527	0.7673	0.7845	0.8062
0.40	1.3569	1.3551	1.3525	1.3490	1.3463	1.3427	0.7272	0.7363	0.7462	0.7599	0.7770	0.7974
0.45	1.3384	1.3367	1.3358	1.3336	1.3355	1.3300	0.7240	0.7330	0.7438	0.7561	0.7717	0.7913
0.50	1.3196	1.3178	1.3177	1.3203	1.3172	1.3199	0.7234	0.7321	0.7422	0.7561	0.7693	0.7875
0.60	1.2870	1.2858	1.2863	1.2880	1.2821	1.2894	0.7270	0.7349	0.7449	0.7562	0.7679	0.7850
0.70	1.2612	1.2609	1.2599	1.2603	1.2627	1.2590	0.7346	0.7423	0.7514	0.7610	0.7736	0.7861
0.80	1.2345	1.2359	1.2360	1.2393	1.2390	1.2425	0.7431	0.7505	0.7598	0.7688	0.7791	0.7924
0.90	1.2188	1.2186	1.2182	1.2196	1.2216	1.2225	0.7538	0.7608	0.7686	0.7767	0.7870	0.7979
1.0	1.2039	1.2033	1.2030	1.2036	1.2044	1.2084	0.7637	0.7704	0.7783	0.7855	0.7944	0.8051
1.2	1.1822	1.1810	1.1800	1.1801	1.1804	1.1818	0.7833	0.7891	0.7959	0.8027	0.8103	0.8187
1.4	1.1666	1.1658	1.1648	1.1639	1.1636	1.1639	0.8007	0.8063	0.8122	0.8178	0.8246	0.8321
1.6	1.1554	1.1541	1.1537	1.1527	1.1518	1.1518	0.8154	0.8205	0.8263	0.8316	0.8372	0.8438
1.8	1.1486	1.1462	1.1449	1.1450	1.1434	1.1427	0.8284	0.8329	0.8380	0.8436	0.8484	0.8538
2.0	1.1430	1.1412	1.1392	1.1376	1.1377	1.1362	0.8394	0.8437	0.8482	0.8526	0.8583	0.8629
2.5	1.1347	1.1325	1.1305	1.1288	1.1274	1.1263	0.8604	0.8643	0.8681	0.8718	0.8758	0.8799
3.0	1.1304	1.1282	1.1261	1.1244	1.1225	1.1205	0.8747	0.8782	0.8818	0.8851	0.8885	0.8919
3.5	1.1285	1.1260	1.1235	1.1216	1.1199	1.1179	0.8851	0.8882	0.8913	0.8944	0.8976	0.9007
4.0	1.1277	1.1251	1.1226	1.1203	1.1182	1.1164	0.8928	0.8956	0.8986	0.9013	0.9041	0.9070
4.5	1.1273	1.1248	1.1220	1.1197	1.1175	1.1154	0.8985	0.9013	0.9041	0.9065	0.9091	0.9117
5.0	1.1273	1.1247	1.1219	1.1195	1.1173	1.1150	0.9030	0.9056	0.9082	0.9106	0.9130	0.9154
6.0	1.1276	1.1250	1.1223	1.1200	1.1174	1.1151	0.9091	0.9117	0.9142	0.9165	0.9185	0.9206
8.0	1.1286	1.1259	1.1232	1.1207	1.1185	1.1163	0.9159	0.9181	0.9204	0.9224	0.9243	0.9264
10.	1.1298	1.1271	1.1245	1.1220	1.1197	1.1174	0.9193	0.9213	0.9234	0.9253	0.9272	0.9290
20.	1.1336	1.1309	1.1289	1.1265	1.1243	1.1221	0.9235	0.9254	0.9271	0.9287	0.9303	0.9319
40.	1.1369	1.1343	1.1323	1.1302	1.1282	1.1263	0.9235	0.9252	0.9266	0.9281	0.9295	0.9309
60.	1.1384	1.1360	1.1339	1.1319	1.1301	1.1283	0.9228	0.9245	0.9258	0.9272	0.9286	0.9299
80.	1.1393	1.1370	1.1348	1.1330	1.1312	1.1296	0.9223	0.9239	0.9253	0.9266	0.9278	0.9291
100.	1.1400	1.1377	1.1355	1.1337	1.1321	1.1305	0.9218	0.9234	0.9248	0.9261	0.9273	0.9284
200.	1.1416	1.1396	1.1374	1.1359	1.1344	1.1331	0.9206	0.9220	0.9235	0.9246	0.9256	0.9266
400.	1.1428	1.1410	1.1393	1.1379	1.1366	1.1354	0.9195	0.9209	0.9222	0.9232	0.9241	0.9250
600.	1.1434	1.1417	1.1403	1.1390	1.1378	1.1366	0.9190	0.9203	0.9215	0.9224	0.9233	0.9241
800.	1.1437	1.1421	1.1409	1.1396	1.1385	1.1374	0.9187	0.9199	0.9210	0.9219	0.9227	0.9235
1000.	1.1439	1.1424	1.1413	1.1401	1.1390	1.1379	0.9185	0.9197	0.9206	0.9215	0.9223	0.9231
∞	1.1458	1.1458	1.1458	1.1458	1.1458	1.1458	0.9167	0.9167	0.9167	0.9167	0.9167	0.9167

See page 501 for Explanation of Tables

TABLE I. Collision Integrals for (8, 6, 4) Potentials

	E^*						F^*					
T^*	$\gamma=0$	$\gamma=0.2$	$\gamma=0.4$	$\gamma=0.6$	$\gamma=0.8$	$\gamma=1.0$	$\gamma=0$	$\gamma=0.2$	$\gamma=0.4$	$\gamma=0.6$	$\gamma=0.8$	$\gamma=1.0$
0	0.8750	0.8750	0.8750	0.8750	0.8750	0.9167	0.8413	0.8413	0.8413	0.8413	0.8413	0.9377
0.01	0.8751	0.8762	0.8781	0.8820	0.8907	0.9144	0.8469	0.8494	0.8544	0.8640	0.8826	0.9323
0.02	0.8750	0.8766	0.8791	0.8837	0.8929	0.9136	0.8471	0.8505	0.8565	0.8669	0.8861	0.9301
0.03	0.8749	0.8768	0.8798	0.8847	0.8941	0.9130	0.8470	0.8512	0.8578	0.8683	0.8874	0.9276
0.04	0.8744	0.8769	0.8800	0.8854	0.8948	0.9124	0.8475	0.8518	0.8588	0.8691	0.8880	0.9252
0.05	0.8744	0.8776	0.8801	0.8859	0.8953	0.9120	0.8478	0.8523	0.8595	0.8698	0.8881	0.9232
0.06	0.8742	0.8771	0.8800	0.8861	0.8956	0.9116	0.8486	0.8538	0.8604	0.8706	0.8884	0.9215
0.07	0.8757	0.8779	0.8811	0.8862	0.8959	0.9113	0.8490	0.8530	0.8604	0.8714	0.8887	0.9200
0.08	0.8765	0.8787	0.8819	0.8876	0.8960	0.9111	0.8467	0.8527	0.8603	0.8709	0.8889	0.9187
0.09	0.8779	0.8798	0.8829	0.8887	0.8971	0.9112	0.8444	0.8509	0.8589	0.8702	0.8877	0.9174
0.10	0.8792	0.8811	0.8841	0.8892	0.8978	0.9114	0.8412	0.8482	0.8569	0.8690	0.8862	0.9152
0.15	0.8790	0.8834	0.8868	0.8928	0.9014	0.9136	0.8217	0.8307	0.8414	0.8561	0.8749	0.9022
0.20	0.8678	0.8721	0.8774	0.8870	0.8971	0.9103	0.8103	0.8192	0.8300	0.8441	0.8625	0.8879
0.25	0.8502	0.8586	0.8641	0.8737	0.8852	0.9006	0.8062	0.8146	0.8248	0.8381	0.8553	0.8776
0.30	0.8347	0.8412	0.8499	0.8596	0.8720	0.8874	0.8066	0.8145	0.8236	0.8358	0.8512	0.8718
0.35	0.8223	0.8286	0.8369	0.8476	0.8597	0.8756	0.8077	0.8151	0.8249	0.8359	0.8500	0.8684
0.40	0.8119	0.8199	0.8289	0.8376	0.8500	0.8651	0.8124	0.8181	0.8259	0.8365	0.8501	0.8671
0.45	0.8053	0.8122	0.8208	0.8321	0.8432	0.8565	0.8149	0.8215	0.8303	0.8380	0.8495	0.8668
0.50	0.8016	0.8070	0.8161	0.8255	0.8383	0.8516	0.8187	0.8251	0.8329	0.8430	0.8520	0.8663
0.60	0.7990	0.8053	0.8127	0.8193	0.8299	0.8432	0.8260	0.8317	0.8400	0.8474	0.8573	0.8697
0.70	0.8013	0.8070	0.8139	0.8217	0.8300	0.8395	0.8344	0.8394	0.8470	0.8530	0.8630	0.8738
0.80	0.8052	0.8113	0.8188	0.8245	0.8332	0.8420	0.8429	0.8477	0.8550	0.8605	0.8678	0.8786
0.90	0.8123	0.8176	0.8238	0.8292	0.8370	0.8457	0.8514	0.8561	0.8620	0.8671	0.8750	0.8830
1.0	0.8196	0.8244	0.8302	0.8359	0.8415	0.8505	0.8591	0.8637	0.8699	0.8741	0.8808	0.8889
1.2	0.8348	0.8391	0.8438	0.8485	0.8542	0.8603	0.8745	0.8781	0.8833	0.8878	0.8934	0.8995
1.4	0.8490	0.8528	0.8572	0.8612	0.8656	0.8708	0.8884	0.8919	0.8962	0.8995	0.9044	0.9103
1.6	0.8613	0.8649	0.8688	0.8726	0.8766	0.8807	0.9002	0.9035	0.9078	0.9108	0.9144	0.9194
1.8	0.8721	0.8754	0.8789	0.8822	0.8860	0.8897	0.9111	0.9138	0.9176	0.9210	0.9239	0.9275
2.0	0.8813	0.8844	0.8877	0.8907	0.8939	0.8974	0.9206	0.9230	0.9263	0.9285	0.9326	0.9353
2.5	0.8991	0.9014	0.9041	0.9068	0.9094	0.9121	0.9397	0.9417	0.9443	0.9459	0.9480	0.9504
3.0	0.9110	0.9133	0.9157	0.9179	0.9203	0.9223	0.9535	0.9550	0.9573	0.9587	0.9603	0.9620
3.5	0.9193	0.9214	0.9236	0.9257	0.9277	0.9298	0.9640	0.9652	0.9669	0.9681	0.9695	0.9710
4.0	0.9253	0.9273	0.9292	0.9312	0.9331	0.9350	0.9722	0.9732	0.9746	0.9755	0.9766	0.9778
4.5	0.9297	0.9316	0.9334	0.9353	0.9371	0.9388	0.9787	0.9795	0.9807	0.9814	0.9823	0.9832
5.0	0.9330	0.9348	0.9366	0.9384	0.9400	0.9417	0.9840	0.9846	0.9856	0.9862	0.9870	0.9877
6.0	0.9375	0.9392	0.9409	0.9425	0.9441	0.9457	0.9917	0.9923	0.9930	0.9937	0.9940	0.9945
8.0	0.9421	0.9437	0.9452	0.9468	0.9483	0.9497	1.0013	1.0015	1.0018	1.0023	1.0027	1.0032
10.	0.9441	0.9457	0.9471	0.9486	0.9500	0.9513	1.0070	1.0071	1.0071	1.0075	1.0078	1.0080
20.	0.9459	0.9473	0.9485	0.9498	0.9510	0.9522	1.0178	1.0177	1.0174	1.0174	1.0175	1.0175
40.	0.9448	0.9461	0.9472	0.9484	0.9495	0.9506	1.0228	1.0227	1.0223	1.0221	1.0220	1.0219
60.	0.9438	0.9452	0.9463	0.9474	0.9484	0.9494	1.0245	1.0244	1.0241	1.0238	1.0236	1.0235
80.	0.9432	0.9445	0.9456	0.9467	0.9477	0.9486	1.0253	1.0252	1.0251	1.0248	1.0246	1.0244
100.	0.9427	0.9439	0.9451	0.9462	0.9471	0.9481	1.0258	1.0257	1.0257	1.0254	1.0252	1.0250
200.	0.9413	0.9425	0.9437	0.9447	0.9455	0.9463	1.0269	1.0268	1.0270	1.0268	1.0267	1.0265
400.	0.9403	0.9414	0.9424	0.9432	0.9440	0.9448	1.0275	1.0275	1.0276	1.0275	1.0275	1.0273
600.	0.9398	0.9408	0.9417	0.9425	0.9432	0.9439	1.0278	1.0277	1.0277	1.0277	1.0276	1.0276
800.	0.9395	0.9405	0.9412	0.9420	0.9427	0.9434	1.0279	1.0278	1.0277	1.0277	1.0277	1.0276
1000.	0.9393	0.9402	0.9409	0.9417	0.9423	0.9430	1.0280	1.0279	1.0277	1.0277	1.0277	1.0276
∞	0.9375	0.9375	0.9375	0.9375	0.9375	0.9375	1.0287	1.0287	1.0287	1.0287	1.0287	1.0287

See page 501 for Explanation of Tables

TABLE II. Collision Integrals for (12, 6, 4) Potentials

	$\Omega^{(1,1)*}$						A^*					
T^*	$\gamma=0$	$\gamma=0.2$	$\gamma=0.4$	$\gamma=0.6$	$\gamma=0.8$	$\gamma=1.0$	$\gamma=0$	$\gamma=0.2$	$\gamma=0.4$	$\gamma=0.6$	$\gamma=0.8$	$\gamma=1.0$
0							0.8696	0.8696	0.8696	0.8696	0.8696	1.0058
0.01	17.189	15.412	13.501	11.437	9.2149	6.8973	0.9168	0.9263	0.9384	0.9541	0.9778	1.0145
0.02	12.040	10.842	9.5800	8.2499	6.8636	5.4699	0.9268	0.9368	0.9491	0.9639	0.9855	1.0160
0.03	9.7638	8.8259	7.8493	6.8367	5.8002	4.7765	0.9342	0.9440	0.9560	0.9705	0.9899	1.0168
0.04	8.4086	7.6262	6.8189	5.9916	5.1555	4.3383	0.9403	0.9498	0.9614	0.9758	0.9931	1.0174
0.05	7.4849	6.8084	6.1159	5.4126	4.7089	4.0257	0.9457	0.9549	0.9659	0.9804	0.9958	1.0180
0.06	6.8043	6.2056	5.5967	4.9834	4.3746	3.7864	0.9501	0.9593	0.9700	0.9843	0.9981	1.0186
0.07	6.2735	5.7368	5.1935	4.6484	4.1114	3.5945	0.9552	0.9633	0.9735	0.9879	1.0003	1.0194
0.08	5.8512	5.3580	4.8672	4.3772	3.8969	3.4355	0.9583	0.9676	0.9772	0.9908	1.0024	1.0203
0.09	5.4971	5.0480	4.5961	4.1508	3.7169	3.3007	0.9625	0.9707	0.9807	0.9944	1.0043	1.0209
0.10	5.1997	4.7837	4.3691	3.9583	3.5623	3.1837	0.9668	0.9743	0.9836	0.9970	1.0071	1.0220
0.15	4.1716	3.8736	3.5805	3.2966	3.0223	2.7634	0.9921	0.9969	1.0029	1.0123	1.0194	1.0300
0.20	3.5272	3.3069	3.0899	2.8786	2.6774	2.4849	1.0210	1.0233	1.0260	1.0318	1.0357	1.0437
0.25	3.0654	2.8996	2.7355	2.5748	2.4211	2.2749	1.0478	1.0479	1.0489	1.0523	1.0543	1.0587
0.30	2.7135	2.5878	2.4612	2.3370	2.2176	2.1034	1.0683	1.0681	1.0679	1.0693	1.0708	1.0740
0.35	2.4367	2.3405	2.2419	2.1442	2.0500	1.9598	1.0832	1.0830	1.0817	1.0831	1.0835	1.0860
0.40	2.2167	2.1400	2.0617	1.9843	1.9094	1.8373	1.0932	1.0938	1.0923	1.0934	1.0935	1.0946
0.45	2.0347	1.9763	1.9123	1.8503	1.7897	1.7319	1.1011	1.0995	1.0996	1.0991	1.1003	1.1011
0.50	1.8814	1.8381	1.7875	1.7365	1.6875	1.6399	1.1077	1.1047	1.1034	1.1046	1.1044	1.1063
0.60	1.6512	1.6222	1.5873	1.5557	1.5222	1.4895	1.1127	1.1106	1.1095	1.1087	1.1089	1.1111
0.70	1.4823	1.4626	1.4404	1.4155	1.3948	1.3734	1.1110	1.1104	1.1110	1.1123	1.1106	1.1114
0.80	1.3528	1.3420	1.3258	1.3107	1.2948	1.2786	1.1110	1.1082	1.1087	1.1090	1.1106	1.1126
0.90	1.2533	1.2461	1.2365	1.2254	1.2149	1.2046	1.1085	1.1072	1.1061	1.1069	1.1079	1.1100
1.0	1.1753	1.1707	1.1636	1.1572	1.1498	1.1426	1.1046	1.1049	1.1043	1.1043	1.1052	1.1068
1.2	1.0557	1.0567	1.0555	1.0530	1.0504	1.0482	1.1025	1.1007	1.1000	1.1012	1.1016	1.1013
1.4	0.97301	0.97667	0.97769	0.97887	0.97922	0.97860	1.0991	1.0978	1.0978	1.0973	1.0976	1.0993
1.6	0.91159	0.91732	0.92070	0.92330	0.92519	0.92717	1.0975	1.0956	1.0953	1.0953	1.0957	1.0957
1.8	0.86473	0.87137	0.87630	0.87980	0.88342	0.88613	1.0966	1.0948	1.0940	1.0943	1.0942	1.0946
2.0	0.82778	0.83471	0.84082	0.84515	0.84949	0.85350	1.0959	1.0950	1.0937	1.0939	1.0936	1.0935
2.5	0.76182	0.77066	0.77785	0.78383	0.78877	0.79368	1.0966	1.0948	1.0937	1.0933	1.0936	1.0933
3.0	0.71782	0.72750	0.73548	0.74248	0.74860	0.75400	1.0984	1.0963	1.0954	1.0944	1.0937	1.0935
3.5	0.68645	0.69642	0.70485	0.71222	0.71884	0.72478	1.1000	1.0984	1.0971	1.0961	1.0953	1.0947
4.0	0.66248	0.67274	0.68145	0.68907	0.69590	0.70209	1.1021	1.1002	1.0990	1.0980	1.0971	1.0964
4.5	0.64327	0.65380	0.66278	0.67062	0.67756	0.68389	1.1042	1.1022	1.1008	1.0997	1.0989	1.0981
5.0	0.62742	0.63819	0.64733	0.65535	0.66247	0.66886	1.1061	1.1041	1.1026	1.1014	1.1004	1.0997
6.0	0.60267	0.61363	0.62301	0.63120	0.63854	0.64515	1.1094	1.1074	1.1058	1.1045	1.1034	1.1025
8.0	0.56877	0.57986	0.58934	0.59776	0.60526	0.61203	1.1142	1.1123	1.1108	1.1094	1.1082	1.1072
10.	0.54553	0.55666	0.56626	0.57471	0.58225	0.58908	1.1176	1.1158	1.1143	1.1129	1.1118	1.1108
20.	0.48364	0.49471	0.50427	0.51271	0.52025	0.52710	1.1262	1.1246	1.1233	1.1221	1.1210	1.1200
40.	0.43117	0.44187	0.45114	0.45932	0.46665	0.47330	1.1318	1.1303	1.1292	1.1282	1.1273	1.1265
60.	0.40339	0.41379	0.42279	0.43075	0.43788	0.44435	1.1341	1.1328	1.1317	1.1308	1.1300	1.1293
80.	0.38480	0.39494	0.40372	0.41149	0.41846	0.42478	1.1354	1.1342	1.1332	1.1324	1.1317	1.1310
100.	0.37097	0.38090	0.38950	0.39710	0.40394	0.41012	1.1364	1.1352	1.1343	1.1335	1.1328	1.1321
200.	0.33109	0.34028	0.34825	0.35531	0.36166	0.36741	1.1387	1.1377	1.1370	1.1363	1.1358	1.1352
400.	0.29540	0.30382	0.31113	0.31761	0.32345	0.32873	1.1402	1.1395	1.1388	1.1383	1.1379	1.1374
600.	0.27627	0.28425	0.29118	0.29731	0.30284	0.30786	1.1407	1.1401	1.1396	1.1391	1.1387	1.1383
800.	0.26342	0.27109	0.27775	0.28365	0.28897	0.29379	1.1409	1.1404	1.1399	1.1395	1.1392	1.1388
1000.	0.25386	0.26129	0.26775	0.27347	0.27862	0.28329	1.1410	1.1405	1.1401	1.1398	1.1395	1.1392
∞							1.1419	1.1419	1.1419	1.1419	1.1419	1.1419

See page 501 for Explanation of Tables

TABLE II. Collision Integrals for (12, 6, 4) Potentials

	B^*						C^*					
T^*	$\gamma=0$	$\gamma=0.2$	$\gamma=0.4$	$\gamma=0.6$	$\gamma=0.8$	$\gamma=1.0$	$\gamma=0$	$\gamma=0.2$	$\gamma=0.4$	$\gamma=0.6$	$\gamma=0.8$	$\gamma=1.0$
0	1.2500	1.2500	1.2500	1.2500	1.2500	1.1852	0.8333	0.8333	0.8333	0.8333	0.8333	0.8889
0.01	1.2553	1.2525	1.2472	1.2375	1.2194	1.1857	0.8293	0.8309	0.8343	0.8414	0.8562	0.8885
0.02	1.2572	1.2526	1.2454	1.2336	1.2148	1.1855	0.8282	0.8309	0.8358	0.8446	0.8605	0.8886
0.03	1.2585	1.2529	1.2445	1.2318	1.2127	1.1859	0.8273	0.8308	0.8367	0.8465	0.8628	0.8886
0.04	1.2594	1.2534	1.2441	1.2308	1.2118	1.1867	0.8265	0.8307	0.8373	0.8478	0.8642	0.8884
0.05	1.2600	1.2535	1.2437	1.2304	1.2117	1.1878	0.8259	0.8305	0.8377	0.8487	0.8651	0.8882
0.06	1.2599	1.2538	1.2438	1.2301	1.2118	1.1893	0.8253	0.8304	0.8380	0.8493	0.8657	0.8878
0.07	1.2624	1.2533	1.2436	1.2303	1.2125	1.1905	0.8255	0.8301	0.8383	0.8497	0.8660	0.8873
0.08	1.2618	1.2563	1.2430	1.2309	1.2132	1.1924	0.8243	0.8305	0.8383	0.8500	0.8662	0.8868
0.09	1.2657	1.2560	1.2466	1.2304	1.2148	1.1942	0.8239	0.8295	0.8388	0.8501	0.8662	0.8863
0.10	1.2710	1.2598	1.2467	1.2341	1.2155	1.1965	0.8229	0.8292	0.8380	0.8506	0.8661	0.8856
0.15	1.3112	1.2915	1.2744	1.2543	1.2362	1.2150	0.8128	0.8223	0.8339	0.8468	0.8630	0.8808
0.20	1.3449	1.3252	1.3059	1.2862	1.2658	1.2456	0.7975	0.8101	0.8235	0.8385	0.8547	0.8727
0.25	1.3610	1.3411	1.3264	1.3105	1.2923	1.2721	0.7834	0.7975	0.8124	0.8282	0.8449	0.8620
0.30	1.3589	1.3465	1.3338	1.3225	1.3060	1.2924	0.7721	0.7872	0.8022	0.8185	0.8348	0.8521
0.35	1.3464	1.3420	1.3343	1.3227	1.3114	1.3001	0.7643	0.7798	0.7950	0.8102	0.8264	0.8429
0.40	1.3321	1.3290	1.3242	1.3159	1.3099	1.2978	0.7592	0.7748	0.7894	0.8044	0.8198	0.8352
0.45	1.3173	1.3154	1.3095	1.3056	1.3002	1.2963	0.7576	0.7714	0.7859	0.8003	0.8151	0.8304
0.50	1.3017	1.2987	1.2987	1.2936	1.2899	1.2871	0.7589	0.7709	0.7842	0.7983	0.8121	0.8264
0.60	1.2686	1.2654	1.2711	1.2682	1.2700	1.2682	0.7619	0.7729	0.7867	0.7977	0.8103	0.8231
0.70	1.2442	1.2454	1.2416	1.2421	1.2453	1.2451	0.7690	0.7804	0.7900	0.8019	0.8127	0.8229
0.80	1.2229	1.2225	1.2239	1.2229	1.2201	1.2237	0.7786	0.7875	0.7980	0.8072	0.8162	0.8268
0.90	1.1993	1.2053	1.2044	1.2063	1.2062	1.2023	0.7873	0.7966	0.8050	0.8143	0.8227	0.8302
1.0	1.1867	1.1886	1.1911	1.1896	1.1916	1.1924	0.7963	0.8049	0.8136	0.8209	0.8290	0.8365
1.2	1.1649	1.1651	1.1654	1.1658	1.1681	1.1700	0.8153	0.8219	0.8286	0.8353	0.8419	0.8479
1.4	1.1489	1.1486	1.1483	1.1483	1.1493	1.1507	0.8310	0.8368	0.8429	0.8482	0.8535	0.8590
1.6	1.1379	1.1368	1.1362	1.1355	1.1361	1.1366	0.8449	0.8497	0.8548	0.8595	0.8642	0.8683
1.8	1.1293	1.1282	1.1274	1.1276	1.1265	1.1268	0.8565	0.8610	0.8654	0.8700	0.8734	0.8772
2.0	1.1224	1.1222	1.1208	1.1211	1.1204	1.1196	0.8661	0.8709	0.8746	0.8788	0.8820	0.8848
2.5	1.1131	1.1114	1.1106	1.1092	1.1093	1.1088	0.8851	0.8884	0.8917	0.8947	0.8979	0.9003
3.0	1.1076	1.1057	1.1043	1.1034	1.1027	1.1017	0.8983	0.9011	0.9037	0.9061	0.9083	0.9103
3.5	1.1035	1.1024	1.1010	1.0999	1.0989	1.0979	0.9073	0.9101	0.9124	0.9145	0.9163	0.9178
4.0	1.1018	1.1001	1.0989	1.0978	1.0968	1.0959	0.9142	0.9166	0.9187	0.9206	0.9223	0.9237
4.5	1.1006	1.0987	1.0974	1.0964	1.0954	1.0945	0.9195	0.9216	0.9235	0.9252	0.9267	0.9280
5.0	1.0997	1.0979	1.0965	1.0954	1.0944	1.0935	0.9236	0.9255	0.9272	0.9287	0.9301	0.9314
6.0	1.0989	1.0971	1.0956	1.0945	1.0934	1.0924	0.9295	0.9311	0.9326	0.9339	0.9350	0.9361
8.0	1.0982	1.0965	1.0953	1.0940	1.0930	1.0920	0.9358	0.9373	0.9386	0.9397	0.9406	0.9415
10.	1.0981	1.0966	1.0952	1.0941	1.0932	1.0922	0.9391	0.9405	0.9416	0.9426	0.9435	0.9443
20.	1.0992	1.0978	1.0967	1.0957	1.0948	1.0940	0.9441	0.9451	0.9459	0.9467	0.9473	0.9479
40.	1.1000	1.0990	1.0981	1.0973	1.0966	1.0960	0.9452	0.9460	0.9467	0.9473	0.9478	0.9483
60.	1.1002	1.0994	1.0986	1.0980	1.0974	1.0969	0.9453	0.9460	0.9466	0.9471	0.9476	0.9480
80.	1.1004	1.0996	1.0990	1.0984	1.0979	1.0974	0.9453	0.9460	0.9465	0.9469	0.9473	0.9477
100.	1.1004	1.0997	1.0992	1.0987	1.0982	1.0978	0.9453	0.9459	0.9464	0.9468	0.9471	0.9475
200.	1.1007	1.1002	1.0998	1.0994	1.0991	1.0988	0.9453	0.9457	0.9460	0.9463	0.9466	0.9468
400.	1.1012	1.1008	1.1004	1.1001	1.0999	1.0996	0.9451	0.9454	0.9456	0.9459	0.9460	0.9462
600.	1.1015	1.1011	1.1008	1.1005	1.1003	1.1001	0.9449	0.9452	0.9454	0.9456	0.9458	0.9459
800.	1.1017	1.1013	1.1010	1.1008	1.1006	1.1004	0.9448	0.9450	0.9453	0.9454	0.9456	0.9457
1000.	1.1018	1.1014	1.1012	1.1009	1.1007	1.1006	0.9447	0.9449	0.9451	0.9453	0.9455	0.9456
∞	1.1019	1.1019	1.1019	1.1019	1.1019	1.1019	0.9444	0.9444	0.9444	0.9444	0.9444	0.9444

See page 501 for Explanation of Tables

TABLE II. Collision Integrals for (12, 6, 4) Potentials

	Ω*						Ω*					
T*	γ=0	γ=0.2	γ=0.4	γ=0.6	γ=0.8	γ=1.0	γ=0	γ=0.2	γ=0.4	γ=0.6	γ=0.8	γ=1.0
0	0.8750	0.8750	0.8750	0.8750	0.8750	0.9167	0.8413	0.8413	0.8413	0.8413	0.8413	0.9377
0.01	0.8754	0.8769	0.8796	0.8845	0.8951	0.9169	0.8499	0.8545	0.8618	0.8728	0.8981	0.9397
0.02	0.8756	0.8776	0.8811	0.8874	0.8981	0.9169	0.8513	0.8573	0.8662	0.8788	0.9041	0.9399
0.03	0.8758	0.8781	0.8822	0.8894	0.8998	0.9169	0.8522	0.8589	0.8689	0.8832	0.9070	0.9396
0.04	0.8759	0.8786	0.8830	0.8908	0.9010	0.9169	0.8530	0.8601	0.8708	0.8866	0.9086	0.9392
0.05	0.8760	0.8790	0.8838	0.8919	0.9019	0.9169	0.8538	0.8612	0.8723	0.8892	0.9097	0.9387
0.06	0.8761	0.8794	0.8845	0.8926	0.9026	0.9169	0.8546	0.8622	0.8735	0.8911	0.9103	0.9380
0.07	0.8759	0.8800	0.8848	0.8933	0.9031	0.9168	0.8556	0.8631	0.8749	0.8922	0.9107	0.9374
0.08	0.8771	0.8802	0.8857	0.8935	0.9038	0.9170	0.8552	0.8640	0.8756	0.8932	0.9110	0.9365
0.09	0.8777	0.8810	0.8865	0.8939	0.9044	0.9168	0.8552	0.8638	0.8763	0.8930	0.9109	0.9361
0.10	0.8783	0.8819	0.8872	0.8951	0.9044	0.9173	0.8541	0.8634	0.8760	0.8932	0.9111	0.9349
0.15	0.8810	0.8859	0.8916	0.8982	0.9078	0.9189	0.8447	0.8571	0.8717	0.8870	0.9068	0.9288
0.20	0.8758	0.8830	0.8907	0.8982	0.9085	0.9186	0.8359	0.8492	0.8642	0.8800	0.8990	0.9201
0.25	0.8643	0.8741	0.8838	0.8926	0.9033	0.9147	0.8322	0.8456	0.8591	0.8741	0.8927	0.9115
0.30	0.8532	0.8640	0.8739	0.8848	0.8964	0.9069	0.8319	0.8437	0.8574	0.8709	0.8879	0.9054
0.35	0.8440	0.8542	0.8653	0.8758	0.8876	0.8986	0.8337	0.8443	0.8567	0.8699	0.8854	0.9011
0.40	0.8359	0.8463	0.8576	0.8677	0.8809	0.8908	0.8357	0.8461	0.8576	0.8697	0.8832	0.8989
0.45	0.8314	0.8418	0.8513	0.8627	0.8728	0.8843	0.8385	0.8468	0.8594	0.8708	0.8840	0.8971
0.50	0.8269	0.8376	0.8480	0.8570	0.8684	0.8779	0.8441	0.8502	0.8600	0.8719	0.8840	0.8967
0.60	0.8234	0.8322	0.8426	0.8522	0.8623	0.8710	0.8503	0.8571	0.8670	0.8743	0.8852	0.8964
0.70	0.8263	0.8339	0.8413	0.8499	0.8591	0.8678	0.8568	0.8639	0.8718	0.8816	0.8896	0.8979
0.80	0.8305	0.8382	0.8454	0.8521	0.8591	0.8662	0.8649	0.8698	0.8780	0.8861	0.8937	0.9026
0.90	0.8372	0.8430	0.8502	0.8565	0.8625	0.8675	0.8723	0.8773	0.8835	0.8906	0.8979	0.9054
1.0	0.8433	0.8485	0.8556	0.8613	0.8670	0.8721	0.8782	0.8836	0.8901	0.8956	0.9024	0.9089
1.2	0.8566	0.8618	0.8669	0.8712	0.8762	0.8809	0.8926	0.8966	0.9014	0.9069	0.9120	0.9168
1.4	0.8697	0.8737	0.8780	0.8821	0.8859	0.8891	0.9043	0.9078	0.9126	0.9164	0.9207	0.9255
1.6	0.8811	0.8848	0.8883	0.8915	0.8947	0.8976	0.9151	0.9178	0.9216	0.9253	0.9290	0.9323
1.8	0.8908	0.8943	0.8974	0.9002	0.9027	0.9050	0.9244	0.9270	0.9300	0.9335	0.9362	0.9394
2.0	0.8992	0.9022	0.9051	0.9077	0.9099	0.9117	0.9323	0.9353	0.9376	0.9408	0.9432	0.9454
2.5	0.9151	0.9176	0.9199	0.9219	0.9235	0.9251	0.9486	0.9503	0.9522	0.9544	0.9569	0.9586
3.0	0.9262	0.9283	0.9300	0.9316	0.9331	0.9343	0.9608	0.9620	0.9634	0.9648	0.9662	0.9676
3.5	0.9340	0.9357	0.9374	0.9387	0.9399	0.9409	0.9696	0.9707	0.9719	0.9730	0.9740	0.9749
4.0	0.9394	0.9411	0.9425	0.9438	0.9448	0.9457	0.9764	0.9774	0.9784	0.9793	0.9801	0.9809
4.5	0.9435	0.9451	0.9464	0.9475	0.9485	0.9493	0.9820	0.9827	0.9835	0.9842	0.9850	0.9856
5.0	0.9467	0.9481	0.9493	0.9504	0.9513	0.9520	0.9866	0.9871	0.9877	0.9882	0.9888	0.9894
6.0	0.9510	0.9523	0.9534	0.9543	0.9551	0.9558	0.9934	0.9937	0.9941	0.9945	0.9948	0.9952
8.0	0.9556	0.9567	0.9577	0.9585	0.9592	0.9598	1.0015	1.0018	1.0021	1.0023	1.0024	1.0026
10.	0.9577	0.9588	0.9597	0.9604	0.9611	0.9617	1.0063	1.0065	1.0067	1.0068	1.0069	1.0070
20.	0.9602	0.9611	0.9618	0.9624	0.9630	0.9635	1.0156	1.0156	1.0156	1.0156	1.0156	1.0156
40.	0.9603	0.9610	0.9615	0.9620	0.9625	0.9629	1.0201	1.0199	1.0198	1.0198	1.0197	1.0197
60.	0.9601	0.9607	0.9612	0.9616	0.9620	0.9624	1.0217	1.0215	1.0213	1.0212	1.0212	1.0211
80.	0.9600	0.9605	0.9609	0.9613	0.9617	0.9620	1.0226	1.0224	1.0222	1.0221	1.0221	1.0219
100.	0.9599	0.9604	0.9608	0.9611	0.9614	0.9617	1.0232	1.0230	1.0228	1.0226	1.0226	1.0224
200.	0.9595	0.9599	0.9602	0.9605	0.9607	0.9609	1.0246	1.0244	1.0242	1.0241	1.0240	1.0238
400.	0.9591	0.9594	0.9597	0.9599	0.9601	0.9603	1.0253	1.0252	1.0250	1.0249	1.0249	1.0247
600.	0.9589	0.9591	0.9594	0.9596	0.9597	0.9599	1.0254	1.0253	1.0252	1.0252	1.0251	1.0250
800.	0.9587	0.9590	0.9592	0.9594	0.9595	0.9597	1.0254	1.0253	1.0253	1.0252	1.0252	1.0251
1000.	0.9586	0.9588	0.9590	0.9592	0.9593	0.9595	1.0254	1.0253	1.0253	1.0253	1.0252	1.0252
∞	0.9583	0.9583	0.9583	0.9583	0.9583	0.9583	1.0258	1.0258	1.0258	1.0258	1.0258	1.0258

See page 501 for Explanation of Tables

TABLE III. Collision Integrals for (16, 6, 4) Potentials

	$\Omega^{(1,1)*}$						A^*					
T^*	γ=0	γ=0.2	γ=0.4	γ=0.6	γ=0.8	γ=1.0	γ=0	γ=0.2	γ=0.4	γ=0.6	γ=0.8	γ=1.0
0							0.8696	0.8696	0.8696	0.8696	0.8696	1.0058
0.01	16.093	14.284	12.383	10.418	8.3866	6.3605	0.9242	0.9333	0.9478	0.9645	0.9882	1.0237
0.02	11.255	10.036	8.7789	7.5146	6.2526	5.0363	0.9357	0.9459	0.9610	0.9773	0.9986	1.0277
0.03	9.1204	8.1620	7.1910	6.2285	5.2871	4.3946	0.9439	0.9548	0.9691	0.9850	1.0043	1.0299
0.04	7.8507	7.0484	6.2472	5.4609	4.7023	3.9901	0.9505	0.9617	0.9752	0.9906	1.0082	1.0314
0.05	6.9858	6.2902	5.6042	4.9360	4.2978	3.7025	0.9563	0.9676	0.9802	0.9949	1.0112	1.0325
0.06	6.3486	5.7316	5.1301	4.5475	3.9955	3.4830	0.9615	0.9727	0.9845	0.9986	1.0138	1.0335
0.07	5.8539	5.2985	4.7616	4.2447	3.7578	3.3076	0.9658	0.9772	0.9884	1.0018	1.0160	1.0344
0.08	5.4547	4.9494	4.4650	3.9999	3.5642	3.1626	0.9709	0.9811	0.9918	1.0048	1.0181	1.0354
0.09	5.1267	4.6601	4.2187	3.7966	3.4024	3.0398	0.9745	0.9856	0.9951	1.0072	1.0201	1.0363
0.10	4.8486	4.4168	4.0099	3.6235	3.2640	2.9339	0.9783	0.9885	0.9987	1.0101	1.0220	1.0371
0.15	3.8978	3.5865	3.2998	3.0293	2.7820	2.5561	1.0005	1.0076	1.0141	1.0233	1.0322	1.0434
0.20	3.3136	3.0799	2.8643	2.6633	2.4782	2.3108	1.0254	1.0286	1.0332	1.0377	1.0449	1.0527
0.25	2.9011	2.7214	2.5556	2.4006	2.2582	2.1284	1.0477	1.0494	1.0510	1.0542	1.0581	1.0637
0.30	2.5888	2.4485	2.3188	2.1973	2.0848	1.9822	1.0660	1.0646	1.0663	1.0677	1.0713	1.0754
0.35	2.3430	2.2323	2.1292	2.0324	1.9428	1.8608	1.0796	1.0791	1.0784	1.0796	1.0815	1.0845
0.40	2.1452	2.0565	1.9739	1.8958	1.8233	1.7569	1.0892	1.0875	1.0865	1.0876	1.0896	1.0913
0.45	1.9834	1.9113	1.8442	1.7807	1.7214	1.6671	1.0943	1.0939	1.0930	1.0937	1.0948	1.0970
0.50	1.8489	1.7892	1.7345	1.6823	1.6333	1.5888	1.0983	1.0978	1.0974	1.0974	1.0990	1.1002
0.60	1.6362	1.5973	1.5606	1.5239	1.4903	1.4592	1.1026	1.1016	1.1004	1.1014	1.1027	1.1042
0.70	1.4820	1.4546	1.4271	1.4034	1.3795	1.3571	1.1021	1.1023	1.1020	1.1018	1.1028	1.1045
0.80	1.3644	1.3446	1.3262	1.3068	1.2908	1.2756	1.0994	1.0997	1.1008	1.1023	1.1018	1.1028
0.90	1.2717	1.2584	1.2448	1.2324	1.2198	1.2081	1.0976	1.0968	1.0976	1.0991	1.0996	1.1015
1.0	1.1978	1.1888	1.1796	1.1701	1.1616	1.1535	1.0952	1.0940	1.0946	1.0958	1.0967	1.0982
1.2	1.0881	1.0851	1.0801	1.0762	1.0720	1.0680	1.0898	1.0890	1.0906	1.0903	1.0916	1.0927
1.4	1.0106	1.0102	1.0096	1.0081	1.0067	1.0054	1.0863	1.0863	1.0862	1.0871	1.0880	1.0888
1.6	0.95331	0.95523	0.95629	0.95723	0.95777	0.95760	1.0836	1.0838	1.0840	1.0841	1.0846	1.0861
1.8	0.90908	0.91240	0.91536	0.91776	0.91894	0.92035	1.0822	1.0823	1.0821	1.0820	1.0828	1.0834
2.0	0.87415	0.87906	0.88236	0.88553	0.88824	0.89007	1.0814	1.0808	1.0812	1.0812	1.0811	1.0820
2.5	0.81243	0.81891	0.82396	0.82794	0.83175	0.83508	1.0805	1.0799	1.0799	1.0802	1.0802	1.0802
3.0	0.77127	0.77879	0.78492	0.78992	0.79423	0.79779	1.0812	1.0806	1.0800	1.0798	1.0797	1.0802
3.5	0.74175	0.74981	0.75645	0.76205	0.76679	0.77098	1.0824	1.0816	1.0809	1.0805	1.0803	1.0803
4.0	0.71939	0.72776	0.73468	0.74057	0.74564	0.75010	1.0837	1.0828	1.0822	1.0817	1.0813	1.0811
4.5	0.70159	0.71027	0.71738	0.72343	0.72869	0.73332	1.0850	1.0841	1.0834	1.0829	1.0824	1.0822
5.0	0.68696	0.69584	0.70318	0.70935	0.71470	0.71944	1.0864	1.0853	1.0846	1.0841	1.0835	1.0833
6.0	0.66395	0.67322	0.68079	0.68722	0.69273	0.69762	1.0890	1.0877	1.0868	1.0862	1.0856	1.0853
8.0	0.63286	0.64214	0.64997	0.65659	0.66232	0.66738	1.0925	1.0915	1.0905	1.0898	1.0891	1.0886
10.	0.61159	0.62102	0.62887	0.63557	0.64137	0.64649	1.0951	1.0941	1.0932	1.0925	1.0919	1.0913
20.	0.55536	0.56478	0.57266	0.57940	0.58530	0.59042	1.1016	1.1007	1.0999	1.0993	1.0990	1.0982
40.	0.50763	0.51680	0.52448	0.53105	0.53682	0.54183	1.1055	1.1048	1.1042	1.1037	1.1033	1.1029
60.	0.48217	0.49110	0.49860	0.50502	0.51062	0.51556	1.1071	1.1065	1.1060	1.1056	1.1052	1.1049
80.	0.46499	0.47374	0.48108	0.48738	0.49283	0.49771	1.1080	1.1074	1.1070	1.1065	1.1063	1.1060
100.	0.45214	0.46073	0.46794	0.47412	0.47946	0.48429	1.1086	1.1081	1.1077	1.1073	1.1070	1.1067
200.	0.41459	0.42263	0.42939	0.43520	0.44019	0.44476	1.1102	1.1098	1.1094	1.1091	1.1089	1.1087
400.	0.38027	0.38773	0.39402	0.39942	0.40417	0.40833	1.1112	1.1109	1.1106	1.1104	1.1102	1.1100
600.	0.36152	0.36866	0.37466	0.37983	0.38435	0.38836	1.1116	1.1113	1.1111	1.1109	1.1107	1.1106
800.	0.34877	0.35568	0.36149	0.36650	0.37089	0.37476	1.1117	1.1115	1.1113	1.1111	1.1109	1.1108
1000.	0.33918	0.34592	0.35159	0.35647	0.36074	0.36453	1.1118	1.1115	1.1114	1.1112	1.1111	1.1110
∞							1.1118	1.1118	1.1118	1.1118	1.1118	1.1118

See page 501 for Explanation of Tables

TABLE III. Collision Integrals for (16, 6, 4) Potentials

	B^*						C^*					
T^*	$\gamma=0$	$\gamma=0.2$	$\gamma=0.4$	$\gamma=0.6$	$\gamma=0.8$	$\gamma=1.0$	$\gamma=0$	$\gamma=0.2$	$\gamma=0.4$	$\gamma=0.6$	$\gamma=0.8$	$\gamma=1.0$
0	1.2500	1.2500	1.2500	1.2500	1.2500	1.1852	0.8333	0.8333	0.8333	0.8333	0.8333	0.8889
0.01	1.2561	1.2533	1.2477	1.2376	1.2191	1.1868	0.8286	0.8304	0.8339	0.8413	0.8567	0.8877
0.02	1.2576	1.2534	1.2453	1.2332	1.2141	1.1862	0.8275	0.8302	0.8354	0.8446	0.8609	0.8879
0.03	1.2585	1.2535	1.2438	1.2304	1.2114	1.1857	0.8267	0.8301	0.8366	0.8468	0.8634	0.8881
0.04	1.2599	1.2535	1.2428	1.2286	1.2098	1.1857	0.8260	0.8300	0.8374	0.8484	0.8650	0.8882
0.05	1.2605	1.2534	1.2422	1.2275	1.2088	1.1859	0.8253	0.8300	0.8381	0.8497	0.8662	0.8883
0.06	1.2611	1.2534	1.2416	1.2267	1.2084	1.1863	0.8249	0.8300	0.8387	0.8506	0.8671	0.8883
0.07	1.2617	1.2533	1.2415	1.2262	1.2081	1.1870	0.8243	0.8300	0.8391	0.8514	0.8677	0.8882
0.08	1.2635	1.2531	1.2413	1.2261	1.2084	1.1878	0.8242	0.8299	0.8395	0.8520	0.8682	0.8880
0.09	1.2635	1.2545	1.2409	1.2263	1.2087	1.1889	0.8233	0.8302	0.8396	0.8525	0.8686	0.8878
0.10	1.2676	1.2549	1.2429	1.2260	1.2097	1.1900	0.8230	0.8299	0.8401	0.8527	0.8688	0.8876
0.15	1.2921	1.2733	1.2553	1.2368	1.2196	1.2004	0.8167	0.8268	0.8384	0.8524	0.8680	0.8850
0.20	1.3191	1.2975	1.2793	1.2584	1.2390	1.2192	0.8066	0.8194	0.8335	0.8481	0.8639	0.8802
0.25	1.3298	1.3149	1.2969	1.2790	1.2593	1.2409	0.7960	0.8110	0.8261	0.8419	0.8574	0.8737
0.30	1.3359	1.3197	1.3035	1.2904	1.2752	1.2588	0.7881	0.8034	0.8189	0.8349	0.8509	0.8670
0.35	1.3289	1.3193	1.3050	1.2933	1.2803	1.2687	0.7822	0.7980	0.8132	0.8290	0.8447	0.8600
0.40	1.3157	1.3070	1.2996	1.2889	1.2809	1.2679	0.7785	0.7937	0.8092	0.8241	0.8395	0.8538
0.45	1.3032	1.2943	1.2893	1.2808	1.2762	1.2666	0.7768	0.7917	0.8065	0.8210	0.8357	0.8491
0.50	1.2857	1.2845	1.2769	1.2737	1.2683	1.2632	0.7767	0.7918	0.8055	0.8196	0.8334	0.8466
0.60	1.2581	1.2562	1.2543	1.2535	1.2491	1.2465	0.7820	0.7948	0.8067	0.8198	0.8318	0.8433
0.70	1.2324	1.2277	1.2321	1.2300	1.2297	1.2295	0.7889	0.7997	0.8126	0.8226	0.8332	0.8438
0.80	1.2105	1.2107	1.2061	1.2089	1.2107	1.2104	0.7971	0.8081	0.8174	0.8283	0.8376	0.8459
0.90	1.1925	1.1923	1.1930	1.1897	1.1909	1.1928	0.8063	0.8160	0.8255	0.8333	0.8419	0.8502
1.0	1.1781	1.1786	1.1776	1.1786	1.1777	1.1764	0.8156	0.8245	0.8325	0.8406	0.8476	0.8540
1.2	1.1532	1.1531	1.1542	1.1560	1.1564	1.1572	0.8325	0.8395	0.8470	0.8534	0.8593	0.8648
1.4	1.1365	1.1364	1.1367	1.1375	1.1383	1.1397	0.8476	0.8541	0.8597	0.8651	0.8701	0.8744
1.6	1.1249	1.1243	1.1241	1.1243	1.1246	1.1253	0.8606	0.8662	0.8712	0.8754	0.8793	0.8833
1.8	1.1161	1.1160	1.1150	1.1142	1.1151	1.1154	0.8718	0.8769	0.8808	0.8842	0.8880	0.8911
2.0	1.1094	1.1086	1.1087	1.1079	1.1074	1.1079	0.8812	0.8854	0.8895	0.8925	0.8952	0.8981
2.5	1.0986	1.0972	1.0968	1.0968	1.0963	1.0959	0.8989	0.9021	0.9052	0.9081	0.9102	0.9120
3.0	1.0922	1.0911	1.0904	1.0896	1.0893	1.0892	0.9112	0.9139	0.9162	0.9182	0.9200	0.9219
3.5	1.0884	1.0873	1.0864	1.0856	1.0849	1.0849	0.9201	0.9223	0.9242	0.9259	0.9273	0.9287
4.0	1.0857	1.0848	1.0839	1.0831	1.0825	1.0818	0.9265	0.9285	0.9302	0.9317	0.9329	0.9339
4.5	1.0839	1.0829	1.0821	1.0814	1.0808	1.0802	0.9314	0.9332	0.9347	0.9361	0.9371	0.9381
5.0	1.0827	1.0816	1.0808	1.0801	1.0795	1.0789	0.9353	0.9368	0.9382	0.9394	0.9404	0.9413
6.0	1.0813	1.0801	1.0792	1.0785	1.0778	1.0773	0.9410	0.9422	0.9433	0.9442	0.9451	0.9458
8.0	1.0797	1.0788	1.0779	1.0771	1.0765	1.0760	0.9472	0.9483	0.9491	0.9498	0.9505	0.9511
10.	1.0790	1.0781	1.0773	1.0767	1.0760	1.0755	0.9505	0.9514	0.9522	0.9528	0.9534	0.9539
20.	1.0785	1.0777	1.0771	1.0765	1.0760	1.0756	0.9558	0.9564	0.9569	0.9573	0.9577	0.9580
40.	1.0783	1.0778	1.0773	1.0769	1.0768	1.0763	0.9575	0.9579	0.9583	0.9586	0.9588	0.9591
60.	1.0781	1.0777	1.0774	1.0771	1.0770	1.0766	0.9579	0.9582	0.9585	0.9588	0.9589	0.9592
80.	1.0780	1.0777	1.0774	1.0772	1.0771	1.0768	0.9581	0.9584	0.9586	0.9588	0.9589	0.9592
100.	1.0779	1.0777	1.0775	1.0772	1.0771	1.0769	0.9582	0.9584	0.9586	0.9588	0.9589	0.9591
200.	1.0778	1.0777	1.0775	1.0774	1.0773	1.0772	0.9584	0.9586	0.9587	0.9588	0.9589	0.9590
400.	1.0780	1.0778	1.0777	1.0776	1.0776	1.0775	0.9585	0.9586	0.9586	0.9587	0.9588	0.9588
600.	1.0781	1.0780	1.0779	1.0778	1.0777	1.0776	0.9584	0.9585	0.9586	0.9586	0.9588	0.9587
800.	1.0782	1.0781	1.0780	1.0779	1.0778	1.0778	0.9584	0.9585	0.9585	0.9586	0.9586	0.9587
1000.	1.0782	1.0781	1.0780	1.0779	1.0778	1.0778	0.9583	0.9584	0.9585	0.9585	0.9586	0.9586
∞	1.0781	1.0781	1.0781	1.0781	1.0781	1.0781	0.9583	0.9583	0.9583	0.9583	0.9583	0.9583

See page 501 for Explanation of Tables

TABLE III. Collision Integrals for (16, 6, 4) Potentials

	Ω^*						P^*					
T^*	$\gamma=0$	$\gamma=0.2$	$\gamma=0.4$	$\gamma=0.6$	$\gamma=0.8$	$\gamma=1.0$	$\gamma=0$	$\gamma=0.2$	$\gamma=0.4$	$\gamma=0.6$	$\gamma=0.8$	$\gamma=1.0$
0	0.8750	0.8750	0.8750	0.8750	0.8750	0.9167	0.8413	0.8413	0.8413	0.8413	0.8413	0.9377
0.01	0.8755	0.8771	0.8803	0.8856	0.8964	0.9172	0.8513	0.8562	0.8637	0.8769	0.9002	0.9407
0.02	0.8756	0.8780	0.8817	0.8883	0.8993	0.9173	0.8532	0.8593	0.8687	0.8845	0.9065	0.9415
0.03	0.8757	0.8786	0.8827	0.8899	0.9009	0.9173	0.8544	0.8614	0.8720	0.8889	0.9099	0.9420
0.04	0.8759	0.8791	0.8836	0.8912	0.9021	0.9174	0.8553	0.8630	0.8744	0.8918	0.9122	0.9423
0.05	0.8761	0.8796	0.8845	0.8922	0.9031	0.9175	0.8561	0.8643	0.8762	0.8938	0.9138	0.9424
0.06	0.8763	0.8798	0.8852	0.8931	0.9038	0.9176	0.8568	0.8655	0.8778	0.8952	0.9151	0.9423
0.07	0.8768	0.8802	0.8859	0.8938	0.9045	0.9176	0.8573	0.8665	0.8790	0.8964	0.9160	0.9422
0.08	0.8765	0.8811	0.8864	0.8946	0.9051	0.9178	0.8580	0.8673	0.8802	0.8972	0.9167	0.9419
0.09	0.8772	0.8807	0.8874	0.8951	0.9057	0.9179	0.8581	0.8683	0.8810	0.8981	0.9173	0.9415
0.10	0.8779	0.8816	0.8875	0.8959	0.9063	0.9181	0.8579	0.8688	0.8817	0.8986	0.9175	0.9412
0.15	0.8807	0.8851	0.8917	0.8991	0.9092	0.9195	0.8531	0.8667	0.8811	0.8987	0.9164	0.9372
0.20	0.8775	0.8848	0.8921	0.9012	0.9106	0.9202	0.8478	0.8622	0.8775	0.8946	0.9124	0.9314
0.25	0.8710	0.8799	0.8889	0.8982	0.9087	0.9184	0.8451	0.8589	0.8741	0.8908	0.9074	0.9254
0.30	0.8625	0.8738	0.8827	0.8937	0.9035	0.9133	0.8438	0.8579	0.8727	0.8878	0.9038	0.9207
0.35	0.8540	0.8660	0.8761	0.8871	0.8976	0.9076	0.8453	0.8577	0.8721	0.8866	0.9019	0.9166
0.40	0.8474	0.8590	0.8708	0.8815	0.8916	0.9020	0.8475	0.8600	0.8727	0.8861	0.8999	0.9142
0.45	0.8436	0.8542	0.8654	0.8760	0.8866	0.8965	0.8493	0.8620	0.8739	0.8868	0.8999	0.9119
0.50	0.8406	0.8511	0.8615	0.8724	0.8821	0.8917	0.8522	0.8640	0.8758	0.8874	0.8998	0.9116
0.60	0.8377	0.8477	0.8585	0.8678	0.8763	0.8847	0.8608	0.8702	0.8790	0.8900	0.9007	0.9112
0.70	0.8390	0.8477	0.8575	0.8661	0.8740	0.8818	0.8673	0.8761	0.8858	0.8939	0.9030	0.9119
0.80	0.8441	0.8518	0.8585	0.8666	0.8743	0.8809	0.8736	0.8823	0.8907	0.8995	0.9070	0.9142
0.90	0.8495	0.8571	0.8638	0.8692	0.8763	0.8819	0.8808	0.8880	0.8957	0.9030	0.9103	0.9176
1.0	0.8555	0.8631	0.8690	0.8747	0.8799	0.8846	0.8877	0.8942	0.9006	0.9076	0.9139	0.9200
1.2	0.8688	0.8744	0.8792	0.8845	0.8883	0.8924	0.9001	0.9052	0.9115	0.9164	0.9216	0.9265
1.4	0.8808	0.8856	0.8898	0.8936	0.8968	0.9000	0.9112	0.9163	0.9206	0.9252	0.9294	0.9332
1.6	0.8918	0.8956	0.8991	0.9023	0.9051	0.9073	0.9209	0.9253	0.9294	0.9328	0.9361	0.9397
1.8	0.9012	0.9046	0.9075	0.9100	0.9124	0.9144	0.9297	0.9337	0.9367	0.9394	0.9428	0.9454
2.0	0.9091	0.9122	0.9148	0.9169	0.9189	0.9206	0.9373	0.9403	0.9436	0.9461	0.9482	0.9509
2.5	0.9243	0.9267	0.9286	0.9303	0.9315	0.9328	0.9520	0.9543	0.9566	0.9589	0.9605	0.9621
3.0	0.9348	0.9365	0.9381	0.9395	0.9406	0.9415	0.9631	0.9647	0.9662	0.9678	0.9691	0.9708
3.5	0.9421	0.9437	0.9450	0.9461	0.9469	0.9477	0.9714	0.9727	0.9738	0.9749	0.9758	0.9769
4.0	0.9474	0.9488	0.9499	0.9509	0.9517	0.9523	0.9777	0.9788	0.9797	0.9806	0.9813	0.9821
4.5	0.9514	0.9526	0.9536	0.9545	0.9552	0.9558	0.9827	0.9835	0.9844	0.9851	0.9856	0.9864
5.0	0.9544	0.9555	0.9564	0.9572	0.9578	0.9584	0.9868	0.9874	0.9881	0.9887	0.9892	0.9898
6.0	0.9587	0.9596	0.9604	0.9610	0.9616	0.9620	0.9931	0.9934	0.9938	0.9942	0.9945	0.9950
8.0	0.9632	0.9640	0.9647	0.9652	0.9658	0.9661	1.0006	1.0009	1.0010	1.0012	1.0014	1.0016
10.	0.9655	0.9662	0.9668	0.9673	0.9678	0.9680	1.0050	1.0052	1.0053	1.0054	1.0055	1.0056
20.	0.9685	0.9690	0.9695	0.9698	0.9702	0.9704	1.0134	1.0135	1.0135	1.0135	1.0135	1.0135
40.	0.9691	0.9695	0.9698	0.9701	0.9703	0.9706	1.0174	1.0173	1.0173	1.0173	1.0173	1.0172
60.	0.9692	0.9695	0.9698	0.9700	0.9702	0.9704	1.0188	1.0187	1.0186	1.0186	1.0186	1.0185
80.	0.9692	0.9695	0.9697	0.9699	0.9700	0.9702	1.0196	1.0194	1.0194	1.0193	1.0193	1.0192
100.	0.9693	0.9695	0.9697	0.9698	0.9699	0.9701	1.0201	1.0200	1.0199	1.0198	1.0197	1.0197
200.	0.9692	0.9694	0.9695	0.9696	0.9697	0.9698	1.0214	1.0212	1.0211	1.0210	1.0209	1.0209
400.	0.9691	0.9692	0.9693	0.9694	0.9695	0.9695	1.0221	1.0220	1.0218	1.0218	1.0217	1.0216
600.	0.9689	0.9690	0.9691	0.9692	0.9693	0.9693	1.0222	1.0220	1.0220	1.0220	1.0220	1.0219
800.	0.9688	0.9689	0.9690	0.9691	0.9692	0.9692	1.0222	1.0221	1.0221	1.0221	1.0221	1.0220
1000.	0.9688	0.9689	0.9690	0.9690	0.9691	0.9691	1.0222	1.0221	1.0221	1.0221	1.0221	1.0220
∞	0.9688	0.9688	0.9688	0.9688	0.9688	0.9688	1.0225	1.0225	1.0225	1.0225	1.0225	1.0225

See page 501 for Explanation of Tables

TABLE IV. Collision Integrals for $(n, 4)$ Potentials

	$\Omega^{(1,1)*}$					A^*				
T^*	n=6	n=10	n=14	n=18	n=300	n=6	n=10	n=14	n=18	n=300
0						0.8696	0.8696	0.8696	0.8696	0.8696
0.01	24.741	18.227	16.538	15.769	13.776	0.8836	0.9109	0.9211	0.9266	0.9444
0.02	17.267	12.780	11.573	11.024	9.6074	0.8901	0.9195	0.9319	0.9388	0.9605
0.03	13.951	10.370	9.3812	8.9307	7.7747	0.8957	0.9261	0.9397	0.9473	0.9714
0.04	11.973	8.9336	8.0771	7.6861	6.6884	0.9004	0.9318	0.9462	0.9542	0.9800
0.05	10.632	7.9548	7.1885	6.8386	5.9506	0.9043	0.9366	0.9517	0.9602	0.9871
0.06	9.6469	7.2303	6.5340	6.2140	5.4082	0.9077	0.9414	0.9566	0.9655	0.9932
0.07	8.8816	6.6715	6.0249	5.7297	4.9883	0.9115	0.9446	0.9613	0.9701	0.9987
0.08	8.2604	6.2183	5.6149	5.3390	4.6509	0.9162	0.9486	0.9656	0.9749	1.0035
0.09	7.7394	5.8447	5.2787	5.0161	4.3722	0.9220	0.9526	0.9693	0.9783	1.0079
0.10	7.2913	5.5257	4.9897	4.7450	4.1373	0.9289	0.9572	0.9737	0.9829	1.0120
0.15	5.6789	4.4210	4.0087	3.8150	3.3439	0.9745	0.9861	0.9972	1.0038	1.0310
0.20	4.6263	3.7185	3.4021	3.2490	2.8780	1.0206	1.0196	1.0234	1.0265	1.0413
0.25	3.8791	3.2114	2.9699	2.8501	2.5606	1.0561	1.0489	1.0477	1.0481	1.0519
0.30	3.3196	2.8270	2.6422	2.5493	2.3299	1.0821	1.0711	1.0675	1.0654	1.0575
0.35	2.8962	2.5262	2.3836	2.3124	2.1517	1.0997	1.0872	1.0816	1.0775	1.0617
0.40	2.5659	2.2848	2.1759	2.1225	2.0108	1.1117	1.0989	1.0920	1.0861	1.0631
0.45	2.3012	2.0842	2.0075	1.9660	1.8957	1.1201	1.1080	1.0969	1.0922	1.0634
0.50	2.0880	1.9252	1.8649	1.8370	1.8009	1.1254	1.1109	1.1021	1.0952	1.0621
0.60	1.7671	1.6745	1.6449	1.6309	1.6529	1.1292	1.1155	1.1073	1.0998	1.0581
0.70	1.5369	1.4916	1.4826	1.4830	1.5440	1.1319	1.1169	1.1061	1.0993	1.0529
0.80	1.3681	1.3544	1.3606	1.3684	1.4609	1.1314	1.1158	1.1037	1.0960	1.0479
0.90	1.2387	1.2483	1.2638	1.2791	1.3961	1.1309	1.1141	1.1022	1.0932	1.0433
1.0	1.1374	1.1630	1.1886	1.2069	1.3444	1.1300	1.1122	1.0994	1.0907	1.0391
1.2	0.98964	1.0386	1.0735	1.1005	1.2675	1.1289	1.1085	1.0954	1.0853	1.0322
1.4	0.88850	0.95070	0.99396	1.0252	1.2137	1.1279	1.1064	1.0918	1.0814	1.0273
1.6	0.81438	0.88550	0.93462	0.96927	1.1747	1.1274	1.1064	1.0895	1.0787	1.0231
1.8	0.75829	0.83726	0.88897	0.92626	1.1450	1.1295	1.1047	1.0885	1.0769	1.0201
2.0	0.71435	0.79838	0.85326	0.89217	1.1216	1.1317	1.1047	1.0877	1.0759	1.0179
2.5	0.63692	0.72906	0.78940	0.83211	1.0812	1.1353	1.1070	1.0876	1.0746	1.0139
3.0	0.58595	0.68339	0.74696	0.79208	1.0557	1.1404	1.1092	1.0887	1.0749	1.0113
3.5	0.54943	0.65052	0.71653	0.76339	1.0381	1.1452	1.1118	1.0903	1.0758	1.0097
4.0	0.52171	0.62536	0.69337	0.74169	1.0252	1.1495	1.1145	1.0919	1.0768	1.0087
4.5	0.49956	0.60532	0.67490	0.72445	1.0155	1.1537	1.1170	1.0936	1.0779	1.0080
5.0	0.48166	0.58883	0.65975	0.71031	1.0078	1.1568	1.1192	1.0952	1.0790	1.0075
6.0	0.45337	0.56287	0.63583	0.68810	0.99663	1.1626	1.1233	1.0982	1.0813	1.0070
8.0	0.41457	0.52743	0.60345	0.65813	0.98295	1.1714	1.1288	1.1022	1.0844	1.0065
10.	0.38810	0.50301	0.58122	0.63776	0.97486	1.1776	1.1329	1.1053	1.0867	1.0066
20.	0.31887	0.43811	0.52225	0.58402	0.95823	1.1931	1.1432	1.1126	1.0924	1.0067
40.	0.26237	0.38335	0.47218	0.53850	0.94823	1.2039	1.1501	1.1172	1.0958	1.0067
60.	0.23364	0.35460	0.44555	0.51417	0.94384	1.2087	1.1531	1.1191	1.0972	1.0066
80.	0.21495	0.33547	0.42765	0.49773	0.94111	1.2115	1.1548	1.1202	1.0979	1.0066
100.	0.20135	0.32131	0.41428	0.48539	0.93916	1.2135	1.1560	1.1210	1.0985	1.0066
200.	0.16378	0.28087	0.37545	0.44922	0.93379	1.2184	1.1589	1.1229	1.0999	1.0068
400.	0.13258	0.24529	0.34028	0.41591	0.92905	1.2221	1.1607	1.1241	1.1008	1.0070
600.	0.11694	0.22649	0.32122	0.39759	0.92642	1.2238	1.1614	1.1245	1.1010	1.0071
800.	0.10690	0.21399	0.30833	0.38508	0.92458	1.2248	1.1617	1.1246	1.1011	1.0071
1000.	0.09967	0.20475	0.29868	0.37565	0.92316	1.2255	1.1619	1.1247	1.1011	1.0071
						1.2344	1.1639	1.1258	1.1010	1.0084

See page 501 for Explanation of Tables

TABLE IV. Collision Integrals for $(n, 4)$ Potentials

	B^*					C^*				
T^*	n=6	n=10	n=14	n=18	n=300	n=6	n=10	n=14	n=18	n=300
0	1.2500	1.2500	1.2500	1.2500	1.2500	0.8333	0.8333	0.8333	0.8333	0.8333
0.01	1.2581	1.2548	1.2558	1.2563	1.2575	0.8283	0.8298	0.8289	0.8284	0.8272
0.02	1.2622	1.2568	1.2574	1.2578	1.2582	0.8256	0.8287	0.8278	0.8273	0.8263
0.03	1.2641	1.2584	1.2586	1.2590	1.2585	0.8237	0.8277	0.8270	0.8265	0.8258
0.04	1.2629	1.2595	1.2597	1.2600	1.2585	0.8228	0.8268	0.8262	0.8258	0.8255
0.05	1.2624	1.2608	1.2605	1.2607	1.2585	0.8223	0.8262	0.8256	0.8252	0.8253
0.06	1.2666	1.2610	1.2608	1.2614	1.2583	0.8217	0.8259	0.8251	0.8247	0.8253
0.07	1.2766	1.2607	1.2597	1.2623	1.2582	0.8202	0.8251	0.8245	0.8242	0.8252
0.08	1.2918	1.2643	1.2630	1.2623	1.2580	0.8176	0.8246	0.8246	0.8238	0.8252
0.09	1.3070	1.2697	1.2640	1.2639	1.2578	0.8137	0.8236	0.8235	0.8236	0.8252
0.10	1.3274	1.2776	1.2680	1.2653	1.2576	0.8088	0.8223	0.8231	0.8227	0.8252
0.15	1.3957	1.3269	1.2993	1.2870	1.2567	0.7771	0.8084	0.8155	0.8178	0.8256
0.20	1.4164	1.3596	1.3291	1.3095	1.2559	0.7470	0.7897	0.8031	0.8090	0.8257
0.25	1.4168	1.3728	1.3416	1.3228	1.2529	0.7248	0.7731	0.7909	0.8002	0.8265
0.30	1.4016	1.3695	1.3468	1.3268	1.2467	0.7098	0.7603	0.7821	0.7927	0.8275
0.35	1.3817	1.3599	1.3371	1.3215	1.2378	0.7001	0.7517	0.7748	0.7879	0.8294
0.40	1.3624	1.3460	1.3251	1.3066	1.2273	0.6945	0.7467	0.7711	0.7840	0.8319
0.45	1.3461	1.3303	1.3084	1.2942	1.2162	0.6929	0.7455	0.7680	0.7833	0.8353
0.50	1.3254	1.3098	1.2933	1.2799	1.2034	0.6921	0.7435	0.7689	0.7831	0.8392
0.60	1.2902	1.2793	1.2604	1.2537	1.1791	0.6957	0.7474	0.7720	0.7893	0.8479
0.70	1.2616	1.2530	1.2388	1.2253	1.1571	0.7038	0.7547	0.7803	0.7952	0.8574
0.80	1.2427	1.2313	1.2156	1.2057	1.1374	0.7142	0.7636	0.7882	0.8042	0.8670
0.90	1.2258	1.2093	1.2003	1.1869	1.1204	0.7251	0.7725	0.7983	0.8129	0.8761
1.0	1.2118	1.1962	1.1811	1.1736	1.1070	0.7360	0.7830	0.8064	0.8224	0.8847
1.2	1.1913	1.1732	1.1590	1.1484	1.0870	0.7568	0.8012	0.8248	0.8389	0.9002
1.4	1.1769	1.1576	1.1425	1.1313	1.0719	0.7750	0.8180	0.8400	0.8536	0.9128
1.6	1.1684	1.1471	1.1308	1.1198	1.0611	0.7914	0.8329	0.8534	0.8665	0.9230
1.8	1.1612	1.1375	1.1222	1.1110	1.0531	0.8051	0.8441	0.8649	0.8774	0.9314
2.0	1.1561	1.1320	1.1153	1.1042	1.0472	0.8167	0.8546	0.8743	0.8867	0.9386
2.5	1.1499	1.1224	1.1049	1.0933	1.0372	0.8394	0.8746	0.8926	0.9039	0.9517
3.0	1.1473	1.1174	1.0990	1.0866	1.0307	0.8552	0.8882	0.9054	0.9160	0.9604
3.5	1.1466	1.1144	1.0953	1.0826	1.0264	0.8666	0.8979	0.9144	0.9246	0.9666
4.0	1.1466	1.1128	1.0928	1.0798	1.0234	0.8749	0.9051	0.9210	0.9309	0.9712
4.5	1.1472	1.1119	1.0913	1.0778	1.0208	0.8813	0.9106	0.9261	0.9357	0.9747
5.0	1.1474	1.1115	1.0902	1.0765	1.0188	0.8858	0.9149	0.9301	0.9395	0.9774
6.0	1.1487	1.1113	1.0892	1.0749	1.0166	0.8924	0.9210	0.9360	0.9451	0.9815
8.0	1.1514	1.1112	1.0878	1.0730	1.0128	0.8996	0.9274	0.9421	0.9512	0.9862
10.	1.1537	1.1118	1.0875	1.0721	1.0112	0.9031	0.9308	0.9455	0.9545	0.9890
20.	1.1602	1.1142	1.0876	1.0711	1.0079	0.9067	0.9353	0.9507	0.9599	0.9938
40.	1.1657	1.1159	1.0879	1.0706	1.0063	0.9054	0.9360	0.9521	0.9617	0.9958
60.	1.1683	1.1165	1.0878	1.0703	1.0057	0.9039	0.9358	0.9524	0.9622	0.9965
80.	1.1699	1.1168	1.0878	1.0701	1.0053	0.9028	0.9357	0.9525	0.9625	0.9968
100.	1.1711	1.1171	1.0878	1.0700	1.0051	0.9020	0.9355	0.9526	0.9626	0.9970
200.	1.1741	1.1178	1.0878	1.0698	1.0046	0.8995	0.9351	0.9527	0.9629	0.9974
400.	1.1765	1.1187	1.0881	1.0699	1.0045	0.8974	0.9346	0.9527	0.9630	0.9976
600.	1.1776	1.1191	1.0883	1.0700	1.0045	0.8963	0.9343	0.9526	0.9630	0.9977
800.	1.1783	1.1194	1.0884	1.0701	1.0045	0.8956	0.9341	0.9525	0.9630	0.9977
1000.	1.1789	1.1195	1.0885	1.0701	1.0045	0.8951	0.9340	0.9525	0.9629	0.9977
∞	1.1852	1.1200	1.0884	1.0700	1.0044	0.8889	0.9333	0.9524	0.9630	0.9978

See page 501 for Explanation of Tables

TABLE IV. Collision Integrals for $(n, 4)$ Potentials

	Ω^*					P^*				
T^*	n=6	n=10	n=14	n=18	n=300	n=6	n=10	n=14	n=18	n=300
0	0.8750	0.8750	0.8750	0.8750	0.8750	0.8413	0.8413	0.8413	0.8413	0.8413
0.01	0.8732	0.8753	0.8754	0.8755	0.8759	0.8390	0.8484	0.8508	0.8515	0.8550
0.02	0.8726	0.8755	0.8756	0.8757	0.8763	0.8384	0.8496	0.8525	0.8535	0.8582
0.03	0.8719	0.8757	0.8758	0.8758	0.8767	0.8380	0.8506	0.8534	0.8548	0.8605
0.04	0.8718	0.8756	0.8760	0.8760	0.8770	0.8384	0.8514	0.8542	0.8559	0.8622
0.05	0.8717	0.8755	0.8760	0.8761	0.8773	0.8384	0.8521	0.8549	0.8568	0.8636
0.06	0.8722	0.8753	0.8762	0.8763	0.8776	0.8371	0.8530	0.8556	0.8575	0.8647
0.07	0.8732	0.8761	0.8765	0.8763	0.8779	0.8341	0.8530	0.8564	0.8583	0.8658
0.08	0.8746	0.8768	0.8768	0.8760	0.8781	0.8297	0.8531	0.8570	0.8592	0.8666
0.09	0.8758	0.8777	0.8771	0.8770	0.8783	0.8244	0.8519	0.8567	0.8597	0.8675
0.10	0.8768	0.8789	0.8779	0.8768	0.8786	0.8184	0.8502	0.8568	0.8594	0.8682
0.15	0.8706	0.8816	0.8808	0.8801	0.8789	0.7941	0.8363	0.8499	0.8558	0.8725
0.20	0.8504	0.8732	0.8779	0.8785	0.8800	0.7840	0.8263	0.8427	0.8512	0.8730
0.25	0.8292	0.8608	0.8695	0.8724	0.8789	0.7814	0.8220	0.8392	0.8486	0.8758
0.30	0.8118	0.8473	0.8599	0.8643	0.8779	0.7838	0.8213	0.8381	0.8481	0.8774
0.35	0.7981	0.8352	0.8500	0.8574	0.8763	0.7870	0.8225	0.8399	0.8498	0.8803
0.40	0.7882	0.8276	0.8424	0.8518	0.8755	0.7903	0.8244	0.8423	0.8515	0.8822
0.45	0.7818	0.8203	0.8388	0.8469	0.8753	0.7946	0.8297	0.8433	0.8546	0.8853
0.50	0.7776	0.8163	0.8346	0.8450	0.8758	0.7984	0.8316	0.8478	0.8561	0.8879
0.60	0.7752	0.8136	0.8303	0.8424	0.8791	0.8064	0.8391	0.8547	0.8652	0.8938
0.70	0.7788	0.8154	0.8335	0.8428	0.8845	0.8160	0.8465	0.8621	0.8711	0.9001
0.80	0.7847	0.8202	0.8381	0.8486	0.8909	0.8248	0.8545	0.8686	0.8777	0.9068
0.90	0.7920	0.8257	0.8436	0.8543	0.8975	0.8339	0.8622	0.8764	0.8842	0.9130
1.0	0.7999	0.8331	0.8494	0.8605	0.9042	0.8427	0.8703	0.8826	0.8912	0.9186
1.2	0.8161	0.8472	0.8633	0.8732	0.9166	0.8595	0.8841	0.8966	0.9031	0.9289
1.4	0.8312	0.8609	0.8757	0.8850	0.9270	0.8741	0.8973	0.9076	0.9138	0.9376
1.6	0.8455	0.8727	0.8870	0.8957	0.9357	0.8877	0.9096	0.9180	0.9234	0.9443
1.8	0.8562	0.8829	0.8966	0.9050	0.9428	0.8996	0.9186	0.9272	0.9318	0.9501
2.0	0.8656	0.8918	0.9047	0.9127	0.9488	0.9100	0.9274	0.9348	0.9391	0.9549
2.5	0.8851	0.9082	0.9203	0.9276	0.9599	0.9310	0.9452	0.9504	0.9533	0.9639
3.0	0.8979	0.9198	0.9310	0.9379	0.9674	0.9465	0.9580	0.9620	0.9639	0.9701
3.5	0.9069	0.9277	0.9385	0.9451	0.9728	0.9584	0.9675	0.9706	0.9719	0.9746
4.0	0.9132	0.9334	0.9439	0.9503	0.9767	0.9675	0.9750	0.9772	0.9779	0.9780
4.5	0.9179	0.9377	0.9479	0.9542	0.9798	0.9749	0.9809	0.9824	0.9827	0.9809
5.0	0.9214	0.9409	0.9510	0.9572	0.9822	0.9804	0.9857	0.9867	0.9867	0.9831
6.0	0.9262	0.9453	0.9553	0.9614	0.9854	0.9890	0.9930	0.9934	0.9928	0.9864
8.0	0.9309	0.9499	0.9599	0.9660	0.9897	0.9998	1.0015	1.0010	1.0000	0.9907
10.	0.9329	0.9520	0.9621	0.9682	0.9918	1.0060	1.0067	1.0057	1.0042	0.9933
20.	0.9339	0.9541	0.9649	0.9714	0.9954	1.0177	1.0166	1.0145	1.0124	0.9979
40.	0.9317	0.9537	0.9653	0.9722	0.9968	1.0229	1.0216	1.0186	1.0161	0.9997
60.	0.9301	0.9533	0.9652	0.9723	0.9973	1.0244	1.0233	1.0202	1.0175	1.0003
80.	0.9290	0.9530	0.9652	0.9724	0.9976	1.0252	1.0243	1.0210	1.0182	1.0006
100.	0.9282	0.9527	0.9652	0.9725	0.9978	1.0256	1.0249	1.0216	1.0187	1.0008
200.	0.9259	0.9521	0.9650	0.9726	0.9982	1.0264	1.0262	1.0230	1.0200	1.0015
400.	0.9239	0.9514	0.9648	0.9725	0.9983	1.0267	1.0268	1.0236	1.0206	1.0019
600.	0.9230	0.9510	0.9646	0.9723	0.9983	1.0268	1.0269	1.0238	1.0207	1.0020
800.	0.9224	0.9508	0.9645	0.9723	0.9983	1.0269	1.0269	1.0238	1.0207	1.0019
1000.	0.9220	0.9507	0.9644	0.9722	0.9983	1.0269	1.0269	1.0237	1.0207	1.0019
∞	0.9167	0.9500	0.9643	0.9722	0.9983	1.0268	1.0277	1.0241	1.0211	1.0018

See page 501 for Explanation of Tables

TABLE V. Asymptotic Forms of $\Omega^{(1,1)*}$

$T^* \rightarrow 0$:

$$\Omega^{(1,1)*} = \frac{1.4714}{(T^*)^{1/2}}\left[\frac{3n(1-\gamma)}{n(3+\gamma)-12(1+\gamma)}\right]^{1/2} \quad \text{for } \gamma \neq 1 \quad \text{(from Ref. 19)}$$

$$\Omega^{(1,1)*} = \frac{1.1874}{(T^*)^{1/3}}\left(\frac{n}{n-6}\right)^{1/3} \quad \text{for } \gamma = 1 \quad \text{(from Ref. 18)}$$

$T^* \rightarrow \infty$:

$$\Omega^{(1,1)*} = \frac{f(n)}{(T^*)^{2/n}}\left[\frac{12(1+\gamma)}{n(3+\gamma)-12(1+\gamma)}\right]^{2/n}$$

n	6	8	10	12	14	16	18	300	∞
$f(n)$	0.8363	0.8661	0.8869	0.9022	0.9133	0.9229	0.9310	0.9950	1

Values calculated from Ref. 18, except for $n = 12$ which is from Ref. 17

TABLE VI. Effective Reduced Temperatures for Minima and Maxima in the Mobility

Potential		T^*_{min}	T^*_{max}	Potential		T^*_{min}	T^*_{max}
(8, 6, 4):	$\gamma = 0$	—	1.89	(16, 6, 4):	$\gamma = 0$	—	1.21
	$\gamma = 0.2$	—	1.81		$\gamma = 0.2$	—	1.12
	$\gamma = 0.4$	0.051	1.68		$\gamma = 0.4$	0.201	1.01
	$\gamma = 0.6$	0.122	1.63		$\gamma = 0.6$	0.313	0.900
	$\gamma = 0.8$	0.177	1.54		$\gamma = 0.8$	0.504	0.702
	$\gamma = 1$	0.244	1.42		$\gamma = 1$	—	—
(12, 6, 4):	$\gamma = 0$	—	1.43	$(n, 4)$:	$n = 6$	—	2.37
	$\gamma = 0.2$	—	1.35		$n = 10$	—	1.61
	$\gamma = 0.4$	0.153	1.27		$n = 14$	—	1.31
	$\gamma = 0.6$	0.224	1.17		$n = 18$	—	1.13
	$\gamma = 0.8$	0.309	1.07		$n = 300$	—	0.419
	$\gamma = 1$	0.420	0.950		$n = \infty$	—	0.36

See page 501 for Explanation of Tables

APPENDIX D

EXCITATION IN ELECTRON-METASTABLE HELIUM COLLISIONS

Excitation in electron-metastable helium collisions*

M. R. Flannery, W. F. Morrison, and B. L. Richmond

School of Physics, Georgia Institute of Technology, Atlanta, Georgia 30332
(Received 14 October 1974)

The $2^{1,3}P$, $3^{1,3}S$, $3^{1,3}P$, $3^{1,3}D$ and $4^{1,3}P$ excitations arising from e-He($2^{1,3}S$) collisions are examined by application of the Born and of the Vainshtein, Presnyakov, and Sobel'man approximations. Total excitation cross sections are calculated for the above transitions for electron impact energy E up to 500 eV. Contrary to expectation, excitation to the $3^{1,3}D$ and $3^{1,3}S$ states dominate the $3^{1,3}P$ and $4^{1,3}P$ excitations except at incident energies above 100 eV.

I. INTRODUCTION

While theoretical and experimental knowledge of collisions between electrons and ground-state atomic species has increased significantly during the past decade, relatively little[1] is known with any great certainty about collisions involving metastables. In a high-density gas discharge, metastable states are populated predominantly by dissociative recombination

$$e + He_2^+ \rightarrow He + He^* \tag{1}$$

between slow electrons and molecular ions formed initially by the rapid three-body association process

$$He^* + 2He \rightarrow He_2^+ + He. \tag{2}$$

In (1), the excited levels with principal quantum number $n \geq 3$ (except, perhaps, the $3^{1,3}S$ states) are depleted by associative ionization (or the Hornbeck-Molnar process)

$$He^{**} + He \rightarrow He_2^+ + e \tag{3}$$

thereby ensuring that the $2^{1,3}S$ metastable states, which are also formed by direct electron-impact excitation from the ground state, are the dominant excited atomic species. The rates of the subsequent collision processes involving the metastables are very important to the analysis of gaseous discharges and gaseous nebulae[2] and are at present unknown. In vacuum uv-lasers, for example, excited molecular states He_2^* are formed mainly by

$$He^* + 2He \rightarrow He_2^* + He \tag{4}$$

which radiate photons of wavelength ~610 Å to the dissociative ground state, thereby ensuring automatic population inversion. The metastable He* formed via (1) is primarily depleted by the excitation processes,

$$e + He(2^{1,3}S) \rightarrow e + He(n^{1,3}L), \quad n = 2\text{—}4;\ L = S,\ P,\ D \tag{5}$$

the cross sections for which would critically affect the over-all formation rate of He_2^* by (4). Any information on the above processes (5) is very scarce.

In an effort to systematically explore the various processes involving metastables, we will consider in this paper the excitation cross sections for (5) by using initially the simpler theoretical approaches—the Born[1] and the Vainshtein, Presnyakov, and Sobel'man (VPS) approximations.[3] Various effects such as the repulsion between the incident and excited electrons, effective-charge, and electron-exchange effects are included to first order in the VPS method. Not only will this present investigation establish some remarkable properties of the cross sections but also will provide the additional insight to the collision needed as a basis for more refined descriptions.

II. THEORY

According to the Born approximation[1] for electron-atom collisions, the total cross section for excitation of state n from an initial state i of the target atom is given by

$$Q_{in}(k_i) = \frac{8\pi}{k_i^2 a_0^2} \int_{k_i - k_n}^{k_i + k_n} |F_{in}(\mathbf{K})|^2 \frac{dK}{K^3} \tag{6}$$

in atomic units (a_0^2), where

$$F_{in}(\mathbf{K}) = \langle \phi_i(\mathbf{r}_1, \mathbf{r}_2) | \sum_{j=1}^{2} \exp(i\mathbf{K}\cdot\mathbf{r}_j) | \phi_n(\mathbf{r}_1, \mathbf{r}_2) \rangle \tag{7}$$

is generalized form factor connecting states i and n of atomic helium, the bound electrons at $\mathbf{r}_1$ and $\mathbf{r}_2$ being described by the set of wave functions $\phi_n(\mathbf{r}_1, \mathbf{r}_2)$ with eigenenergies ϵ_n. The vector $\mathbf{K} = \mathbf{k}_i - \mathbf{k}_n$, where $\mathbf{k}_i$ and $\mathbf{k}_n$ are the initial and final wave numbers of relative motion, is the momentum change suffered by the collision. From a knowledge of the form factor (7), the excitation cross sections are easily calculated from (6).

In Born's approximation, however, and in more refined descriptions, e.g., the close-coupling method, the total wave function for the collision system is expanded in terms of unperturbed atomic states, the interaction between the incoming electron and the atom being treated as a perturbation, assumed small. In this instance, the averaged attraction of the incident electron with the screened nucleus is of primary importance, while details of repulsion with the atomic electrons is ignored in the wave function describing the relative motion. However, when an atom is initially in an excited state, the electron is generally quite distant from the core [for H(n), $\langle r_1 \rangle = n^2 a_0$; for He($2^1S$), $\langle r_{12} \rangle = 5.3 a_0$] and hence, the incident electron is subjected not to the averaged field of the orbital electron about the core but actually to two strong Coulomb fields—the e-e repulsion and the e-core attraction. These two fields reduce to the averaged field only for distant encounters.

For electron-hydrogen scattering, Vainshtein *et al.*[3] have introduced a method whereby a product of Coulombic functions is chosen to represent the zero-order (unperturbed) wave function for the e-H relative motion. The method achieved notable success for e-H(1s) excitation and ionization. The extension of their analysis to

e-He($2^{1,3}S$) collisions is straightforward, and results in the cross section,

$$Q_{in}=\frac{8\pi}{k_i^2 a_0^2}\int_{k_i-k_n}^{k_i+k_n}|F_{in}(\mathbf{K})|^2[f(\nu,x)]^2\frac{dK}{K^3} \tag{8}$$

in which the integrand of (6) is multiplied by the square of the factor,

$$f(\nu,x)=\left(\frac{\pi\nu}{\sinh\pi\nu}\right)F(-i\nu,i\nu,1,x), \tag{9}$$

where F is a hypergeometric function with arguments

$$x=\frac{2\epsilon_{ni}+K^2}{2\epsilon_{ni}+3K^2}, \quad \nu=k_i^{-1} \text{ or } [k_i+(2\epsilon_i)^{1/2}]^{-1} \tag{10}$$

in which $\epsilon_{ni}=\epsilon_n-\epsilon_i$ is the excitation energy in atomic units (27.2 eV) and where the second value of ν in (10) is designed to account for the fact that the atomic electrons are bound so as to give an effective-charge effect.

The effect of exchange between the incident and atomic electrons is ignored by (6) and (8). Its acknowledgment involves explicit inclusion of spin functions. For singlet-singlet transitions the over-all spin state for the (e-He) system is a doublet and the total wave function for the three electrons denoted by 1, 2, and 3 is, in a two-state treatment, given by,

$$\Psi^S(1,2;3)=(N_S/\sqrt{3})\sum_{1,2,3}^{\text{cyclic}}[\Psi_i^S(1,2)F_i(3) + \Psi_n^S(1,2)F_n(3)]\chi^-(1,2;3)\equiv\Psi_i+\Psi_n, \tag{11}$$

where $F_n(3)$ is the wave function describing the projectile-target relative motion, where

$$\chi^-(1,2;3)=(1/\sqrt{2})(\alpha_1\beta_2-\beta_1\alpha_2)\alpha_3 \tag{12}$$

is the normalized doublet spin function, and where $\Psi_n^S(1,2)=\Psi_n^S(2,1)$ is the symmetrical spatial wave function for singlet helium. The over-all wave function Ψ^S, normalized by N_S, is antisymmetric with respect to interchange of *any* two electrons. The Born approximation to the amplitude for scattering by angle θ is therefore

$$F_{in}(\theta)=-\frac{1}{4\pi}\frac{2me^2}{\hbar^2}\sum_{m_{s_1}}\sum_{m_{s_2}}\sum_{m_{s_3}}\langle\Psi_n|V|\Psi_i\rangle_{r_1,r_2,r_3}, \tag{13}$$

where $V(\mathbf{r}_1,\mathbf{r}_2,\mathbf{r}_3)$ is the e-He electrostatic interaction and $F_i(3)=\exp(i\mathbf{k}_i\cdot\mathbf{r})$. On performing the cyclic summations in (11), on summing over the spin substates $m_s=\pm\frac{1}{2}$ in (13) and on using the orthonormal properties of the spin functions α_i and β_i, then, the scattering amplitude reduces, after some analysis, to

$$F_{in}^{SS}(\theta)=N_S^2(f_{in}-g_{in}), \tag{14}$$

where

$$f_{in}(\theta)=-\frac{1}{4\pi}\frac{2me^2}{\hbar^2}\langle\Psi_n^S(1,2)F_n(3)|V|\Psi_i^S(1,2)F_i(3)\rangle \tag{15}$$

is the scattering amplitude for *direct* collisions alone and

$$g_{in}(\theta)=-\frac{1}{4\pi}\frac{2me^2}{\hbar^2}\langle\Psi_n^S(3,2)F_n(1)|V|\Psi_i^S(1,2)F_i(3)\rangle \tag{16}$$

represents the scattering amplitude for *exchange* collisions in which electrons 1 and 3 have been interchanged. By taking $F_{i,n}$ to be a plane wave, then (14)–(16) gives rise to the Born-Oppenheimer approximation.[1] By taking F_n to be a plane wave and F_i to be a product of unperturbed Coulombic waves, then

$$g_{in}^{\text{VPS}}=(K^2/2k_i^2)f(\nu,\tfrac{1}{4})f_{in}^B, \tag{17}$$

$$f_{in}^B=f_{in} \quad \text{with } F_{i,n}=\exp(i\mathbf{k}_{i,n}\cdot\mathbf{r}_3),$$

for the exchange amplitude can eventually be derived from application of the VPS approximation which also assumes $\langle\Psi_i|\Psi_n\rangle=\delta_{in}$ and hence $N_S=1$ in (14). Then, the total cross section including exchange for singlet-singlet transitions is finally

$$Q_{in}^{1,1}(k_i)=\frac{2\pi k_n}{k_i}\int|F_{in}^{SS}(\theta)|^2\,d(\cos\theta) \tag{18}$$

$$=\frac{8\pi}{k_i^2a_0^2}\int_{k_i-k_n}^{k_i+k_n}\frac{|F_{in}(K)|^2}{K^3}\left(f(\nu,x)-\frac{K^2}{2k_i^2}f(\nu,\tfrac{1}{4})\right)^2dK.$$

For the triplet-triplet transitions in (5), the over-all antisymmetric spatial-spin state function can either belong to a doublet or as a quartet spin state. Scattering in the doublet mode occurs in one-third of all collisions while two-thirds of all collisions are in a quartet mode. The total wave function analogous to (11) is therefore

$$\Psi^T(1,2;3)=(N_T/\sqrt{3})\sum_{1,2,3}^{\text{cyclic}}[\Psi_i^A(1,2)F_i(3) + \Psi_n^A(1,2)F_n(3)]\chi_{Q,D}^*(1,2;3) \equiv\Psi_i+\Psi_n \tag{19}$$

in which $\Psi_i^A(1,2)$ is the antisymmetric spatial wave function for triplet helium and where the three-electron normalized spin functions are

$$\chi_Q^*(1,2;3)=\begin{cases}\alpha_1\alpha_2\alpha_3, & M_S=+\frac{3}{2}\\ (1/\sqrt{3})(\alpha_1\alpha_2\beta_3+\alpha_1\beta_2\alpha_3+\beta_1\alpha_2\alpha_3), & M_S=+\frac{1}{2}\end{cases} \tag{20a}$$

for the quartet spin state with total magnetic components $M_S=\frac{3}{2}$ and $\frac{1}{2}$, and

$$\chi_D^*(1,2;3)=(1/\sqrt{6})[2\alpha_1\alpha_2\beta_3-\alpha_3(\alpha_1\beta_2+\alpha_2\beta_1)], \quad M_S=+\tfrac{1}{2} \tag{20b}$$

represents the doublet state. The functions appropriate to states with negative magnetic quantum numbers are obtained from (12) and (20) by the $\alpha_i \longrightarrow \beta_i$ interchange for each of the three electrons in the corresponding function for positive M_S.

By substituting (19) and (20) in (13) and by performing the cyclic summations, then after lengthy, although straightforward, analysis,

$$F_{in}^{TT}(D)=N_T(f_{in}+g_{in}) \tag{21a}$$

and

$$F_{in}^{TT}(Q)=N_T(f_{in}-2g_{in}) \tag{21b}$$

are obtained for the scattering amplitudes in the doublet (D) and quartet (Q) modes, respectively. Since one-third and two-thirds of all collisions are in the D and Q

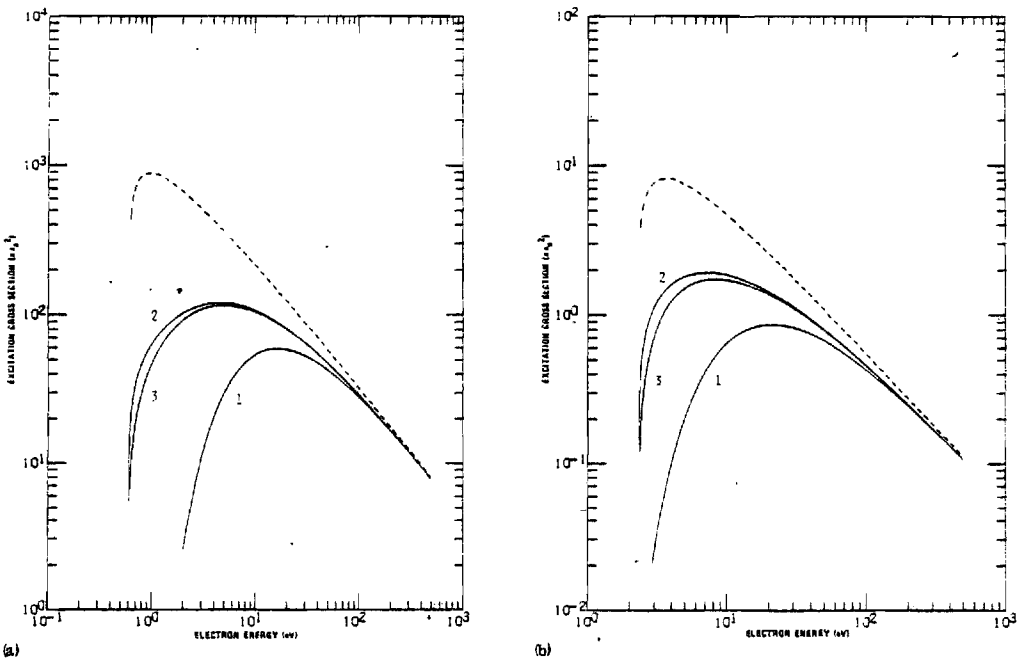

FIG. 1. (a) The 2^1P and (b) the 3^1S cross sections for excitation arising from e-He(2^1S) collisions as a function of electron impact energy. Broken curve: Born approximation, (6) in text; solid curve: VPS approximation, 1, 2—(8)—(10) in text, with and without effective charge, 3—(18) with effective charge and exchange.

modes, respectively, then

$$|F_{in}^{TT}(\theta)|^2 = \tfrac{1}{3}|F_{in}^{TT}(D)|^2 + \tfrac{2}{3}|F_{in}^{TT}(Q)|^2 \tag{22a}$$

$$= |f_{in}|^2 - 2\mathrm{Re}(f_{in}g_{in}^*) + 3|g_{in}|^2. \tag{22b}$$

Hence, the total excitation cross section for triplet-triplet transitions is then

$$Q_{in}^{3,3}(k_i) = 2\pi\frac{k_n}{k_i}\int |F_{in}^{TT}(\theta)|^2\, d(\cos\theta) \tag{23a}$$

$$= \frac{8\pi}{k_i^2 a_0^2}\int \frac{|F_{in}(K)|^2}{K^3}\left(\left[f(\nu,x)\right]^2 - \frac{K^2}{k_i^2}f(\nu,\tfrac{1}{4})f(\nu,x) + \tfrac{3}{8}\frac{K^4}{k_i^4}\left[f(\nu,\tfrac{1}{4})\right]^2\right) dK \tag{23b}$$

on application of the VPS approximations (8) and (17) for f_{in} and g_{in}, respectively. Note that at high impact energies, the function $f(\nu,x) \to 1$ so that the Born and the Ochkur[4] approximations are recovered for the direct and exchange scattering amplitudes, respectively. The Ochkur method is a simplification to the original Born-Oppenheimer approximation mentioned above and is therefore based on the use of plane waves for the relative motion.

III. RESULTS AND DISCUSSION

The theory outlined above has been applied to the examination of the excitation processes,

$$e + \mathrm{He}(2^{1,3}S) \to e + \mathrm{He}(n^{1,3}L), \quad n = 2\text{—}4,\ L = S,\ P,\ D, \tag{24}$$

for incident-electron energies E from threshold up to 500 eV. Highly accurate form factors (3) have already been computed by Kim and Inokuti[5] from the extremely reliable correlated wave functions of Weiss.[6] The following four sets of cross-section calculations were performed for each transition in (24)—the Born approximation B given by (6), and the three VPS approximations given by (8)—(10), with and without the effective charge, and by (18) and (23) which include the additional effect of electron exchange in singlet-singlet and triplet-triplet transitions, respectively.

In Figs. 1—4 are presented the Born and VPS cross sections (in $\pi a_0^2 = 0.88\times10^{-16}$ cm^2) calculated to within 1% accuracy as a function of impact energy E (eV). The present Born values agree with those previously given by Kim and Inokuti[5] for the 2^1S-2^1P and the triplet-triplet transitions. The optical line strengths S for the $2^{1,3}S$-$2^{1,3}P$ transitions are the largest (25.5 and 57.7 atomic units, respectively[7]) and hence it is only to be expected that the collision cross sections for these excitations dominate. However, Fig. 3 demonstrates a remarkable feature at low E when the collisional excitations are in the following descending order $3^1D > 3^1S > 3^1P > 4^1P$. At high $E > 100$ eV, the natural order $3^1P > 3^1D > 3^1S > 4^1P$ is followed when the cross sections

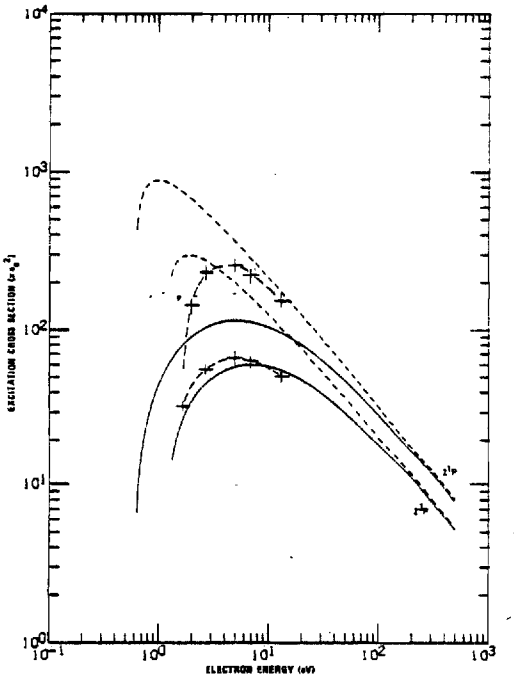

FIG. 2. The $2^{1,3}P$ cross sections for excitation arising from e-He($2^{1,3}S$) collisions. (---): Born approximation; (——); VPS approximation (3) with effective charge and exchange; (OOOO): close-coupling results of Burke *et al.* (Ref. 8).

$\sim E^{-1}\ln E$ for the optically allowed transitions, and $\sim E^{-4}$ for the optically forbidden transitions. For the singlet transitions $\sigma(3^1S) > \sigma(3^1P)$ from threshold up to ~12 eV, while $\sigma(3^1D)$ remains greater than $\sigma(3^1P)$ up to 100 eV. Figure 4 demonstrates that similar behavior occurs also for the triplet transitions, the crossover point for the cross sections being shifted however to higher energies, i.e., $\sigma(3^3S) > \sigma(3^3P)$ for $E < 100$ eV and $\sigma(3^3D) > \sigma(3^3P)$ for $E < 1000$ eV.

The basic reason for this unexpected behavior is that the line strength for the $2^{1,3}S$-$3^{1,3}P$ transitions in helium is abnormally small, i.e., 2.5 atomic units[7] to be compared with the value[7] 18.8 for the $2s$-$3p$ transition in atomic hydrogen. The importance of the quadrupole and higher-order optically forbidden multipole terms relative to the optically allowed dipole term is therefore strong such that the optically forbidden collisional excitations dominate the optically allowed excitation at low and intermediate impact energies.

The effects acknowledged by the various VPS approximations are demonstrated in Fig. 1 for the 2^1P and the 3^1S excitations which were found to be representatives of the optically allowed and forbidden transitions in (24). The use, as in (8) with $\nu = k^{-1}$, of the zero-order Coulombic functions for the relative motion (instead of a plane wave) yields, in general, cross sections which are lower than the Born values in the low- and intermediate-energy region and which eventually converge onto the correct Born limit at high energies. The optically allowed transitions are affected more by this inclusion than are the optically forbidden excitations. When the effective charge is acknowledged by the use of $\nu = [k_i + (2\epsilon_i)^{1/2}]^{-1}$ in (8) and (9), all the cross sections are significantly increased. The additional inclusion of exchange, as by (18) and (23), causes a relatively smaller decrease. The use of more-refined wave functions for the relative motion thus appears to be more important than the inclusion of exchange.

This claim is further supported in Fig. 2 by the close-coupling study of Burke *et al.*[8] who included distortion and exchange effects in the solution near threshold of the equations[1] closely coupling all the $n = 2$ states. The close-coupling results lie in general between Born and VPS treatments except at the lowest E. The agreement exhibited in Fig. 2 between the VPS and close-coupling approximations for the 2^3S-2^3P is remarkable. The singlet excitation cross sections are, in general, greater than those for the triplet excitations.

In Figs. 3 and 4 are displayed the comparison of the Born cross sections with the VPS approximation (with effective charge and exchange) for the singlet-singlet and triplet-triplet transitions to the $n = 3$ and 4 states. Convergence to the Born limit is attained at high energies. The dip in the Born 3^3P and 4^3P cross sections at

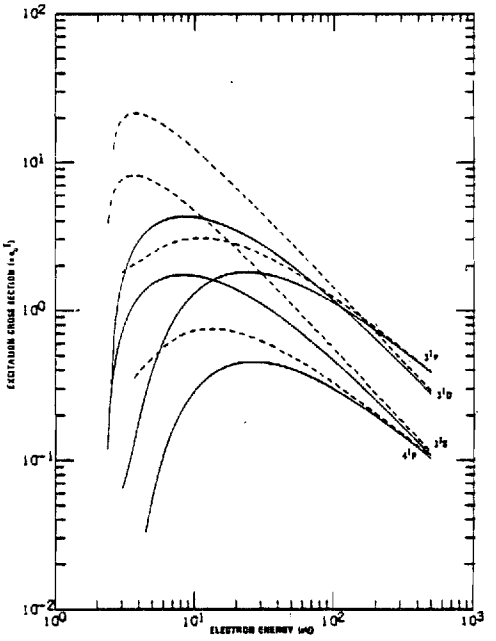

FIG. 3. The 3^1S, 3^1P, 3^1D, and 4^1P excitations arising from e-He(2^1S) collisions. Broken curve: Born approximation; solid curve: VPS approximation (3) with effective charge and exchange.

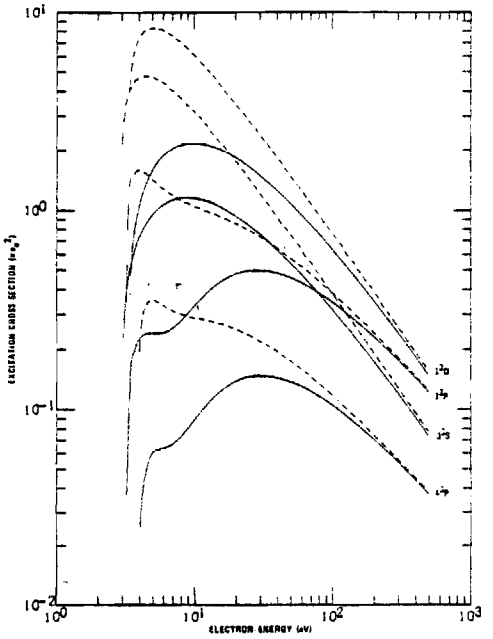

FIG. 4. The 3^3S, 3^3P, 3^3D, and 4^3P excitations arising from e-He(2^3S) collisions. Broken curve: Born approximation; solid curve: VPS approximation (3) with effective charge and exchange.

10 eV is a direct result of a zero occurring in the corresponding form factors (7), and this dip is further reflected in the VPS curves which are increasing with E at 10 eV.

In conclusion, total excitation cross sections for transitions arising from electron-metastable helium transitions have been derived from two different approximations. In the Born approximation, the incident relative motion is represented by a plane wave unaffected by the target, while in the VPS method, the relative motion is taken as a product of two Coulomb waves arising from the incident electron-atomic electron repulsion and the incident electron-atomic core attraction. The differences exhibited in the various sets of cross-section curves is a measure of the importance of obtaining accurate wave functions for the relative motion. At present, the situation is difficult to assess without resorting to more-refined theoretical treatments as, for example, the close-coupling or multichannel eikonal approach.[9] However, in the absence of any experimental data and since the above two approximations correspond to the two extremes of relative motion, each set of curves in the figures simply display the present theoretical uncertainty in finding reliable cross sections for excitation out of metastable helium. Application of the VPS approximation to the $1s$-$2s$ and $1s$-$2p$ excitations and the ionization of atomic hydrogen by electron impact does yield, however, cross sections[3,10] in good agreement with experiment. The agreement exhibited between the VPS and close-coupling methods for the 2^3S-2^3P excitation is also encouraging.

However, all the figures clearly indicate the need that theoretical treatments more refined than above must closely couple all the excitation channels together. The 3^1P cross section is smaller than both the 3^1D and 3^1S cross sections at low energies such that it would be affected by the presence of the 3^1D-3^1P and 3^1S-3^1P dipole couplings which would therefore tend to enhance the 3^1P excitation at low energies. Thus for impact energies $E < 100$ eV, it is highly desirable to closely couple all the 2^1S, 2^1P, 3^1S, 3^1P, and 3^1D channels. Such an investigation would involve the solution of up to ten coupled differential equations and is quite difficult.

*Research sponsored by the Air Force Aerospace Research Laboratories, Air Force Systems Command, United States Air Force, Contract F 33615-74-C-4003.

[1] B. L. Moiseiwitsch and S. J. Smith, Rev. Mod. Phys. 40, 238 (1968).
[2] D. E. Osterbrock, Ann. Rev. Astron. Astrophys. 2, 95 (1964).
[3] L. Vainshtain, L. Presnyakov, and I. Sobel'man, Sov. Phys. Phys.-JETP 18, 1383 (1964).
[4] V. I. Ochkur, Sov. Phys.-JETP 18, 503 (1964).
[5] Y-K. Kim and M. Inokuti, Phys. Rev. 181, 205 (1969). The authors wish to thank Dr. Y-K. Kim for sending us detailed tables of the form factors which were only partially given in this reference.
[6] A. W. Weiss, J. Res. Natl. Bur. Stand. (U.S.) A 71, 163 (1967).
[7] W. L. Wiese, M. W. Smith, and B. M. Glennon, *Atomic Transition Probabilities*, Natl. Bur. Stand. Publication No. NSRDS-NBS4 (U.S. GPO, Washington, D.C., 1966), Vol. 1.
[8] P. G. Burke, J. W. Cooper, and S. Ormonde, Phys. Rev. 183, 245 (1969).
[9] M. R. Flannery and K. J. McCann, Phys. Rev. 10, 2264 (1974).
[10] L. P. Presnyakov, Sov. Phys.-JETP 20, 760 (1965).

BIBLIOGRAPHY

1. E. W. McDaniel and E. A. Mason, "The Mobility and Diffusion of Ions in Gases," J. Wiley & Sons, New York, 1973.

2. J. O. Hirschfelder, C. F. Curtiss, and R. B. Bird, "Molecular Theory of Gases and Liquids," J. Wiley & Sons, New York, 1954.

3. A. Dalgarno and A. Williams, Proc. Phys. Soc. 72, 274-6, (1959).

4. B. H. Bransden, "Atomic Collision Theory," W. A. Benjamin, Inc., New York, 1970.

5. L. I. Schiff, "Quantum Mechanics," McGraw-Hill Book Company, New York, 1968.

6. M. S. Childs, "Molecular Collision Theory," Academic Press, New York, 1974.

7. J. E. G. Farina, "Quantum Theory of Scattering Processes," Pergamon Press, New York, 1973.

8. E. Merzbacher, "Quantum Mechanics," J. Wiley and Sons, Inc., New York, 1970.

9. G. W. Catlow, M. R. C. McDowell, J. J. Kaufmann, L. M. Sachs, and E. S. Chang, J. Phys. B, 3, 833, (1970).

10. A. S. Dickinson, J. Phys. B, 2, 1, 387-401, (1968).

11. H. T. Wood, J. Chem. Phys., 54, 3, 997, (1971).

12. H. O'Hara and F. J. Smith, Comp. Phys. Com., 2, 47-54, (1971).

13. C. W. Clenshaw and A. R. Curtiss, Num. Math., 2, 197-205, (1960).

14. M. Kennedy and F. J. Smith, Mol. Phys., 13, 5, 443-448, (1967).

15. R. W. Hamming, "Numerical Methods for Scientists and Engineers," McGraw Hill Book Company, Inc., New York, 1962.

16. D. R. Hartree, "The Calculation of Atomic Structures," J. Wiley and Sons, Inc., New York, 1957.

17. A. C. Allison, J. Comp. Phys. 6, 378-391, (1970).

18. A. C. Allison, Comp. Phys. Com. 3, 173-179, (1972).

BIBLIOGRAPHY (Continued)

19. R. E. Langer, Phys. Rev. 51, 669, (1937).

20. P. F. Byrd and M. D. Friedman, "Handbook of Elliptic Integrals for Engineers and Physicist," Lange, Maxwell, and Springer, London, 1954.

21. S. Peyerimhoff, J. Chem. Phys., 43, 3, 998, (1965).

22. H. P. Weise, H. U. Mittmann, A. Ding, and H. Henglein, Z. Naturforsch. A 26, 1122, (1971).

23. H. U. Mittmann, H. P. Weise, A. Ding, and H. Henglein, Z. Naturforsch. A 26, 1112, (1971).

24. R. Klingbeil, J. Chem. Phys., 57, 3, 1066, (1972).

25. W. G. Rich, S. M. Bobbio, R. L. Champion, and L. D. Doverspike, Phys. Rev. A, 4, 6, 2253, (1971).

26. S. Y. Kim and R. G. Gordon, J. Chem. Phys., 60, 1, 1, (1974).

27. R. G. Gordon and M. Waldman, J. Chem. Phys. to be published.

28. M. Barat, D. Dhuicq, R. Francois, and V. Sidis, J. Phys. B, 6, 2072, (1973).

29. C. Kubach and V. Sidis, J. Phys. B, 6, L289, (1973).

30. H. R. Skullerud, J. Phys. B, 6, 918, (1973).

31. P. C. Hariharan and V. Staemmler, Chem. Phys. 15, 409, (1976).

32. A. Dalgarno, M. R. C. McDowell, and A. Williams, Phil. Trans. R. Soc. A, 250, 411-25, (1958).

33. W. F. Morrison, G. R. Akridge, H. W. Ellis, R. Y. Pai, and E. W. McDaniel, L. A. Viehland, and E. A. Mason, J. Chem. Phys., 63, 5, 2238, (1975).

34. B. F. Junker and J. C. Browne, Abstr. 6th Int. Conf. on the Physics of Electronic and Atomic Collisions, Cambridge, Mass.: MIT Press, 220-21, (1969).

35. F. J. Rogers, Phys. Rev. A, 4, 3, 1145, (1971).

36. R. J. Munn, E. A. Mason, and F. J. Smith, J. Chem. Phys. 41, 12, 3978, (1964).

BIBLIOGRAPHY (Continued)

37. R. J. Munn, F. J. Smith, and E. A. Mason, J. Chem. Phys. 42, 2, 537, (1965).

38. S. Imam-Rahajoe, C. F. Curtiss, and R. B. Bernstein, J. Chem. Phys. 42, 2, 530, (1965).

39. R. B. Bernstein and K. H. Kramer, J. Chem. Phys. 38, 10, 2507, (1963).

40. D. R. Bates, "Quantum Theory," Academic Press Inc., New York, 1961.

41. K. W. Ford and J. A. Wheeler, Ann. Phys. (N.Y.) 7, 259, (1959).

42. N. F. Mott and H. S. W. Massey, "The Theory of Atomic Collisions," 3rd ed., Oxford, at the Clarendon Press, 1965.

43. I. R. Gatland, L. A. Viehland, and E. A. Mason, J. Chem. Phys. (in press).

44. I. R. Gatland, W. F. Morrison, H. W. Ellis, M. G. Thackston, E. W. McDaniel, M. H. Alexander, L. A. Viehland, and E. A. Mason, J. Chem. Phys., 66, 11, 5121, (1977).

45. M. McFarland, D. L. Albritton, F. C. Fehsenfeld, E. E. Ferguson, and A. L. Schmeltekopf, J. Chem. Phys. 59, 6610, (1973).

46. O. J. Orient, J. Phys. B 4, 1257, (1971).

47. O. J. Orient, J. Phys. D 7, 2266, (1974).

48. H. W. Ellis, R. Y. Pai, E. W. McDaniel, E. A. Mason, and L. A. Viehland, (to be published).

49. L. A. Viehland and E. A. Mason, Ann. Phys. 91, 2, (1975).

50. G. R. Akridge, H. W. Ellis, R. Y. Pai, and E. W. McDaniel, J. Chem. Phys. 62, 4578, (1975).

51. H. Inouye and S. Kita, J. Chem. Phys. 57, 1301 (1972).

52. K. Hoselitz, Proc. Roy. Soc. A 177, 200, (1941).

53. L. A. Viehland. E. A. Mason, W. F. Morrison, and M. R. Flannery, Atomic Data and Nuclear Data Tables 16, 495-514, (1975).

54. J. R. Taylor, "Scattering Theory," J. Wiley and Sons, New York, 1972.

BIBLIOGRAPHY (Continued)

55. A. S. Davydov, "Quantum Mechanics," NEO Press, Ann Arbor, Michigan, 1966.

56. L. Vainshtein, L. Presnyakov, and I. Sobel'man, JETP 18, 1383, (1964).

57. D. S. F. Crothers and R. McCarrol, Proc. Phys. Soc. 86, 753, (1965).

58. L. Presnyakov, I. Sobel'man, and L. Vainshtein, Proc. Phys. Soc. 89, 511, (1966).

59. D. S. F. Crothers, Proc. Phys. Soc. 91, 855, (1967).

60. J. P. Coleman, "Case Studies in Atomic Collision Physics," E. W. McDaniel and M. R. C. McDowell editors, North-Holland Publishing Company, Amsterdam, 1969.

61. A. Nordsieck, Phys. Rev. 93, 785, (1954).

62. W. L. Fite and R. T. Brockman, Phys, Rev. 112, 215, (1958).

63. W. L. Fite, R. F. Stebbings, and R. T. Brockman, Phys. Rev. 116, 356, (1959).

64. R. F. Stebbings, W. L. Fite, D. G. Hummer, and R. T. Brockman, Phys. Rev. 119, 1939, (1960).

65. R. F. Stebbings, W. L. Fite, A. G. Hummer, and R. T. Brockman, Phys. Rev. 124, 2051, (1961).

66. H. L. Kyle and M. R. C. McDowell, J. Phys. B. 2, 2, 15, (1969).

67. M. R. Flannery, W. F. Morrison, and B. L. Richmond, J. Applied Phys., 46, 3, 1186, (1975).

68. V. I. Ochkur, JETP 18, 503, (1964).

69. Y-K. Kim and M. Inokuti, Phys. Rev. 181, 205, (1969).

70. P. G. Burke, J. W. Cooper, and S. Ormoude, Phys. Rev. 183, 245, (1969).

71. M. R. Flannery, J. Phys. B. 8, 15, 2470, (1975).

72. H. S. W. Massey and C. B. O. Mohr, Proc. Roy. Soc. A146, 880, (1934).

73. W. Rothenstein, Proc. Phys. Soc. (London) A 67, 673, (1954).

VITA

Walter Fredrick Morrison, Jr., is a native of Birmingham, Alabama. He received his B.S. Degree in Physics, with Honors, in 1971 and his M.S. Degree in Physics in 1973 from the Georgia Institute of Technology.

Between the years 1973 and 1976 Mr. Morrison was employed as a Graduate Teaching and Research assistant while conducting research toward his doctoral degree. In January 1976 Mr. Morrison entered active duty with the U. S. Army and was assigned to the Ballistic Research Laboratory, Aberdeen Proving Ground, Maryland where he completed work on his doctoral dissertation. His publications include:

"Excitation in Electron-Metastable Helium Collisions," M. R. Flannery, W. F. Morrison, and B. L. Richmond, J. Applied Phys., 46, 3, 1186, (1975).

"Test of the Li^+-He Interaction Potential," W. F. Morrison, G. R. Akridge, H. W. Ellis, R. Y. Pai, and E. W. McDaniel, L. A. Viehland, and E. A. Mason, J. Chem. Phys., 63, 5, 2238, (1975).

"Tables of Transport Collision Integrals for (n,6,4) Ion-Neutral Potentials," L. A. Viehland, E. A. Mason, W. F. Morrison, and M. R. Flannery, Atomic Data and Nuclear Data Tables 16, 495-514, (1975).

"The Li^+-He Interaction Potential," I. R. Gatland, W. F. Morrison, H. W. Ellis, M. G. Thackston, E. W. McDaniel, M. H. Alexander, L. A. Viehland, and E. A. Mason, J. Chem. Phys., 66, 11, 5121, (1977).

Mr. Morrison is a member of Tau Beta Pi, Phi Kappa Phi, Sigma Pi Sigma, and the American Physical Society. He is married to the former Julia DuVal Harris of Richmond, Virginia.